CHEMISTRY OF LOW-VALENT PLATINUM DIMERS

Thesis by

Miriam Heinrichs Zietlow

In Partial Fulfillment of the Requirements

for the Degree of

Doctor of Philosophy

California Institute of Technology

Pasadena, California

1989

(Submitted August 8, 1988)

Under certain circumstances there are few hours in life more agreeable than the hour dedicated to the ceremony known as afternoon tea. There are circumstances in which, whether you partake of the tea or not—some people of course never do,—the situation is in itself delightful.

Henry James

The Portrait of a Lady

ACKNOWLEDGMENTS

It's hard to believe that I've been at Caltech for five years! I won't say that "I've had the time of my life" here, but there are some people who have made this place pleasant and deserve some thanks.

First there's Harry, a man whom I have great respect for as a person and as a scientist. He is one of the most generous people I have ever met and I have greatly enjoyed interacting with him, learning from him, listening to his stories and laughing.

Then, of course there is the rest of the Gray group, past and present: Janet, Tom, Mike, Tad, David, Erica, Holden, Ramy, John, Mark, Wayne, and the bio-group; some of whom deserve special recognition. When I joined the group, it consisted of a bunch of men and one woman; I leave the group with the same ratio. Good luck Erica. Tad "Dude" and David "the Mav", who have been with me during my five years here and have been responsible, knowingly or unknowingly, for much of my amusement. Jenny, a great roommate and the perfect person to be writing a thesis with; she always knows when to take a break — "How 'bout a movie?" Ramy, a really sweet guy, the best washboard around, and now even a convertible — What more could a girl want? Holden, a very "bright" young man who has the incredible responsibility of leading "such a hard life"; best of all, though, he's a Tarheel born and Tarheel bred. And then there's John "Johnny Dollar", who never did get a little red wagon — well, I don't think you'll need one now.

I want to thank all those people who helped me along on my first and "will it ever end" linear chains project: Bill Schaefer, Les Butler, Basil Swanson, and especially Steve Conradson.

Lunchtime — that midday break necessary to regain my sanity; I want to say THANKS to all my long-time regular lunch buddies; Paula, Marie, Scott, Debbie, and "H".

Every year, around July, I never got enough sleep during it, but I always felt better after it — the Southern California Inorganic Photochemistry (SCIP) conference. I'll miss those meetings and the people, especially Carl, Cris, and Dick.

Although I'm not a big fan of Southern California, there are two things here that I will truly miss: Claro's Italian Deli and the people there, and, most importantly, the Santa Anita Race Track. GO Winning Colors!!! GO Willy!!!

Words cannot begin to express how grateful I am for all the patience, encouragement, and love that my husband, Tom, and my parents have given me. Tom, you are my best friend, my "sweetie"; one of the best things that ever happened to me was having to work late on a Friday night. My mother and father, Mami and Papi, not a typical set of parents — maybe that's why I love them so much.

And lastly, I want to thank God for all that He has done for me in the past, at the present, and in the future.

to my Mother, my Father, Ashes

and Tom

ABSTRACT

Physical and chemical properties of low-valent platinum dimers, namely $[Pt_2(P_2O_5H_2)_4]^{4-}$ and $Pt_2(\mu\text{-dppm})_2Cl_2$, have been investigated using a variety of structural and spectroscopic techniques.

Platinum(II) d^8-d^8 dimers have been shown to exhibit much thermal and photochemical reactivity. Chapter 2 describes studies aimed at elucidating the excited state reduction potential of $[Pt_2(P_2O_5H_2)_4]^{4-}$, Pt_2, in organic media. By conducting excited state electron transfer studies using derivatized pyridiniums and benzophenones, the Pt_2 excited state reduction potential has been estimated to be ~2 V. The Pt_2 complex undergoes partial oxidation to form Pt(II,III) linear chains. Chapter 3 describes the structural and spectroscopic techniques used to determine the translational symmetries of these $[Pt_2(P_2O_5H_2)_4X]^{4-}$ (X = Cl, Br), Pt_2X, chains. Pt_2Br has been found to be intermediate between $(AAB)_n$ and $(AABCCB)_n$, while, Pt_2Cl is of $(AABCCB)_n$ translational symmetry. Investigations into the electronic transitions of Pt_2Cl and Pt_2Br were conducted using high pressure techniques and are presented in Chapter 4. The Pt_2X electronic spectrum exhibits bands attributable to the reduced Pt_2 complex and the oxidized Pt_2X_2 complex ($[Pt_2(P_2O_5H_2)_4X_2]^{4-}$) along with an intervalence charge-tranfer band characteristic of a mixed-valence solid.

Photophysical investigations of a new luminescent chromophore, $Pt_2(\mu\text{-dppm})_2Cl_2$, a d^9-d^9 dimer, and its analogs are described in Chapter 5. The absorption band directly responsible for the observed emission is believed to be very weak and, as of yet, unobserved. Attempts to determine the spin multiplicty and approximate energy of this unobserved transition are described in Chapter 6. Excited-state

energy transfer studies indicate that this absorption band is a triplet transition at ~13,000 cm^{-1}. Although, the $Pt_2(\mu\text{-dppm})_2Cl_2$ excited state is non-luminescent in fluid solution, it has been shown to undergo thermal electron transfer to tetracyanoethylene and photo-induced electron transfer to methylviologen. These experiments are presented in Chapter 7. Preliminary studies, described in Chapter 8, of non-bridged d^9-d^9 platinum(I) dimers have shown that $[Pt_2(CNCH_3)_6]^{2+}$ serves as a versatile precursor in the synthesis of new d^8-d^8 A-frame complexes.

TABLE OF CONTENTS

LIST OF FIGURES

Chapter 1

Chapter2

Chapter 3

Chapter 4

Chapter 5

LIST OF TABLES

Chapter 4

Chapter 5

Chapter 6

Chapter 7

CHAPTER 1

Introduction

INTRODUCTION

A photo-excited molecule is best envisioned as a new species possessing physical and chemical properties distinct from its corresponding ground state molecule. Photophysical studies of various molecular chromophores (namely monomers,[1,2] dimers,[3,4] and clusters[5,6]) have resulted in elaborate and detailed descriptions of the physical properties of their excited states. During these studies, certain chromophores have been recognized as possessing great photochemical potential in the areas of solar energy conversion and small molecule activation.[1,7] One such molecular chromophore is the d^8-d^8 dimer.

First synthesized by Roundhill and coworkers,[8] $[Pt_2(P_2O_5H_2)_4]^{4-}$, Pt_2, is a particularly interesting member of this class of molecules. Its structure can be described as two face-to-face square planar monomeric fragments, which are hooked together by four bridging ligands (see Figure 1.1)[9]; hence, the "idealized" point group is D_{4h}. The molecular orbital diagrams for all d^8-d^8 species have the same basic features, which are illustrated in Figure 1.2. Since all the electrons are spin paired, the ground state is a singlet. The lowest energy excited state is obtained when an electron is promoted from the $d\sigma^*$ orbital to the $p\sigma$ orbital; for Pt_2 this transition is $A_{1g} \rightarrow A_{2u}$.[10,11] From group theory, the $(d\sigma^*)^2 \rightarrow (d\sigma^*)(p\sigma)$ transition is fully allowed along the z direction,[10,11] thus the extinction coefficient for the $^1A_{1g} \rightarrow {}^1A_{2u}$ transition is expected to be 10^3 - 10^4 M^{-1} cm^{-1}; the actual value being 3.45×10^4 M^{-1} cm^{-1}.[10,11] The $^1A_{1g} \rightarrow {}^3A_{2u}$ transition is formally spin forbidden; however due to spin-orbit coupling it is observed in the absorption spectrum with an $\varepsilon = 110$ M^{-1} cm^{-1}.[10,11]

While these features are common to all d^8-d^8 dimers, the exact

Figure 1.1 Structure of $[Pt_2(P_2O_5H_2)_4]^{4-}$.

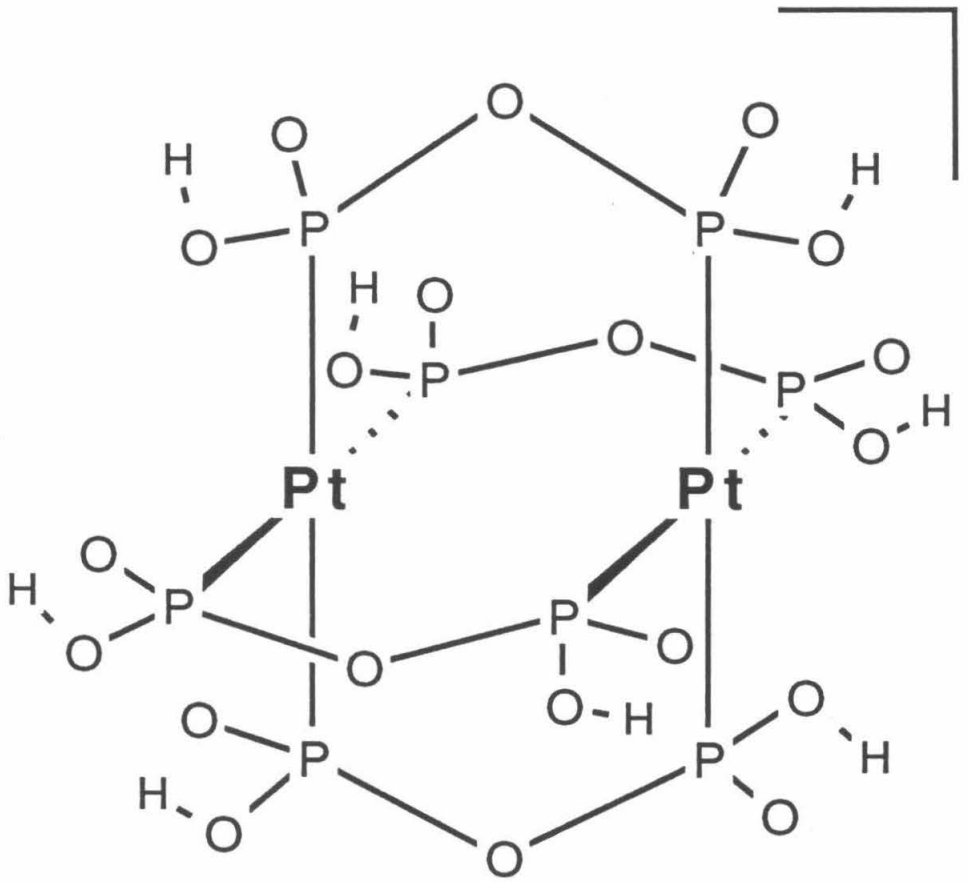

4 -

Figure 1.2 Molecular orbital diagram for a d^8-d^8 dimer built from a d^8 monomer.

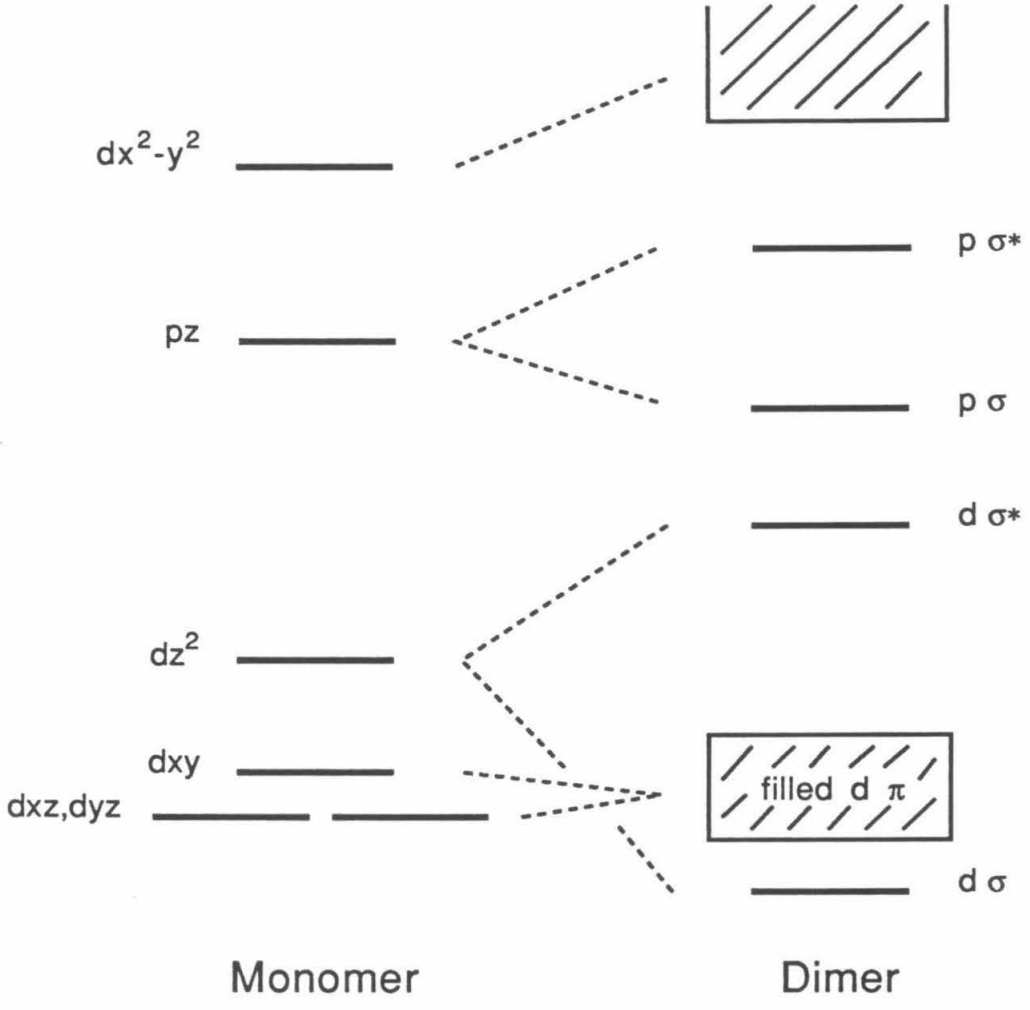
dx2-y2
pz
dz2
dxy
dxz,dyz
p σ*
p σ
d σ*
filled d π
d σ
Monomer
Dimer

energies of the singlet-singlet and singlet-triplet transitions are a function of the metal and type of ligands, as well as constraints on the metal-metal distance due to the size of the bridging ligand. These factors cause the singlet-singlet and singlet-triplet transitions in Pt_2 to lie at relatively high energies; 27100 cm^{-1} (369 nm) and 22200 cm^{-1} (451 nm) respectively (see Figure 1.3). The molecular orbital diagram predicts that $Pt_2(pop)_4$ contains no formal metal-metal bonds; however, configurational mixing of orbitals results in a ground state metal-metal interaction. The excited state is predicted to have a formal metal-metal single bond; evidence for this is observed in low temperature absorption spectroscopy, where the vibrational transitions are well resolved,[10] and in time-resolved resonance Raman spectroscopy.[12,13] The formation of a metal-metal single bond in the excited state has important implications in the photochemistry arising from this state.

The most appealing feature of all d^8-d^8 dimers is their observed luminescence. Although all d^8-d^8 dimers studied thus far luminesce to some extent, emission observed for Pt_2 is truly remarkable, with a quantum yield of emission greater than 0.50 (see Figure 1.3).[14] The majority of the emission results from radiative decay from the triplet excited state (phosphorescence) with a luminescence lifetime of 10 μs at room temperature. Emission from the singlet excited state (fluorescence) is also observed; its luminescence lifetime is estimated to be 40 ps.[10,11] Due to the shortness of the fluorescent lifetime, it is unlikely that any bimolecular photochemistry will occur directly from the singlet excited state.

These properties of Pt_2 can be used to investigate the correlation

Figure 1.3 Electronic absorption (——) and corrected emission (----) spectra (taken from reference 10b) of an aqueous solution (300 K) of $K_4[Pt_2(P_2O_5H_2)_4]$; (left scale, $\varepsilon \times 10^{-4}$ M^{-1} cm^{-1} values).

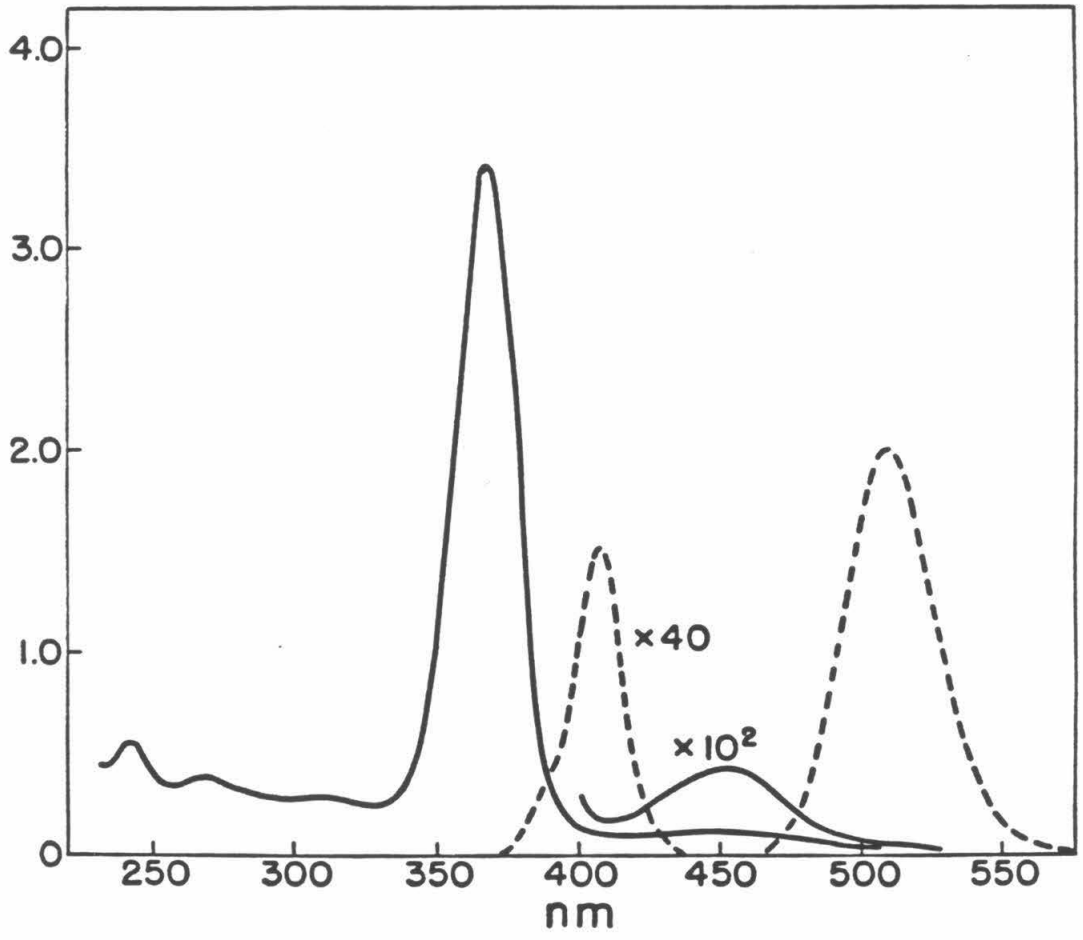
4.0
3.0
2.0
1.0
0
250
300
350
400
450
500
550
nm
×40
×10²

of one electron potentials with photoreactivity involving one or more electrons. Chapter 2 describes quenching experiments designed to investigate the photoreactivity of the triplet excited state in organic media.

The Pt_2 dimer crystallizes in the tetragonal space group P4/mbm as infinite chains along the c axis when K^+ is present as the counterion.[9] Oxidation of the Pt_2 structure by the introduction of different groups, which act as bridges between the dimers, creates d^7-d^8 systems which exhibit interesting conduction properties.[15,16] The results of X-ray diffraction studies and Raman experiments, which offer a clearer structural view of these linear chain systems, are discussed in Chapter 3.

In addition to bond length changes in the $Pt_2(P_2O_5H_2)_4$ core resulting from oxidation by halogen, the molecular orbital description of the $[Pt_2(P_2O_5H_2)_4X]^{4-}$ chains changes. Chapter 4 investigates the effects of pressure on the electronic absorption spectra for $[Pt_2(P_2O_5H_2)X_n]^{4-}$ (n = 0,1,2); these results have increased our insight into the structural and electronic factors which dominate in the molecular orbital description of these systems.[17]

In addition to being desirable candidates for photophysical study, d^8-d^8 dimers participate in many interesting photochemical reactions. Two types of reaction classes, established thus far, which result in net photochemistry are (*i*) bimolecular oxidative-additon reactions initiated by electron transfer[18,19] and (*ii*) hydrogen atom abstraction reactions.[20-24] In both of these reactions, steric restrictions imposed by the bridging ligands of the d^8-d^8 starting material force substrate addition to occur in the axial position, resulting in the formation of d^7-d^7 dimers as products. Because of this steric re-

striction, it is difficult to envision photochemical, concerted addition of small molecules such as CO_2, CS_2, and SO_2. If the metal-metal core were made more assessible to substrates such that adjacent coordination sites were available, concerted small molecule addition may be possible.

It is with this thought in mind that the photophysical and photochemical study of the nearly planar d^9-d^9 platinum dimer $Pt_2(\mu\text{-dppm})_2Cl_2$ (dppm = bis(diphenylphosphino)methane) and its analogs was undertaken (see Figure 1.4 and Table 1.1).[25,26] Both platinum and palladium d^9-d^9 complexes, $M_2(\mu\text{-dppm})_2Cl_2$ (M = Pt, Pd), have been shown to thermally add small molecules across the metal-metal bond to form the corresponding d^8-d^8 A-frame complexes (see Figure 1.5).[27-33] The palladium dimers failed to exhibit any detectable luminescence; therefore the photochemical study of these complexes centered about the platinum dimers. Investigation into their photophysical properties is described in Chapter 5. More detailed information about the d^9-d^9 excited state reactivity is presented in Chapters 6 and 7 where energy transfer and electron transfer studies on these complexes are described. And in closing, Chapter 8 briefly discusses preliminary investigations on non-bridging d^9-d^9 dimers. Unlike the nearly planar dppm bridged complexes, these molecules have a staggered geometry.[34] Their thermal and photochemical reactivity is dominated by homolytic metal-metal bond cleavage reactions similar to those observed for the d^7-d^7 $M_2(CO)_{10}$ (M = Mn, Re) complexes.[35-37]

Figure 1.4 Structure and ORTEP drawing (taken from reference 26) of $Pt_2(\mu\text{-dppm})_2Cl_2 \cdot 0.5CH_2Cl_2$.

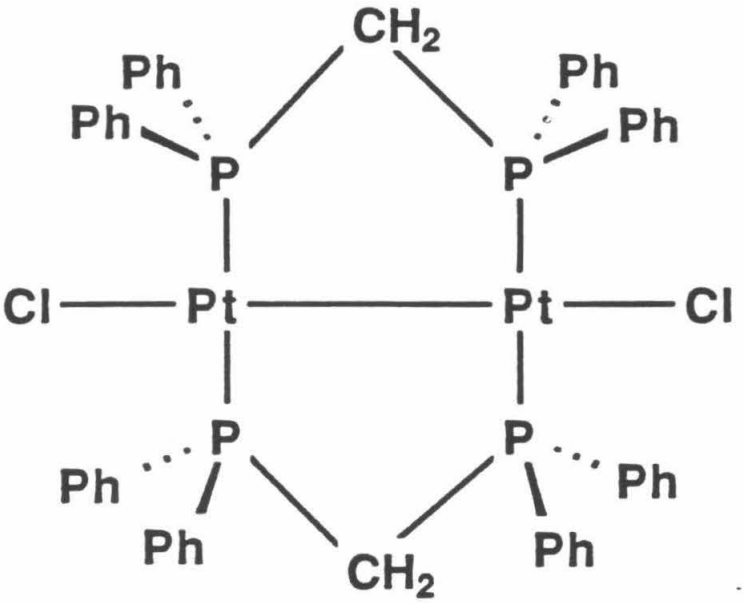
CH2
Ph
Ph
Ph
Ph
P
P
Cl
Pt
Pt
Cl
P
P
Ph
Ph
Ph
Ph
CH2

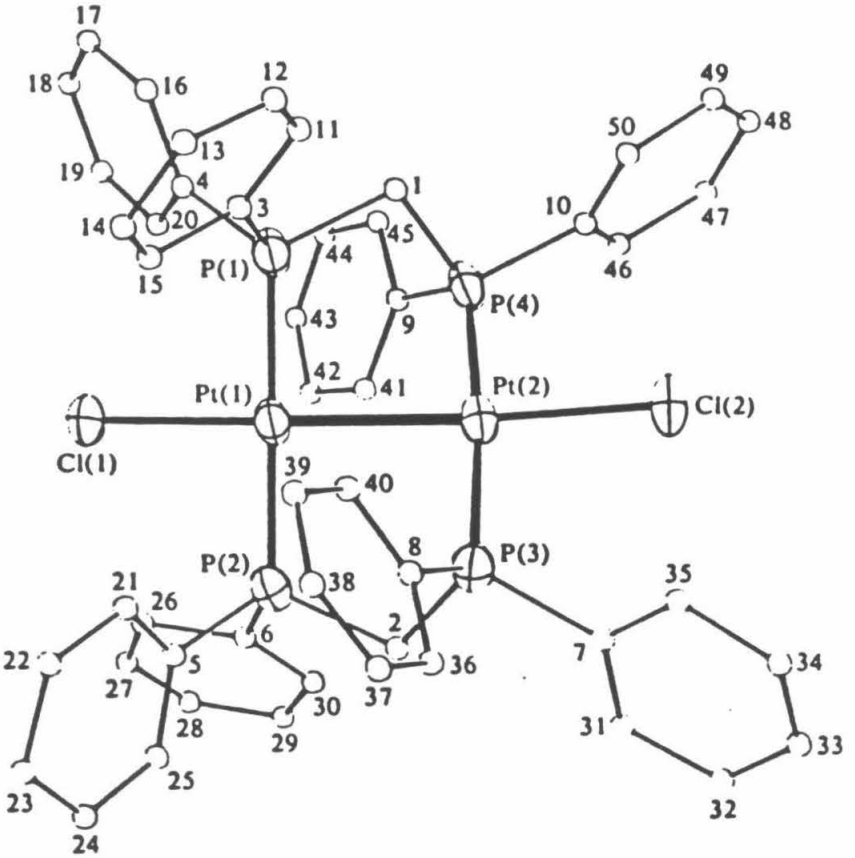
P(1)
P(2)
P(3)
P(4)
Pt(1)
Pt(2)
Cl(1)
Cl(2)

Table 1.1

Selected Bond Lengths and Bond Angles of $Pt_2(\mu\text{-dppm})_2Cl_2$ †

Bond Lengths (Å)		Bond Angles (°)	
Pt(1) - Pt(2)	2.651(1)	Cl(1) - Pt(1) - Pt(2)	178.5(2)
Pt(1) - Cl(1)	2.408(5)	P(1) - Pt(1) - P(2)	175.6(2)
Pt(2) - Cl(2)	2.401(5)	Cl(1) - Pt(1) - P(1)	90.2(2)
Pt(1) - P(1)	2.294(7)	Cl(1) - Pt(1) - P(2)	89.6(2)
Pt(1) - P(2)	2.264(7)	Pt(2) - Pt(1) - P(1)	89.3(2)
Pt(2) - P(3)	2.259(7)	Pt(2) - Pt(1) - P(2)	91.0(2)
Pt(2) - P(4)	2.250(7)		
		Cl(2) - Pt(2) - Pt(1)	175.7(2)
		P(3) - Pt(2) - P(4)	172.9(2)
		Cl(2) - Pt(2) - P(3)	94.3(2)
		Cl(2) - Pt(2) - P(4)	92.2(2)
		Pt(1) - Pt(2) - P(3)	88.7(2)
		Pt(1) - Pt(2) - P(4)	85.0(2)

† Data taken from reference 26.

Figure 1.5 Known thermal chemistry of $Pt_2(\mu\text{-dppm})_2Cl_2$.

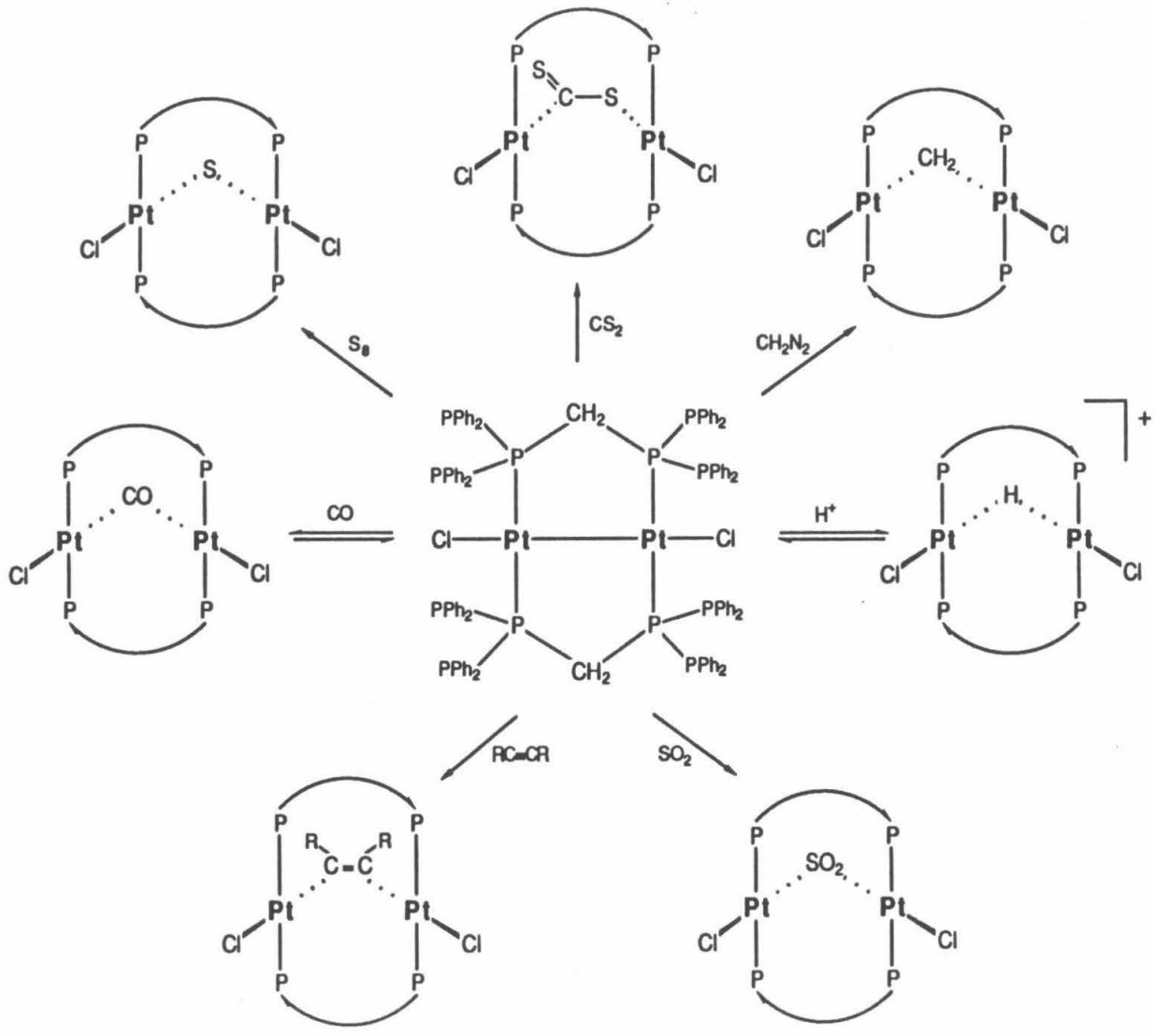
CS2
S8
CH2N2
CO
H+
RC≡CR
SO2
PPh2
CH2
Pt
Cl
P
S
C
R
SO2
H
+

REFERENCES

1. Kalyanasundaram, K. *Coord. Chem. Rev.* **1982**, *159*, 244.
2. Winkler, J. R.; Gray, H. B. *Inorg. Chem.* **1985**, *24*, 346.
3. Trogler, W. C.; Solomon, E. I.; Trajberg, I.; Ballhausen, C. J.; Gray, H. B. *Inorg. Chem.* **1977**, *16*, 828.
4. Rice, S. F.; Gray, H. B. *J. Am. Chem. Soc.* **1981**, *103*, 1593.
5. Maverick, A. W.; Najdzionek, J. S.; Mackenzie, D.; Nocera, D. G.; Gray, H. B. *J. Am. Chem. Soc.* **1983**, *105*, 1878.
6. Zietlow, T. C.; Hopkins, M. D.; Gray, H. B. *J. Solid State Chem.* **1985**, *57*, 112.
7. Gray, H. B.; Maverick, A. W. *Science* **1981**, *214*, 1201.
8. Sperline, R. R.; Dickson, M. K.; Roundhill, D. M. *J. Chem. Soc. Chem. Commun.* **1977**, 62.
9. Filomena Dos Remedios Pinto, M. A.; Sadler, P. J.; Neidle, S.; Sanderson, M. R.; Subbiah A.; Kuroda, R. *J. Chem. Soc. Chem. Commun.* **1980**, 13.
10. (a) Rice, S. F.; Gray, H. B. *J. Am. Chem. Soc.* **1983**, *105*, 4571. (b) Che. C.-M.; Butler, L. G.; Gray, H. B. *J. Am. Chem. Soc.* **1981**, *103*, 7796.
11. Fordyce, W. A.; Brummer, J. G.; Crosby, G. A. *J. Am. Chem. Soc.* **1981**, *103*, 7061.
12. Stein, R. B.; Dickson, M. K.; Roundhill, D. M. *J. Am. Chem. Soc.* **1983**, *105*, 3489.
13. Che, C.-M.; Butler, L. G.; Gray, H. B.; Crooks, R. M.; Woodruff, W. H. *J. Am. Chem. Soc.* **1983**, *105*, 5492.
14. Heuer, W. B.; Trotten, M. D.; Rodman, G. S.; Herbert, E. J.; Tracy, H. J.; Nagle, J. K. *J. Am. Chem. Soc.* **1984**, *106*, 1163.

15. Che, C.-M.; Herbstein, F. H.; Schaefer, W. P.; Marsh, R. E.; Gray, H. B. *J. Am. Chem. Soc.* **1983**, *105*, 4604.

16. Butler, L. G.; Zietlow, M. H.; Che, C.-M.; Schaefer, W. P.; Sridhar, S.; Grunthaner, P. J.; Swanson, B. I.; Clark, R. J. H.; Gray, H. B. *J. Am. Chem. Soc.* **1988**, *110*, 1155.

17. Stroud, M. A.; Drickamer, H. G.; Zietlow, M. H.; Gray, H. B.; Swanson, B. I. *J. Am. Chem. Soc.* **1988**, in press.

18. Marshall, J. L.; Stiegman, A. E.; Gray, H. B. *A. C. S. Symp. Ser.* **1986**, *307*, 166.

19. Caspar, J. V.; Gray, H. B. *J. Am. Chem. Soc.* **1984**, *106*, 3029.

20. Roundhill, D. M.; Atherton, S. J. *Inorg. Chem.* **1986**, *25*, 4071.

21. Harvey, E. L.; Stiegman, A. E.; Vlcek, A.; Gray, H. B. *J. Am. Chem. Soc.* **1987**, *109*, 5233.

22. Vlcek, A.; Gray, H. B. *J. Am. Chem. Soc.* **1987**, *109*, 286.

23. Roundhill, D. M.; Atherton, S. J.; Shen, Z. P. *J. Am. Chem. Soc.* **1987**, *109*, 6076.

24. Vlcek, A.; Gray, H. B. *Inorg. Chem.* **1987**, *26*, 1997.

25. Brown, M. P.; Puddephatt, R. J.; Rashidi, M.; Manojlović-Muir, Lj.; Muir, K. W.; Solomun, T.; Seddon, K. R. *Inorg. Chim. Acta*, **1977**, *23*, L33.

26. Manojlović-Muir, Lj.; Muir, K. W.; Solomun, T. *Acta Cryst.* **1979**, *B35*, 1237.

27. Brown, M. P.; Puddephatt, R. J.; Rashidi, M.; Seddon, K. R. *J. Chem. Soc. Dalton Trans.* **1978**, 516.

28. Brown, M. P.; Puddephatt, R. J.; Rashidi, M.; Seddon, K. R. *J. Chem. Soc. Dalton Trans.* **1978**, 1540.

29. Brown, M. P.; Fisher, J. R.; Puddephatt, R. J.; Seddon, K. R.;

Inorg. Chem. **1979**, *18*, 2808.

30. Cameron, T. S.; Gardner, P. A.; Grundy, K. R. *J. Organomet. Chem.* **1981**, *212*, 135.
31. Benner, L. S.; Balch, A. L. *J. Am. Chem. Soc.* **1978**, *100*, 6099.
32. Olmstead, M. M.; Hope, H.; Benner, L. S.; Balch, A. L. *J. Am. Chem. Soc.* **1977**, *99*, 5502.
33. Balch, A. L.; Benner, L. S.; Olmstead, M. M. *Inorg. Chem.* **1979**, *18*, 2996.
34. Goldberg, S. Z.; Eisenberg, R., *Inorg. Chem.* **1976**, *15*, 535.
35. Boehm, J. R.; Doonan, D. J.; Balch, A. L. *J. Am. Chem. Soc.* **1976**, *98*, 4845.
36. Miller, T. D.; St. Clair, M. A.; Reinking, M. K.; Kubiak, C. P. *Organometallics* **1983**, *2*, 767.
37. Reinking, M. K.; Kullberg, M. L.; Cutler, A. R.; Kubiak, C. P. *J. Am. Chem. Soc.* **1985**, *107*, 3517.

CHAPTER 2

Electron Transfer Studies of $(TBA)_4[Pt_2(P_2O_5H_2)_4]$

INTRODUCTION

Several experiments were performed which attempted to establish the ground and excited state redox properties of $[Pt_2(P_2O_5H_2)_4]^{4-}$, Pt_2, in water.[1-4] Cyclic voltammograms were measured; however, the redox couples of Pt_2 were irreversible, suggesting that the oxidized and reduced species of Pt_2 are very short lived. Hence only estimates of the oxidation and reduction potentials were obtained. Fairly good approximations for the excited state redox values were obtained through oxidative and reductive quenching studies.[1,3-5] From these investigations it was determined that Pt_2 was both a strong reducing agent[3,4] and a strong oxidant in water.[1] The modified Latimer diagram for Pt_2 in water is illustrated in Figure 2.1.

Since the potassium salt of Pt_2 is only soluble in water, attempts to find routes to new photochemical reactions were hampered by the limited solvent selection. Metathesis of the potassium salt to tetrabutylammonium, TBA^+, yielded a salt soluble in a variety of solvents. Along with the increase in solvent selection, the reactivity of the dimer appeared to increase in non-aqueous media, which led to new questions concerning the reducing power of the dimer. This chapter describes electron transfer quenching experiments designed to probe the reducing power of Pt_2 in acetonitrile.

Figure 2.1 Modified Latimer diagram for $K_4[Pt_2(P_2O_5H_2)_4]$ (E in V *vs.* SCE) in water.

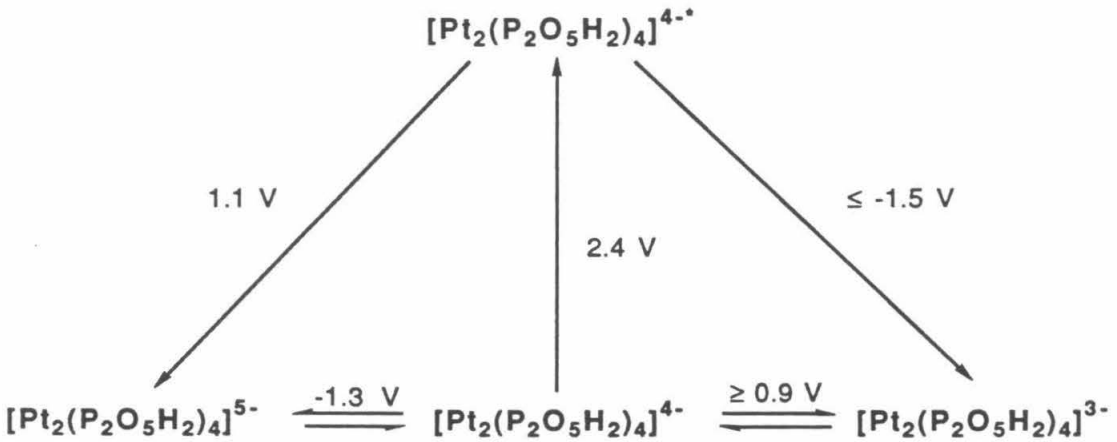
[Pt2(P2O5H2)4]4-•
1.1 V
2.4 V
≤ -1.5 V
[Pt2(P2O5H2)4]5-
-1.3 V
[Pt2(P2O5H2)4]4-
≥ 0.9 V
[Pt2(P2O5H2)4]3-

EXPERIMENTAL

Materials

All solvents, unless otherwise noted, were reagent grade and used as received without further purification.

$K_4[Pt_2(P_2O_5H_2)_4]$ and $(TBA)_4[Pt_2(P_2O_5H_2)_4]$: The potassium salt of Pt_2 was prepared by the published procedure.[6] Metathesis of the potassium salt to the tetrabutylammonium salt was carried out in the dark following, for the most part, the published procedure.[7] For improved results: $K_4[Pt_2(P_2O_5H_2)_4]$ (0.25 g) was dissolved in 10 mL of water. A 4:1 molar excess of tetrabutlyammonium chloride (TBACl) in 30 mL of CH_2Cl_2 was added to the Pt_2 solution with vigorous shaking. The platinum complex was extracted into the organic layer (yellow) and separated. The $(TBA)_4[Pt_2(P_2O_5H_2)_4]$ was precipitated from CH_2Cl_2 by adding an excess of dry diethyl ether (~ 100 mL).

Pyridinium hexafluorphosphates. The pyridinium hexafluorphosphate quenchers were prepared and recrystallized by Dr. Janet Marshall and used as received.[8]

Benzophenone and its derivatives. Benzophenone (Adrich, 99%), 4-methylbenzophenone (Aldrich, 97%), 4-fluorobenzophenone (Aldrich, 97%), 4-methoxybenzophenone (Aldrich, 97%), 4-dimethoxyaminobenzophenone (Aldrich, 98%) were recrystallized from hot 2:1:1 (v/v/v) water:acetone:ether and used without further purification.

Methylviologen hexafluorphosphate. Methylviologen dichloride hydrate (Aldrich) was dissoved in a minimum amount of water to which a saturated solution of potassium hexafluorophosphate, KPF_6, (Aldrich, 98%) was added. Methylviologen hexafluorophosphate precipitated immediately, was filtered, washed with water, and recrystallized from hot

2:1:1 (v/v/v) water:acetone:ether yielding long white needles.

Tetrabutylammonium hexafluorophosphate, $TBAPF_6$. Equal molar concentrations of saturated tetrabutylammonium bromide, TBABr, (Aldrich, 98%) in water and saturated KPF_6 in water were added together. $TBAPF_6$ precipitated, was filtered, and recrystallized from hot absolute ethanol yielding white needles.

Physical Measurements

Electrochemical Measurements. All cyclic voltammograms were measured using EG&G PAR electronics, Models 175 (Universal Programmer), 173 (Potentiostat/Galvanostat) and 179 (Digital Coulometer) with a Houston Instruments 2000 X-Y Recorder. The reference electrode was a standard calomel electrode, SCE; both the working and auxiliary electrodes were platinum wires. The cyclic voltammograms were measured in acetonitrile (Burdick and Jackson, UV grade) solutions, purged with N_2, with 0.1 M $TBAPF_6$ as the supporting electrolyte. Measurements were made at both 200 and 500 mV sec^{-1} scan rates.

Stern-Volmer Quenching Procedures. Rate constants obtained from luminescence lifetime quenching data were measured using a Nd:YAG pulsed laser system described previously.[9] Rate constants obtained from emission intensity quenching data were measured using an emission spectrophotometer constructed at Caltech and described elsewhere.[10] All emission spectra were recorded and corrected for monochromator and photomultiplier tube response using the OLIS fluorimetry programs.[11]

Samples for all electron transfer measurments were prepared by placing Pt_2 (~1 mg) was placed in a two-compartment spectrophotometric cell (referred to as a quenching cell) equipped with two teflon vacuum

valves and consisting of a square cuvette (1 cm pathlength) and a round bottom flask (pyrex, ~15 mls.). Exactly 4 mL of acetonitrile (Burdick and Jackson, UV grade) was added to the round bottom flask of the quenching cell and the solution was freeze/pump/thawed a minimum of 6 times on a high vacuum line (limiting pressure < 10^{-3} Torr). Quencher solutions were added to the square compartment in aliquots of known concentration; the quencher solvent was distilled off under vacuum to leave behind known quantities of the solid quencher. The quenching cell was re-evacuated while the already evacuated solution was sealed in the round bottom compartment to maintain the oxygen-free conditions of the experiment.

RESULTS and DISCUSSION

As in the case of the cyclic voltammograms measured for Pt_2 in water, those measured in acetonitrile showed irreversible redox couples.

Initial electron transfer quenching experiments were performed using a series of pyridinum quenchers with reduction potentials of -0.67 V to -1.85 V *vs.* SCE (see Table 2.1).[8] (Energy transfer quenching can be ruled out since the pyridiniums' triplet energy is too high to make it a competitive process with electron transfer.) Data were collected using luminescent lifetime techniques (excitation wavelength 355 nm and emission wavlength 515 nm) and the electron transfer rates were calculated by fitting the lifetime and concentration values to the Stern-Volmer equation:

$$\tau_0/\tau = 1 + k_q[Q]\tau_0 \ .$$

(τ_0 is the phosporescent excited state lifetime in the absence of quencher, τ is the phosporescent excited state lifetime at various quencher concetrations [Q], and k_q is the quenching rate constant.) An example of Stern-Volmer quenching is illustrated in Figure 2.2.

The value of k_q for all pyridinium quenchers used was on the order of 10^9 - 10^{10} M^{-1} sec^{-1}, which is the upper limit for diffusion controlled reactions in acetonitrile. Even 2,6,-dimethyl-4-methoxy-N-methyl-pyridinium, with a reduction potential of -1.85 V, had a quenching rate constant of 1.5×10^9 M^{-1} sec^{-1}, which is remarkably high (Table 2.1). The high quenching rate constants and the relatively insignificant drop off with increasing negative reduction potentials which were observed can be explained by electrostatic interactions. In

Table 2.1

Electron Transfer Data Using Pyridiniums

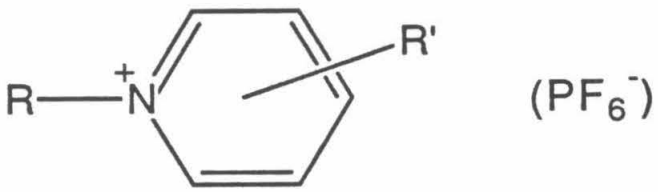

Quencher	R	R'	E (A/A$^-$) V *vs.* SCE	k_q
4-Cyano-N-methylpyridinium	CH_3	4-CN	-0.67	2.0×10^{10}
4-Carbomethoxy-N-methylpyridinium	CH_3	4-CO_2CH_3	-0.78	3.2×10^{10}
4-Amido-N-methylpyridinium	CH_3	3-$CONH_2$	-1.14	1.4×10^{10}
4-Ethylpyridinium	CH_3		-1.36	4.1×10^{10}
2-Methoxy-N-methylpyridinium	CH_3	2-OCH_3	-1.48	6.7×10^{10}
4-Methoxy-N-methylpyridinium	CH_3	4-OCH_3	-1.49	5.9×10^{10}
2,6-Dimethyl-4-methoxy-N-methylpyridinium	CH_3	2,6-$(CH_3)_2$ 4-OCH_3	-1.85	3.2×10^{10}

Figure 2.2 Stern-Volmer plot of the electron transfer quenching of $(TBA)_4[Pt_2(P_2O_5H_2)_4]$ with 2-methoxy-N-methyl-pyridinium ($E_{1/2}$ ~ -1.48 V *vs.* SCE).

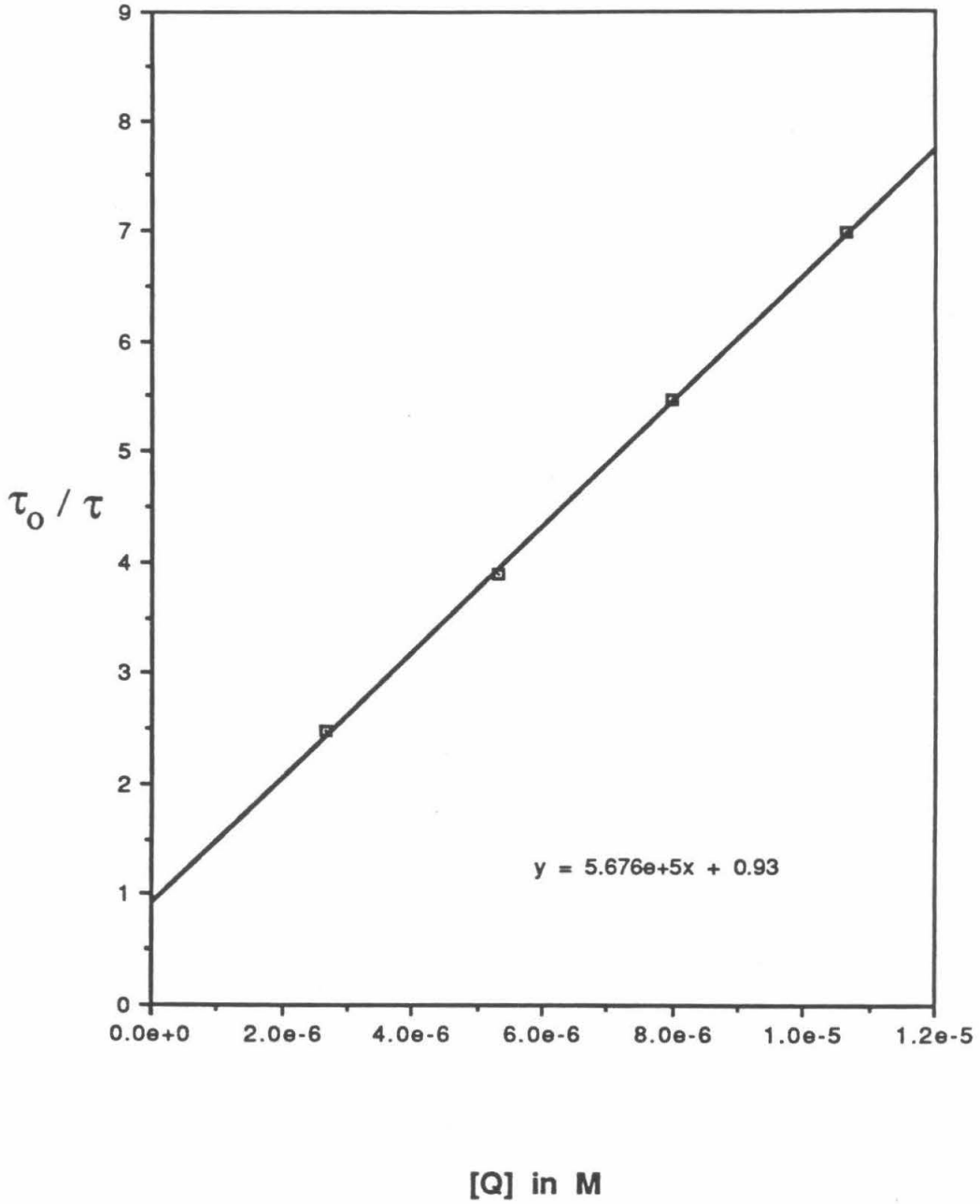
9
8
7
6
5
4
3
2
1
0
τ_o / τ
y = 5.676e+5x + 0.93
0.0e+0
2.0e-6
4.0e-6
6.0e-6
8.0e-6
1.0e-5
1.2e-5
[Q] in M

solution, the positively charged pyridinium quenchers are attracted to the high negative charge (4-) of Pt_2; therefore, they congregate about the dimer, setting up a non-random, non-uniformly distributed, quencher-dimer localized system. When the laser pulse excites the platinum dimer, one electron transfer to a closely associated quencher molecule is easily facilitated, resulting in the observed high quenching rate constants. Along the same lines, attempts to gather quenching rate data using methylviologen, MV^{2+}, as the electron acceptor caused precipitation of an orange solid presumed to be Pt_2 tight-ion paired with the MV^{2+} cation. These results indicated that in order to get a more accurate description of the bimolecular electron transfer rate, neutral or negatively charged electron acceptors are required.

The second series of quenchers used were derivatized benzophenones with reduction potentials ranging from -1.86 V to -2.03 V *vs.* SCE (see Table 2.2). The cyclic voltammograms of the derivatized benzophenones showed quasi-reversible reduction couples. The peak to peak separation in all samples was significantly greater than 59 mV and the peak heights for the forward and back waves were not equivalent; however, reproducible $E_{1/2}$ values at different scan rates were obtained.

Electron transfer rates between Pt_2 and the various derivatized benzophenones were determined using emission intensity quenching techniques since lifetime data obtained from laser excitation of the phosphorescent excited state exhibited biphasic behavior. The observed biphasic behavior of the lifetime data was ascribed to energy transfer from the excited benzophenone quencher to the Pt_2 dimer. The electronic absorption spectrum of the derivatized benzophenones clearly

showed significant absorption at 355 nm. Thus, the derivatized benzophenones were excited by the laser pulse, then underwent energy transfer to the ground state Pt_2 to produce Pt_2^*. The biphasic lifetime decay reflected the fact that Pt_2 excitation to Pt_2^* was no longer occurring only from the laser pulse, but occurred as a result of the energy transfer mechanism as well.

In using the emission intensity quenching technique, Pt_2 was excited by continuous irradiation at 436 nm (a wavelength at which none of the derivatized benzophenones had any absorption). The decrease in phosphorescent intensity was monitored with respect to increasing quencher concentrations (see Figure 2.3). Once again Stern-Volmer kinetics:

$$\Phi_0/\Phi = 1 + k_q[Q]\tau_0$$

were used to determine the quenching rate constants; see Table 2.2. (Φ_0 is the intensity of the emission band at 516.7 nm in the absence of quencher, and Φ is the intensity of the emission band at 516.7 nm at various quencher concentrations.)

The quenching rate constant obtained for benzophenone, whose reduction potential is quite similar to that of 2,6,-dimethyl-4-methoxy-N-methyl-pyridinium, was an order of magnitude less than that obtained for the pyridinium quencher (1.0×10^8 M^{-1} sec^{-1} for benzophenone *vs.* 1.5×10^9 M^{-1} sec^{-1} for the pyridinium quencher). This result supports the notion that the strong electrostatic attraction between the positively charged pyridinium quenchers and Pt_2 led to quenching rate constants which were anomalously high.

The quenching rate constant obtained for the quencher with the most

Table 2.2

Electron Transfer Data Using Benzophenones

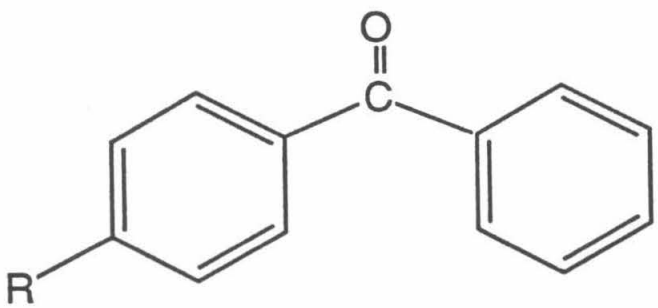

Quencher	R	E (A/A$^-$) V *vs.* SCE	k_q
Benzophenone	H	-1.86	1.0×10^8
4-Methylbenzophenone	CH_3	-1.89	8.5×10^7
4-Fluorobenzophenone	F	-1.89	8.5×10^7
4-Methoxybenzophenone	OCH_3	-1.98	4.8×10^7
4-Dimethylaminobenzophenone	$N(CH_3)_2$	-2.03	4.6×10^7

Figure 2.3 (a) Emission intensity quenching of $(TBA)_4[Pt_2(P_2O_5H_2)_4]$ with 4-dimethylaminobenzophenone (5.3×10^{-4} M aliquot additions of quencher).

(b) Stern-Volmer plot of the electron transfer quenching of $(TBA)_4[Pt_2(P_2O_5H_2)_4]$ with 4-dimethylaminobenzophenone.

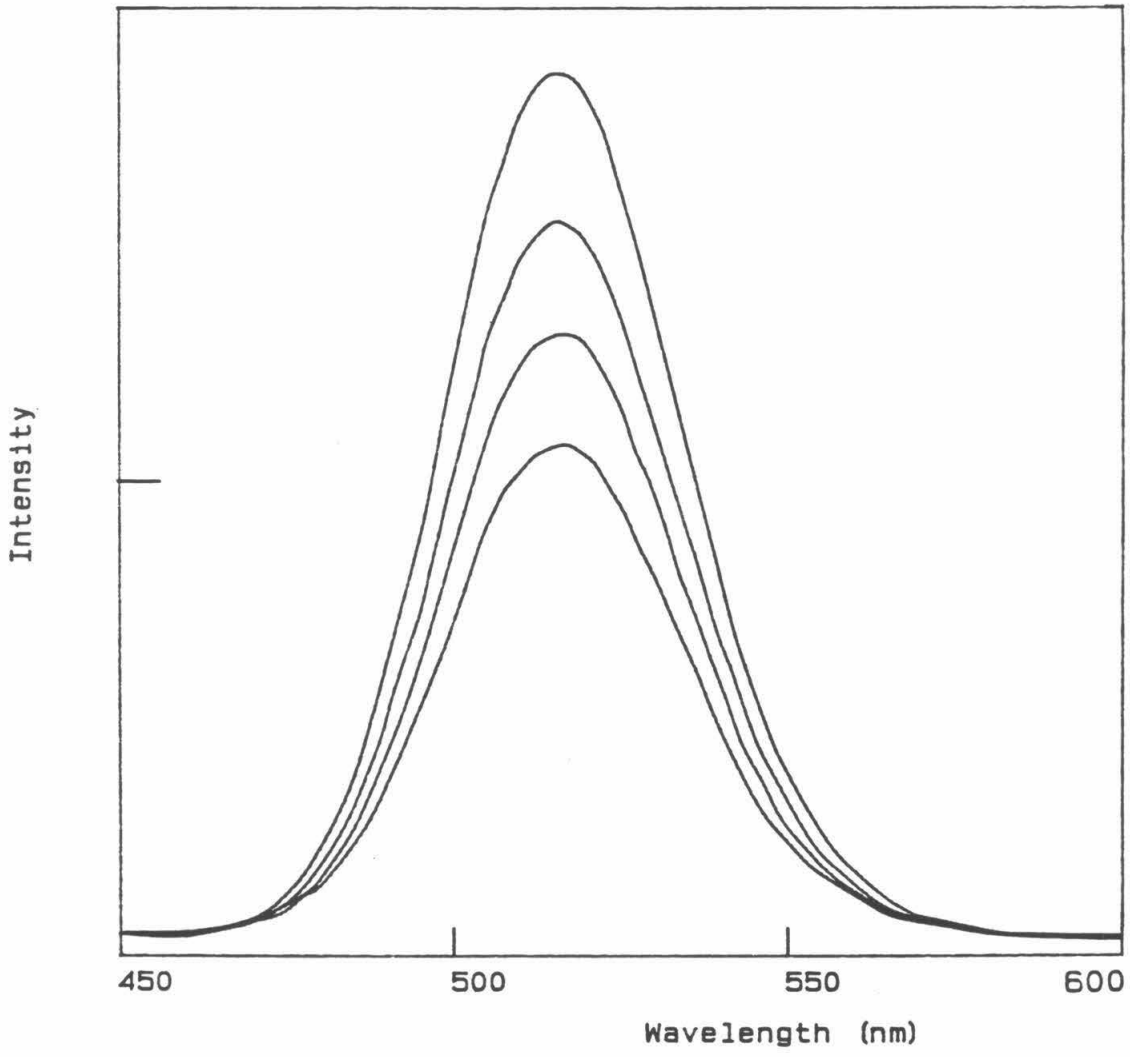
Intensity
450
500
550
600
Wavelength (nm)

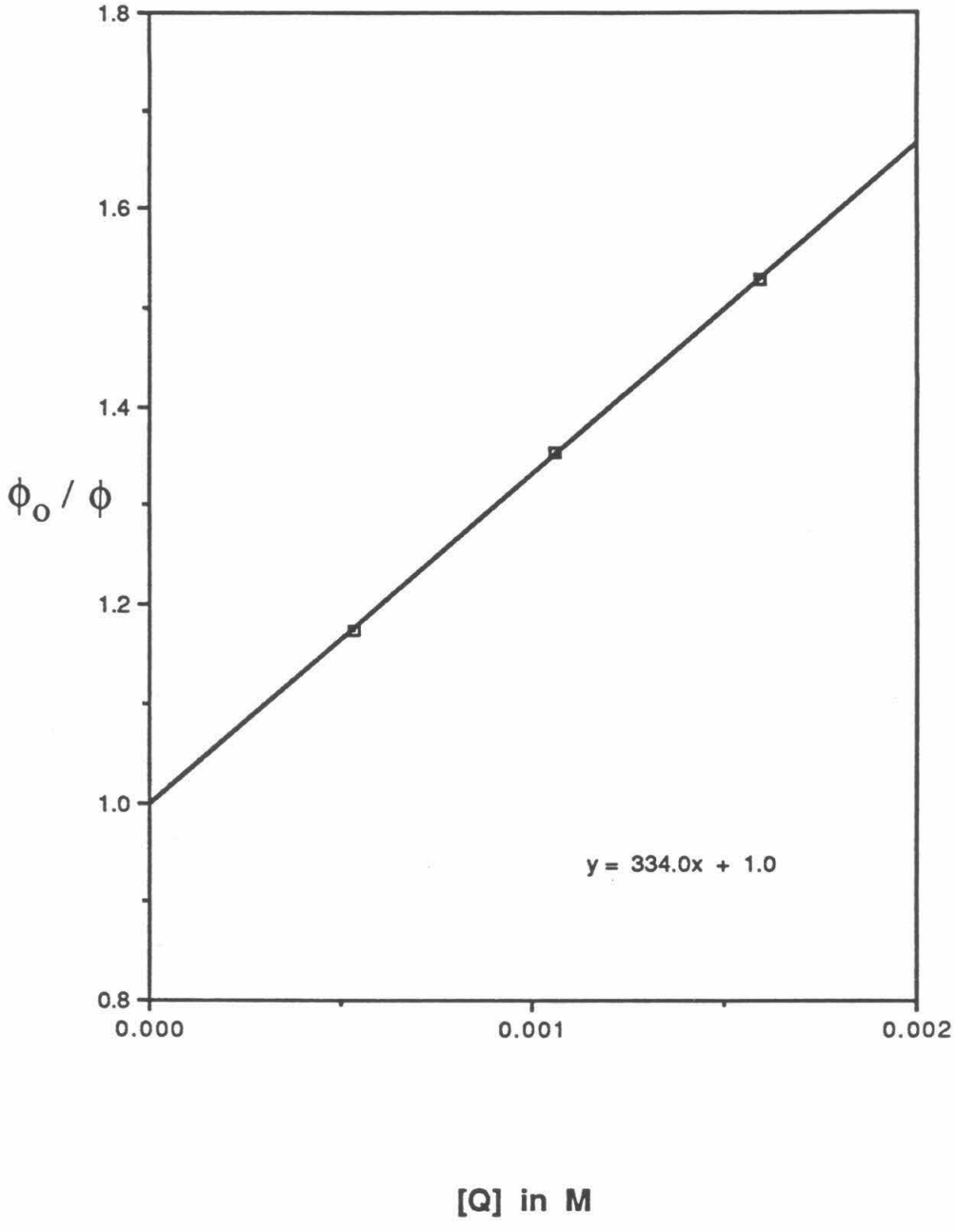
1.8
1.6
1.4
1.2
1.0
0.8
ϕ_o / ϕ
y = 334.0x + 1.0
0.000
0.001
0.002
[Q] in M

negative reduction potential, 4-dimethylaminobenzophenone, was 4.6 × 10^7 M^{-1} sec^{-1}, suggesting the Pt_2^* has an oxidation potential of about -2.0 V.

A plot of $RT\ln k_q$ *vs.* the quencher reduction potential, should yield a slope whose value is 0.5 by Marcus theory for outer-sphere electron transfer;[12,13] however for the benzophenone data the fit to Marcus theory was poor. One reason for the poor fit may be that the electron transfer is not occurring by a purely outer-sphere mechanism, but may be partially facilitated by an inner-sphere process as well. However, since the reduction potential range of the quenchers is less than 0.2 V, and the change in the quenching rate constant is less than one order of magnitude, the data range is insufficiently broad to allow any definite conclusions to be drawn.

REFERENCES

1. Heuer, W. B.; Trotten, M. D.; Rodman, G. S.; Herbert, E. J.; Tracy, H. J.; Nagle, J. K. *J. Am. Chem. Soc.* **1984**, *106*, 1163.
2. Che, C.-M.; Atherton, S. J.; Butler, L. G.; Gray, H. B. *J. Am. Chem. Soc.* **1984**, *106*, 5143.
3. Che, C.-M.; Butler, L. G.; Gray, H. B. *J. Am. Chem. Soc.* **1981**, *103*, 7796.
4. Nocera, D. G.; Maverick, A. W.; Winkler, J. R.; Che, C.-M.; Gray, H. B. "Inorganic Chemistry: Toward the 21st Century" (M. H. Chisholm, ed.) A. C. S. Symposium Series No. 211, Am. Chem. Soc.: Washington, D. C., 1983, pp 21-33.
5. Bryan, S. A.; Dickson, M. K.; Roundhill D. M. *J. Am. Chem. Soc.* **1984**, *106*, 1882.
6. Che, C.-M.; Butler, L. G.; Grunthaner, P. J.; Gray, H. B. *Inorg. Chem.* **1985**, *24*, 4662.
7. Stiegman, A. E.; Rice, S. F.; Gray, H. B.; Miskowski, W. M. *Inorg. Chem.* **1987**, *26*, 1112.
8. Marshall, J. L.; Stobart, S. R.; Gray, H. B. *J. Am. Chem. Soc.* **1984**, *106*, 3027.
9. Parker, C. A.; Rees, W. T. *Analyst* **1960**, *85*, 587.
10. Nocera, D. G.; Winkler, J. R.; Yocom, K. M.; Bordignon, E.; Gray, H. B. *J. Am. Chem. Soc.* **1984**, *106*, 5145.
11. Emission curves were corrected using the OLIS model 3820 Data System Fluorimetry program, SpexR Version 4.02.
12. Marcus, R. A. *J. Chem. Phys.* **1965**, *43*, 679.
13. Marcus, R. A. *J. Chem. Phys.* **1956**, *24*, 966.

CHAPTER 3

Translational Symmetries in the Linear-Chain Semiconductors $K_4[Pt_2(P_2O_5H_2)_4X]\cdot nH_2O$ (X = Cl, Br)

INTRODUCTION

Materials having anisotropic electrical conductivity, whether built from aromatic organic molecules or transition metal complexes, have been the subject of much contemporary research.[1-7] The electronic properties of a linear chain are determined by the extent of interaction between neighboring atoms along the chain and by the translational symmetry of the linear chain. While the importance of the overlap between atomic orbitals of neighboring atoms in the linear chain has been discussed,[8-10] little attention has been directed to the desired characteristics of the translational symmetry[11] required for optimization of a property such as electrical conductivity. Indeed, the mechanisms of electrical transport in these materials are unknown. To date, the variety of translational symmetry types in linear chains has been limited. $K_2Pt(CN)_4Br_{0.3} \cdot 3.2H_2O$ is typical of the near perfect $(A)_n$ symmetry found in most linear chain systems made from mononuclear transition metal complexes.[5,12] Tetrathiofulvalenium tetracyanoquinodimethanide, TTF-TCNQ, with $(A)_n$ along each of the two segregated stacks of TTF cations and TCNQ anions, is representative of 1-dimensional organic conductors.[1,4,13] Salts of tetramethyltetraselenafulvalene, such as $[(TMTSF)_2(ReO_4)]$, also have this symmetry, and are members of the first class of linear chain compounds that has been found to undergo a transition to a superconductive phase.[14-16]

Our group has been concerned with the bonding in d^8-d^8 transition metal dimers, such as $Rh_2b_4^{2+}$ (b = diisocyanopropane).[18-22] The rhodium dimer has interesting photophysical properties resulting from metal-metal interactions. For example, the lowest excited electronic state ($^3A_{2u}$; $(d\sigma)^2(d\sigma^*)^1(p\sigma)^1$) possesses a relatively strong Rh-Rh

bond.[20,21] Interestingly, some of the rhodium isocyanides are 1-dimensional materials.[22] In our studies of d^8-d^8 platinum complexes, we discovered a material that contained a linear chain of $[Pt_2(P_2O_5H_2)_4]^{4-}$ units bridged by a halide ion[23-26] and having a metallic luster. The 300 K X-ray structure of Pt_2Br (Pt_2X = $K_4[Pt_2(P_2O_5H_2)_4X]$; X = Cl, Br, I) has been reported;[27] it revealed an apparent $(AAB)_n$ linear chain system that prompted us to investigate the properties of this unusual system. Some of the possible translational geometries for the three-atom repeat unit of Pt_2X are shown in Figure 3.1. In this chapter, focus is placed on the structures of the 1-dimensional materials, their Raman spectra, and which of these structural schemes are valid for the Pt_2X system.

During the course of this work, the preparation and room temperature X-ray structures of an analogous 1-dimensional system, $Ni_2(CH_3CS_2)_4I$ and $Pt_2(CH_3CS_2)_4I$, were reported.[28] Also, the 300 K structure of $K_4[Pt_2(P_2O_5H_2)_4Cl]\bullet 3H_2O$ has been independently determined and reported, together with Raman and infrared data for $K_4[Pt_2(P_2O_5H_2)_4X]\bullet nH_2O$ (X = Cl, Br, I).[29] Band theory calculations have been done for the general Pt_2X system.[11]

Figure 3.1 Translational symmetries for $K_4[Pt_2(P_2O_5H_2)_4X]$ (X = Cl, Br).

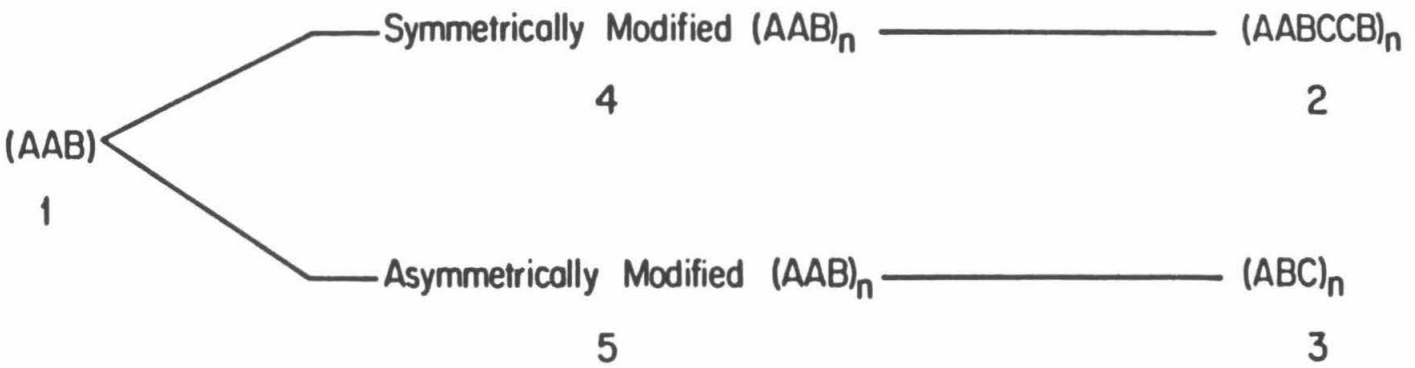

Scheme 1: $(AAB)_n$ $-Pt^{2.5}-Pt^{2.5}-X-Pt^{2.5}-Pt^{2.5}-X-Pt^{2.5}-Pt^{2.5}-X-$

Scheme 2: $(AABCCB)_n$ $-Pt^{2}-Pt^{2}-X-Pt^{3}-Pt^{3}-X-Pt^{2}-Pt^{2}-X-$

Scheme 3: $(ABC)_n$ $-Pt^{2}-Pt^{3}-X-Pt^{2}-Pt^{3}-X-Pt^{2}-Pt^{3}-X-$

Scheme 4: $-Pt^{2.5+\delta}-Pt^{2.5+\delta}-X-Pt^{2.5-\delta}-Pt^{2.5-\delta}-X-Pt^{2.5+\delta}-Pt^{2.5+\delta}-X-$

Scheme 5: $-Pt^{2.5+\delta}-Pt^{2.5-\delta}-X-Pt^{2.5+\delta}-Pt^{2.5-\delta}-X-Pt^{2.5+\delta}-Pt^{2.5-\delta}-X-$

EXPERIMENTAL

Materials

Preparation of $K_4[Pt_2(P_2O_5H_2)_4Cl]\cdot 3H_2O$, Pt_2Cl: The preparations of both Pt_2Cl and Pt_2Br are similar in that Pt_2 and Pt_2X_2 (Pt_2 = $K_4[Pt_2(P_2O_5H_2)_4]$ and Pt_2X_2 = $K_4[Pt_2(P_2O_5H_2)_4X_2]$; X = Cl, Br, I) are the reactants. However, an improved method for preparing the reduced parent metal dimer, $K_4[Pt_2(P_2O_5H_2)_4]\cdot 2H_2O$, was used.[25] $K_4[Pt_2(P_2O_5H_2)_4]$ (0.08 g) and $K_4[Pt_2(P_2O_5H_2)_4Cl_2]$ (0.08 g) were dissolved in a minimum amount of water together with 0.4 g KNO_3. Absolute methanol was added dropwise until a dark precipitate began to form. A few drops of water were added to clarify the solution. The solution was then cooled slowly to 5°C and allowed to stand for 2 days. The bronze crystals were filtered and dried. [Analysis calculated for $K_4[Pt_2(P_2O_5H_2)_4Cl]\cdot 3H_2O$ (%): Pt, 32.19; P, 20.45; Cl, 2.93. Found: Pt, 32.4; P, 20.6; Cl, 2.82.]

Alternatively, 2 mL of chlorine water were added to a solution of 0.4 g $K_4[Pt_2(P_2O_5H_2)_4]$ in 5 mL of H_2O. A saturated solution of KCl in 5 mL H_2O was added next, followed by several drops of methanol to see if the dark precipitate was observed. Crystals were obtained in the same manner as that stated above.

Preparation of $K_4[Pt_2(P_2O_5H_2)_4Br]\cdot 3H_2O$, Pt_2Br: Pt_2Br was prepared from $K_4[Pt_2(P_2O_5H_2)_4]$ by the published procedure.[27]

The appearance of Pt_2X under transmitted light shows some sample dependence resulting in subtle differences in the Raman data.[30]

Physical Measurements

Crystal Structure Determinations. The general features of both

crystal structure determinations were the same. The parameters of Pt_2Cl at 22 K, and Pt_2Cl at 300 K were refined in the tetragonal space group, P4/mbm (#127). A summary of the crystal and intensity collection data for both structures is given in Table 3.1. The crystals were mounted with epoxy on glass fibers. The 300 K diffraction data were taken on a Syntex $P2_1$; low temperature data sets were taken on a locally modified Syntex $P\bar{1}$ diffractometer.[31] Both diffractometers were equipped with graphite-monochromated Mo Kα X-radiation (λ = 0.71073 Å). Cell dimensions, given in Table 3.1, were determined from the setting angles of 15 reflections with $25^\circ<2\Theta<30^\circ$. The temperatures reported for the Syntex $P\bar{1}$ data sets have error limits of ± 1 K.

Data were collected by Θ-2Θ scans at 2°/minute from $(2\Theta(K\alpha_1)-1^\circ$ to $2\Theta(K\alpha_2)+1^\circ)$. The three check reflections collected after every 97 reflections showed a slight decrease in intensity in all crystals (~3%). Variances, $\sigma^2(I)$, were assigned on the basis of counting statistics plus an additional term, $(0.024 \cdot I)^2$, to account for fluctuations proportional to the diffracted intensity. Intensities were corrected for Lorentz and polarization effects and crystal decay. Using the crystal dimensions and the linear absorption coefficient, the data were corrected for absorption by Gaussian integrations over an 8×8×8 grid. All structures were refined using full-matrix least-squares techniques, minimizing $\Sigma w(F_o^2-F_c^2)^2$, where $w = 1/\sigma^2(F_o^2)$. For both structures, final difference maps were somewhat noisy, particularly in the plane containing the potassium ions and the water molecules. Alternative descriptions of the water would be consistent with the data. Residual peaks and holes (up to ±2.9 $eÅ^{-3}$) near the potassium ion positions suggest that some changes could be made in their description, but we

Table 3.1

Crystal and Intensity Data Collection Summary.
(Space group is P4/mbm (#127), with z=2.)

	Pt_2Cl at 300 K	Pt_2Cl at 22 K
Molecular Formula	$K_4[Pt_2(P_2O_5H_2)_4Cl]\cdot 3H_2O$	$K_4[Pt_2(P_2O_5H_2)_4Cl]\cdot 3H_2O$
a, Å	13.283(3)	13.170(4)
c, Å	8.125(3)	8.077(3)
crystal dimensions, mm	0.10×0.14×0.26	0.22×0.15×0.08
Absorption Coefficient μ(Mo Kα) cm^{-1}	114.8	116.9
Transmission Coefficient (min, max)	0.221, 0.343	0.193, 0.407
2Θ Limits, deg	3.0-75.0	5.0-80.0
Number of Reflections Collected	4112	3335
Unique Reflections	2095	1428
Number of Reflections with I>0	1820	1333
Refined Parameters	63	61
R[a]	0.056	0.036
GOF[b]	2.2	2.0

[a] $R = (\Sigma|F_o - |F_c||)/\Sigma F_o$, based upon data with I>0
[b] $GOF = [\Sigma w(F_o^2 - F_c^2)^2/(n-p)]^{1/2}$

did not develop a good alternative model. The maps suggest that the halide and potassium occupancies may be non-stoichiometric, but we have not been able to pursue this. Calculations were done with programs of the CRYM X-ray computing system plus ORTEP;[32] scattering factors were taken from the standard compilations.[33] Hydrogen atoms were ignored in the calculations.

Pt_2Cl at 22 K. A different Pt_2Cl crystal was used for the low temperature study than that which was used for the room temperature structure. This second crystal was cooled to 22 K in incremental steps at which time the unit cell dimensions were determined using the same 15 reflections as used to determine the cell dimensions at room temperature. No extra reflections were found at low temperature, thus confirming the choice of cell dimensions.

During data collection, the temperature was maintained at 22± 1 K. A full orthorhombic data set was taken and used for refinement in both orthorhombic and tetragonal unit cells; 3335 reflections were scanned in the range $5^\circ<2\Theta<80^\circ$. Systematic absences in the diffractometer data of h0l, where h = 2n+1, and 0kl, where k = 2n+1, were consistent with space group P4/mbm (#127). The data were merged to give 1428 independent reflections, all of which were used in the structure solution and refinement. Although lattice cell constants and the goodness of fit did not indicate that an orthorhombic distortion had occurred, checks were made for both a doubled unit cell and for an orthorhombic distortion. Scans were taken in reciprocal space along [100], [010], [001], and [110] axes with the output of the counter circuit connected to a chart recorder. No extra reflections were observed along any axis that would indicate a radical change in cell dimension.[34-36]

Initially, refinement proceeded with ordered platinum atoms but two-site disordered bridging chloride ions. Because this yielded highly anisotropic platinum thermal parameters (U_{11} = U_{22} = 0.0029(1), U_{33} = 0.0082(1)), an alternative model was refined, with the platinum atom also disordered between two sites. Allowing the two half-populated platinum atoms to move along the stacking axis gave a Pt-Pt site separation of 0.142(2) Å,[29] or Pt-Pt bond distances of 2.685(2) Å, 2.827(2) Å, or 2.969(2) Å, depending, as will be discussed later, on the overall translational symmetry. The final R value and goodness of fit were essentially the same as in the ordered model. An ORTEP of the Pt_2Cl unit is presented in Figure 3.2a, and a partial drawing of the structure illustrating the 1-dimensional stacking unit is shown in Figure 3.2b; atomic coordinates are given in Table 3.2.

Pt_2Cl at Room Temperature. An earlier collected and refined data set was re-evaluated based upon the findings of Pt_2Cl at 22 K. The bridging halide was represented by a two site model with isotropic thermal parameters. One fully populated water site, W(1), was found, with additional sites of lower partial population in the region near K(1). The structure was refined with both a single platinum atom site and with a two-site model; both gave the same values for the R-index and the goodness of fit. Because spectral data indicate that both Pt_2 and Pt_2Cl_2 are present in the crystal, the parameters for the model with two platinum sites are reported herein. A partial drawing of the structure illustrating the 1-dimensional stacking unit is shown in Figure 3.2b; atomic coordinates are listed in Table 3.3.

Raman Spectroscopy. The Raman data were collected by Dr. Steven D.

Figure 3.2 (a) ORTEP drawing of a $[Pt_2(P_2O_5H_2)_4Cl]^{4-}$ molecule.

(b) ORTEP drawings of all $[Pt_2(P_2O_5H_2)_4X]^{4-}$ structures. Ellipsoids are drawn at the 50% probability level.

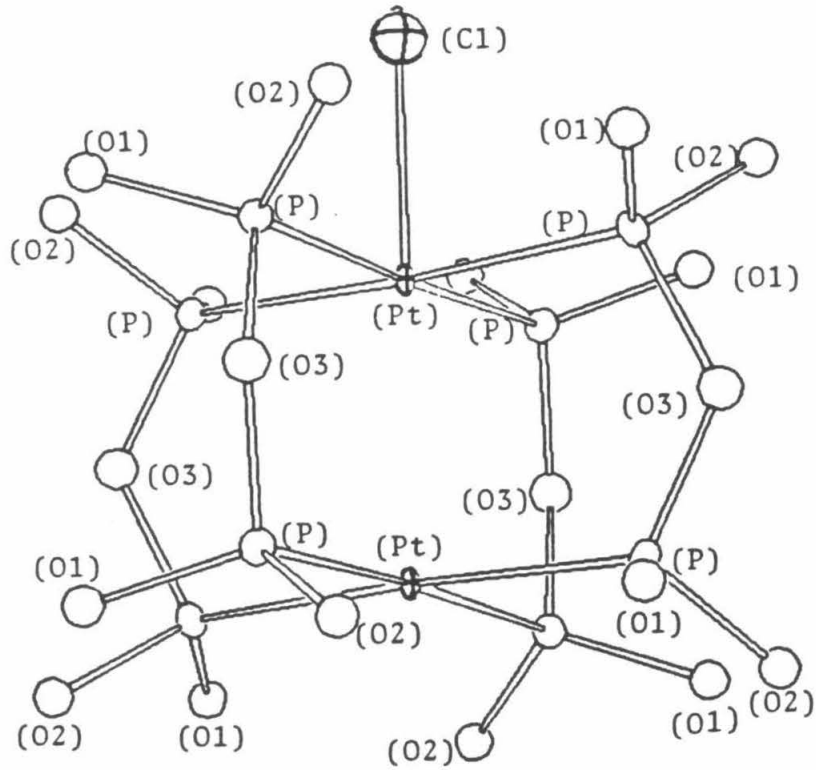
(Cl)
(O2)
(O1)
(O1)
(O2)
(P)
(P)
(O2)
(O1)
(P)
(Pt)
(P)
(O3)
(O3)
(O3)
(O3)
(P)
(Pt)
(P)
(O1)
(O1)
(O2)
(O2)
(O1)
(O2)
(O1)
(O2)

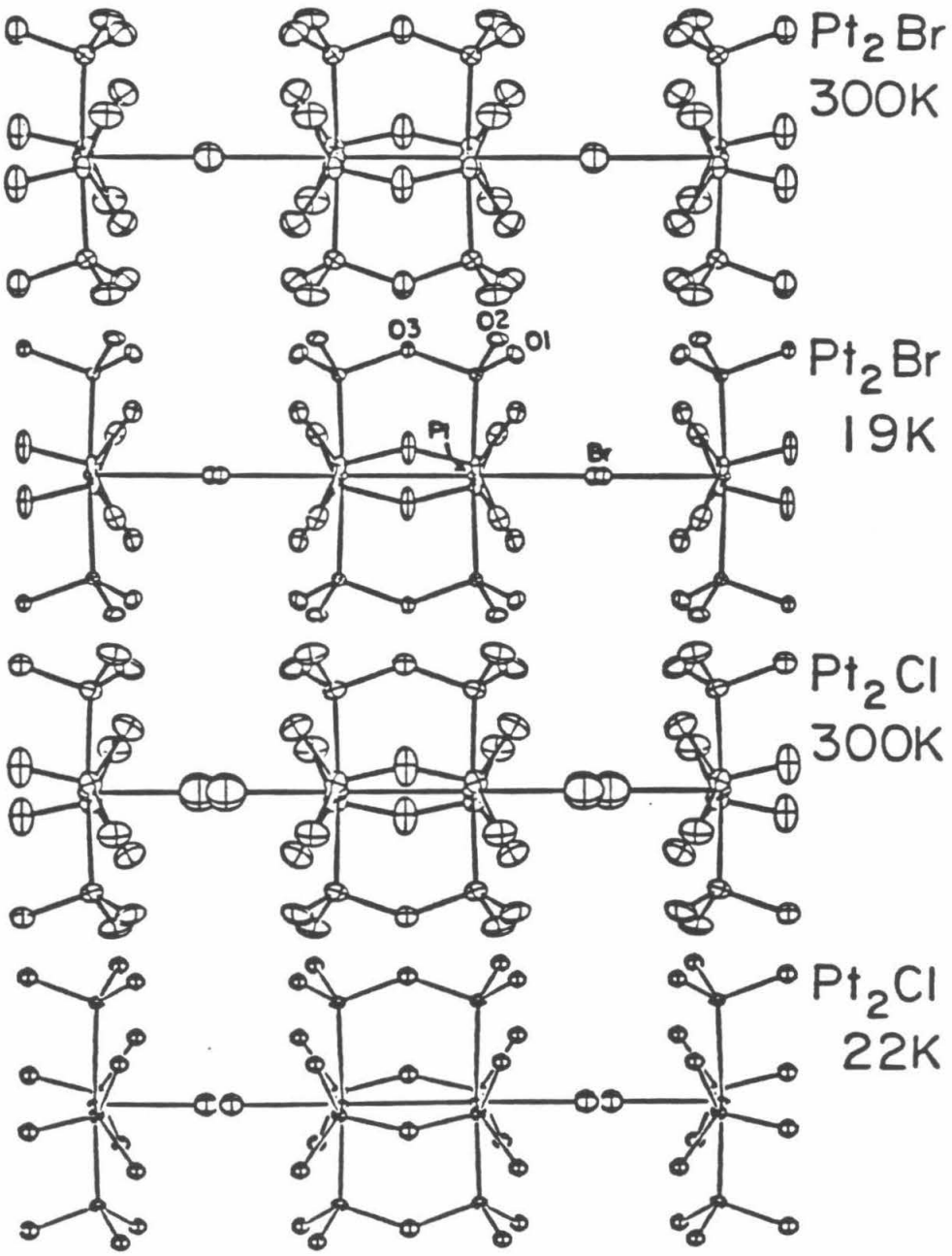
Pt2Br
300K
O3
O2
O1
Pt
Br
Pt2Br
19K
Pt2Cl
300K
Pt2Cl
22K

Table 3.2

Parameters for Pt_2Cl at 22 K.
x, y, z and $U_{eq} \times 10^4$

Atom	x	y	z	U_{eq}[a]	POP†
PtA	0	0	3338(2)	0.22(3)*	2.0
PtB	0	0	3162(1)	0.22(3)*	2.0
Cl	0	0	316(9)	287(10)	2.0
K1	2772(2)	7772	0	150(3)	4.0
K2	3892(2)	8892	5000	134(3)	4.0
P	1173(1)	1325(1)	3174(1)	90(2)	16.0
O1	2161(2)	1073(2)	2140(4)	122(6)	16.0
O2	807(2)	2353(2)	2572(4)	129(7)	16.0
O3	1659(4)	1510(3)	5000	156(10)	8.0
W1	1030(10)	6030	5000	1.5(2)*	3.0
W2	0	5000	2272(60)	1.3(6)*	0.6
W3	0	5000	909(60)	0.8(7)*	0.5
W4	649(40)	5649	0	1.4(6)*	0.7
W5	612(30)	5612	2835(41)	1.1(5)*	1.2

[a] $U_{eq} = 1/3(U_{11} + U_{22} + U_{33})$
* B (iso)

† Atoms per unit cell

Table 3.3

Parameters for Pt_2Cl at 300 K.
x, y, z and $U_{eq} \times 10^4$

Atom	x	y	z	U_{eq} [a]	POP†
PtA	0	0	3321(2)	1.0(.3)*	2.0
PtB	0	0	3180(2)	1.1(.3)*	2.0
Cl	0	0	373(8)	668(18)	2.0
K1	2742(3)	7742	0	402(5)	4.0
K2	3874(3)	8874	5000	389(4)	4.0
P	1174(1)	1304(1)	3181(2)	212(2)	16.0
O1	2158(3)	1035(3)	2189(6)	340(8)	16.0
O2	833(3)	2325(3)	2570(6)	363(9)	16.0
O3	1640(5)	1492(5)	5000	437(14)	8.0
W1	1014(14)	6014	5342(21)	3.1(3)*	3.2
W2	410(54)	5410	2186(76)	7.9(14)*	1.6
W3	0	5000	586(**)	5.2(24)*	0.4
W4	632(**)	5632	0	4.1(20)*	0.4
W5	4373(**)	9373	1134(**)	3.0(26)*	0.4

[a] $U_{eq} = 1/3(U_{11} + U_{22} + U_{33})$ * B (iso)
** esd ≥ 100 † Atoms per unit cell

Conradson at the Los Alamos National Laboratory, Los Alamos, New Mexico. Raman spectra of single crystals of Pt_2Cl and Pt_2Br were obtained using 676.4 nm excitation at several temperatures in the range 25-300 K. The crystals were mounted in a cell containing *ca.* 150 psi (room temperature) of He in order to minimize local heating. The cell was coupled to the cold end of an Air Products Displex closed-cycle cryostat and the temperature monitored and controlled using thermocouples. The spectra were obtained using a SPEX 1401 double monochromator with excitation from a Spectra Physics 171 Kr^+ laser.

RESULTS

Given the 300 and 19 K structure of Pt_2Br reported earlier,[37] these efforts were directed towards establishing the structural variations that occur in Pt_2Cl and Pt_2Br and how they may be related to the conduction properties observed in these systems.

Structural Data on Pt_2Cl: Pt_2Cl retains a tetragonal unit cell on cooling to 22 K. The Pt_2Cl unit cell dimensions contracted with temperature in a fashion similar to that observed in Pt_2Br.[37] It is interesting to note that the unit cell did not double in size along any unit cell axis, although this has been seen in other 1-dimensional systems. Also, no evidence for an orthorhombic distortion was found nor was any tilting of the Pt-Cl-Pt unit with respect to the stacking axis observed.

Tables 3.2 and 3.3 list the final parameters of the models used to describe the two structures. Tables 3.4 and 3.5 compare selected bond distances and angles of Pt_2, Pt_2Br (300 and 19 K) and Pt_2Cl (300 and 22 K). The Pt_2Cl structures were refined with a two-site model for the bridging chloride and both one- and two-site models for the platinum atoms. At both room temperature and at 22 K the chloride ion sites were well-separated and refined smoothly. At room temperature the Pt could be refined in a single site; changing to a two-site model gave nearly identical results. The resulting $(AABCCB)_n$ translational symmetry is in better accord with spectral data, which will be discussed below, and thus we have accepted it. Upon cooling Pt_2Cl to 22 K, the chloride and platinum positions remain disordered, and the two-site model is retained. This model is not statistically better than a

Table 3.4

Selected Bond Distances

	Pt_2[a]	Pt_2Br[b]	Pt_2Br[c]	Pt_2Cl[c]	Pt_2Cl[c]
T(K)	300	300	19	300	22
Pt-Pt	2.925(1)	2.793(1)	2.781(1)	2.729(2)	2.685(2)
				2.958(2)	2.969(2)
Pt-X (short)	----	2.699(1)	2.579(4)	2.281(7)	2.441(7)
				2.395(7)	2.299(7)
Pt-X (long)	----	----	2.778(4)	2.886(7)	2.951(7)
				3.001(7)	2.809(7)
ΔX	----	0	0.199(5)	0.606(9)	0.510(10)
Pt-P	2.320(5)	2.334(1)	2.331(1)	2.334(2)	2.335(2)
				2.331(2)	2.331(2)
P-O(H)	1.579(9)	1.562(4)	1.572(4)	1.577(4)	1.581(3)
P=O	1.519(9)	1.505(4)	1.509(4)	1.514(4)	1.518(3)
P-O (bridging)	1.623(6)	1.618(3)	1.621(6)	1.622(6)	1.626(5)
P•••P	2.980(6)	2.935(2)	2.924(2)	2.956(2)	2.949(1)
O(H)•••O	2.505(19)	2.487(5)	2.482(5)	2.476(6)	2.479(4)
K(1)•••O(H)	2.848(14)	2.915(5)	2.861(8)	2.884(10)	2.828(7)
K(1)•••O	2.847(13)	2.912(6)	2.887(8)	2.873(10)	2.850(7)

[a]References 23 and 40. [b]Reference 27. [c]This work.

Table 3.5

Seclected Bond Angles

	Pt_2[a]	Pt_2Br[b]	Pt_2Br[c]	Pt_2Cl[c]	Pt_2Cl[c]
T(K)	300	300	19	300	22
Pt-Pt-P	90.67(10)	91.74(2)	91.75(3)	92.78(6)	93.25(5)
				89.97(6)	89.76(5)
Pt-P-O(H)	114.0(5)	113.4(1)	113.1(1)	114.3(2)	114.7(1)
				112.7(2)	112.7(1)
Pt-P=O	118.0(5)	117.3(2)	117.5(2)	118.7(2)	118.4(1)
				117.7(2)	117.1(1)
Pt-P-O (bridge)	110.3(4)	110.4(2)	110.4(2)	109.0(2)	108.7(2)
				111.7(2)	112.1(2)
P-O-P	133.3(9)	130.2(3)	128.9(4)	131.4(4)	130.2(3)

[a]References 23 and 40. [b]Reference 27. [c]This work.

single-site platinum model (the R factor and goodness of fit are each improved by only 0.01) but, as in the room-temperature case, it has been adopted because of spectroscopic results. Listings of observed and calculated structure factors and anisotropic thermal parameters are tabulated in Appendix I.

Raman Spectroscopy: The Raman spectra of Pt_2Cl and Pt_2Br at *ca.* 25 K are shown in Figure 3.3; these spectra are similar to those reported by Kurmoo and Clark[29b]. The wavenumbers of the bands observed for Pt_2Cl are significantly different from those reported earlier,[29b] owing to the fact that different excitation wavelengths were used to obtain the Raman spectra. For Pt_2Cl, we employed 514.5 nm excitation, which is close to the IVCT absorption maximum, while Kurmoo and Clark employed 647.1 nm excitation. We note that the Raman spectrum of Pt_2Br also exhibits unusual relative intensity changes with excitation wavelength. The origin of these differences has been investigated by Swanson and coworkers.[30] Kurmoo and Clark concluded that, on the basis of X-ray work at room temperature, both Pt_2Cl and Pt_2Br consist of polar dimers (Scheme 3 with $(ABC)_n$ translational symmetry) and assigned the band observed at ~152 cm^{-1} in the Pt_2Cl spectrum to the Pt-Pt stretch. The Pt(III)-Pt(III) stretch in the fully oxidized form, Pt_2Cl_2, is observed at 158 cm^{-1} and the Pt(II)-Pt(II) stretch in the reduced form, Pt_2, is at 115 cm^{-1}. If a polar dimer represents the true structure for Pt_2Cl, we would expect a Pt-Pt stretching mode intermediate in wavenumber to those found for Pt_2 and Pt_2Cl_2. Accordingly, we believe that the ~152 cm^{-1} band (155 cm^{-1} in our spectrum) of Pt_2Cl should be assigned to the Pt(III)-Pt(III) stretch of the oxidized

unit in a chain with $(AABCCB)_n$ translational symmetry. The band at 119 cm^{-1} in Pt_2Cl is attributed to the Pt(II)-Pt(II) stretch of the reduced unit in the chain. The fact that the two bands assigned to Pt-Pt stretching in Pt_2Cl are quite close to those observed for the fully oxidized and fully reduced forms suggests strong valence localization for Pt_2Cl. The band at ~301 cm^{-1} in Pt_2Cl is attributed to the symmetric Pt(III)-Cl stretch.

The Raman spectrum of Pt_2Br shows bands at ~117 and ~122 cm^{-1}. While the band at 117 cm^{-1} is quite close to the Pt(II)-Pt(II) stretching frequency of Pt_2, the 122 cm^{-1} feature is significantly lower than the 132 cm^{-1} Pt(III)-Pt(III) stretching frequency of Pt_2Br_2.[29] Furthermore, the Pt-Br stretch of Pt_2Br is 211 cm^{-1}, by contrast to 223 cm^{-1} for Pt_2Br_2. The energies for the Pt-Br and "Pt(III)-Pt(III)" stretching modes are inconsistent with complete valence localization and $(AABCCB)_n$ translational symmetry. The two Pt-Pt stretches could result from coupling of two Pt-Pt bonds of equal or nearly equal strengths, as would be expected for Schemes 3, 4, and 5 (Figure 3.1). However, the appearance of only one band attributable to a Pt-Br stretching mode suggests that Scheme 4, the symmetrically modified $(AAB)_n$ structure, provides the best description. The bands at ~132 and ~223 cm^{-1} are sample dependent in their intensities and wavenumbers (note that Clark and Kurmoo reported a band at 137 cm^{-1}). We attribute these two bands to Pt-Pt and Pt-Br stretches, respectively, of a local state. The presence of local states in these systems has been investigated by Swanson and coworkers.[30] The observed Raman bands and their assignments are given in Tables 3.6 and 3.7.

The relative intensities of the bands attributed to the Pt-Pt and

Figure 3.3 Raman spectra of $[Pt_2(P_2O_5H_2)_4X]^{4-}$ (X = Cl, Br) at resonance with the intervalence band.

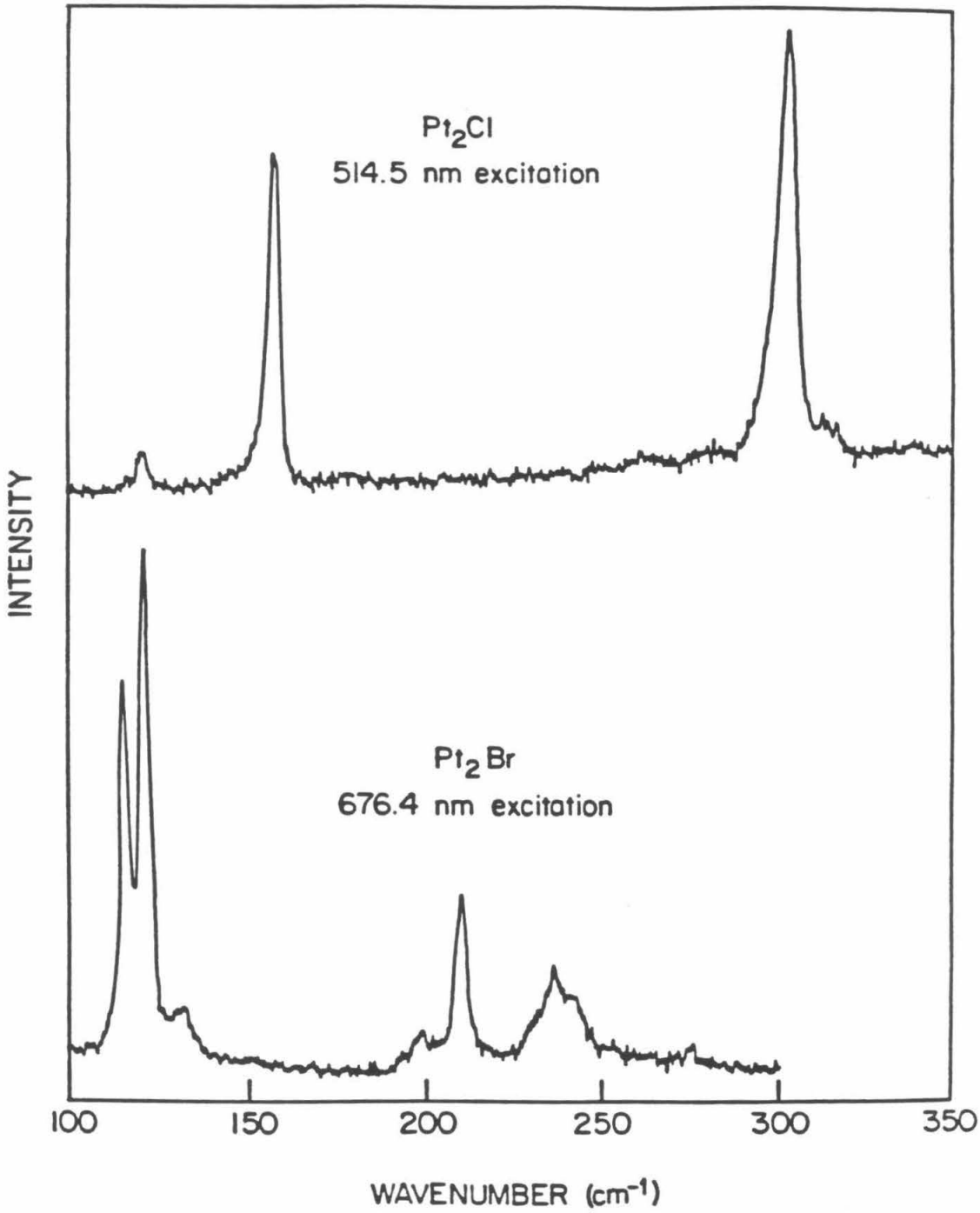
Pt2Cl
514.5 nm excitation
Pt2Br
676.4 nm excitation
INTENSITY
100
150
200
250
300
350
WAVENUMBER (cm-1)

Table 3.6

Raman Bands for Pt_2Cl

Assignment	This work[a] (cm^{-1})	Clark and Kurmoo[b] (cm^{-1})
ν_1 (Pt^{II}-Pt^{II})	119 (mw)	125.8 (mw)
ν_2 (Pt^{III}-Pt^{III})	155 (vs)	152.3 (vs)
ν_3'	260 (mw)	263 (mw)
ν_3 (Pt^{III}-Cl)	301 (vs)	291.3 (vs)
$\nu_1 + \nu_3$	419 (mw)	418 (w)
$\nu_2 + \nu_3$	453 (m)	443 (ms)
$\nu_3' + \nu_3$	557 (mw)	552 (w)
$2\nu_3$	598 (m)	583 (ms)

Abbreviations: m=medium, v=very, w=weak, s=sharp.

[a] λ_0=514.5 nm, 25 K, single crystal.

[b] Reference 29, λ_0=647.1 nm, 80 K, $K[ClO_4]$ disk matrix.

Table 3.7

Raman Bands for Pt_2Br

Assignment	This work[a] (cm^{-1})	Clark and Kurmoo[b] (cm^{-1})
δ (Pt-Pt-Br)	93 (w)	93 (w)
ν_1 (Pt-Pt)	116.5 (vs)	117 (vs)
ν_2 (Pt-Pt)	122 (vs)	122 (vs)
ν_2' (Pt-Pt)[c]	132 (mw)	137 (mw)
?	193 (mw)	195 (mw)
ν_3 (Pt-Br)	211 (m)	210 (m)
ν_3' (Pt-Br)[c]	223 (w)	223 (w)
$2\nu_1$	231 (sh)	
$\nu_1 + \nu_2$	236 (m)	
$2\nu_2$	241 (m)	239 (m)
$\nu_2 + \nu_3$	332 (mw)	330 (mw)
$3\nu_2$	360 (mw)	355 (mw)
$2\nu_2 + \nu_3$	454 (w)	450 (w, br)
$4\nu_2$	474 (w,br)	475 (w, br)

Abbreviations: m=medium, v=very, w=weak, s=sharp, sh=shoulder, br=broad.

[a] λ_0=676.4 nm, 25 K, single crystal.

[b] Reference 29, λ_0=647.1 nm, 80 K, $K[ClO_4]$ disk matrix.

[c] Raman bands attributed to local states; see text.

Pt-X stretching modes also provide information concerning the structures of these materials. The ν(Pt-Cl) is intense relative to the ν(Pt-Pt) bands of the Pt_2Cl complex, while ν(Pt-Br) is weak relative to the ν(Pt-Pt) bands of Pt_2Br. These observations are consistent with a significant shift of the Cl atom from the central position between the dimer units but with the Br atom being quite close to this special position.

The Raman spectra of Pt_2Cl and Pt_2Br do not change significantly in going from 25 K to room temperature, indicating that there is no structural phase transformation over this temperature range. The energies and widths of the Raman bands do vary slightly with temperature, as is expected.

DISCUSSION

A tetragonal unit cell has been found for the parent dimer, Pt_2, and the 1-dimensional materials, Pt_2Cl and Pt_2Br. The *c* axis length is very similar for Pt_2Cl and Pt_2Br systems, and only slightly reduced for Pt_2. Although the *c* axis lengths are similar, there is a significant difference in the halide separations between the chloride (0.606(9) Å) and the bromide (0.199(5) Å)[37]. This difference is larger than expected from the difference in radius between Cl and Br (0.15 Å), although similar to that found for Wolframs's red salts.[38] We conclude that the $Pt_2(P_2O_5H_2)_4$ cores and the K^+ ions form a stable arrangement. We note the disorder found in the water positions and the fact that no disorder was evident in the K^+ ion positions. Replacement of K^+ by Na^+ causes a major structural change in Pt_2 (from tetragonal to an orthorhombic unit cell);[25] thus, we conclude that the alkali metal ion

metal ion has an important structural influence.

This regular array of potassium ions and Pt-Pt units fixes the coordination environment for bridging chloride or bromide (with potassium as the counter ion) as a tetragonal cavity approximately 5.34 Å long. This distance corresponds to the Pt-Pt distance between neighboring dimers along the stacking axis. From the structures of fully oxidized Pt_2X_2 complexes, one finds the following Pt-X bond distances: Pt-Cl = 2.407(2), Pt-Br = 2.572(1), and Pt-I = 2.742(1) Å.[27,29,39] Thus a chloride ion is not constrained along the *c* axis, a bromide ion just fits, and an iodide ion is too large for the cavity (which may explain why the iodide complex does not crystallize in the same space group).

The translational symmetries ($(AAB)_n$, $(ABC)_n$ and $(AABCCB)_n$) shown in Schemes 1-5 (Figure 3.1) illustrate different structural arrangements for Pt_2X, and imply different patterns of platinum oxidation states; however, attempts by Butler *et al.*[37] to assign the oxidation states of the platinum atoms by ESCA did not yield much useful information. In fact, the ESCA measurements provided no conclusive evidence to suggest multiple platinum oxidation states or differing chemical environments for the platinum, bridging bromide or iodide, or ligated phosphorus atoms.

From earlier work on Pt_2Br at 19 K,[37] the Pt_2Br structure was fitted by a single site model for the platinum atoms and a two-site model for the bridging bromide ion. Of the translational symmetries schematically described in Figure 3.1, the only ones that permit relatively well-defined platinum atom positions and two-site disorder of

the bridging halide are Schemes 3, 4, and 5 with $(ABC)_n$, symmetrically modified $(AAB)_n$, and asymmetrically modified $(AAB)_n$ translational symmetries, respectively. The separation between the linear chains of atoms in these structures is large, 9.3 Å, and thus the interchain structural correlation is expected to be weak. A randomly ordered set of chains of Schemes 3, 4, and 5 will have equal numbers of chains pointing to the left and to the right; an average yields the X-ray diffraction results observed for Pt_2Br at 19 K.

The polar dimer of $(ABC)_n$ translational symmetry and the asymmetrically modified $(AAB)_n$ translational symmetry should yield spectra in which there are two bands attributable to Pt-Br stretches. Since only one such Raman band is observed for Pt_2Br, schemes 3 and 5 can be ruled out. Thus Scheme 4, the "intermediate" between the extremes of $(AAB)_n$ and $(AABCCB)_n$, best describes the Pt_2Br structure. Scheme 4, with the symmetrically modified $(AAB)_n$ translational symmetry, requires both a short and a long Pt-Br bond; at 19 K, bond distances of 2.579(4) and 2.778(4)Å were found. At least in the limit of a short chain, we would not expect a large energy barrier for halide "atom transfer",[40] as shown below:

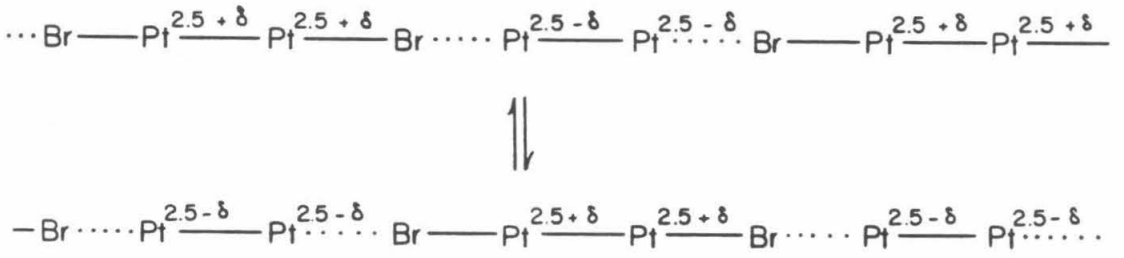

Halide motion should be thermally activated and, at 300 K, would be rapid. The 300 K X-ray structural results are consistent with either

fast halide motion in an upper vibrational state, or a centrally positioned bromide. We recall, however, that the room temperature Raman spectrum shows evidence for a band attributable to a Pt-Br stretch, demonstrating that the bromide ion remains slightly shifted, even at room temperature, from the special position equidistant from neighboring Pt atoms. Scheme 4 also allows for a very slight variation in Pt-Pt bond length, such that it may or may not (depending upon the sensitivity of the technique and the value of δ) be possible to resolve two distinct Pt-Pt bonds. Raman data do, in fact, give evidence for two bands attributable to Pt-Pt stretches, these being very close in wavenumber (*ca.* 116.5 and 122 cm^{-1}), whereas the X-ray data do not require two distinct Pt-Pt bond lengths. (Comparison of the isotropic thermal ellipsoids for the Pt atoms in Pt_2Br at 19 K[37] and in Pt_2Cl at 22 K shows that the Pt atom thermal motion in Pt_2Br (0.074 Å) is larger than that in Pt_2Cl (0.053 Å).) Thus there may, in fact, be two distinct Pt-Pt bonds in the Pt_2Br structure. The Pt-Pt distance of 2.781(1)Å at 19 K, which reflects a formal Pt-Pt bond order of 0.5, is intermediate between that observed for the reduced dimer, Pt_2, $d_{(Pt-Pt)}$ = 2.925(1) Å[23,41] and the fully oxidized Pt_2Br_2, $d_{(Pt-Pt)}$ = 2.716(1) Å.[29c,39]

The translational symmetry of the Pt_2Cl structure is different from that of Pt_2Br. The Pt_2Cl structural data were refined using a two-site model for the halide and both a one-site and two-site model for the platinum centers giving nearly identical results. The Pt_2Cl Raman spectrum resembles a superposition of the Raman spectra of Pt_2 and Pt_2Cl_2. Quite simply, Pt_2Cl appears, at both room temperature and 22

K, to be a combination of equal amounts of Pt_2 and Pt_2Cl_2 alternating along the chain. Therefore, the translational symmetry of Pt_2Cl is assigned as $(AABCCB)_n$ (Scheme 2, Figure 3.1).

Whangbo and Canadell have performed band calculations using extended Hückel methods and halide p- and metal d-orbitals on a model for the Pt_2X systems, $Pt_2(HCS_2)_4I$.[11] They have discussed the results both in terms of a possible Peierls instability of a metallic system, and in terms of localized electronic states of a non-metallic system. In neither limit did the $(ABC)_n$ translational symmetry represent an energy minimum; instead $(AABCCB)_n$ was predicted to be more stable than $(AAB)_n$ by 4 kJ mol^{-1}. The results show that the subtle balance of forces (i.e., electron-phonon coupling, etc.) in the Pt_2X systems gives rise to different ground state structures for Pt_2Cl and Pt_2Br.

Pt_2Br is a moderate semiconductor, with conductivity 10^6 times greater than that of Reihlen's green, $[Pt^{II}(etn)_4][Pt^{IV}(etn)_4Br_2]\bullet 4H_2O$ (etn = ethylamine)[38], but 10^6 times weaker than that of $K_2[Pt(CN)_4]Br_{0.3}\bullet 3.2H_2O$. We note that an analogous system that uses iodide ion as the bridging unit between metal dimers, $Pt_2(CH_3CS_2)_4I$, forms a structure at 300 K with translational symmetry that is virtually $(AAB)_n$.[28,29] The conductivity of this material is comparable to that of Pt_2Br.

In conclusion, the translational symmetry, $(AAB)_n$, which we anticipated for Pt_2Br, was not found in any structure, although the observed structure is only slightly different from this translational symmetry. Consideration of the cavity size between Pt_2 units indicates

that bromide is more appropriate than chloride for creating a highly symmetric 1-dimensional material with $(AAB)_n$ symmetry. Chloride, which is not as well suited for the K^+/Pt_2 framework as bromide, leads to the $(AABCCB)_n$ structure. The Pt_2Cl and Pt_2Br complexes provide an interesting example of how competing interactions in a quasi 1-dimensional system lead to different ground state structures. An understanding of the relationship between the structures of these materials, the nature of the local states, and the macroscopic properties such as conductivity is essential in developing materials with useful properties.

REFERENCES

1. Williams, J. M.; Beno, M. A.; Wang, H. H.; Leung, P. C. W.; Emge, T. J.; Geiser, U.; Carlson, K. D. *Acc. Chem. Res.* **1985**, *18*, 261.
2. Miller, J. S., Ed. "Extended Linear Chain Compounds"; Plenum: New York, 1982; Vol. 1-3.
3. Monceau, P., Ed. "Electronic Properties of Inorganic Quasi-One-Dimensional Compounds"; D. Reidel: Boston, 1985: Vol. 1,2.
4. Ibers, J. A.; Pace, L. J.; Martinsen, J.; Hoffman, B. M. *Struct. and Bond.* **1982**, *50*, 1.
5. Stucky, G. D.; Schultz, A. J.; Williams, J. M. *Ann. Rev. Mater. Sci.* **1977**, *7*, 301.
6. Toombs, G. A. *Phys. Rev.* **1978**, *40*, 181.
7. Friend, R. H.; Jerome, D. *J. Phys. C: Solid State Phys.* **1979**, *12*, 1441.
8. Whangbo, M.-H.; Hoffmann, R. *J. Am. Chem. Soc.* **1978**, *100*, 6093.
9. Hoffmann, R.; Christian, M.; Gray, H. B. *J. Am. Chem. Soc.* **1984**, *106*, 2001.
10. Whangbo, M.-H. *Acc. Chem. Res.* **1983**, *16*, 95.
11. Whangbo, M.-H.; Canadell, E. *Inorg. Chem.* **1986**, *25*, 1762.
12. Peters, C.; Eagen, C. F. *Inorg. Chem.* **1976**, *15*, 782.
13. Schultz, A. J.; Stucky, G. D.; Blessing, R. H.; Coppens, P. *J. Am. Chem. Soc.* **1976**, *98*, 3194.
14. Jerome, D.; Mazaud, A.; Ribault, M.; Bechgaard, K. *J. Phys. Lett.* **1980**, *41*, L195.
15. Bechgaard, K.; Carneiro, K.,; Olsen, M.; Rasmussen, F. B.; Jacobsen, C. S. *Phys. Rev. Lett.* **1981**, *46*, 852.
16. Bechgaard, K.; Rasmussen, F. B.; Olsen, M.; Rindorf, G.; Jacobsen,

C. S.; Pedersen, H. J.; Scott, J. C. *J. Am. Chem. Soc.* **1981**, *103*, 2440.

17. Mann, K. R.; Gordon, II, J. G.; Gray, H. B. *J. Am. Chem. Soc.* **1975**, *97*, 3553.
18. Balch, A. L.; Olmstead, M. M. *J. Am. Chem. Soc.* **1976**, *98*, 2354.
19. Sigal, I. S.; Gray, H. B. *J. Am. Chem. Soc.* **1981**, *103*, 2220.
20. Rice, S. F.; Gray, H. B. *J. Am. Chem. Soc.* **1981**, *103*, 1593.
21. Dallinger, R. F.; Miskowski, V. M.; Gray, H. B.; Woodruff, W. H. *J. Am. Chem. Soc.* **1981**, *103*, 1595.
22. Gordon, II, J. G.; Williams, R.; Hsu, C.-H.; Cuellar, E.; Samson, S.; Mann, K.; Gray, H. B.; Hadek, V.; Somoano, R. *Ann. New York Acad. Sci.* **1978**, *313*, 580.
23. Filomena Dos Remedios Pinto, M. A.; Sadler, P. J.; Neidle, S.; Sanderson, M. R.; Subbiad, A.; Kuroda, R. *J. Chem. Soc., Chem. Commun.* **1980**, 13.
24. Che, C.-M.; Butler, L. G.; Gray, H. B. *J. Am. Chem. Soc.* **1981**, *103*, 7796.
25. Che, C.-M.; Butler, L. G.; Grunthaner, P. J.; Gray, H. B. *Inorg. Chem.* **1985**, *24*, 4662.
26. Isci, H.; Mason, W. R. *Inorg. Chem.* **1985**, *24*, 1761.
27. Che, C.-M.; Herbstein, F. H.; Schaefer, W. P.; Marsh, R. E.; Gray, H. B. *J. Am. Chem. Soc.* **1983**, *105*, 4606.
28. (a) Bellitto, C.; Flamini, A.; Gastaldi, L.; Scaramuzza, L. *Inorg. Chem.* **1983**, *22*, 444. (b) Bellito, C.; Dessy, G.; Fares, V. *Inorg. Chem.* **1985**, *24*, 2815.
29. (a) Clark, R. J. H.; Kurmoo, M. *J. Chem. Soc., Dalton Trans.* **1985**, 579. (b) Kurmoo, M.; Clark, R. J. H. *Inorg. Chem.* **1985**, *24*, 4420.

(c) Clark, R. J. H.; Kurmoo, M.; Dawes, H. M.; Hursthouse, M. B. *Inorg. Chem.* **1986**, *25*, 409.

30. Swanson, B. I.; Conradson, S. D.; Stroud, M. A.; Zietlow, M. H.; Gray, H. B., manuscript in preparation.
31. Samson, S.; Goldish, E.; Dick, J. *J. Appl. Cryst.* **1980**, *13*, 425.
32. (a) Duchamp, D. J. Paper B-17, American Crystallographic Association Meeting, Bozeman, Montana, 1964. (b) Johnson, C. K. "ORTEP, A Fortran Thermal Ellipsoid Plot Program (ORNL-3794)" Oak Ridge National Laboratory: Oak Ridge, Tenn., 1965.
33. *International Table for Crystallography;* Kynoch: Birmingham, England, 1974; Vol. IV, p. 72.
34. Kistenmacher, T. J.; Destro, R.; Marsh, R. E.; Samson, S. *Mol. Cryst. Liq. Cryst.* **1980**, *62*, 173.
35. Williams, R.; Lowe Ma, C.; Samson, S.; Khanna, S. K.; Somoano, R. B. *J. Chem. Phys.* **1980**, *72*, 3781.
36. Lowe Ma, C.; Williams, R.; Samson, S. *J. Chem. Phys.* **1981**, *74*, 1966.
37. Butler, L. G.; Zietlow, M. H.; Che, C.-M.; Schaefer, W. P.; Sridhar, S.; Grunthaner, P. J.; Swanson, B. I.; Clark, R. J. H.; Gray, H. B. *J. Am. Chem. Soc.* **1988**, *110*, 1155.
38. Clark, R. J. H. In "Advances in Infrared and Raman Spectroscopy"; Clark, R. J. H.; Hester, R. E., Eds.; Wiley: Chichester, 1984; Vol. 11, Chapter 3.
39. Alexander, K. A.; Bryan, S. A.; Fronczek, F. R.; Fultz, W. C.; Reingold, A. L.; Roundhill, D. M.; Stein, P.; Watkins, S. F. *Inorg. Chem.* **1985**, *24*, 2803.
40. Burdett, J. K. *Inorg. Chem.* **1978**, *17*, 2537.

41. Marsh, R. E.; Herbstein, F. H. *Acta Crystallogr., Sect. B* **1983**, *39*, 280.

42. Conradson, S. D.; Dallinger, R. F.; Swanson, B. I.; Clark, R. J. H.; Croud, V. B. *Chem. Phys. Lett.* **1987**, *135*, 463.

43. (a) Baeriswyl, D.; Bishop, A. *J. Phys. C: Solid State Phys.* **1988**, in press. (b) Baeriswyl, D.; Bishop, A. *Physics Scripta* **1988**, in press.

CHAPTER 4

Pressure Dependence of the Electronic Spectra of $K_4[Pt_2(P_2O_5H_2)_4X_n]$ (X = Cl, Br; n = 0, 1, 2)

INTRODUCTION

An important characteristic of quasi-one-dimensional, halide-bridged, mixed-valence transition metal complexes, MX, is that their physical properties may be controlled by varying the transition metal complex ions, the halogen, and external pressure.[1-7] These materials exhibit an intense intervalence charge-transfer excitation, the IVCT band, that is polarized along the chain axis. Resonance Raman spectra obtained by exciting into the IVCT band are also highly polarized along the chain axis and the frequencies of the Raman-enhanced modes have been used along with IVCT band energy as a measure of the extent of valence delocalization.[1c] These highly anisotropic semiconductors are generally in the trapped-valence limit, with the metal atoms in alternating valence states. These and similar systems have recently been recognized as examples of commensurate charge-density-wave (CDW) systems.[6,8,9] They exhibit a large distortion of the halogen from the central position between the metal dimers due to a Peierls instability.

Linear MMX chain complexes, $K_4[Pt_2(P_2O_5H_2)_4X]\cdot 3H_2O$, X=Cl,Br ($Pt_2X$), are of particular interest[10-14] because they are more valence delocalized and show smaller distortions of the halide sublattice relative to the MX systems. Early structural work on Pt_2Br indicated that the halogen was centrally located between the Pt dimers.[11] However, theoretical calculations suggested that there should be a distorted halide sublattice and some mixed-valence character.[13] Recent experimental studies have shown that there is a small distortion of the halogen from the central position in Pt_2Br.[10,14] In contrast, Pt_2Cl is in the strongly trapped-valence limit with a large distortion of the chloride from the central position (see Chapter 3).

Original interest in investigating these types of systems under high pressure was inspired by the research of Interrante and coworkers.[15] They investigated similar linear chain MX complexes and found that the conductivity could be increased by as much as nine orders of magnitude at 14.0 GPa, presumably because of a decrease in the Peierls gap with increasing pressure. This tremendous pressure dependence made these types of materials good candidates for spectroscopic studies. Tanino, *et al.*[5] measured the effects of high pressure on the lattice parameters, optical gaps, luminescence peaks, and the X-ray absorption near edge structure of MX complexes. It was concluded that the Peierls gap decreases with increasing pressure.

The effects of pressure on the electronic spectra of Pt_2Cl, Pt_2Br, $(TBA)_4[Pt_2(P_2O_5H_2)_4]$ (Pt_2), and $K_4[Pt_2(P_2O_5H_2)_4Cl_2]$ (Pt_2Cl_2) have been investigated in order to gain insight into the structural changes that can occur in these materials. The energy maximum of the IVCT band provides a direct diagnostic of the extent of valence delocalization in the monohalide complexes.[16] In addition, study of the other bands in the electronic spectra should yield valuable information on the effects of pressure on the electronic structures of the complexes. The magnitude and direction of the pressure-induced changes of the energy of the transitions provide information on changes in ligand field splitting and changes in the bond strength of the Pt-Pt complexes.

EXPERIMENTAL

Materials

All solvents were reagent grade and used without further purification.

The platinum dimers $K_4[Pt_2(P_2O_5H_2)_4]$, Pt_2, and $K_4[Pt_2(P_2O_5H_2)_4]$, Pt_2Cl_2, were prepared by published procedures.[14,17,18] Linear chain complexes, $K_4[Pt_2(P_2O_5H_2)_4Cl]$, Pt_2Cl, and $K_4[Pt_2(P_2O_5H_2)_4Br]$, Pt_2Br, were prepared as described in the experimental section of Chapter 3.

Physical Measurements

The high pressure electronic absorption measurements were performed by Dr. Mary Ann Stroud with technical assistance from Dr. Stephen F. Agnew, Dr. Philip D. Stroud and Mr. Douglas G. Eckhart at the Los Alamos National Laboratory, Los Alamos, New Mexico.

Pressure was generated using a gasketed Merrill-Basset diamond anvil cell with an inconel gasket. The high energy working range of the cell was limited to 41700 cm^{-1} because of the strong absorption by nitrogen impurities in the diamonds. A ruby fluorescence pressure calibration method was used to determine pressures. Absorption measurements were obtained at room temperature using a Perkin Elmer 330 spectrophotometer. The instrument was modified for DAC work by using a 100 W tungsten-halogen lamp source and by adding a Harrick 5 to 1 beam condenser to the sample chamber.[19]

Fluorescence measurements were obtained on a SPEX Model 1403 3/4-m double monochromator equipped with a Princeton Applied Research photon counting system. Typically, the 514.5 nm line of a Spectra-Physics 171 argon laser was used as the exciting line. The cell was allowed to

equilibrate after each pressure increase and ruby fluorescence was routinely checked before and after the data collection to insure that the pressure had not varied significantly. When possible, the fluorescence from several rubies located in different parts of the cell were measured and the average value was used to estimate the pressure. Pressure gradients of as large as 0.4 GPa were observed at high pressures. Because of problems with sample degradation, the laser power at the sample was kept to less than 20 mW. For Pt_2Cl_2, Pt_2, and Pt_2Br, all pressure effects were reversible. Degradation of the Pt_2Cl sample was a problem. Peak positions were always reversible; however, intensity changes and weak additional features in the release spectra were observed when sample degradation had occurred.

For Pt_2Cl_2, a 3-5% mixture of Pt_2Cl_2 in $KClO_4$ was prepared and mixed for several minutes in a dental amalgamator. The sample was loaded into the cell immediately after mixing. Pressure was applied to the sample until the salt fused and the sample became transparent. The cell was released to zero pressure before the run was started. The Pt_2 crystals were ground in mineral oil under flowing N_2. When the crystals were ground in air, the electonic absorption spectra suggested that the sample was reacting. Samples prepared by minimal grinding of Pt_2Br single crystals with $KClO_4$ in a mortar and pestle resulted in the best obtainable electronic spectra. Single crystals of Pt_2Cl were ground in air and under flowing N_2. Mineral oil or $KClO_4$ was used as the pressurizing medium.

Sample-dependent high-energy scattering was observed in the electronic spectra. After correction for this scattering tail had been made, peak locations were determined using a cursor. Polynomial fits

of all the energy *vs.* pressure electronic data were determined. For many of the electronic transitions, the ambient-pressure peak locations were somewhat dependent on the sample preparation, though the pressure-induced shifts were not. Most likely, the major cause of these differences was varying particle size. In order to compare the relative pressure-induced shift of the energy of a transition in the different runs, an energy correction factor was subtracted from each run. The correction factor, ν_0, was determined by minimizing the standard deviation of a polynomial fit to the data. Wherever a significant energy difference resulted between runs, the ν_0 values are noted.

RESULTS and DISCUSSION

Pt_2, Pt_2Cl_2, Pt_2Cl, and Pt_2Br contain Pt_2P_8 units of D_{4h} symmetry built by four bi-nucleating pyrophosphite ligands, $[(HO_2P)_2O^{2-}]$ (see Figure 1.1). The potassium salts of the fully reduced complex, Pt_2, and the monohalides, Pt_2Cl and Pt_2Br, are isostructural with the metal-metal bond aligned along the z axis of the tetragonal unit cell, P4/mbm, as illustrated in Figure 3.2b. In the monohalides, the Pt_2 units form an infinite linear chain in the z direction. The larger the distortion of the halogen from the central position, the larger the trapped-valence character of the chain. In Pt_2Cl, which is in the trapped-valence limit, the halogen is displaced 0.25 Å from the central position at 22 K[14] and the charge on the alternating Pt dimers is close to Pt(II)-Pt(II) and Pt(III)-Pt(III). In the Pt_2Br complex, the halogen is displaced only 0.1Å from the central position at 19 K,[14] and the charge on the Pt atoms is more delocalized. The ambient-pressure energies of all the electronic transitions studied as a function of pressure are listed in Table 4.1.

Pt_2Cl_2. Two electronic transitions were studied as a function of pressure in Pt_2Cl_2, $d_{xz},d_{yz} \rightarrow d\sigma^*$ and $\sigma(X) \rightarrow d\sigma^*$ (Figure 4.1).[20] The $d\sigma \rightarrow d\sigma^*$ transition has been assigned to an absorption (at about 46,500 cm^{-1}) that is too high in energy to be observed in a diamond anvil cell. The smoothed absorption spectra of Pt_2Cl_2 at 0.1 and 9 GPa are shown in Figure 4.2.

The $d_{xz},d_{yz} \rightarrow d\sigma^*$ transition shifts blue with increasing pressure at a rate of 300 cm^{-1}/GPa from its position at 28,100 cm^{-1}. The shift is linear over the pressure range studied (Figure 4.3a). Increasing pressure enhances the overlap between the d_{z^2} orbitals on adjacent Pt

Table 4.1

Ambient-Pressure Energies of Electronic Transitions (in cm^{-1})

Transition	Pt_2Cl_2	Pt_2	Pt_2Br	Pt_2Cl
$d_{xz},d_{yz} \rightarrow d\sigma^*$	28,100			
$\sigma(X) \rightarrow d\sigma^*$	34,500		32,800	35,400
$d\sigma^* \rightarrow p\sigma$		26,700	27,600	26,400
$d_{xz},d_{yz} \rightarrow p\sigma$		40,200		
$d\sigma^* \rightarrow d_{x^2-y^2}$		35,300		
unassigned				25,600
IVCT			16,100	18,600

Figure 4.1 Energy level diagram for $[Pt_2(P_2O_5H_2)_4Cl_2]^{4-}$ at ambient pressure.

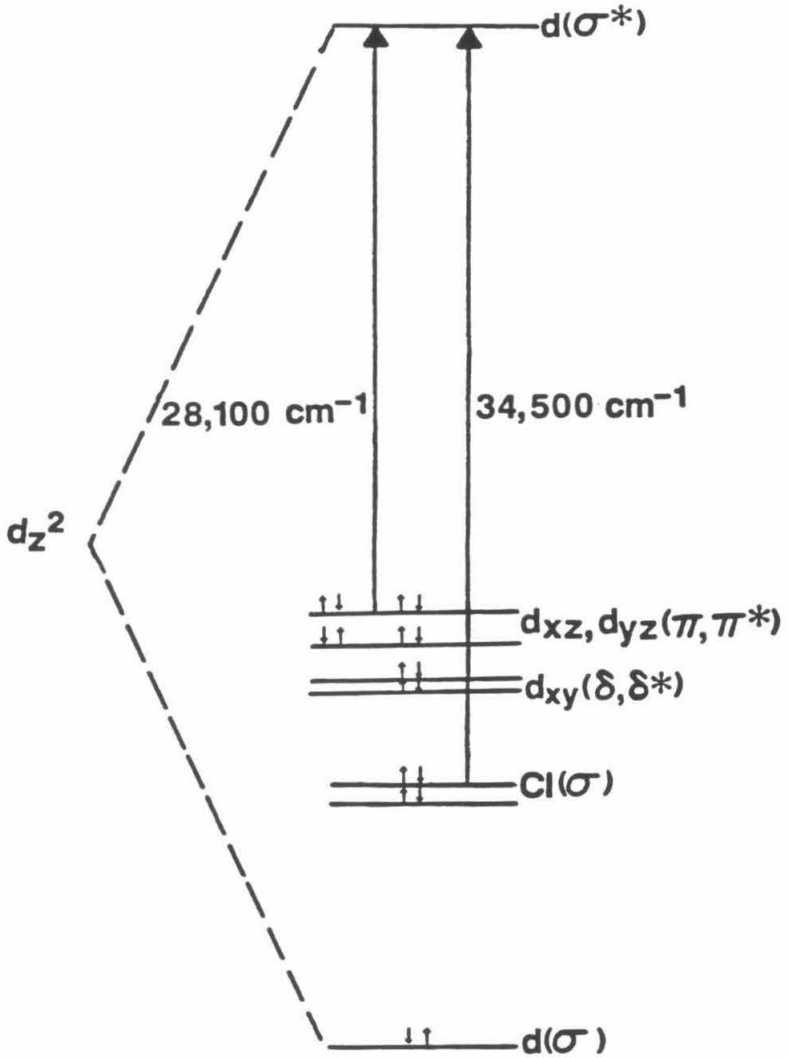
d(σ*)
28,100 cm⁻¹
34,500 cm⁻¹
dz²
dxz, dyz(π, π*)
dxy(δ, δ*)
Cl(σ)
d(σ)

Figure 4.2 Smoothed electronic absorption spectra of $[Pt_2(P_2O_5H_2)_4Cl_2]^{4-}$ at 0.1 and 9.0 GPa.

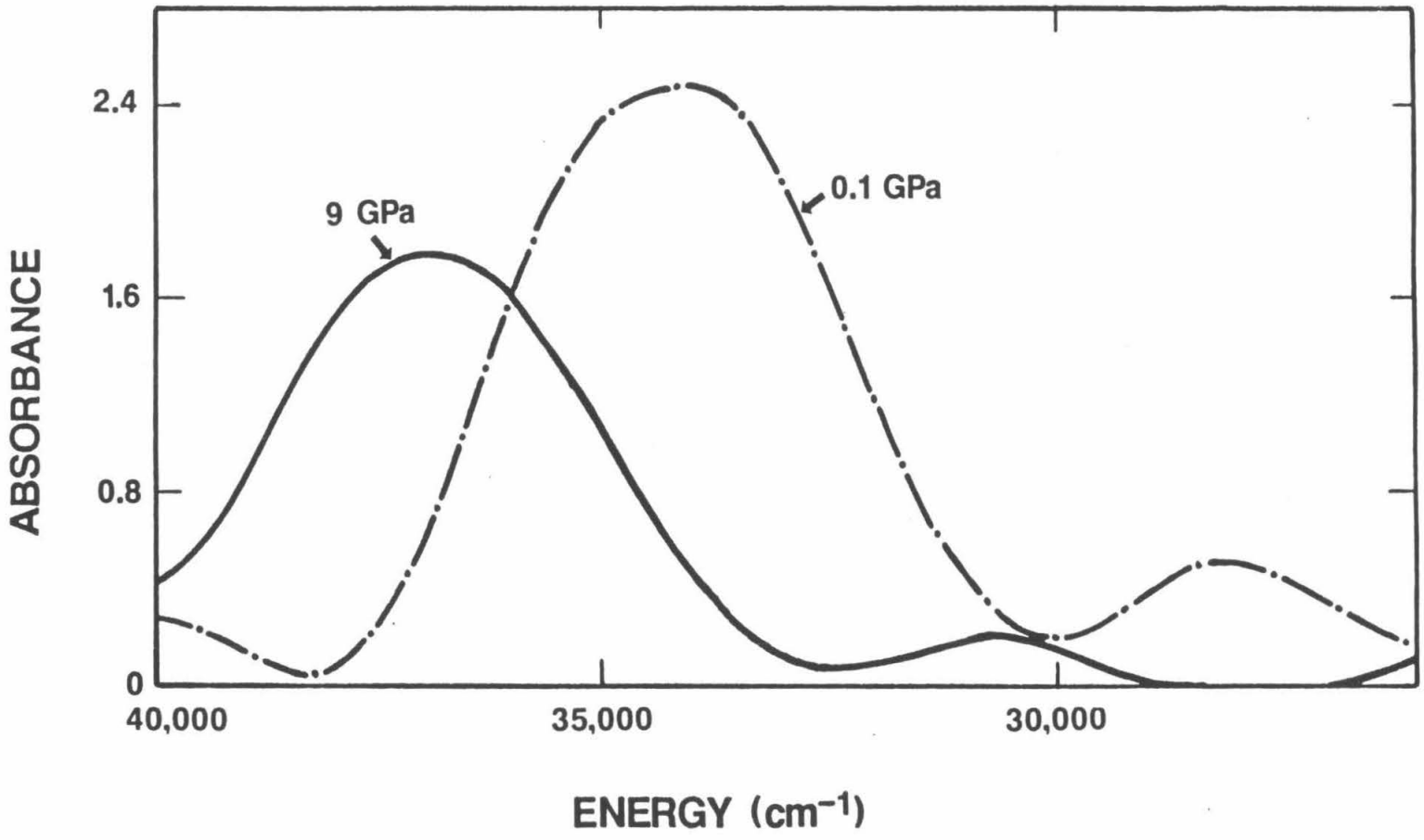
ABSORBANCE
2.4
1.6
0.8
0
9 GPa
0.1 GPa
40,000
35,000
30,000
ENERGY (cm^{-1})

Figure 4.3 (a) Pressure shift of the $d_{xz}, d_{yz} \rightarrow d\sigma^*$ transition in $[Pt_2(P_2O_5H_2)_4Cl_2]^{4-}$.

(b) Pressure shift of the $\sigma(Cl) \rightarrow d\sigma^*$ transition in $[Pt_2(P_2O_5H_2)_4Cl_2]^{4-}$.

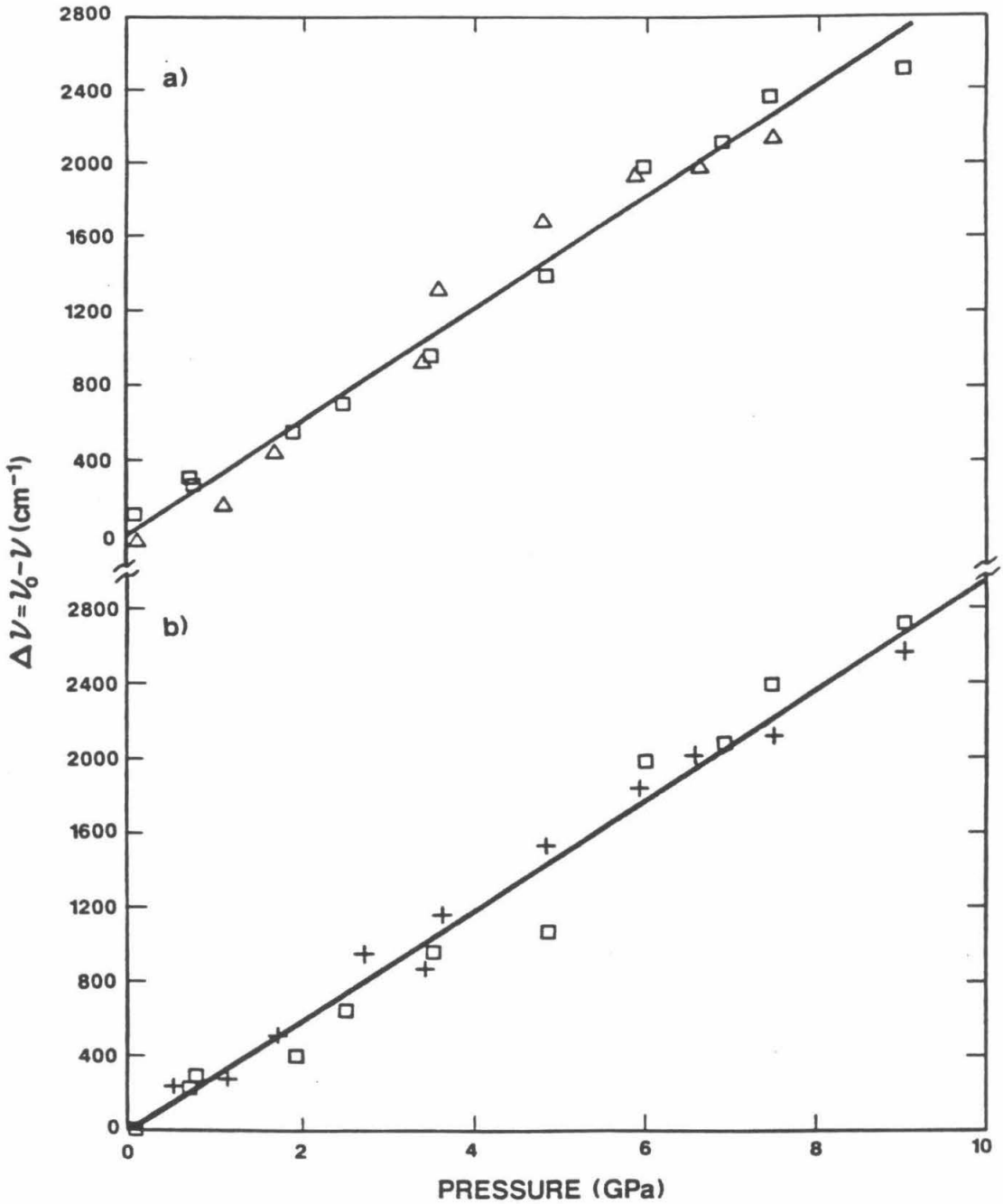
a)
b)
2800
2400
2000
1600
1200
800
400
0
$\Delta\nu = \nu_0 - \nu$ (cm^{-1})
0
2
4
6
8
10
PRESSURE (GPa)

atoms, thereby destabilizing $d\sigma^*$. The two sets of d_{xz},d_{yz} orbitals interact only weakly, so the shift of the d_{xz},d_{yz} → $d\sigma^*$ transition is attributed to the pressure-induced destabilization of $d\sigma^*$. Any increase in the splitting of the d_{xz},d_{yz} orbitals would reduce the magnitude of the observed blue shift.

The energy of the σ(Cl) → $d\sigma^*$ transition also blue shifts linearly, at a rate of 300 cm^{-1}/GPa from 34,500 cm^{-1} (Figure 4.3b). Accordingly, this blue shift is attributed mainly to the destabilization of $d\sigma^*$ with increasing pressure.

Pt_2. The MO diagram of the d^8-d^8 Pt_2 complex is given in Chapter 1 (Figure 1.2); however, for convenience the energy levels are presented again in Figure 4.4. The effects of pressure on three electronic transitions, d_{xz},d_{yz} → $p\sigma$, $d\sigma^*$ → $p\sigma$, and $d\sigma$ → $d_{x^2-y^2}$,[21] have been investigated (Figure 4.5).

The d_{xz},d_{yz} → $p\sigma$ transition in Pt_2 (40,200 cm^{-1} at ambient pressure) exhibits a linear blue shift of 190 cm^{-1}/GPa with increasing pressure (Figure 4.6a). An explanation of the observed shift is that the p_z orbitals are coupled strongly to d_{z^2} orbitals on adjacent Pt atoms, while the d_{xz},d_{yz} orbitals experience only very weak π interactions. This pattern of interactions with increasing pressure results in a destabilization of p_z relative to d_{xz},d_{yz}.

The $d\sigma^*$ → $d_{x^2-y^2}$ energy (ambient-pressure energy of 35,400 cm^{-1}) exhibits unusual nonlinear behavior with increasing pressure. The $d\sigma^*$ → $d_{x^2-y^2}$ transition shifts red up to 5.5 GPa at an initial rate of about 230 cm^{-1}/GPa, then levels off and begins to shift blue until at least 10.0 GPa (Figure 4.6b). This transition is expected to be affected both by increased splitting of $d\sigma$ and $d\sigma^*$, resulting from

Figure 4.4 Energy level diagram for $[Pt_2(P_2O_5H_2)_4]^{4-}$ at ambient pressure.

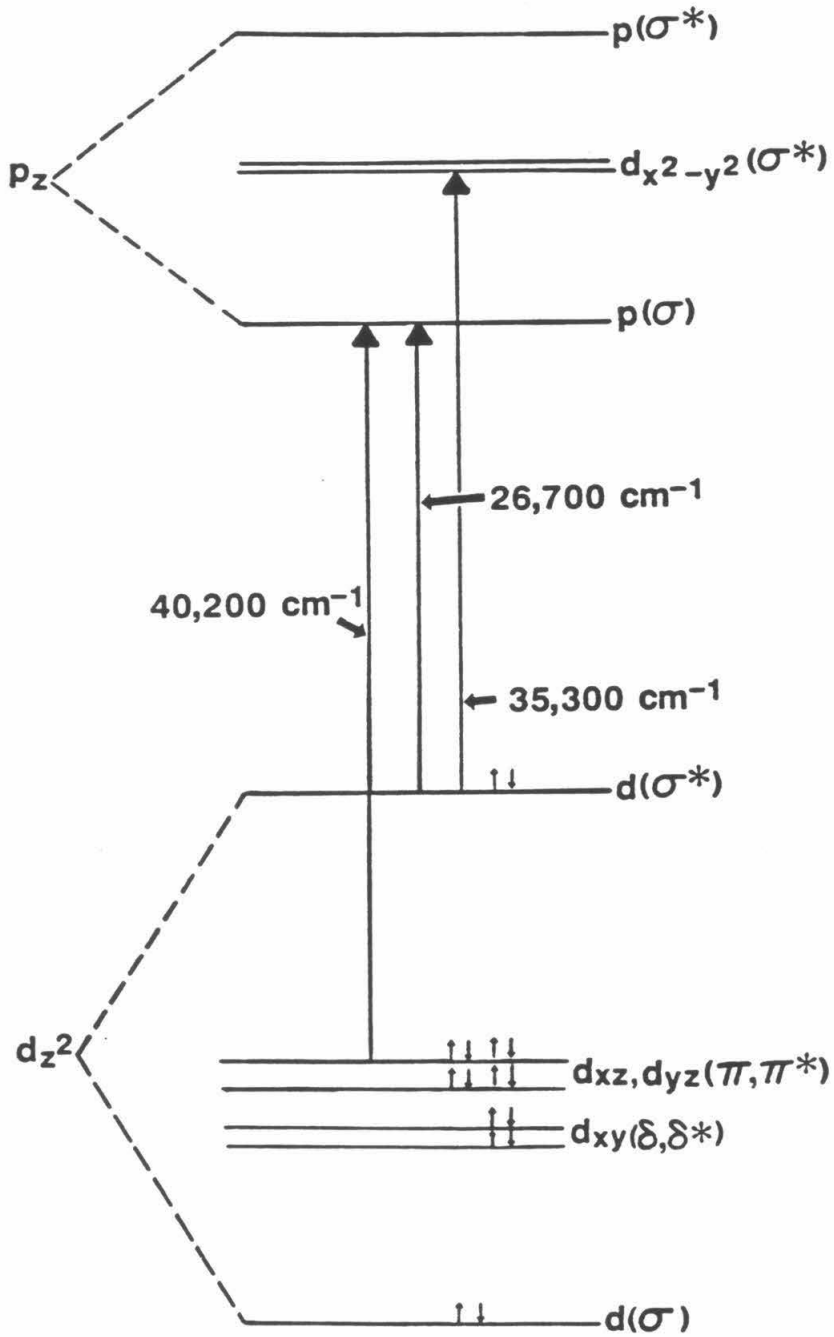
p(σ*)
pz
dx2-y2(σ*)
p(σ)
26,700 cm-1
40,200 cm-1
35,300 cm-1
d(σ*)
dz2
dxz,dyz(π,π*)
dxy(δ,δ*)
d(σ)

Figure 4.5 Smoothed electronic absorption spectra of $[Pt_2(P_2O_5H_2)_4]^{4-}$ at 0.1, 5.2, and 11.7 GPa.

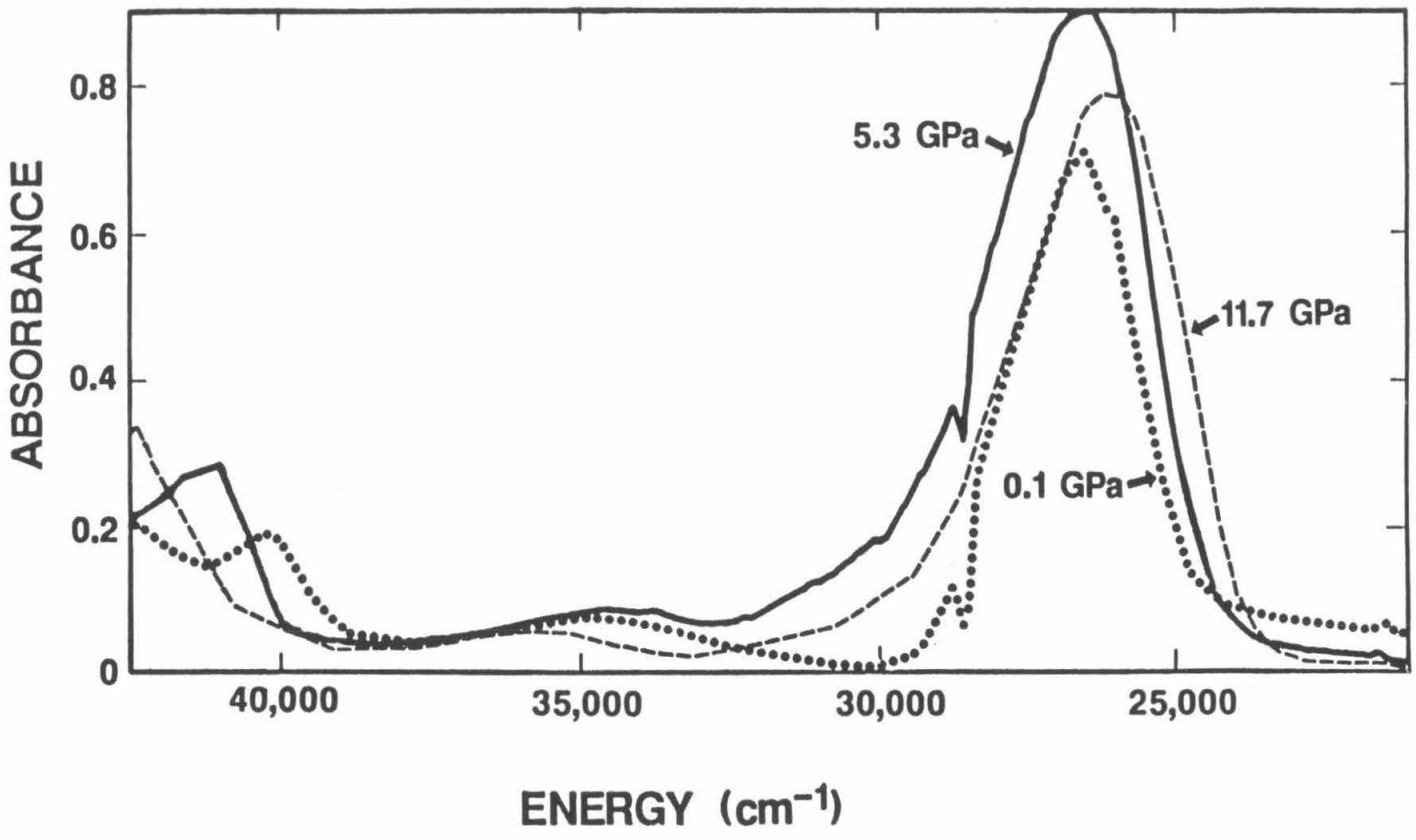
ABSORBANCE
0.8
0.6
0.4
0.2
0
40,000
35,000
30,000
25,000
ENERGY (cm⁻¹)
5.3 GPa
11.7 GPa
0.1 GPa

Figure 4.6 (a) Pressure shift of the $d_{xz}, d_{yz} \rightarrow p\sigma$ transition in $[Pt_2(P_2O_5H_2)_4]^{4-}$.

(b) Pressure shift of the $d\sigma^* \rightarrow d_{x^2-y^2}$ transition in $[Pt_2(P_2O_5H_2)_4]^{4-}$.

(c) Pressure shift of the $d\sigma^* \rightarrow p\sigma$ transition in $[Pt_2(P_2O_5H_2)_4]^{4-}$.

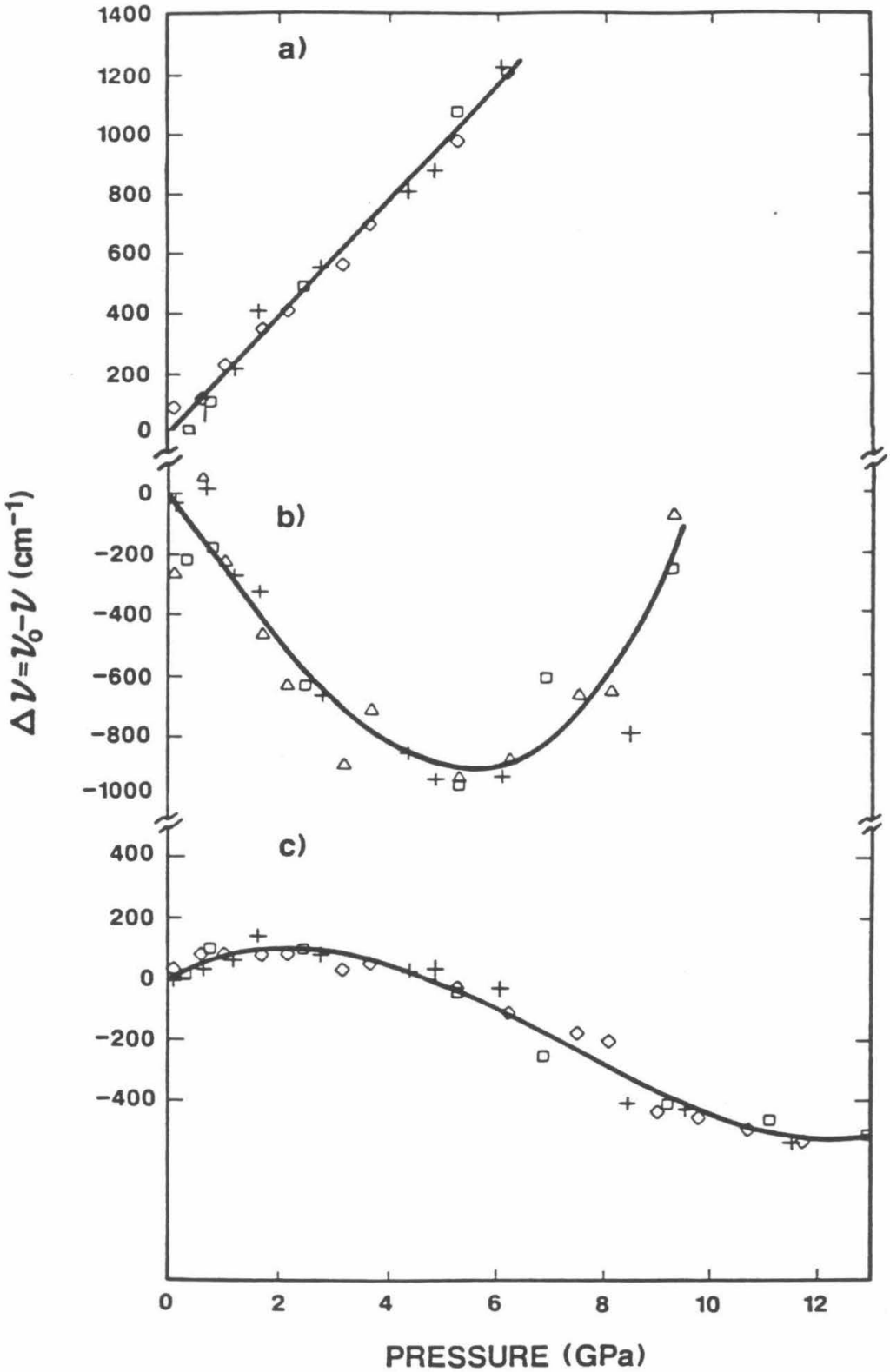
a)
b)
c)
1400
1200
1000
800
600
400
200
0
-200
-400
-600
-800
-1000
0
2
4
6
8
10
12
PRESSURE (GPa)
$\Delta\nu=\nu_0-\nu$ (cm^{-1})

greater overlap of the d_{z^2} orbitals on adjacent Pt atoms, and an increased ligand field that destabilizes $d_{x^2-y^2}$ relative to d_{z^2}. In the absence of large changes in the ligand field splitting, an increase in the overlap of adjacent d_{z^2} orbitals would lead to a red shift, and it is reasonable that this is the dominant effect at low pressure. At higher pressures, increased ligand field splitting between $d_{x^2-y^2}$ and d_{z^2} begins to dominate and the $d\sigma^* \rightarrow d_{x^2-y^2}$ transition shifts to the blue. The strong nonlinearity of the ligand field effect is attributed to nonlinear compression of the P-Pt bonds as the pressure is increased. At low pressure, compression along the *a* and *b* crystallographic axes results in compression of the interchain separation and little or no change in the P-Pt bonds. At higher pressure, as the interchain interactions stiffen, the P-Pt bonds begin to compress, thereby destabilizing $d_{x^2-y^2}$.

There is little shift in the 26,700 cm^{-1} energy of $d\sigma^* \rightarrow p\sigma$ up to 5.0 GPa, though the transition does appear to initially shift slightly to the blue. At higher pressures, a significant red shift is observed; this shift appears to level off at ca. 11.0 GPa. Increased splitting of $d\sigma$ and $d\sigma^*$ would result in a red shift of the $d\sigma^* \rightarrow p\sigma$ transition. The $d\sigma^*$ and $p\sigma$ levels are coupled, and any increase in the coupling as the pressure is raised would tend to repel $d\sigma^*$ and $p\sigma$, resulting in a blue shift. For the $d\sigma^* \rightarrow p\sigma$ transition, there is probably a delicate balance between these two effects. Because a weak shift is observed, other effects also may significantly influence the behavior of this transition. At higher pressures, when the transition begins to red shift, increased coupling between the phosphorus σ orbital and $d\sigma^*$ occurs. Increased $\sigma(P)$-d_{z^2} coupling is expected at higher pressures in

light of the observed pressure shift of the $d\sigma^* \rightarrow d_{x^2-y^2}$ transition. This effect suggests that the energy of the $d\sigma^*$ orbital may be tuned in binuclear complexes by varying the bridging ligand. For monohalide complexes, the ligands may be used to control the extent of delocalization of the chain.

The weak 22,000 cm^{-1} absorption attributable to the triplet $d\sigma^* \rightarrow p\sigma$ transition[21] initially shifts weakly blue with increasing pressure. The weak 31,800 cm^{-1} shoulder is probably the $d\sigma^* \rightarrow d_{x^2-y^2}$ triplet,[21] which shifts red with increasing pressure.

Pt_2Br. A diagram of the electronic transitions in Pt_2Br is shown in Figure 4.7. The absorption spectrum of Pt_2Br is a superposition of electronic transitions in Pt_2 and Pt_2Br_2, modified slightly depending on the degree of delocalization, and an additional broad low energy band, which is the IVCT band characteristic of the mixed-valence complex itself (Figure 4.8). The highest energy transition observed in this study, 32,800 cm^{-1} at ambient pressure, shifts to higher energy with increasing pressure at a rate of 270 cm^{-1}/GPa (Figure 4.9a). The rate of the shift is within 10% of the observed shift of the $\sigma(Cl) \rightarrow d\sigma^*$ transition in Pt_2Cl_2 and it is linear over the pressure range studied. The band position at ambient pressure is very close to that of $\sigma(Br) \rightarrow d\sigma^*$ in Pt_2Br_2 (32,800 cm^{-1}),[17,22] and the absorption is intense. Based on this evidence, the band is assigned to the $\sigma(Br) \rightarrow d\sigma^*$ transition.

The pressure-induced energy change of the 27,600 cm^{-1} transition is shown in Figure 4.9b. The energy of the transition shifts weakly to the red with increasing pressure and appears to level off above 5.0 GPa. Based on our analysis of the Pt_2Cl_2 and Pt_2 results, a red shift

Figure 4.7 Energy level diagram for $[Pt_2(P_2O_5H_2)_4Br]^{4-}$ at ambient pressure.

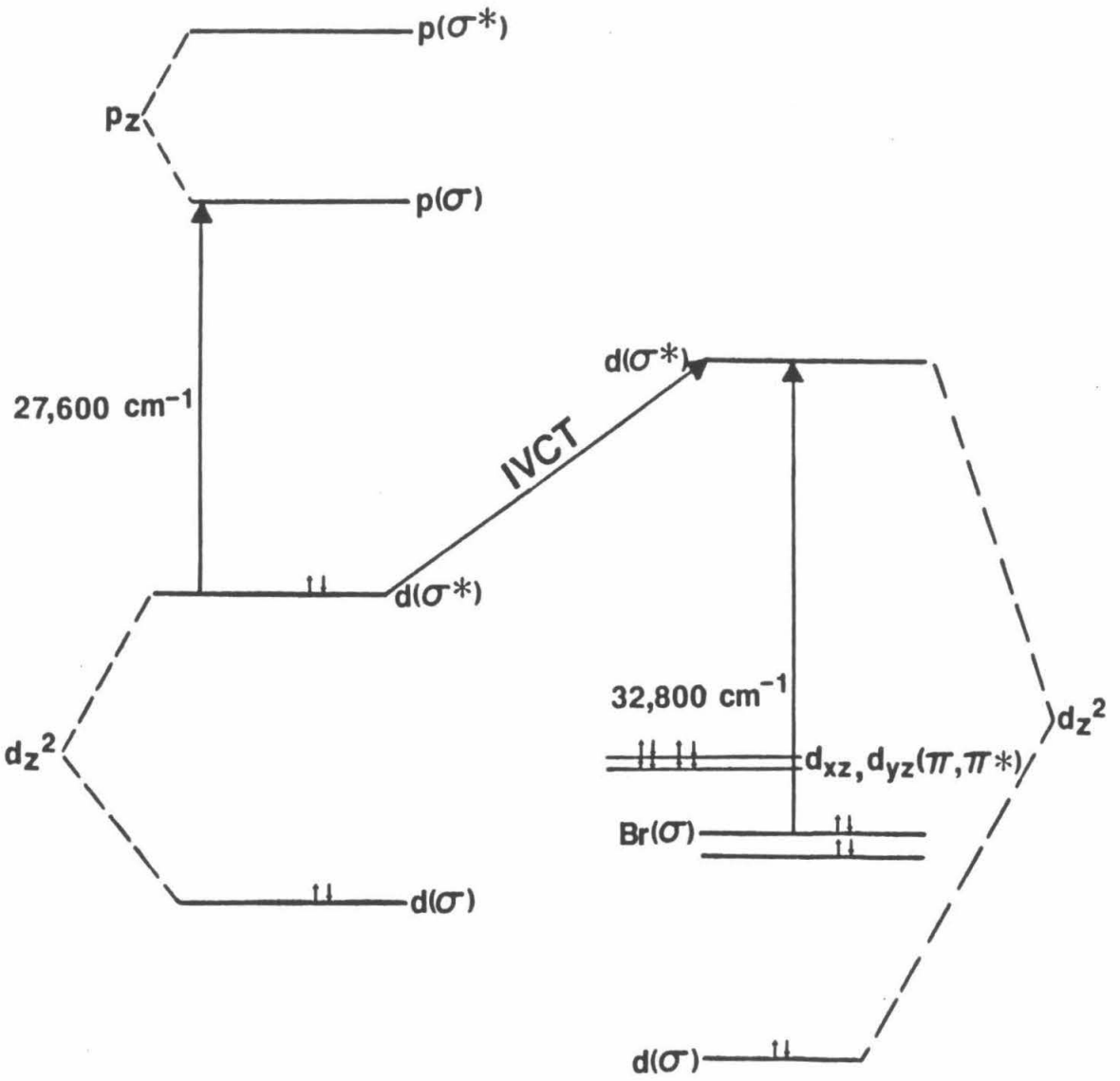
p(σ*)
pz
p(σ)
27,600 cm⁻¹
IVCT
d(σ*)
d(σ*)
dz²
d(σ)
32,800 cm⁻¹
dxz, dyz(π,π*)
Br(σ)
dz²
d(σ)

Figure 4.8 Smoothed electronic absorption spectra of $[Pt_2(P_2O_5H_2)_4Br]^{4-}$ at 0.3, 2.4, 4.9, and 9.4 GPa.

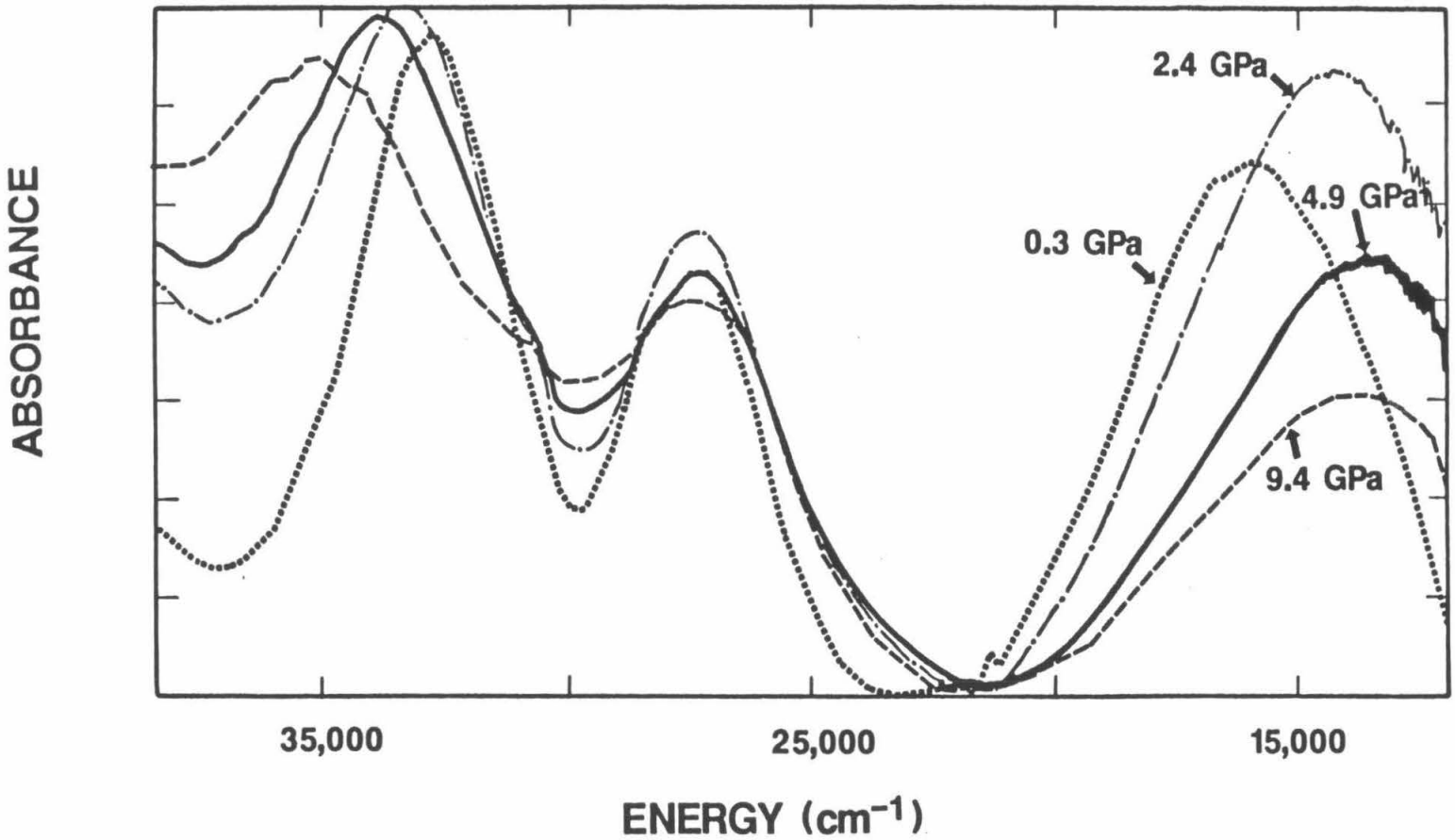
ABSORBANCE
2.4 GPa
4.9 GPa
0.3 GPa
9.4 GPa
35,000
25,000
15,000
ENERGY (cm^{-1})

Figure 4.9 (a) Pressure shift of the $\sigma(Br) \rightarrow d\sigma^*$ transition in $[Pt_2(P_2O_5H_2)_4Br]^{4-}$.

(b) Pressure shift of the $d\sigma^* \rightarrow p\sigma$ transition if $[Pt_2(P_2O_5H_2)_4Br]^{4-}$ (ν_0 = 27,200, 27600, and 27,900 cm^{-1}).

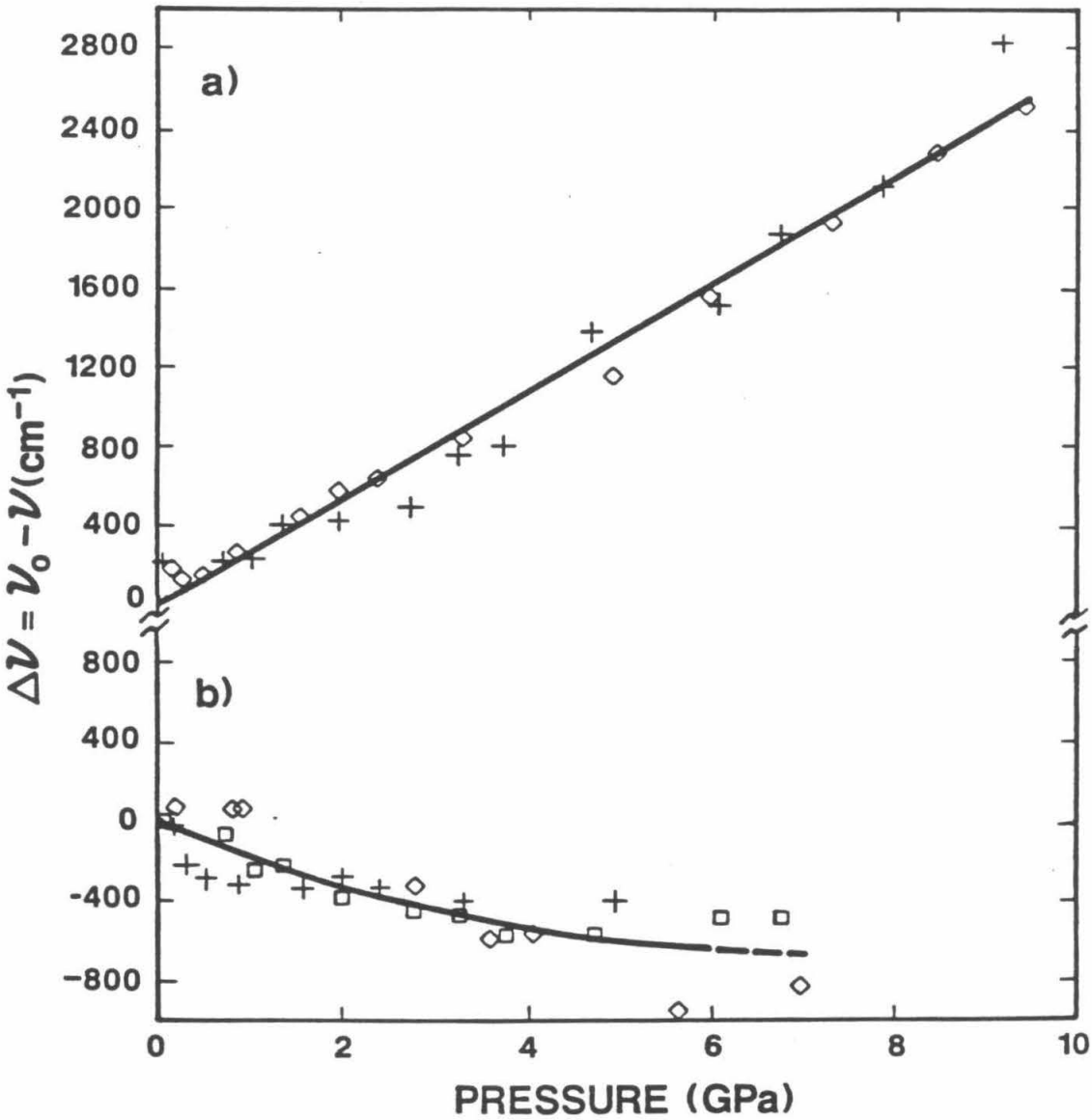
a)
b)
2800
2400
2000
1600
1200
800
400
0
800
400
0
-400
-800
0
2
4
6
8
10
PRESSURE (GPa)
$\Delta\nu = \nu_0 - \nu (cm^{-1})$

of $d\sigma^* \rightarrow p\sigma$ is plausible, while a blue shift is expected for $d_{xz},d_{yz} \rightarrow d\sigma^*$. In Pt_2Br, a red shift of $d\sigma^* \rightarrow p\sigma$ also is expected at high pressure, because of enhanced intermolecular interactions along the metal-metal axis. Accordingly, the intense 27,600 cm^{-1} band is assigned to $d\sigma^* \rightarrow p\sigma$.

Pt_2Cl. The energy level diagram for Pt_2Br (Figure 4.7) can also be utilized in discussing the spectrum of Pt_2Cl, where four electronic transitions have been studied as a function of pressure (Figure 4.10). The highest energy transition observed for Pt_2Cl (35,400 cm^{-1} at ambient pressure) shifts to higher energy with increasing pressure at a rate of 290 cm^{-1}/GPa (Figure 4.11a). The shift is linear with pressure and its magnitude is within 10% of the observed shift of the $\sigma(Cl) \rightarrow d\sigma^*$ transition in Pt_2Cl_2. The energy of the transition at ambient pressure is very close to that of $\sigma(Cl) \rightarrow d\sigma^*$ in Pt_2Cl_2 (Table 4.1). Since the transition is also very intense, it is assigned to $\sigma(Cl) \rightarrow d\sigma^*$.

The weak blue shift, 75 cm^{-1}/GPa, of the transition at 26,700 cm^{-1} is illustrated in Figure 4.11b. A blue shift of the $d_{xz},d_{yz} \rightarrow d\sigma^*$ band has been observed in Pt_2Cl_2 and can be inferred in Pt_2 by taking the difference between the pressure-induced shift of $d_{xz},d_{yz} \rightarrow p\sigma$ and that of $d\sigma^* \rightarrow p\sigma$; however, the shifts in Pt_2Cl_2 and Pt_2 are over twice that of the blue shift observed for the 26,700 cm^{-1} transition in Pt_2Cl. A blue shift is also plausible for $d\sigma^* \rightarrow p\sigma$ if an increase in the coupling between $d\sigma^*$ and $p\sigma$ is the dominant pressure effect. Accordingly, the intense 26,700 cm^{-1} band is assigned to the $d\sigma^* \rightarrow p\sigma$ transition.

There is a very strong pressure-induced linear red shift (-510 cm^{-1}/GPa) of the Pt_2Cl electronic transition with an ambient-pressure

Figure 4.10 Smoothed electronic absorption spectrum of $[Pt_2(P_2O_5H_2)_4Cl]^{4-}$ at 0 and 2.2 GPa.

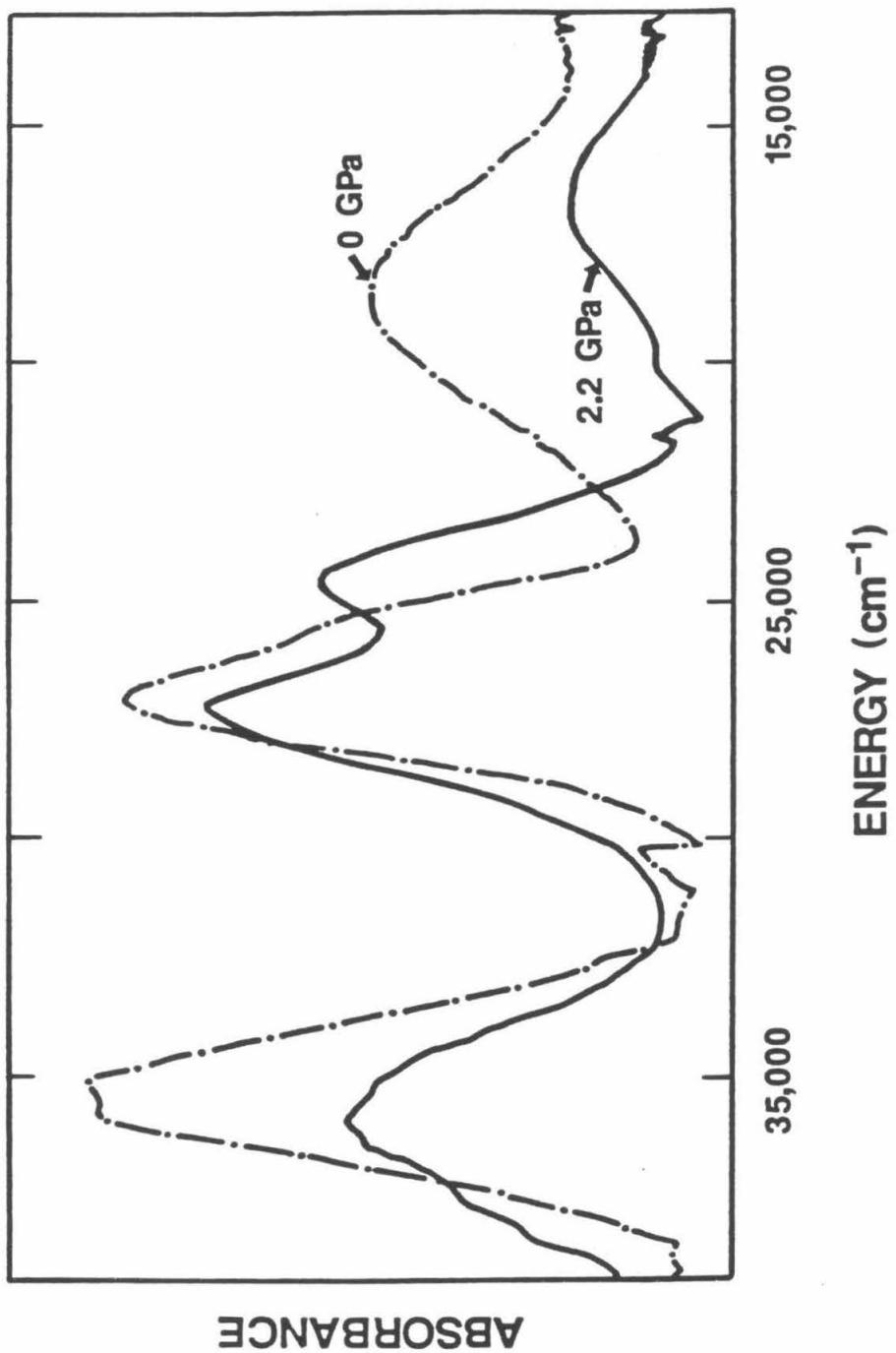
0 GPa
2.2 GPa
35,000
25,000
15,000
ENERGY (cm^{-1})
ABSORBANCE

Figure 4.11 (a) Pressure shift of the $\sigma(Cl) \rightarrow d\sigma^*$ transition in $[Pt_2(P_2O_5H_2)_4Cl]^{4-}$.

(b) Pressure shift of the $d\sigma^* \rightarrow p\sigma$ transition in $[Pt_2(P_2O_5H_2)_4Cl]^{4-}$ (ν_0 = 26,200, 26,800, and 27,100 cm^{-1}).

(c) Pressure shift of the unassigned transition in $[Pt_2(P_2O_5H_2)_4Cl]^{4-}$.

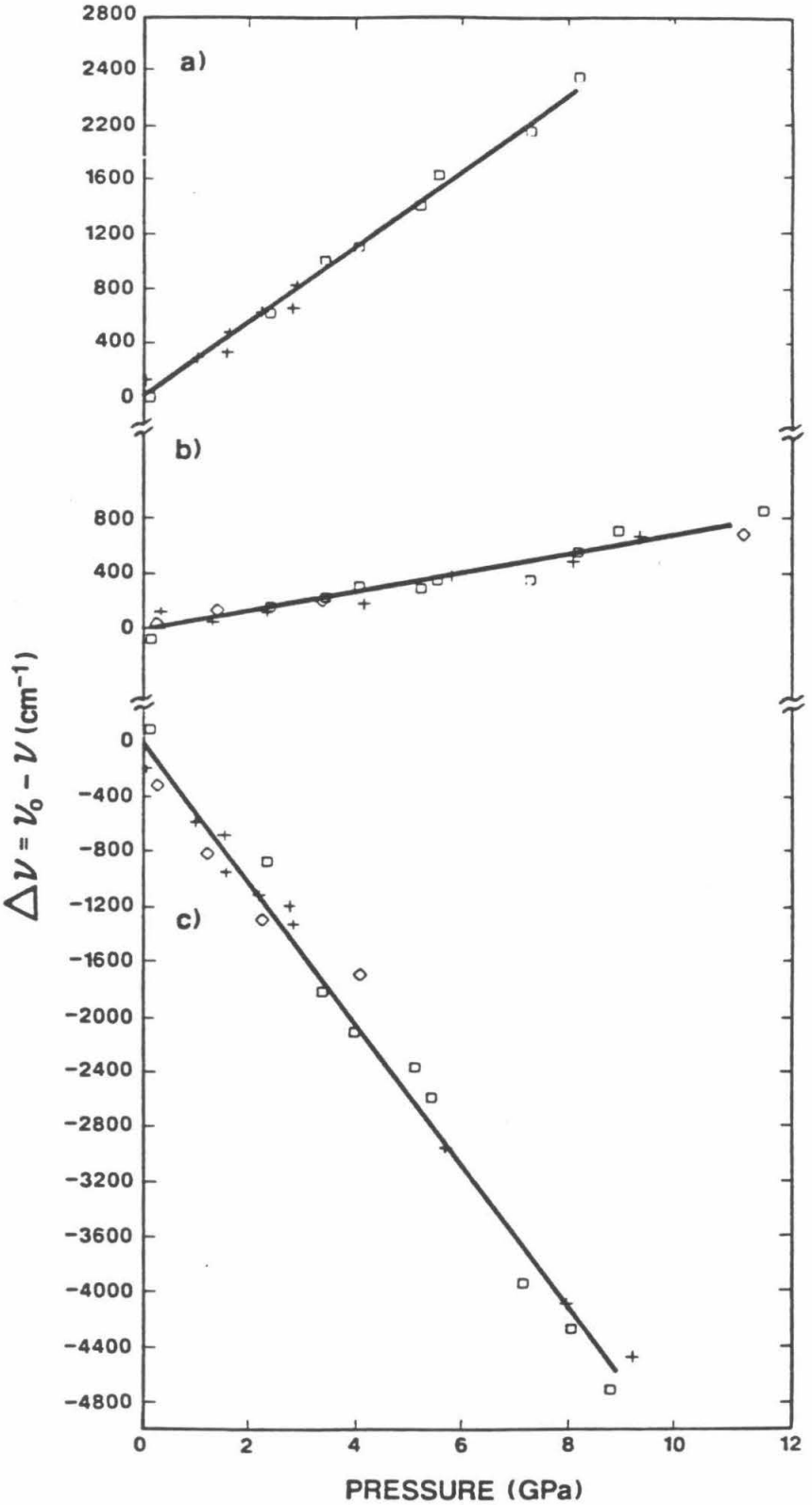
a)
b)
c)
2800
2400
2200
1600
1200
800
400
0
-400
-800
-1200
-1600
-2000
-2400
-2800
-3200
-3600
-4000
-4400
-4800
0
2
4
6
8
10
12
PRESSURE (GPa)
$\Delta\nu = \nu_0 - \nu$ (cm^{-1})

energy of 25,600 cm^{-1}. A weak red shift of the $d\sigma^* \rightarrow p\sigma$ transition has been observed for Pt_2Br and at pressures greater than 5.0 GPa for Pt_2. The magnitude of the red shift of the 25,600 cm^{-1} band is several times larger and for this reason assignment to $d\sigma^* \rightarrow p\sigma$ is unlikely. (In addition, the 26,700 cm^{-1} has already been assigned to the $d\sigma^* \rightarrow p\sigma$ transition.) Another unusual characteristic of this transition is that the intensity of the peak varies considerably with the method of sample preparation. The peak has been observed previously in the electronic spectra of samples in $KClO_4$ pellets,[10] and there is no peak in the Pt_2Br electronic spectrum that exhibits similar behavior. Because of these observations, the peak has not been assigned to a metal-based transition of the ground-state structure. The transition may result from a defect state present in the crystal. Resonance Raman spectra of Pt_2Cl show evidence for fine structure that grows in when the excitation wavelength is tuned to the red of the IVCT band. This fine structure was attributed to a polaronic local state resulting from a deficiency of K^+ ions.[12] On the basis of the Peierls-Hubbard 3/4 filled band model developed by Baeriswyl and Bishop,[6] the energies of the defect electronic transitions are predicted to be to the blue as well as to the red of the IVCT band.

Intervalence Charge-Transfer Excitation. In the limit of a strongly trapped-valence material with a large distortion of the halogen from the central position, the IVCT band corresponds to $d\sigma^* \rightarrow d\sigma^*$ electron transfer along the chain axis from Pt_2 to an adjacent Pt_2X_2 (Figure 4.9). The energy of the IVCT band at ambient pressure in the trapped-valence Pt_2Cl complex is 18,600 cm^{-1}; it is significantly lower (16,100 cm^{-1}) in the more delocalized Pt_2Br complex. (The lower

the energy of the IVCT band, the more delocalized the complex.[16]) In Pt_2Cl and Pt_2Br, as the pressure increases, the IVCT band initially shifts strongly to lower energy and then appears to level off above 4.0 GPa (Figure 4.12). The initial red shift is approximately -750 cm^{-1} /GPa in Pt_2Cl and -1000 cm^{-1} /GPa in Pt_2Br. By way of comparison, the absorption edge of Wolfram's red salt shifts to lower energy at a rate of -1600 cm^{-1} /GPa up to 3.4 GPa.[5c]

The strong red shift of the IVCT band with increasing pressure is consistent with a continuous change toward a symmetric structure with the halogen located equidistant between adjacent Pt dimers. As the halogen becomes more centrally located, there will be a decrease in the energy difference between $d\sigma^*$ orbitals on adjacent Pt dimers. The red shift of the IVCT band will be further enhanced by a decrease in the halide distortion, because the extent of delocalization along the z axis will increase the band character of the $d\sigma^*$ orbitals. Band calculations by Whangbo and Canadell on a related MMX system support these conclusions.[13]

In interpreting pressure-induced changes of the IVCT band, it is important to separate the effects of structural changes from those of changes in orbital overlap. In this case we can establish an upper limit to the red shift caused by increasing overlap by comparing the shifts of the IVCT bands in Pt_2Cl and Pt_2Br. The red shift observed for the IVCT band in Pt_2Br is 4/3 times as large as that observed for Pt_2Cl. Accordingly, at least the increased red shift of the IVCT band in Pt_2Br is attributed to the movement of the Br atom towards the center position relative to the surrounding Pt_2 fragments.

Figure 4.12 Relative energy shifts of the IVCT bands in $[Pt_2(P_2O_5H_2)_4Br]^{4-}$ (ν_0 = 15,700, 16,200, and 16,400 cm^{-1}) and $[Pt_2(P_2O_5H_2)_4Cl]^{4-}$ (ν_0 = 18,400, 18,500, and 18,800 cm^{-1}).

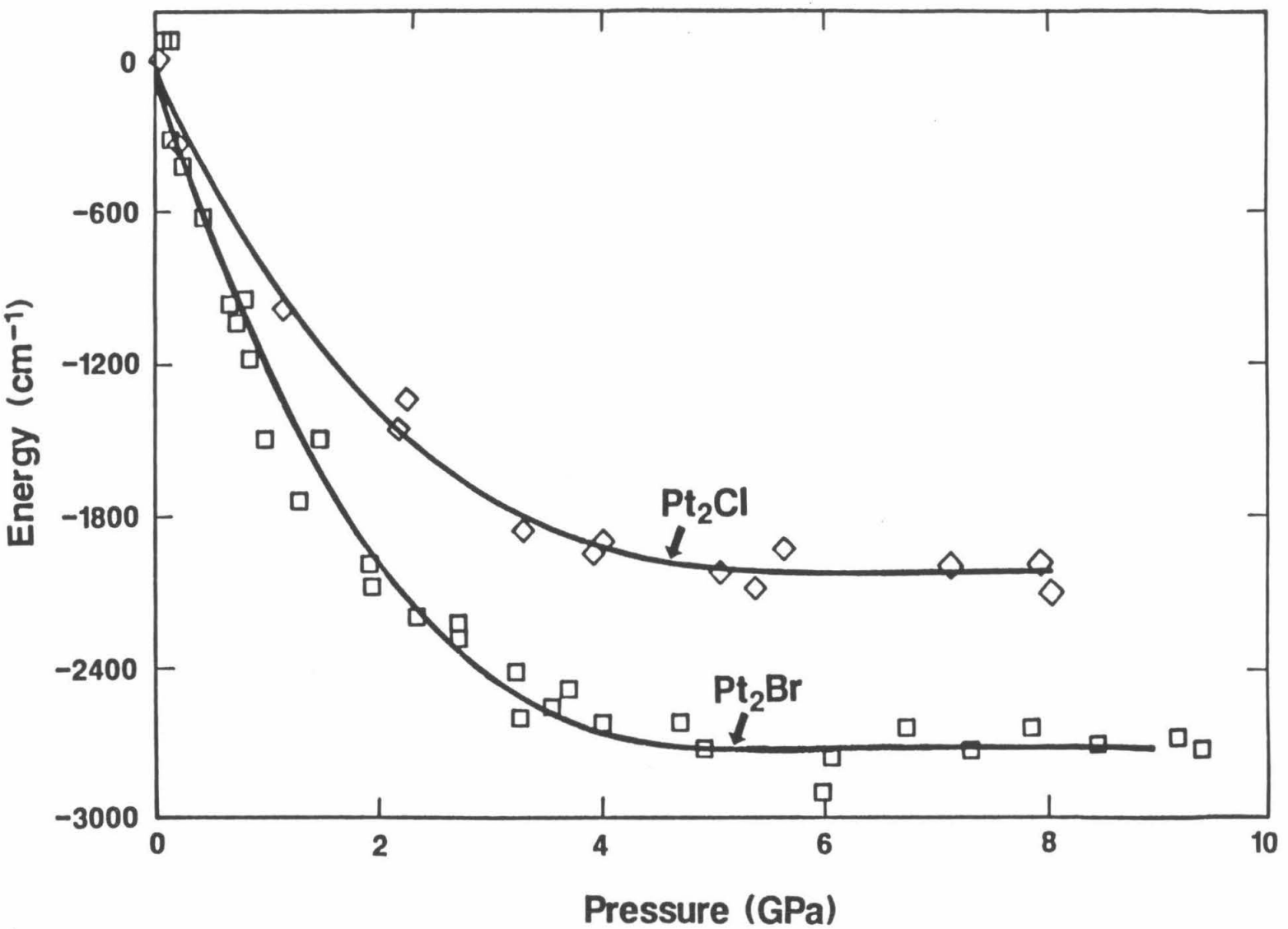
0
-600
-1200
-1800
-2400
-3000
Energy (cm^{-1})
0
2
4
6
8
10
Pressure (GPa)
Pt_2Cl
Pt_2Br

Comparisons of Pt_2Cl_2, Pt_2, and Pt_2X Transitions.

A pressure-induced blue shift of the $d_{xz},d_{yz} \rightarrow d\sigma^*$ transition in Pt_2Cl_2 of approximately 300 cm^{-1}/GPa was observed and a shift of 190 cm^{-1}/GPa can be inferred for Pt_2. It is reasonable for the $d\sigma^*$ orbital in Pt_2Cl_2 to be destabilized more rapidly than in Pt_2 because it is coupled to the halogen orbitals. By way of comparison, the $Mn_2(CO)_{10}$ $d_{xz},d_{yz} \rightarrow d\sigma^*$ transition blue shifts at an initial rate of 500 cm^{-1}/GPa in the solid state.[23] However, the pressure-induced shift of the transition in $Mn_2(CO)_{10}$ is influenced by stabilization of the $d\pi$ levels because of increased π-backbonding with the carbonyl ligands.

The pressure-induced shifts of the $d\sigma^* \rightarrow p\sigma$ transition in Pt_2, Pt_2Br, and Pt_2Cl are compared in Figure 4.13. A weak shift was observed in all three complexes; however, the direction of the shift varies, thereby indicating that there is a delicate balance among several competing effects. Increased coupling between the d_{z^2} and p_z orbitals, which may be somewhat larger in the monohalides because of the presence of the bridging halide, blue shifts $d\sigma^* \rightarrow p\sigma$. This appears to be the dominant effect in Pt_2Cl. The observed red shift in Pt_2Br can be explained in terms of band broadening of the $d\sigma^*$ and $p\sigma$ orbitals due to enhanced intermolecular interactions along the z axis. The band broadening should be larger in Pt_2Br than in Pt_2Cl, since Pt_2Br becomes delocalized more rapidly with increasing pressure.[24] A red shift of the $d\sigma^* \rightarrow p\sigma$ transition also results from an increase in coupling of $d\sigma^*$ with the phosphorus σ orbitals, an effect that becomes important in Pt_2 at high pressure.

Figure 4.13 Relative energy shifts of the $d\sigma^* \rightarrow p\sigma$ transition in $[Pt_2(P_2O_5H_2)_4Cl]^{4-}$, $[Pt_2(P_2O_5H_2)_4]^{4-}$, and $[Pt_2(P_2O_5H_2)_4Br]^{4-}$.

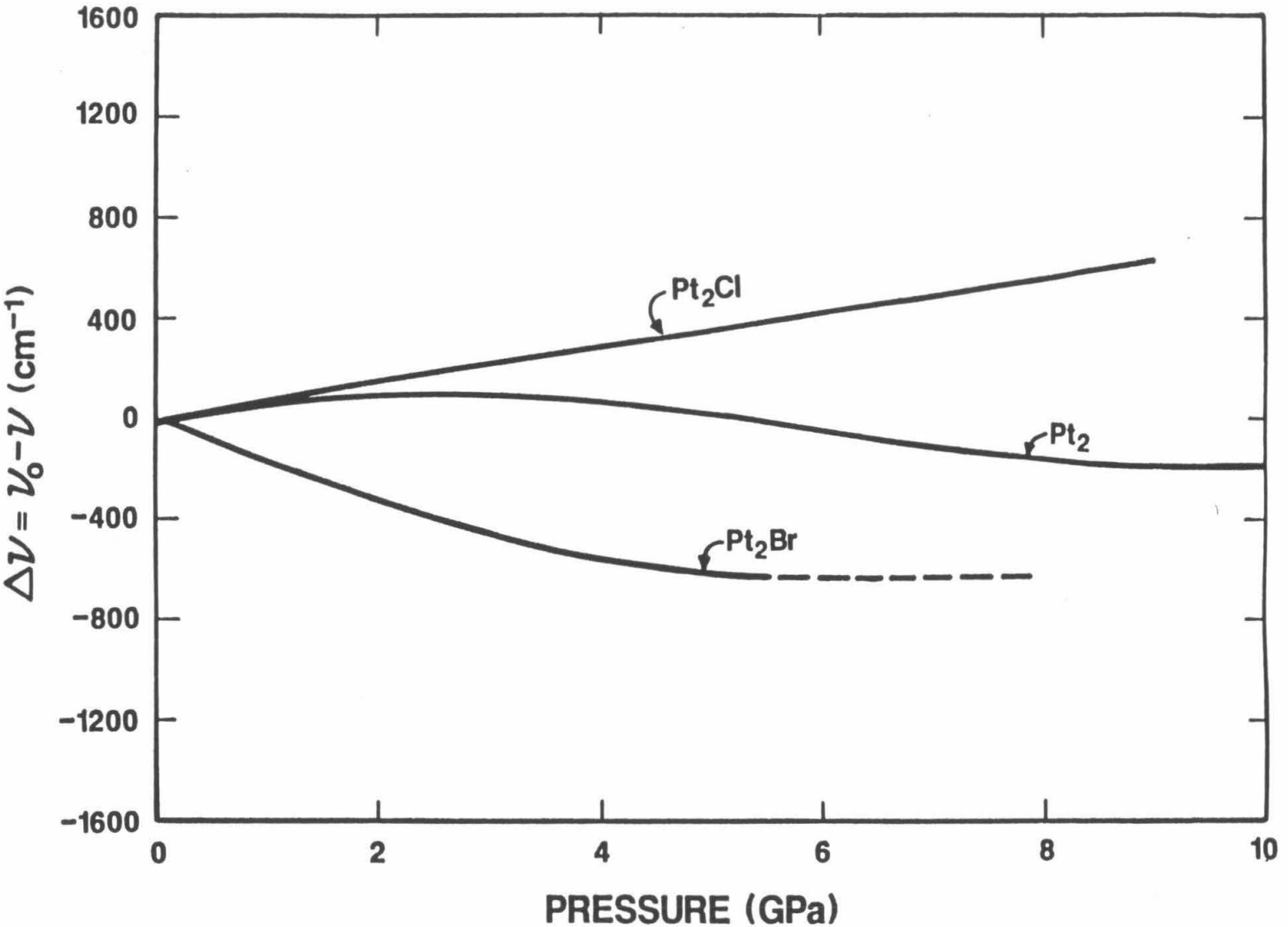
1600
1200
800
400
0
-400
-800
-1200
-1600
0
2
4
6
8
10
PRESSURE (GPa)
$\Delta\nu = \nu_0 - \nu$ (cm^{-1})
Pt_2Cl
Pt_2
Pt_2Br

REFERENCES

1. (a) Clark, R. J. H. *Ann. N. Y. Acad. Sci.* **1978**, *313*, 672. (b) Keller, H. J. *Extended Linear Chain Compounds;* J. S. Miller: Plenum: New York, 1982; pp 357. (c) Clark, R. J. H. *Advances in Infrared and Raman Spectroscopy;* Vol. 11, R. J. H. Clark and R. E. Hester: Wiley: Heyden, 1984; pp 95. (d) Clark, R. J. H. *Mixed Valence Compounds;* D. B. Brown: Reidel: Dordrecht, 1982; pp 271.
2. Clark, R. J. H.; Kurmoo, M. *J. Chem. Soc., Faraday Trans.* **1983**, *79*, 519.
3. Tanaka, M.; Kurita, V. *J. Phys. C.: Solid State Phys.* **1986**, *19*, 3019.
4. Conradson, S. D.; Dallinger, R. F.; Swanson, B. I.; Clark, R. J. H.; Croud, V. B. *Chem. Phys. Lett.* **1987**, *135*, 463.
5. (a) Tanino, H.; Koshizuka, N.; Hoh, K.; Yamashita, M.; Kobayashi, K. *Physica* **1986**, *39*, *140B*, 487. (b) Tanino, H.; Kobayashi, K; Yamashita, M. *Solid State Physics under Pressure;* S. Minomura: Terra Scientific Publ. Co., 1985; pp 115. (c) Tanino, H.; Koshizuka, N.; Kobayashi, K.; Yamashita, M.; Hoh, K. *J. Phys. Soc. Jpn.* **1985**, *54*, 483.
6. (a) Baeriswyl, D.; Bishop, A. R. *J. Phys. C: Solid State Phys.* **1988**, in press. (b) Baeriswyl, D.; Bishop, A. R. *Physics Scripta* **1988**, in press.
7. (a) Tanaka, M.; Kurita, S.; Koyima, T.; Yamada, Y. *Chem. Phys.* **1984**, *91*, 257. (b) Tanaka, M.; Kurita, S. *J. Phys. C. Solid State Phys.* **1986**, *19*, 3019, and references therein.
8. Ueta, M.; Kanzaki, H.; Kobayashi, K.; Toyozawa, Y.; Hanamura, E. *Excitonic Processes in Solids,* Vol. 60, Springer Series in Solid

State Sciences, Berlin, 1986, Ch.9.

9. Onodera, Y. *J. Phys. Soc. Jpn.* **1987**, *56*, 250.

10. Kurmoo, M.; Clark, R. J. H. *Inorg. Chem.* **1985**, *24*, 4420.

11. Che, C.-M.; Herbstein, F. H.; Schaefer, W. P.; Marsh, R. E.; Gray, H. B. *J. Am. Chem. Soc.* **1983**, *105*, 4604.

12. Conradson, S. D.; Stroud, M. A.; Zietlow, M. H.; Swanson, B. I.; Baeriswyl, D.; Bishop, A. R. *Solid State Communications*, **1988**, in press.

13. Whangbo, M.-H.; Canadell, E. *Inorg. Chem.* **1986**, *25*, 1726.

14. Butler, L. G.; Zietlow, M. H.; Che, C.-M.; Schaefer, W. P.; Sridhar, S.; Grunthaner, P. J.; Swanson, B. I.; Clark, R. J. H.; Gray, H. B. *J. Am. Chem. Soc.* **1988**, *110*, 1155.

15. Interrante, L. V.; Browall, K. W.; Bundy, F. P. *Inorg. Chem.* **1974**, *13*, 1158.

16. Clark, R. J. H. *Chem. Soc. Rev.* **1984**, *13*, 219.

17. Che, C.-M.; Schaefer, W. P.; Gray, H. B.; Dickson, M. K.; Stein, P. B.; Roundhill, D. M. *J. Am. Chem. Soc.* **1982**, *104*, 4253.

18. Che, C.-M.; Butler, L. G.; Grunthaner, P. J.; Gray, H. B. *Inorg. Chem.* **1985**, *24*, 4662.

19. The glitches that occurred in some of the electronic spectra at approximately 30,000 and 28,000 cm^{-1} were caused by the lamp change. The glitch at approximately 21,000 cm^{-1} was caused by a grating anomaly.

20. Che, C.-M.; Mak, T. C.; Miskowski, V. M.; Gray, H. B. *J. Am. Chem. Soc.* **1986**, *108*, 7840.

21. Stiegman, A. E.; Rice, S. F.; Gray, H. B.; Miskowski, W. M. *Inorg. Chem.* **1987**, *26*, 1112.

22. Isci, H.; Mason, W. R. *Inorg. Chem.* **1985**, *24*, 1761.

23. Carroll, T. L.; Shapley, J. R.; Drickamer, H. G. *Chem. Phys. Lett.* **1985**, *119*, 340.

24. (a) Stroud, M. A.; Swanson, B. I., manuscript in preparation. (b) See IVCT section of this article. (c) Swanson, B. I.; Stroud, M. A.; Conradson, S. D.; Zietlow, M. H. *Solid State Communications* **1988**, in press.

CHAPTER 5

Photophysics of $[Pt_2(\mu\text{-dppm})_2Y_2]^{n+}$

(Y = Cl, Br; n = 0 or Y = PPh_3, PPh_2Me, $PPhMe_2$; n = 2)

INTRODUCTION

Adjacent coordination sites are necessary for concerted, small molecule addition to a photo-excited metal center to occur. $Pt_2(\mu\text{-dppm})_2Cl_2$ (dppm = bis(diphenylphosphino)methane) and its analogs are good candidates for the study of this type of reactivity. The ligand arrangement about each platinum metal center is square planar with each platinum atom acting as the other platinum's fourth ligand.[1,2] The two bridging dppm ligands are opposite of one another; thus, unlike in the unbridged d^9-d^9 complex $Pt_2(CNCH_3)_6^{2+}$ which adopts a staggered structure,[3] this molecule adopts a more planar (or eclipsed) structure with an ~40° degree twist (see Figure 1.4). Overall, these bridged complexes have four sites available for substrate addition, two adjacent sites above and two below the molecular plane.

These molecules are known to possess a rich thermal chemistry dominated by small molecule addition across the metal-metal bond[4-10] (see Figure 1.5). For example, reacting $Pt_2(\mu\text{-dppm})_2Cl_2$ with CS_2 results in the formation of an A-frame d^8-d^8 dimer in which the CS_2 group bridges the metal centers through a carbon and a sulfur atom.[7]

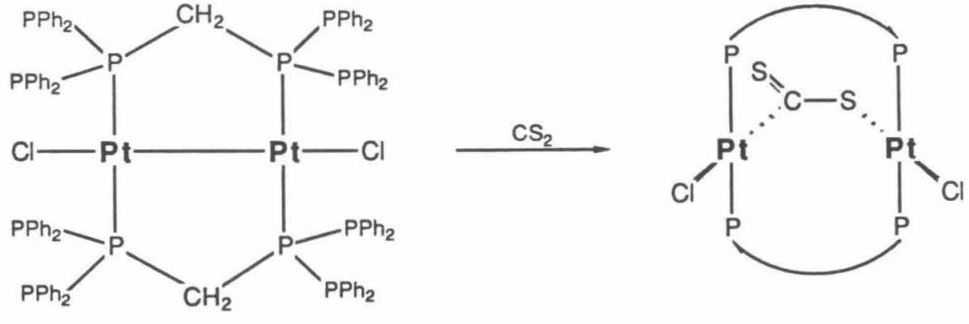

Although the thermal reactivity of these complexes have been explored, no investigations into their photochemistry have been reported.

Having the necessary structural requirements for concerted, small molecule addition, it is worthwhile to evaluate the photochemical potential of this system by gaining some understanding of the nature of the excited state and the factors which govern its reactivity.

EXPERIMENTAL

Materials

All solvents used in the synthesis reactions were used as received without further purification. Solvents used in spectroscopic experiments were purified, if necessary, dried, freeze/pump/thaw degassed (4 cycles), then bulb-to-bulb distilled under vacuum into storage flasks (glass solvent pots equipped with teflon vacuum valves) and again freeze/pump/thaw degassed (3 cycles). Dichloromethane (Burdick and Jackson, UV grade) was dried over calcium hydride and stored over freshly activated Linde 3A molecular sieves. The sieves were activtated by heating under dynamic vacuum ($<10^{-3}$ Torr) for 24 - 48 hours. Significant purification of 2-methyltetrahydrofuran, 2-MeTHF, (Aldrich, 99%) was necessary. The 2-MeTHF was first distilled from a 0.5% suspension of $CuCl_2$ followed by distillation from potassium hydroxide pellets. Finally the 2-MeTHF was dried over calcium hydride and stored over sodium metal and benzophenone. Absolute ethanol (USI Chemicals Co., punctillious) was dried over sodium metal and stored over freshly activated 3A Linde molecular sieves. Methanol (Burdick and Jackson, UV grade) was stored over freshly activated Linde 3A molecular sieves.

Pt(dppm)Cl$_2$: K_2PtCl_4 (Aldrich, 98%) and bis(diphenylphosphino)-methane, dppm, (Aldrich, 97%) were used to prepare Pt(dppm)Cl_2 by a method similar to that used by Westland to prepare Pt(dppe)Cl_2 (dppe = 1,2-bis(diphenylphosphino)ethane).[11] K_2PtCl_4 (0.50 g) and dppm (0.45 g) were refluxed in a mixture of 17 mL ethanol and 17 mL concentrated HCl for 4 1/2 hours. During the course of the reaction the desired product precipitated from the hot mixture as a fine powder. The reaction was completed when the initial red color of K_2PtCl_4 disappeared

and only the white powder product remained. The product was clean and further purification was not necessary. (If desired, the complex may be recrystallized from hot dimethylformamide, DMF, by adding a mixture of petroleum ether and diethyl ether.) The yield is essentially 100%. [Analysis calculated for $Pt_2(dppm)Cl_2$ (%): C, 46.17; H, 3.41. Found: C, 45.99; H, 3.43.]

$Pt_2(\mu\text{-}dppm)_2Cl_2$: The procedure of Brown *et al.*[12] was followed with slight modification. $Pt(dppm)Cl_2$ (1.2 g) was suspended in 20 mL of nitrogen purged ethanol in a round bottom flask equipped with a stir bar. Sodium borohydride, $NaBH_4$, (0.5 g) was suspended in 15 mL of nitrogen purged ethanol in an addition funnel. Over a 40 - 60 minute period, the $NaBH_4$ mixture was added dropwise to the $Pt(dppm)Cl_2$ mixture with rapid stirring; the white mixture began to take on a yellow-brown tinge during the addition. After all the $NaBH_4$ was added, the mixture was stirred for another 5 minutes, then filtered. The solid was rinsed with methanol and water to get rid of any unreacted $NaBH_4$. The impure $[Pt_2(\mu\text{-dppm})_2(\mu\text{-H})(H)_2]Cl$ solid was prepared for the next reaction step by futher rinsing with ethanol, diethyl ether, and lastly benzene. (On occasion, the impure $[Pt_2(\mu\text{-dppm})_2(\mu\text{-H})(H)_2]Cl$ was dried *in vacuo* for 1 hour as suggested in the original procedure.)[12] Next, impure $[Pt_2(\mu\text{-dppm})_2(\mu\text{-H})(H)_2]Cl$ (1.0 g) was supended in 45 mL of benzene and 1.5 mL concentrated HCl and refluxed for 15 minutes. The hot yellow solution was decanted off from the red-brown residue, allowed to cool, and precipitated by adding ~15 mL iso-octane. The final product recrystallized as the lemon-yellow benzene solvate $Pt_2(\mu\text{-dppm})_2Cl_2 \cdot C_6H_6$ in ~70% yield. In most instances, the benzene solvate obtained directly from the reaction was pure; however if further cleaning was necessary,

there were several methods of purification depending upon which solvate was desired. Compounds studied gave acceptable elemental analysis and clean NMR spectra which matched published results.

$Pt_2(\mu\text{-dppm})_2Cl_2$ dissolves in only a few solvents, mainly halocarbons. Recrystallizing $Pt_2(\mu\text{-dppm})_2Cl_2$ from the solvent of choice and precipitating with iso-octane will yield crystals of $Pt_2(\mu\text{-dppm})_2Cl_2$ with the corresponding solvate. $Pt_2(\mu\text{-dppm})_2Cl_2 \cdot C_6H_6$ is not soluble in benzene. If the sample obtained from the reaction mixture needs to be cleaned and the benzene solvate is desired, any impurities present must be washed from the solid. The easiest way to remove the impurities is to stir a suspension of $Pt_2(\mu\text{-dppm})_2Cl_2 \cdot C_6H_6$ in boiling benzene for ~15 minutes, then filter. Repeat this procedure as often as necessary to obtain pure product.

Occasionally during the course of recrystallization, white crystalline specks were observed in addition to the desired yellow $Pt_2(\mu\text{-dppm})_2Cl_2 \cdot$solvate crystals. The white impurity is believed to be $[Pt_2(\mu\text{-dppm})_2(\mu\text{-H})Cl_2]Cl$. Addition of a few drops of triethylamine, NEt_3, clears up this contamination problem.

$Pt(\mu\text{-dppm})_2Br_2 \cdot 0.5CH_2Cl_2$, $[Pt_2(\mu\text{-dppm})_2(PPh_3)_2](PF_6)_2$, $[Pt_2(\mu\text{-dppm})_2(PPh_2Me)_2](PF_6)_2$, $[Pt_2(\mu\text{-dppm})_2(PPhMe_2)_2](PF_6)_2$: These platinum complexes were prepared by the published procedures.[12,13]

$Pd_2(\mu\text{-dppm})_2Cl_2$: This palladium complex was prepared by method 2 of the published procedure.[8]

Physical Measurements

Electronic Absorption Spectropscopy: Electronic absorption spectra were measured using a Cary Model 17 or Shimatzu UV-260 spectrophoto-

meter. Low temperature, 77 K, electronic absorption spectra were measured using the Cary Model 17 spectrophotometer equipped with a quartz optical dewar (copper block base). Samples for the absorption measurements were prepared by placing $Pt_2(\mu\text{-dppm})_2Cl_2$ (~1 mg) into an extra long spectrophotometric cell consisting of a square cuvette (1 cm pathlength) and a teflon vacuum valve.

Emission and Excitation Spectroscopy: Emission spectra were recorded using an emission spectrophotometer constructed at Caltech and described elsewhere.[14] Samples for these measurements (solids and solutions) were placed in NMR tubes equipped with a 14/20 ground glass joint and capped with a septum. Samples were run in aerated, N_2 purged, and degassed solutions; no significant differences were observed. Emission and excitation spectra were measured using a Perkin-Elmer spectrofluorimeter MPF-66 interfaced to a Perkin-Elmer computer. Emission and excitation spectra measured at 77 K were obtained by placing the sample in an NMR tube and immersing the tube in a liquid-nitrogen-filled quartz finger dewar. Samples for these measurements were placed in 3 mm (o.d.) quartz EPR tubes capped with a septum and parafilm. Lower temperature emission and excitation spectra (down to 16 K) were measured by placing the solid sample (adhered on a quartz disk with silicon grease) into a CTI Model 21 cryocooler. The temperature inside the cryocooler was varied with a small resistive heater; a chromel/Au-Fe thermocouple was used to measure the temperature.

Emission Lifetime Measurements: Luminescent lifetime data were collected using a pulsed Nd:YAG laser system described previously.[15] The third harmonic (355 nm) was used as the excitation line. Low

temperature, 77 K experiments were carried out using the before mentioned liquid-nitrogen-filled quartz finger dewar. Samples for these measurements (solids and solutions) were placed in NMR tubes equipped with a 14/20 ground glass joint and capped with a septum. Samples were run in aerated, N_2 purged, and degassed solutions; no significant differences were observed. Variable temperature experiments were performed using a continuous-flow nitrogen gas dewar in which the nitrogen gas was cooled by travelling through copper tubing immersed in a liquid-nitrogen-filled dewar. The temperature was regulated by the speed of gas flow and measured by a copper *vs.* copper nickel (copper-constantan) thermocouple. Variable temperature samples were placed in extra long 5 mm (o.d.) quartz EPR tubes and capped with a septum and parafilm.

Other. Elemental analyses were performed by Mr. Larry Henling and Mr. Fenton Harvey at the Caltech Analytical Laboratory, Pasadena, California.

RESULTS and DISCUSSION

In order to discuss the origin of the chemical reactivity of these d^9-d^9 dimers, a description of their electronic distribution would prove useful; however no detailed molecular orbital (MO) diagram for these systems has been proposed. There may be several reasons for this, one being that the electronic absorption spectra of these complexes are quite complicated and the bands are not well resolved, making the measurement of exact band maxima, peak intensities, and band widths difficult.

A plausible MO diagram may be constructed from MO diagrams of monomeric d^{10} complexes which possess similar geometries and ligand environments. The MO diagram for $[Au(PEt_3)_2]^+$ is shown in Figure 5.1a.[16] Bringing two such diagrams together along the x-axis (designated as the metal-metal bonding axis) results in the diagram illustrated in Figure 5.1b. When axial ligands are added to $Pt_2(P_2O_5H_2)_4^{4-}$, the resulting d^7-d^7 MO diagram has the same basic orbital ordering as the d^8-d^8 MO diagram except with two additional $\sigma(X)$ orbitals and two fewer metal localized electrons (see Figures 4.1 and 4.4). Therefore, addition of axial halides to the d^{10}-d^{10} MO diagram constructed in Figure 5.1b, along the x axis, will most likely change the energies of several of the levels, without perturbing the orbital ordering very much. The MO diagram presented in Figure 5.1c takes these perturbations into account.

From Figure 5.1c, the highest occupied molecular orbital, HOMO, is expected to be $\delta^*(d_{z^2})$. However, depending upon how close the monomer d_{z^2} and d_{xy}, $d_{x^2-y^2}$ levels are, the possiblity that $\pi^*(d_{xy})$ is the HOMO cannot be completely ruled out.

Figure 5.1 (a) Molecular orbital diagram for MP_2 (taken from reference 16).

(b) Proposed molecular orbital diagram for $(MP_2)_2$.

(c) Proposed molecular orbital diagram for $(MP_2)_2X_2$.

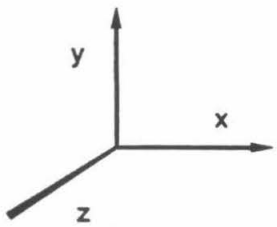
y
x
z

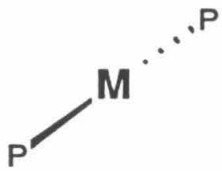
P
M
P

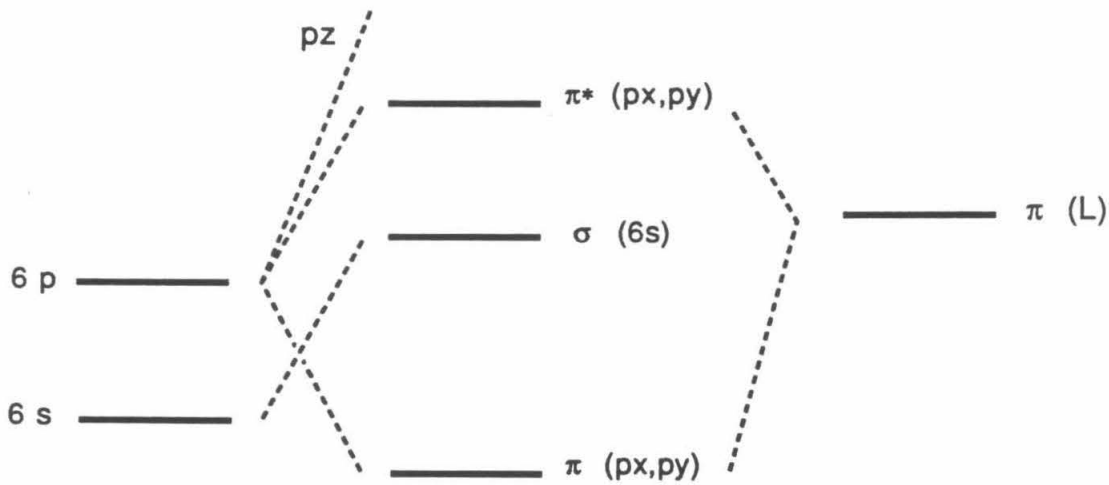
pz
π* (px,py)
σ (6s)
π (px,py)
π (L)
6 p
6 s

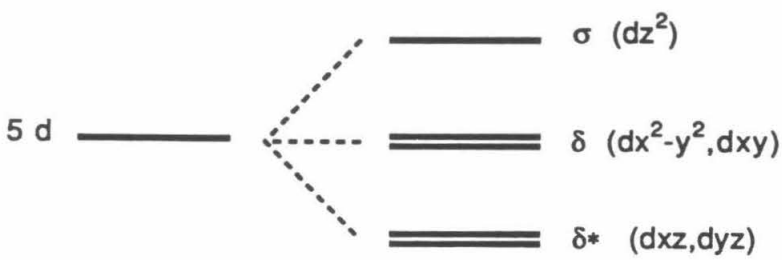
σ (dz²)
δ (dx²-y²,dxy)
δ* (dxz,dyz)
5 d

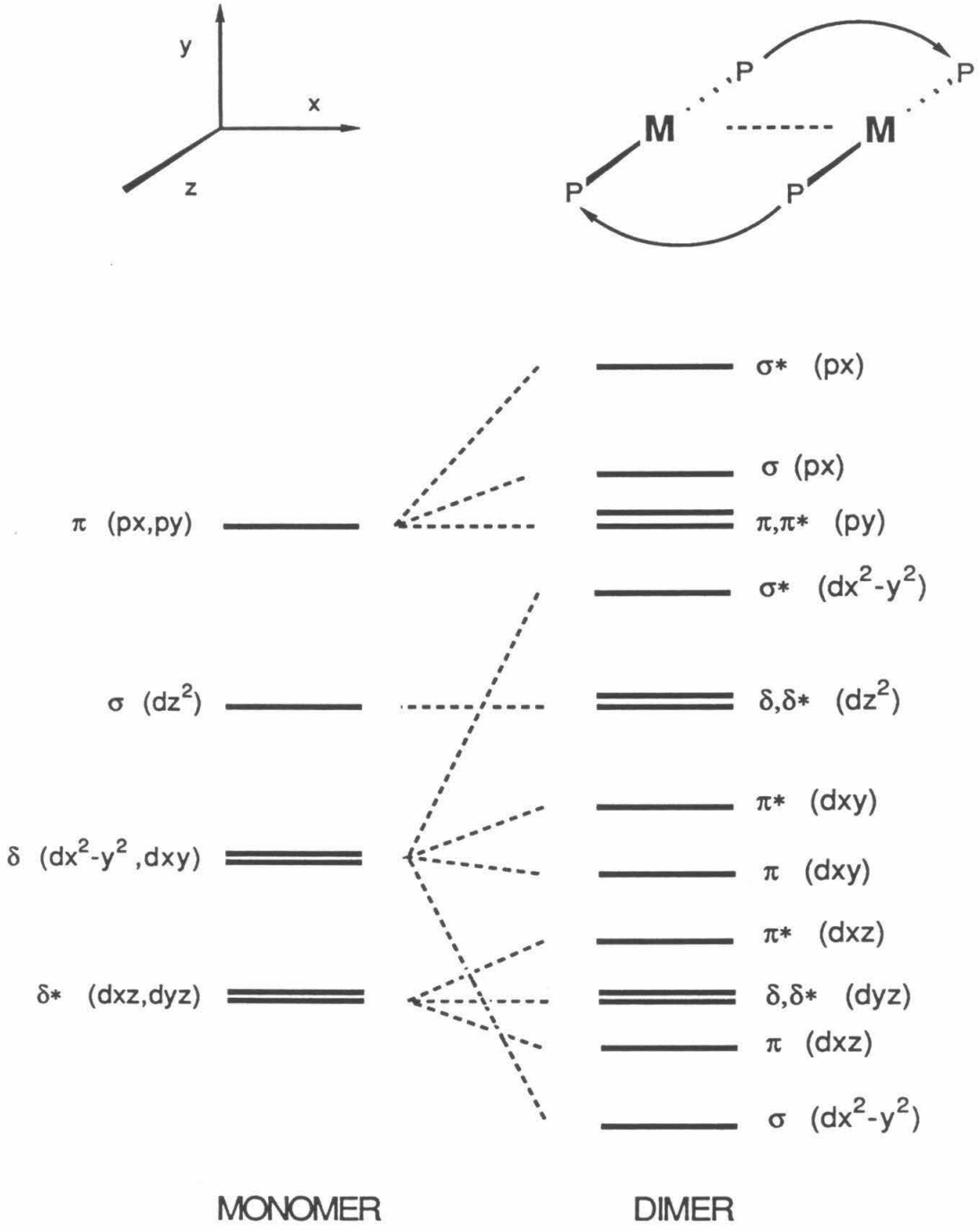
y
x
z
P
P
M
M
P
P
σ* (px)
σ (px)
π (px,py)
π,π* (py)
σ* (dx²-y²)
σ (dz²)
δ,δ* (dz²)
π* (dxy)
δ (dx²-y², dxy)
π (dxy)
π* (dxz)
δ* (dxz,dyz)
δ,δ* (dyz)
π (dxz)
σ (dx²-y²)
MONOMER
DIMER

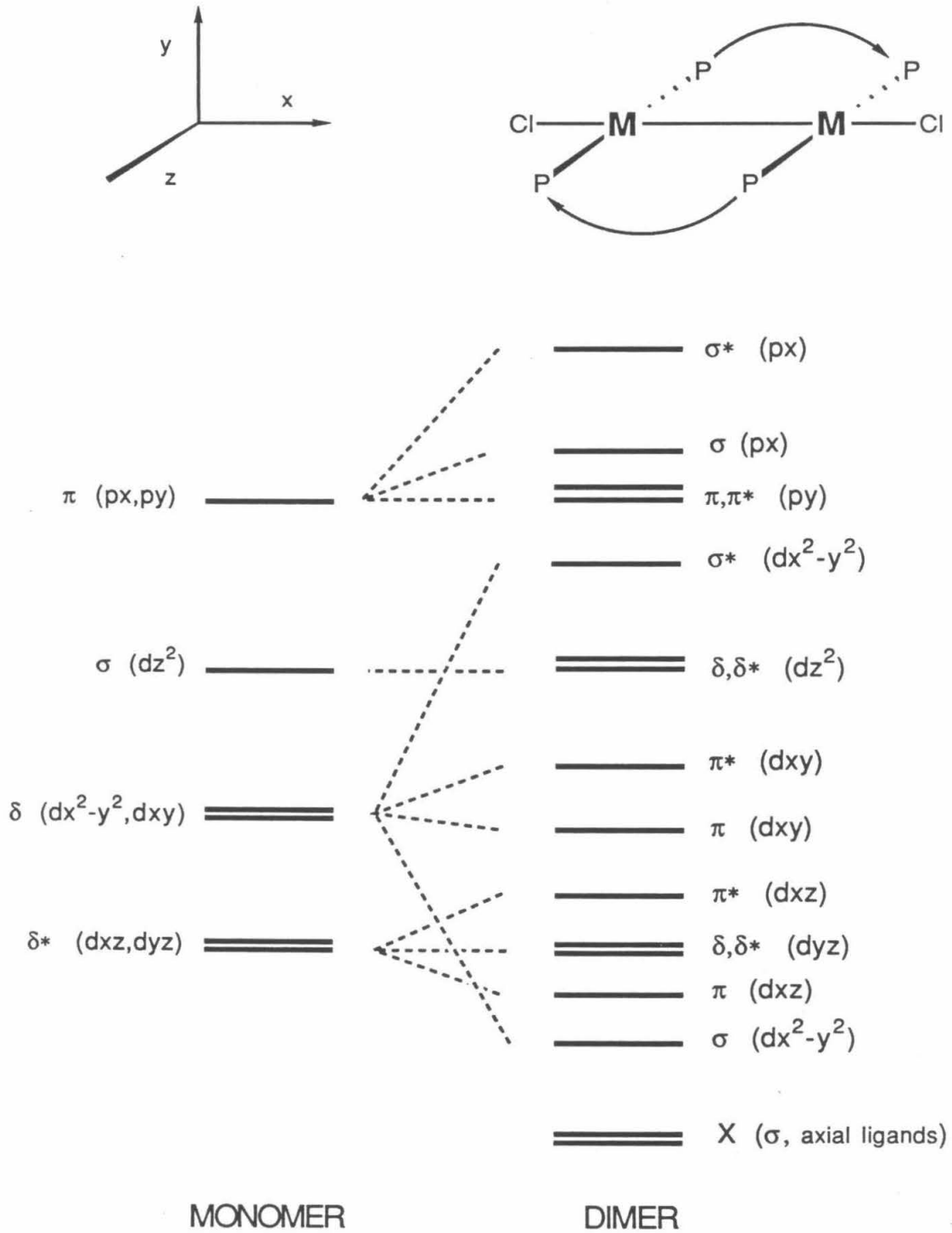
y
x
z
Cl
M
M
Cl
P
P
P
P
σ* (px)
σ (px)
π (px,py)
π,π* (py)
σ* (dx²-y²)
σ (dz²)
δ,δ* (dz²)
π* (dxy)
δ (dx²-y²,dxy)
π (dxy)
π* (dxz)
δ* (dxz,dyz)
δ,δ* (dyz)
π (dxz)
σ (dx²-y²)
X (σ, axial ligands)
MONOMER
DIMER

The lowest unoccupied molecular orbital, LUMO, is predicted to be $\sigma^*(d_{x^2-y^2})$; however, the π(py) orbital cannot be immediately excluded from consideration. In d^{10}-d^{10} systems the HOMO level is $d\sigma^*(d_{x^2-y^2})$ and the LUMO is p_x,p_y; however addition of the axial halide along the x axis in this d^9-d^9 systems may raise the $d\sigma^*(d_{x^2-y^2})$ level up sufficiently, making the $\pi(p_y)$ level lower in energy. On the other hand, photochemically induced oxidative-addition reactions of unbridged d^9-d^9 systems[17-19] show metal-metal bond cleavage and production of Pt(II) $15e^-$ radical species as the predominant reaction intermediate. Similarly, in bridged systems, where the dissociative pathway is unlikely, substrate addition across the metal-metal bond occurs with net metal-metal bond cleavage.[4-6] Therefore, the assignment of the LUMO as $d\sigma^*(d_{x^2-y^2})$ is given additional support considering the observed thermal and photochemical reactivity.

Group theory analysis of the proposed MO diagram predicts several orbitally allowed electronic transitions which are listed in Table 5-1. The first six transitions are most likely to be the lowest energy transition assuming that the σ^* $(d_{x^2-y^2})$ and $\pi\pi^*$ (p_y) orbitals are close in energy.

Crystals of the platinum(I) complexes are yellow in color; whereas, the palladium(I) analogs are more intensely orange colored. The room temperature electronic absorption spectrum of $Pt_2(\mu\text{-dppm})_2Cl_2$ in dichloromethane first reported by Alves *et al.*[20] is shown in Figure 5.2. Three bands are observed; however, they are not well resolved and do not allow for any theoretical analysis. Electronic absorption band maxima of $Pd_2(\mu\text{-dppm})_2Cl_2$ have been reported by Benner *et al.*;[8] the

Figure 5.2 Electronic absorption spectrum of $Pt_2(\mu\text{-dppm})_2Cl_2$ in dichloromethane (300 K).

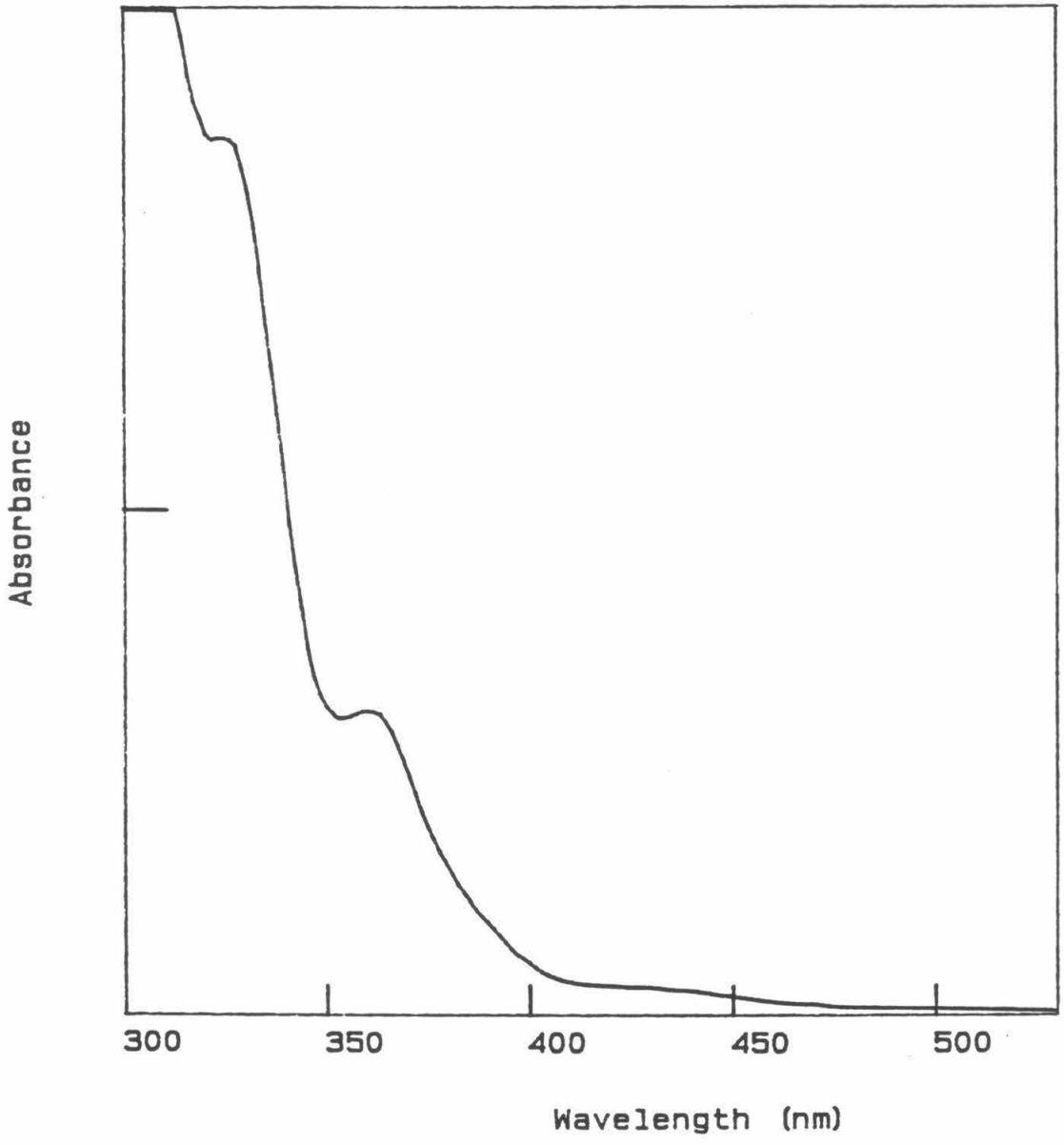
Absorbance
300
350
400
450
500
Wavelength (nm)

Figure 5.3 Electronic absorption spectrum of $Pd_2(\mu\text{-dppm})_2Cl_2$ in dichloromethane (300 K).

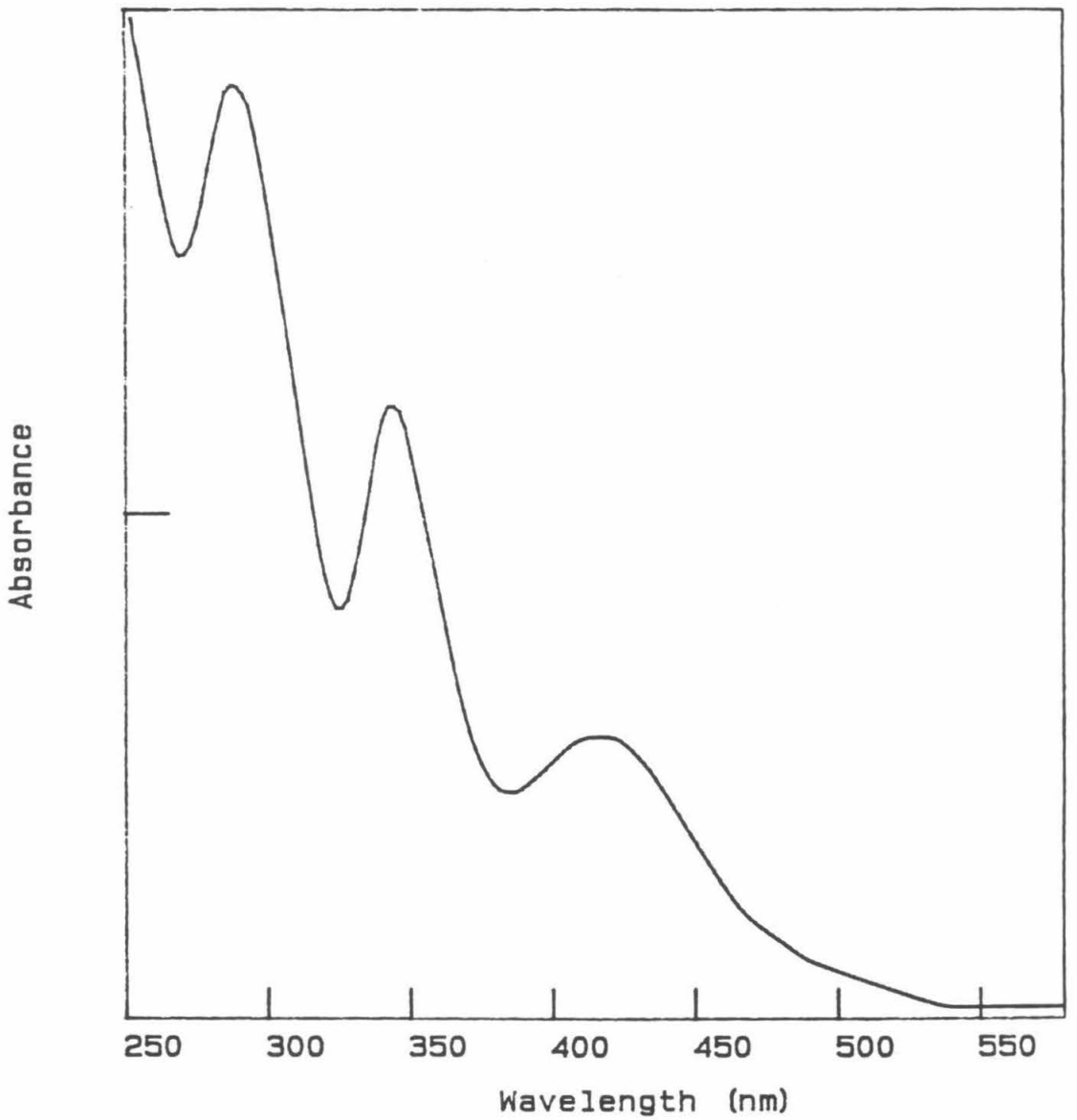
Absorbance
250
300
350
400
450
500
550
Wavelength (nm)

actual spectrum is shown in Figure 5.3. In this spectrum two absorption bands at lower energy are fairly well resolved with a shoulder at higher energy. Surprisingly, the absorption band shapes and extinction coefficients for the platinum(I) and palladium(I) dimers do not look as similar as might be expected for such closely related complexes. More than likely the observed absorption bands do not correspond to the same transitions in the platinum and palladium systems.

Luminescence from the platinum(I) dimers is observed only in the solid state and frozen solution. Similar luminescence is not observed in the analogous palladium system. It was necessary to confirm that the d^9-d^9 molecule present in solution was the species responsible for the observed luminescence, since highly luminescent d^8-d^8 and d^{10}-d^{10} platinum complexes are known and may have been present in trace quantities. Comparison of the excitation spectra of $Pt_2(\mu\text{-dppm})_2Cl_2 \cdot 0.5CH_2Cl_2$ and $Pt_2(\mu\text{-dppm})_2Br_2 \cdot 0.5CH_2Cl_2$ with their absorption spectra verified that the observed luminescence was definitely arising from these d^9-d^9 dimers. (The low temperature solid emission and excitation spectra for $Pt_2(\mu\text{-dppm})_2Cl_2 \cdot 0.5CH_2Cl_2$ and $Pt_2(\mu\text{-dppm})_2Br_2 \cdot 0.5CH_2Cl_2$ are shown in Figures 5.4 and 5.5, respectively.)

The low temperature solid excitation spectrum of $Pt_2(\mu\text{-dppm})_2Cl_2$ revealed the presence of additional electronic transitions at ~380 and ~465 nm which were either completely masked or too weak to detect in solution. This observation prompted further investigation into the electronic absorption spectrum of $Pt_2(\mu\text{-dppm})_2Cl_2$. At low temperature, 77 K, in a 1:1 CH_2Cl_2:2-MeTHF glass (Figure 5.6), the absorption band at 380 nm begins to be resolved, but the absorption band at ~465 nm is

Figure 5.4 (a) Corrected emission spectrum of $Pt_2(\mu\text{-dppm})_2Cl_2 \cdot 0.5CH_2Cl_2$, powder sample, 21 K. Emission maximum at 714 nm.

(b) Corrected excitation spectrum of $Pt_2(\mu\text{-dppm})_2Cl_2 \cdot 0.5CH_2Cl_2$, powder sample, 21 K. Absorption maxima at 465, 429, and 389 nm.

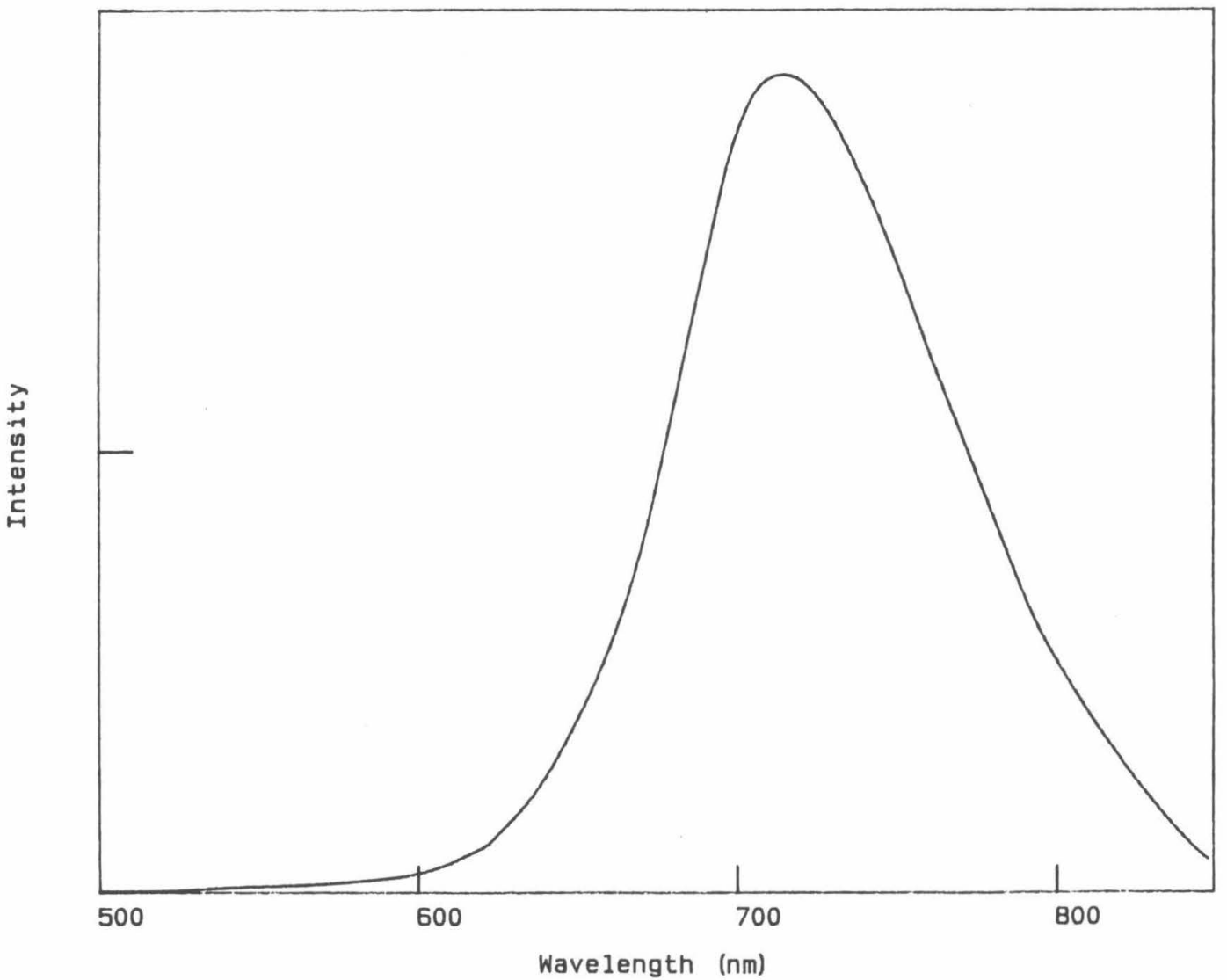
Intensity
500
600
700
800
Wavelength (nm)

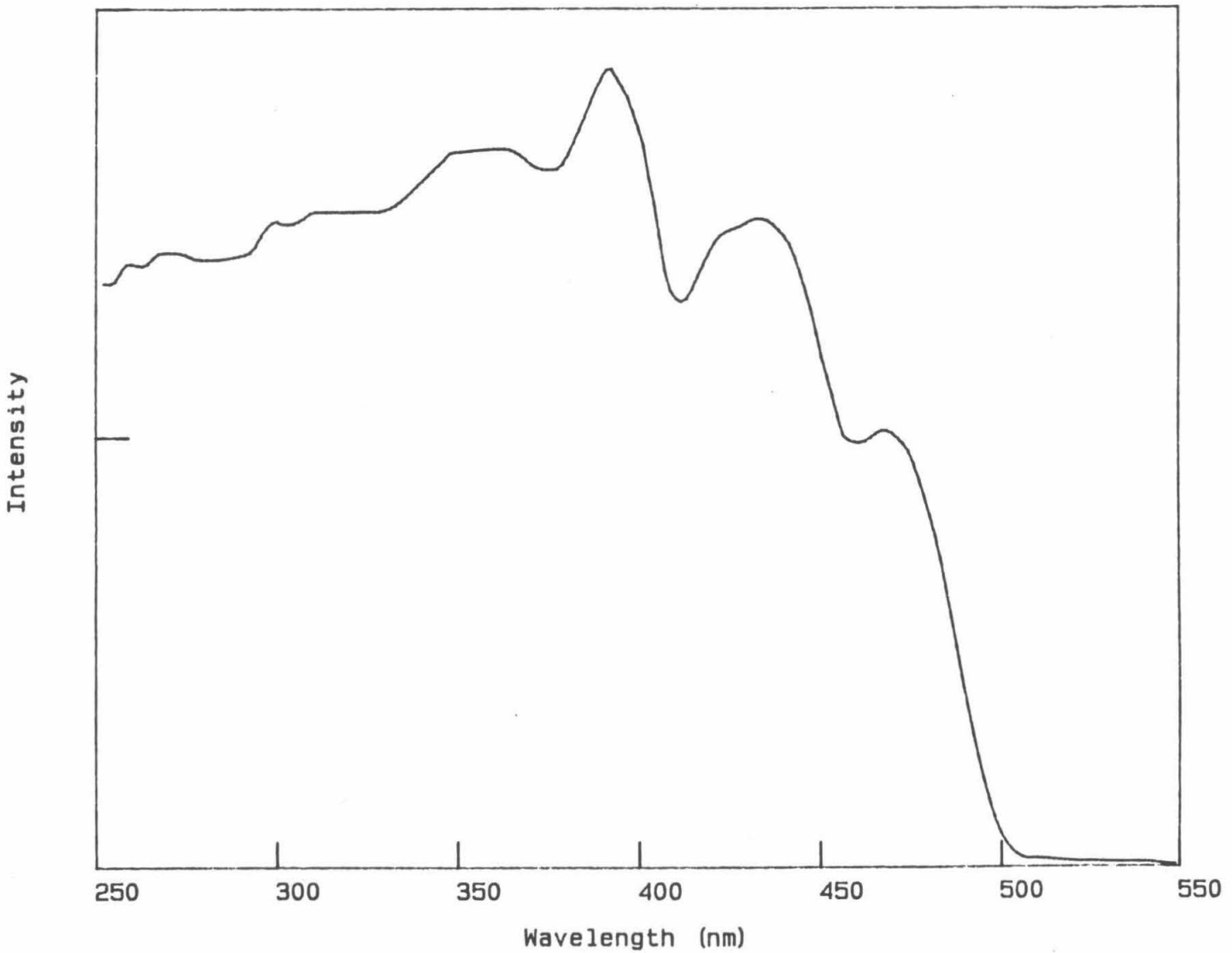
Intensity
250
300
350
400
450
500
550
Wavelength (nm)

Figure 5.5 (a) Corrected emission spectrum of $Pt_2(\mu\text{-dppm})_2Br_2 \cdot 0.5CH_2Cl_2$, powder sample, 16 K. Emission maximum at 716 nm.

(b) Corrected excitation spectrum of $Pt_2(\mu\text{-dppm})_2Br_2 \cdot 0.5CH_2Cl_2$, powder sample, 16 K. Absorption maxima at 478, 441, 390 nm.

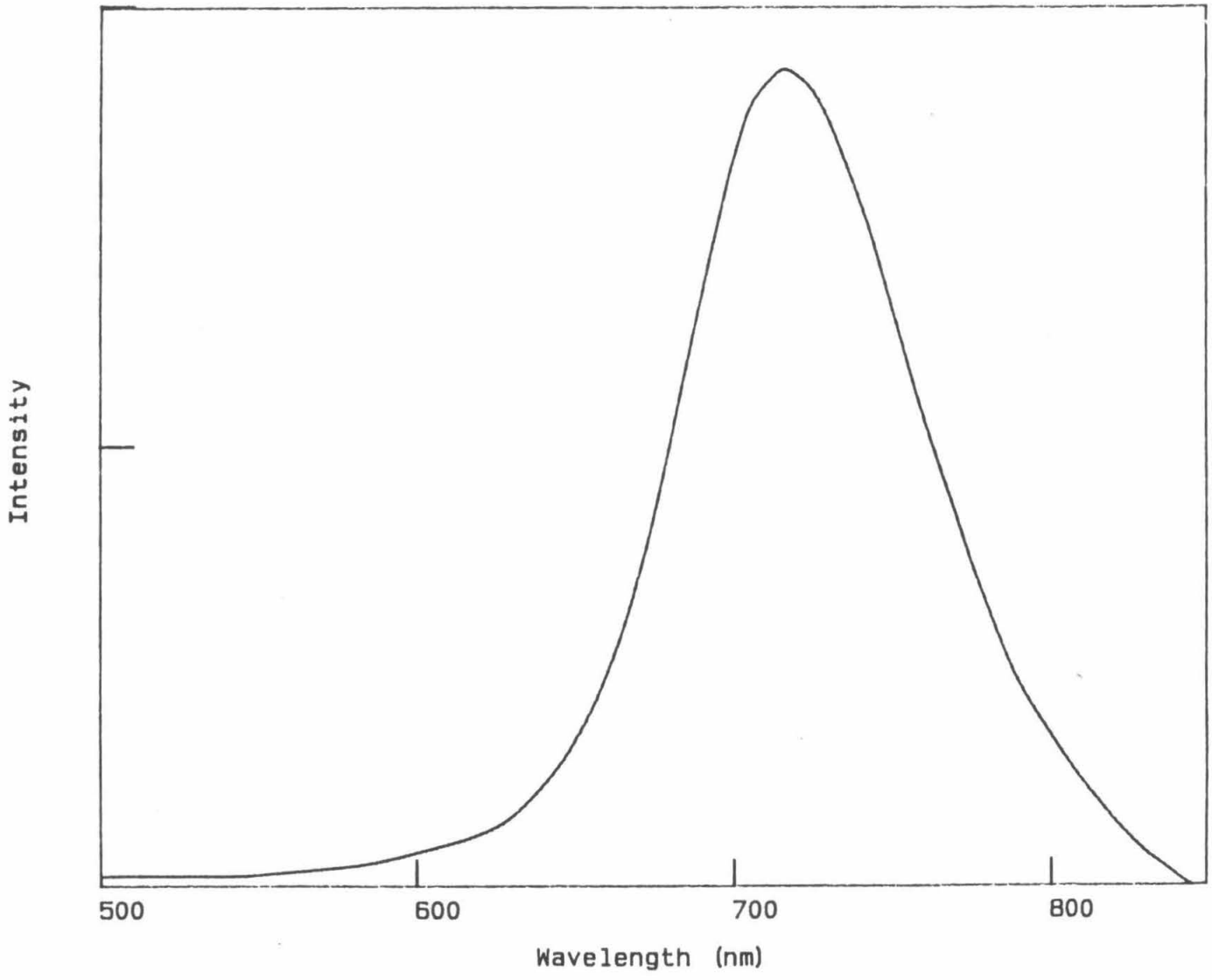
Intensity
500
600
700
800
Wavelength (nm)

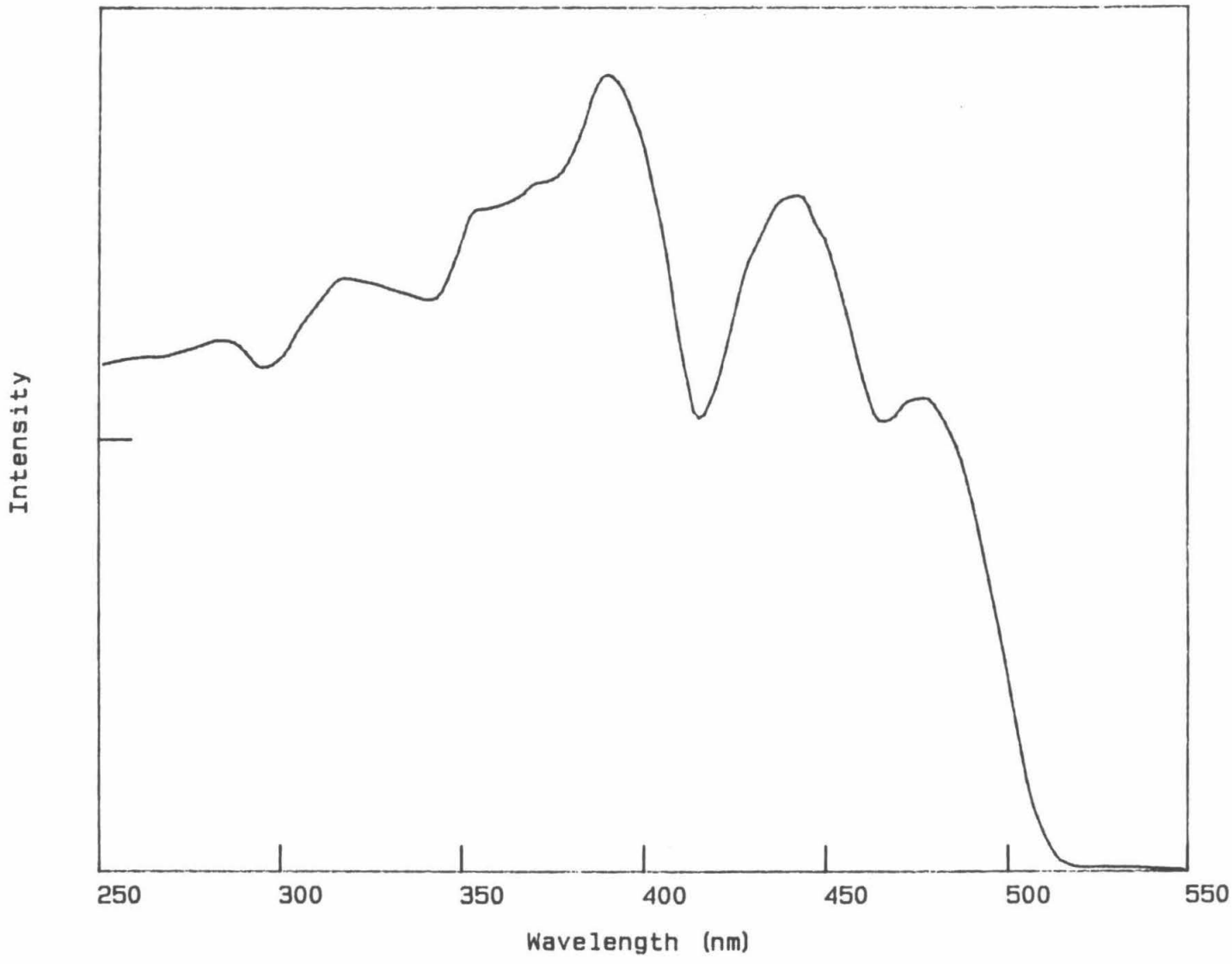
Intensity
250
300
350
400
450
500
550
Wavelength (nm)

Figure 5.6 Electronic absorption spectrum of $Pt_2(\mu\text{-dppm})_2Cl_2$ in a 1:1 dichloromethane:2-methyltetrahydrofuran glass (v/v) at 77 K.

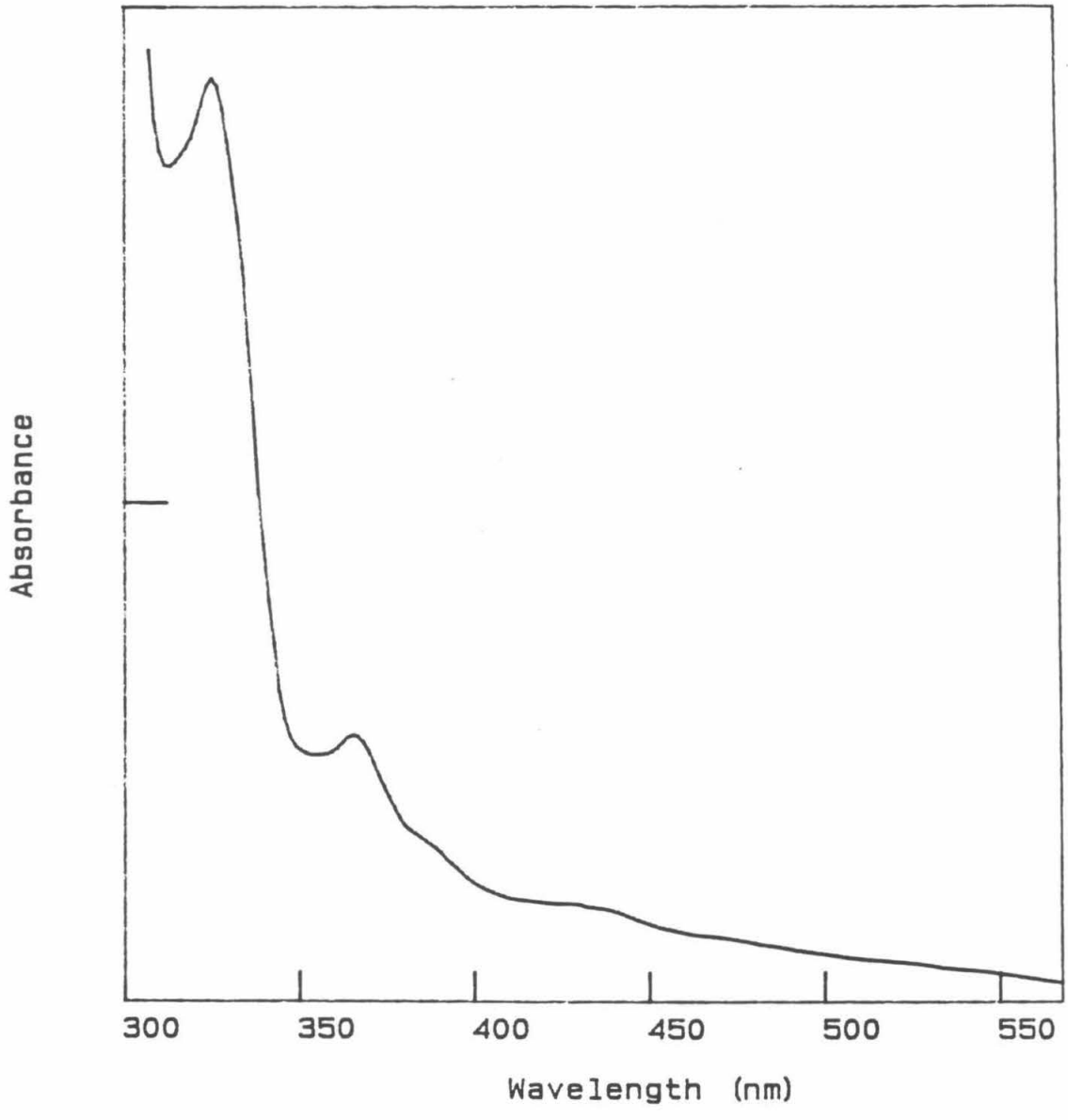
Absorbance
300
350
400
450
500
550
Wavelength (nm)

still too weak to be detected. It appears that single crystal electronic absorption measurements will be required to observe the absorption bands at wavelengths longer tnan 450 nm. Thus, at present, it seems reasonable to estimate that the 465 nm absorption, observed in the solid state excitation spectrum, of $Pt_2(\mu\text{-dppm})_2Cl_2$ is much less than 100 M^{-1} cm^{-1}. (A similar argument may be made for the absorption band at ~478 nm observed in the solid state excitation spectrum of $Pt_2(\mu\text{-dppm})_2Br_2$.)

The extinction coefficients of the two low energy absorption bands of $Pt_2(\mu\text{-dppm})_2Cl_2$ at 427 nm (ε = 200 M^{-1} cm^{-1})[20] and 465 nm (ε < 100 M^{-1} cm^{-1}) indicate that these transitions are most likely spin forbidden, orbitally allowed transitions such as $^3[\delta^*(d_{z^2}) \rightarrow \pi^*(py)]$ or $^3[\delta(d_{z^2}) \rightarrow \sigma^*(d_{x^2-y^2})]$ or spin allowed, orbitally forbidden transitions such as $^1[\delta^*(d_{z^2}) \rightarrow \sigma^*(d_{x^2-y^2})]$. The transitions lying to higher energy (λ > 380 nm) all have extinction coefficients greater than 1000 M^{-1} cm^{-1} and can be assigned to a variety of spin and orbitally allowed transitions (see Table 5.1).

Surprisingly, the luminescence intensity and band maxima of solid samples were found to be dependent upon which solvate was present in the unit cell. Figure 5.7 shows the emission and excitation spectrum of $Pt_2(\mu\text{-dppm})_2Cl_2 \cdot C_6H_6$. The luminescence intensity is much greater and the emission band maxima is significantly shifted to higher energy for the benzene solvate as compared to the dichloromethane solvate. On the other hand, the excitation spectrum for $Pt_2(\mu\text{-dppm})_2Cl_2 \cdot C_6H_6$ has nearly identical peak maxima to the excitation spectrum for $Pt_2(\mu\text{-dppm})_2Cl_2 \cdot 0.5CH_2Cl_2$.

Table 5.1

Orbitally Allowed Transitions assuming D_{2h} symmetry

δ^* (d_{z^2})	→	π^* (py)	y allowed
δ (d_{z^2})	→	σ^* $(d_{x^2-y^2})$	x allowed
δ (d_{z^2})	→	π (p_y)	y allowed
π^* (d_{xy})	→	σ^* $(d_{x^2-y}$	y allowed
π^* (d_{xy})	→	π (p_y)	x allowed
π (d_{xy})	→	π^* (p_y)	x allowed
π^* (d_{xz})	→	σ^* $(d_{x^2-y^2})$	z allowed
δ^* (d_{yz})	→	π^* (p_y)	z allowed
δ (d_{yz})	→	π (p_y)	z allowed
σ $(d_{x^2-y^2})$	→	σ^* $(d_{x^2-y^2})$	x allowed
σ $(d_{x^2-y^2})$	→	π (p_y)	y allowed

Figure 5.7 (a) Corrected emission spectrum of $Pt_2(\mu\text{-dppm})_2Cl_2 \cdot C_6H_6$, powder sample, 20 K. Emission maximum at 672 nm.

(b) Corrected excitation spectrum of $Pt_2(\mu\text{-dppm})2Cl_2 \cdot C_6H_6$, powder sample, 20 K. Absorption maxima at 465, 428, 388 nm.

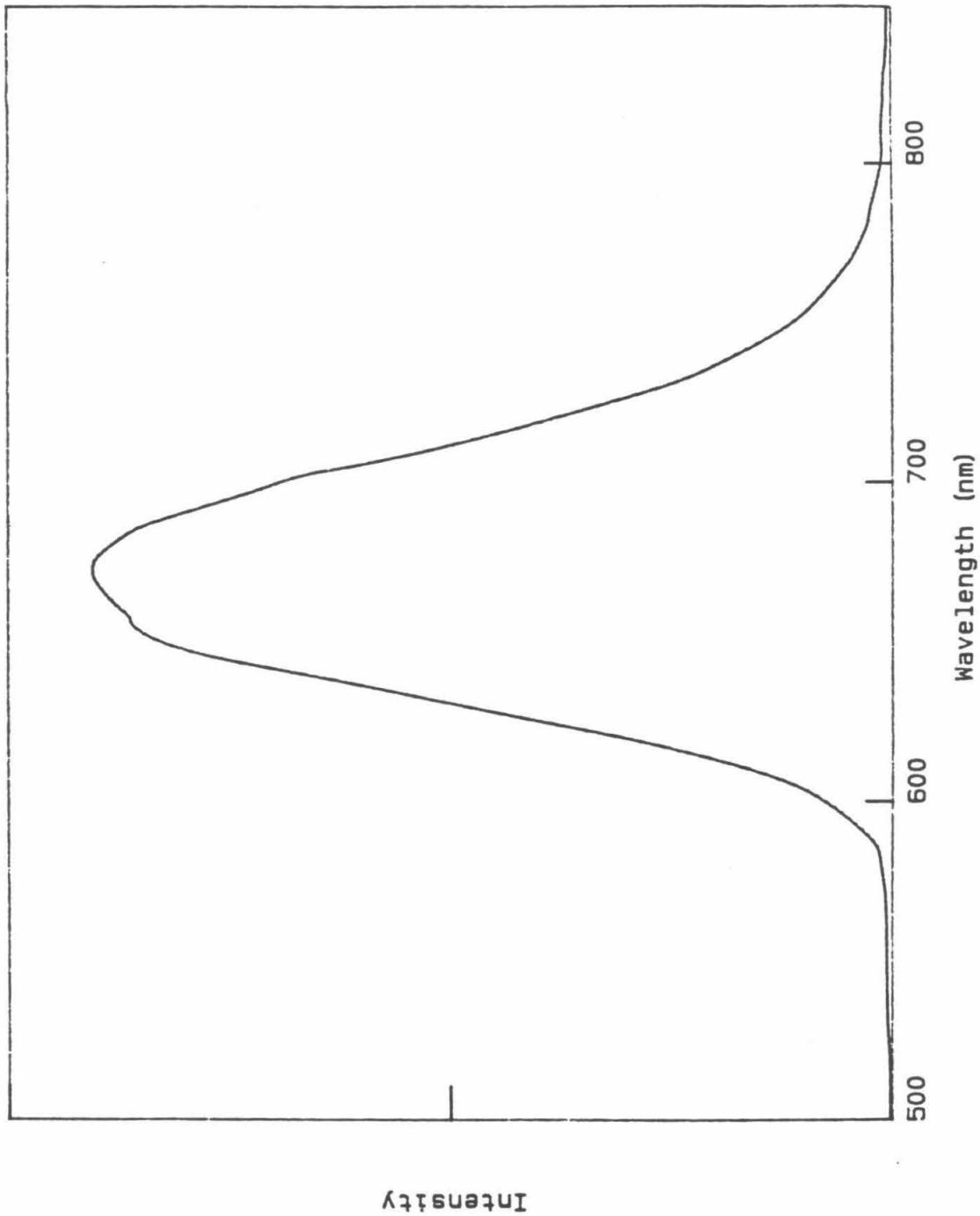
Intensity
500
600
700
800
Wavelength (nm)

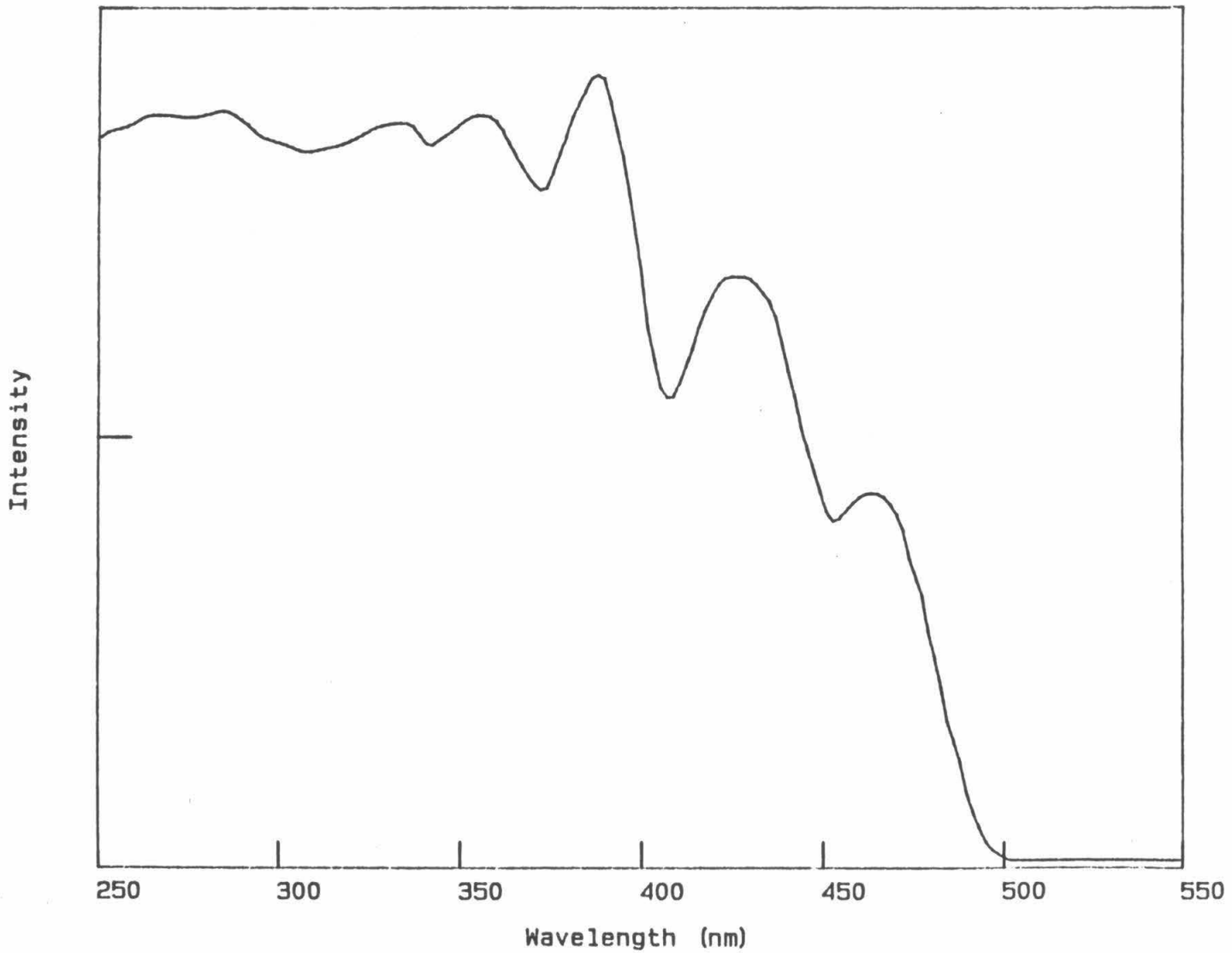
Intensity
250
300
350
400
450
500
550
Wavelength (nm)

Differences in the solid state emission band maxima and lifetimes of $Pt_2(\mu\text{-dppm})_2Cl_2$ complexes are listed in Table 5.2. The longest *lifetime* obtained is that of the benzene solvate, 900 ns; and the shortest lifetime is observed for the dichloromethane solvate, 130 ns.

The general trend of high-energy-emission/long-lifetime and low-energy-emission/short-lifetime is in accord with the energy gap law which relates the non-radiative rate out of an excited state with the energy of the excited state within a given chromophore.[21] This law is based on the extent of vibrational coupling between the zeroeth vibrational level of the excited state, and the higher lying vibrational levels of the ground state.[22] In the case of $Pt_2(\mu\text{-dppm})_2Cl_2 \cdot$solvate, it appears that the solvate is somehow affecting the $Pt_2(\mu\text{-dppm})_2Cl_2$ excited state resulting in an emission-energy/emission-lifetime correlation similar to that predicted by the energy gap law.

These results indicate that the solvate molecule interacts with the excited state in some fashion. One possibility is that this interaction is dependent upon the polarity of the solvate molecule, such that a more polar solvent decreases the emission energy and lifetime. Another possibility is that the π system of the solvate interacts with the unfilled σ^* ($d_{x^2-y^2}$) and $\pi\pi^*$ (p_y) orbitals of the $Pt_2(\mu\text{-dppm})_2Cl_2$ molecule resulting in an increase of the excited state emission energy and lifetime. Unfortunately, the investigation of these suggestions is not straightforward since these complexes do not luminesce in fluid solution.

Additional evidence for solvate interaction with the metal complex is obtained from glass emission and excitation spectra of $Pt_2(\mu\text{-dppm})_2Br_2 \cdot 0.5CH_2Cl_2$ in a 1:1 dichloromethane/2-methyltetrahydrofuran

Table 5.2

Emission Maxima and Lifetimes of $Pt_2(\mu\text{-dppm})_2Cl_2 \cdot$solvate

Solvate	Emission Maximum (nm, 77 K)	Lifetime (ns, 300 K)
$\cdot C_6H_6$	667	870
$\cdot C_6H_5Cl$	674	470
$\cdot CHCl_3$	683	120
$\cdot CH_2Cl_2$	709	71

(v/v) mixed solvent system (see Figure 5.8). The emission spectrum is comprised of two bands, one of which has its maximum at ~626 nm and the other which manifests itself as a shoulder to lower energy, λ_{max} ~705 nm. The lower energy shoulder may be residual dichloromethane interacting with the $Pt_2(\mu\text{-dppm})_2Br_2$ molecule, since $Pt_2(\mu\text{-dppm})_2Br_2 \cdot 0.5CH_2Cl_2$ has its emission maximum at ~716 nm. The higher energy emission band may be ascribed to the interaction of 2-methyl-tetrahydrofuran with the $Pt_2(\mu\text{-dppm})_2Br_2$ excited state. The excitation spectrum of the $Pt_2(\mu\text{-dppm})_2Br_2$ glass, on the other hand, exhibits excitation bands with identical peak maxima to those recorded for the solid excitation spectrum of $Pt_2(\mu\text{-dppm})_2Br_2 \cdot 0.5CH_2Cl_2$. Apparently, the solvate interacts strongly with the lowest energy excited state but not with any of the higher energy states observed in the absorption and excitation spectra. (Similar emission maxima shifts were observed for the $Pt_2(\mu\text{-dppm})_2Cl_2$ complex in this mixed solvent system.)

Considering the sensitivity of the emissive excited state to a single solvate molecule in the crystal, it is not surprising that no luminescence is observed in fluid solution. In fluid solution the relaxation of molecular rigidity and the increased frequency of solvent collision with the $Pt_2(\mu\text{-dppm})_2X_2$ molecule results in more deactivation pathways accessible to the excited state.

In order to gain some information about the primary deactivation pathway available to the excited state in the solid, and also to more clearly chart the effect of temperature on the luminescent lifetime, variable temperature studies on $Pt_2(\mu\text{-dppm})_2Cl_2 \cdot C_6H_6$ were performed.[23] The results show that the lifetime of the excited state is indeed

Figure 5.8 (a) Corrected emission spectrum of $Pt_2(\mu\text{-dppm})_2Br_2 \cdot 0.5CH_2Cl_2$ in a 1:1 dichloromethane:2-methyltetrahydrofuran glass (v/v) at 77 K. Emission maximum at 626 nm with a shoulder at 705 nm.

(b) Corrected excitation spectrum of $Pt_2(\mu\text{-dppm})_2Br_2 \cdot 0.5CH_2Cl_2$ in a 1:1 dichloromethane:2-methyltetrahydrofuran glass (v/v) at 77 K. Absorption maxima at 438, 388, 360, 335 nm.

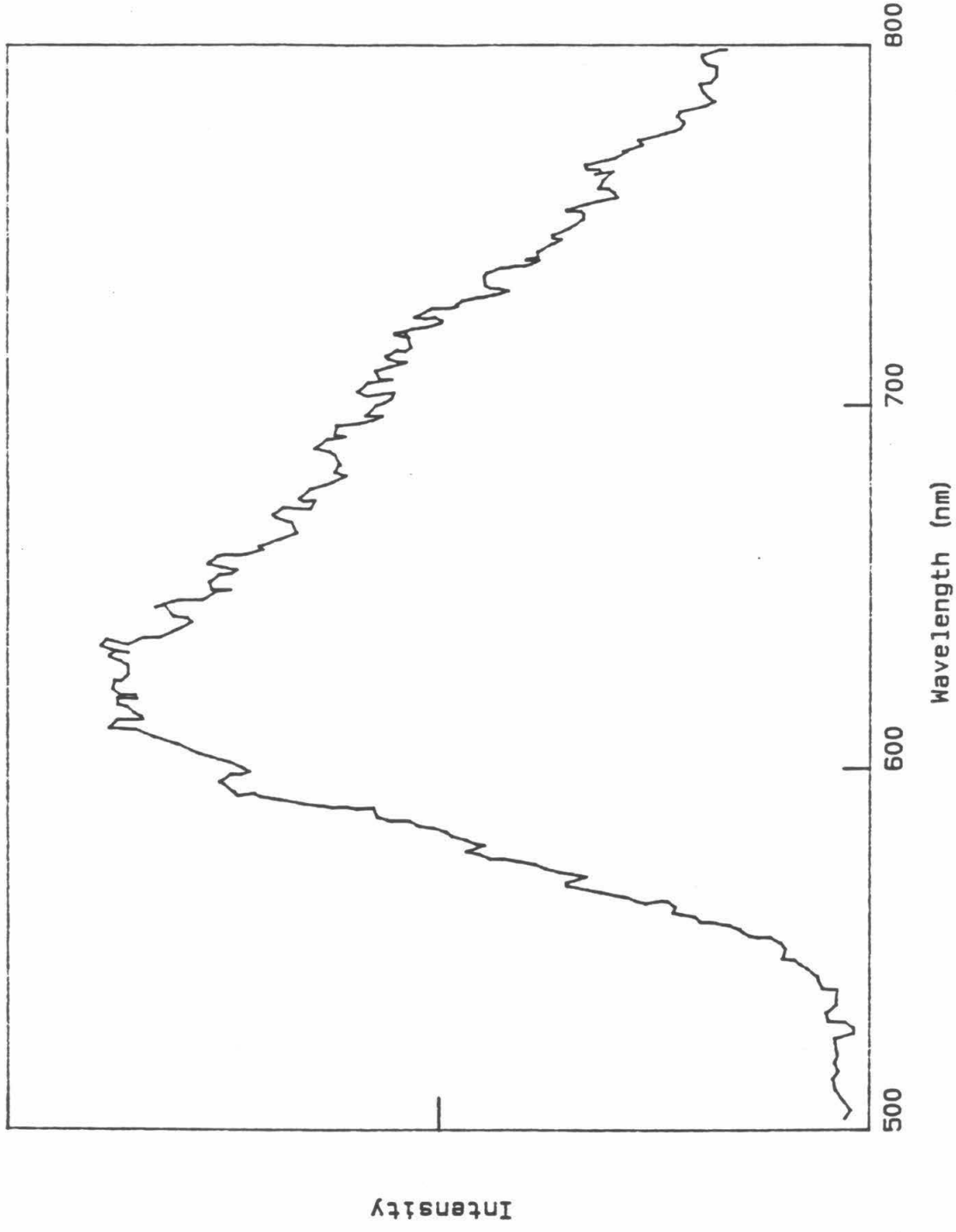
Intensity
500
600
700
800
Wavelength (nm)

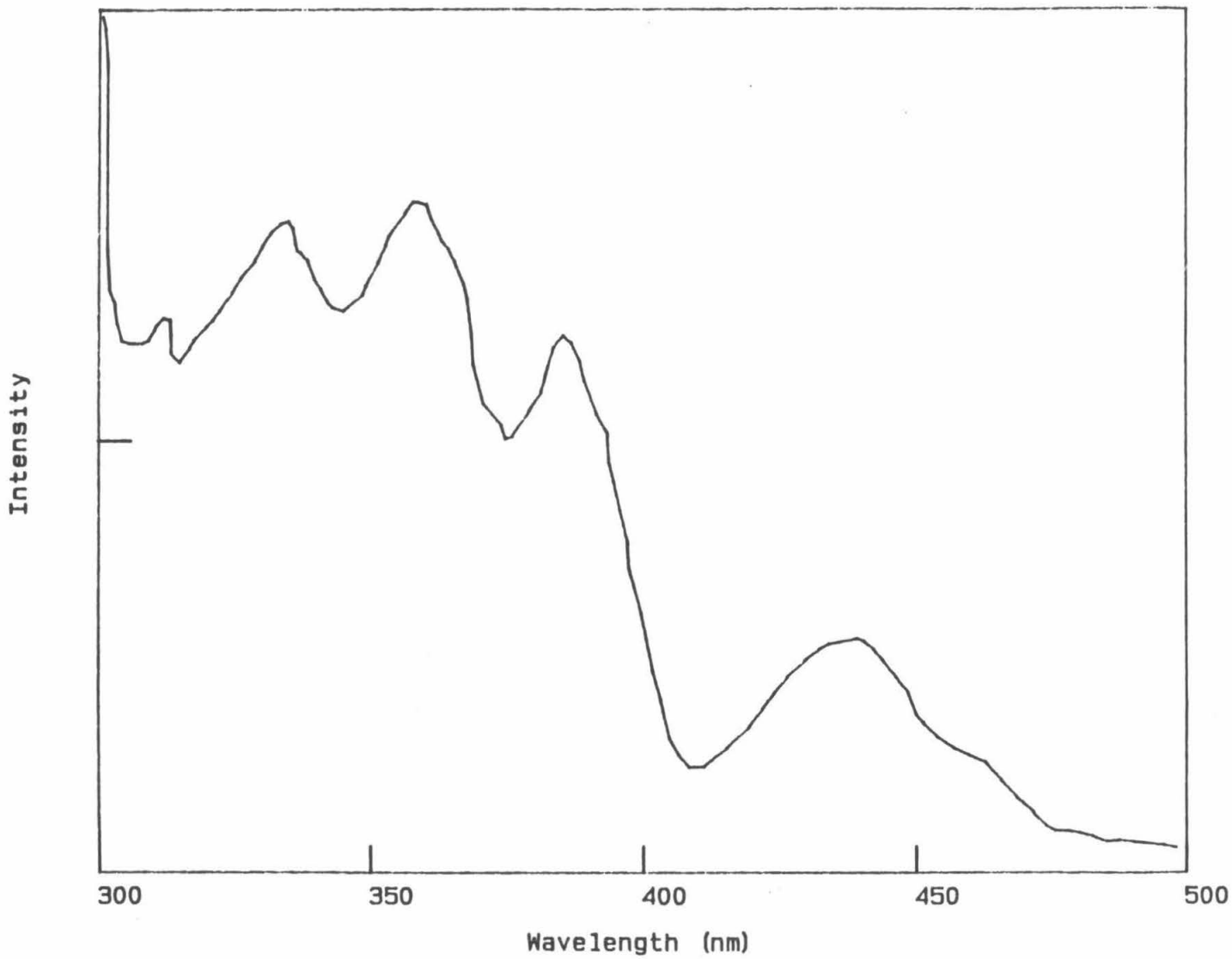
Intensity
300
350
400
450
500
Wavelength (nm)

temperature dependent, increasing from 900 ns at 300 K to 27.3 μs at 77 K. A similarly dramatic increase in the luminescent intensity was observed between 300 and 77 K implying that the variation of the lifetime with temperature is primarily due to variations in the non-radiative rate constant, k_{nr}. Therefore, $k_{obs} \approx k_{nr}$, and the Arrhenius expression may be used in this study. Plotting $ln k_{obs}$ *vs.* 1/T and fitting the linear portion of these data to the Arrhenius expression:

$$k_{obs} = A\exp(-E_a/RT)$$

(where $k_{obs} = 1/\tau_{obs}$, A is the pre-exponential factor, and E_a is the activation energy for the thermally accessible, non-radiative pathway leading to the deactivation of the excited state) yields values of E_a = 1450 cm^{-1} and A = 1 × 10^9 sec^{-1}. The data are listed in Table 5.3 and plotted in Figure 5.9. These results suggest that the major deactivation pathway accessible to the excited state lies ~1450 cm^{-1} to higher energy; however, since there is no vibrational mode readily assignable to this energy, the interpretation of this result is nebulous.

Several cationic phosphine and amine complexes of the form $[Pt_2(\mu\text{-dppm})_2L_2]^{2+}$ were synthesized and studied. Their electronic absorption and emission spectra are presented in Figures 5.10, 5.11, and 5.12. The absorption spectra of the three complexes are nearly identical; two resolved bands at ~400 nm and ~340 nm with molar extinctions in the range of 5000 - 25,000 M^{-1} cm^{-1}. As observed for the neutral halide complexes, the phosphine complexes only luminesce in the solid state and frozen solution, not in fluid solution. Of the three phosphine complexes studied, the PPh_3 adduct exhibits the most intense luminescence with a emission maximum at 583 nm, while the $PPhMe_2$ adduct is the

Table 5.3

$Pt_2(\mu\text{-dppm})_2Cl_2 \cdot C_6H_6$ Variable Temperature Data

τ_{obs} (μs)	k_{obs} (sec^{-1})	ln k_{obs}	T (K)	1/T (× 1000 K)
0.85	1176624	13.98	296	3.38
1.50	667999	13.41	279	3.58
1.87	535407	13.19	273	3.66
2.73	365656	12.81	261	3.83
3.33	300492	12.61	254	3.94
4.47	223620	12.32	243	4.12
5.74	174094	12.07	233	4.29
8.41	118844	11.69	214	4.67
10.01	99898	11.51	203	4.93
11.51	86872	11.37	195	5.13
12.87	77695	11.26	187	5.35
15.28	65445	11.09	172	5.81
17.61	56791	10.95	157	6.37
19.74	50657	10.83	146	6.85
21.13	47320	10.77	135	7.41
22.13	45187	10.72	128	7.84
23.12	43255	10.68	119	8.44
24.70	40483	10.61	110	9.09
26.27	38062	10.55	97	10.31

Figure 5.9 Arrhenius plot for $Pt_2(\mu\text{-dppm})_2Cl_2 \cdot C_6H_6$ (τ measured at 670 nm).

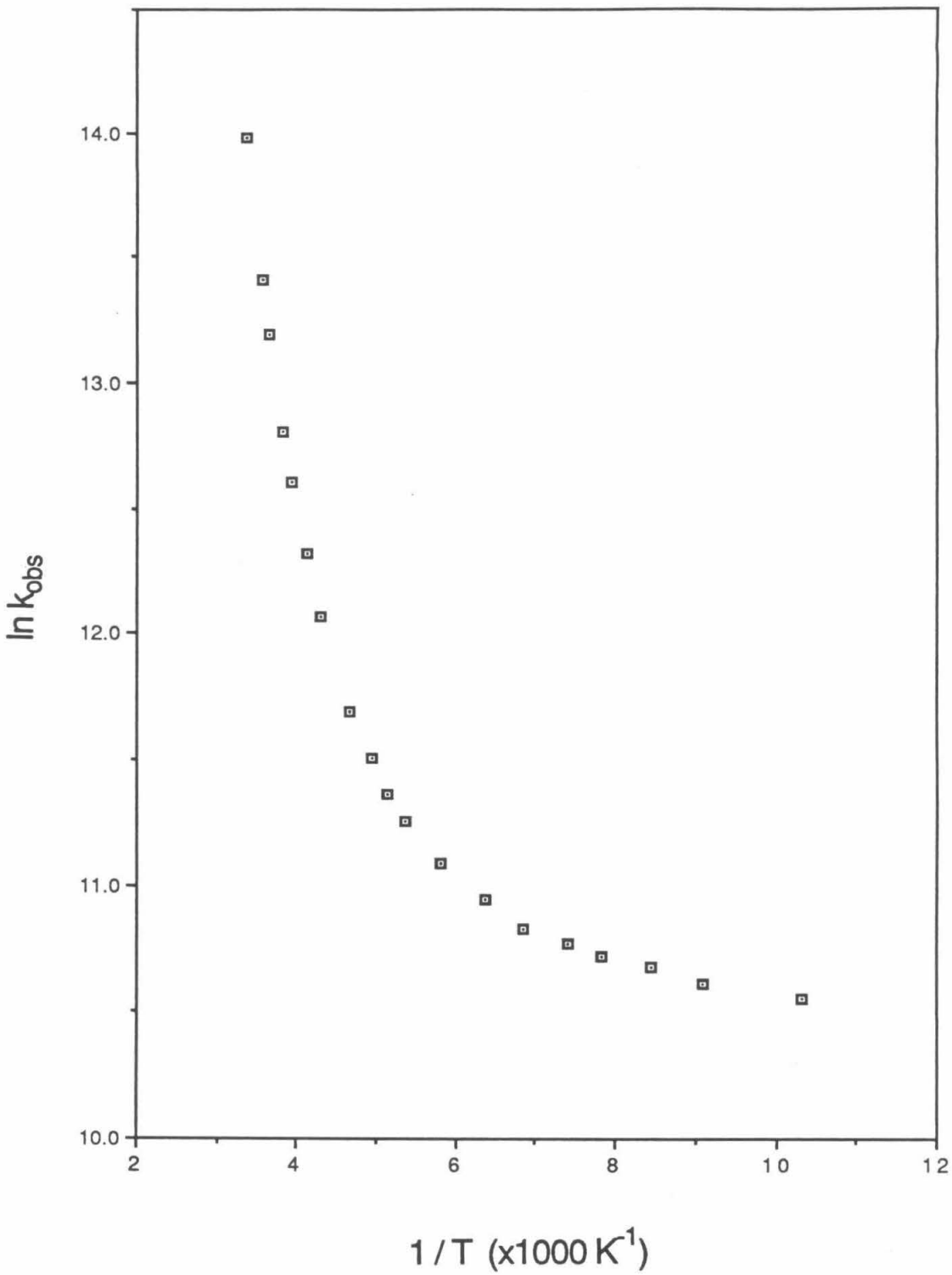
14.0
13.0
12.0
11.0
10.0
ln k_{obs}
2
4
6
8
10
12
1 / T (x1000 K^{-1})

Figure 5.10 (a) Electronic absorption spectrum of $[Pt_2(\mu\text{-dppm})_2(PPh_3)_2](PF_6)_2$ in ethanol (300 K). Absorption maxima at 404 and 350 nm.

(b) Uncorrected emission spectrum of $[Pt_2(\mu\text{-dppm})_2(PPh_3)_2](PF_6)_2$, powder sample, 300 K. Emission maximum at 583 nm. (A grating anomaly occurs at ~667 nm.)

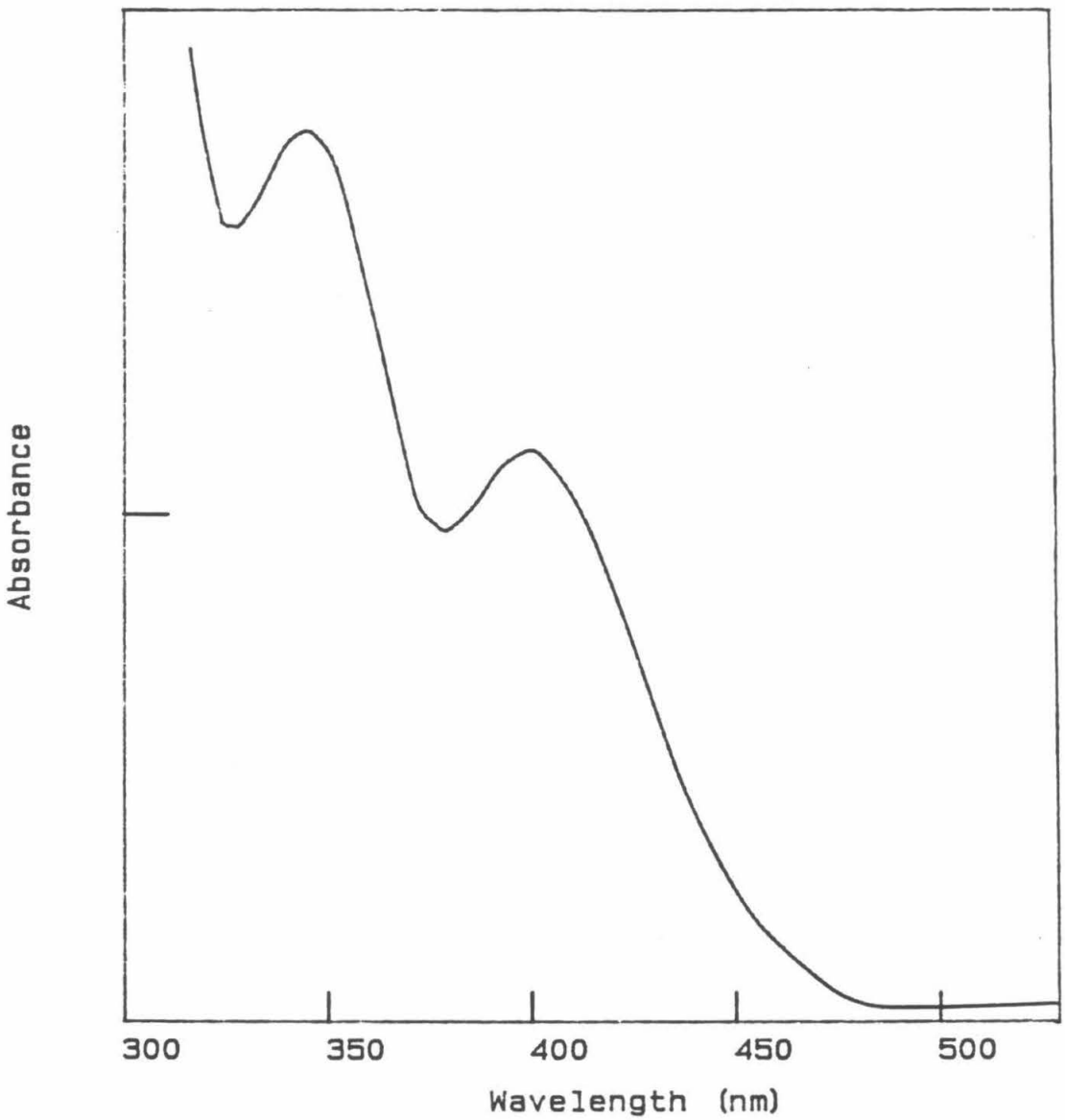
Absorbance
300
350
400
450
500
Wavelength (nm)

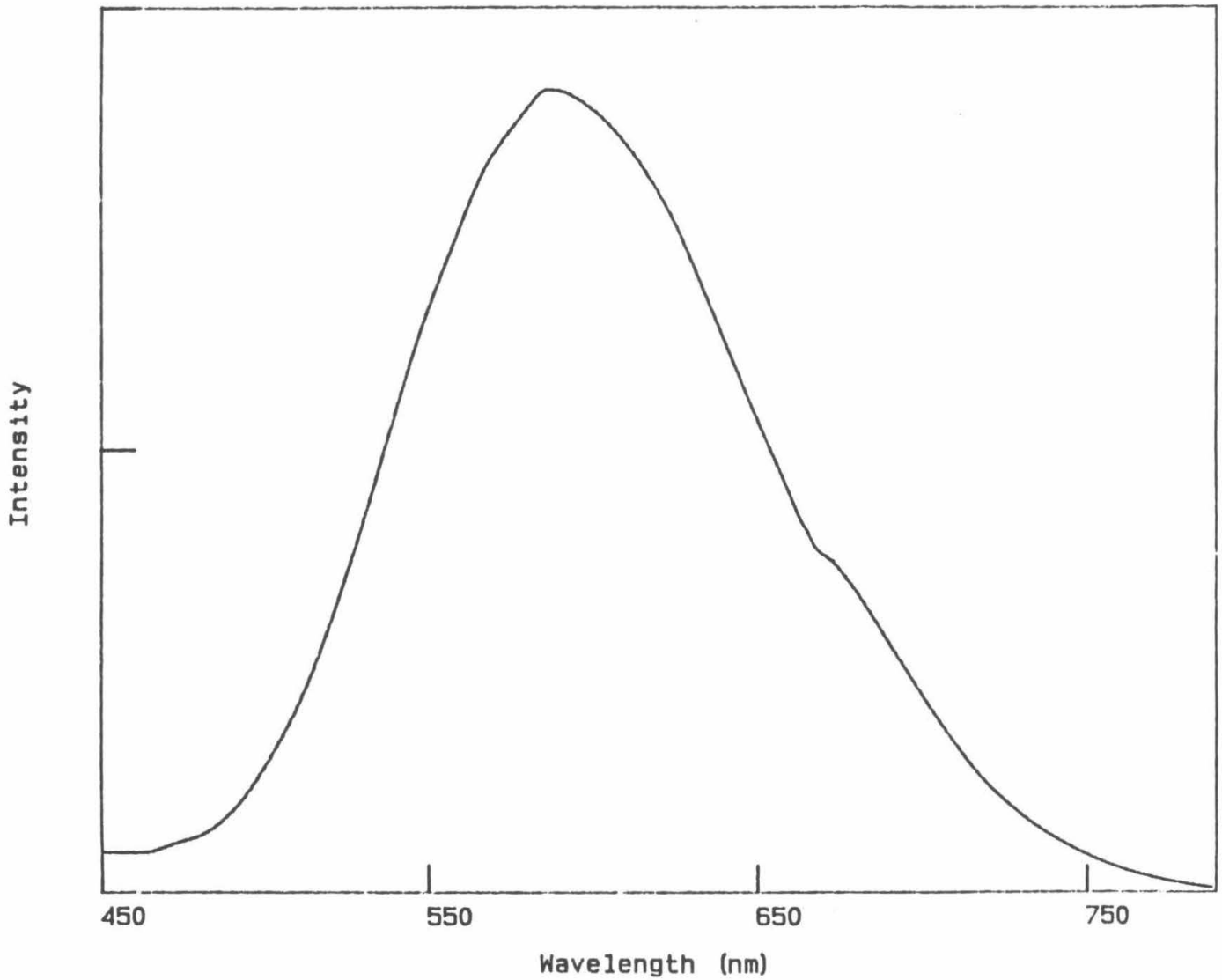
Intensity
450
550
650
750
Wavelength (nm)

Figure 5.11 (a) Electronic absorption spectrum of $[Pt_2(\mu\text{-dppm})_2(PPh_2Me)_2](PF_6)_2$ in acetonitrile (300 K). Absorption maxima at 400 and 335 nm.

(b) Uncorrected emission spectrum of $[Pt_2(\mu\text{-dppm})_2(PPh_2Me)_2](PF_6)_2$, powder sample, 300 K. Emission maximum at 624 nm. (A grating anomaly occurs at ~667 nm.)

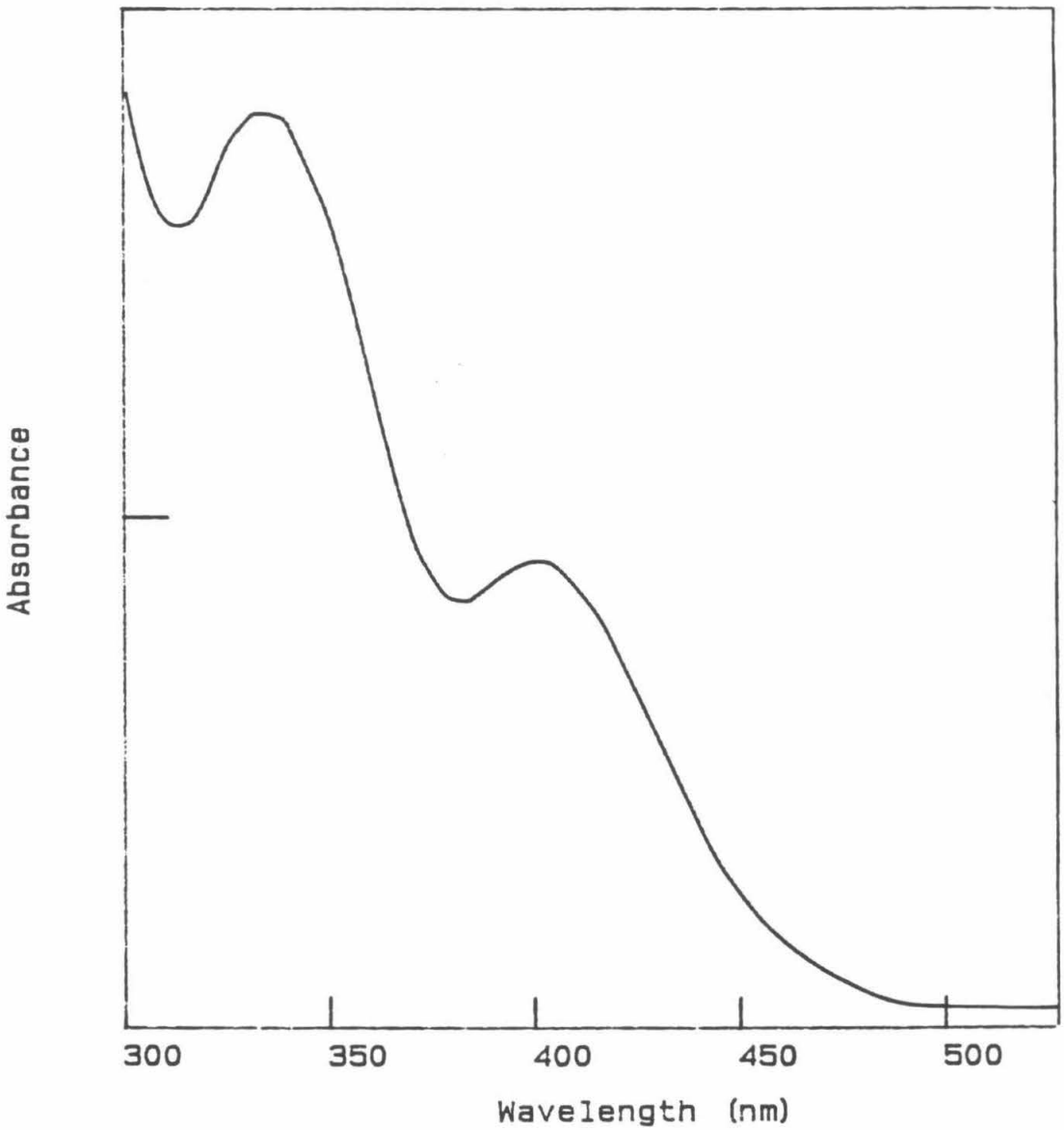
Absorbance
300
350
400
450
500
Wavelength (nm)

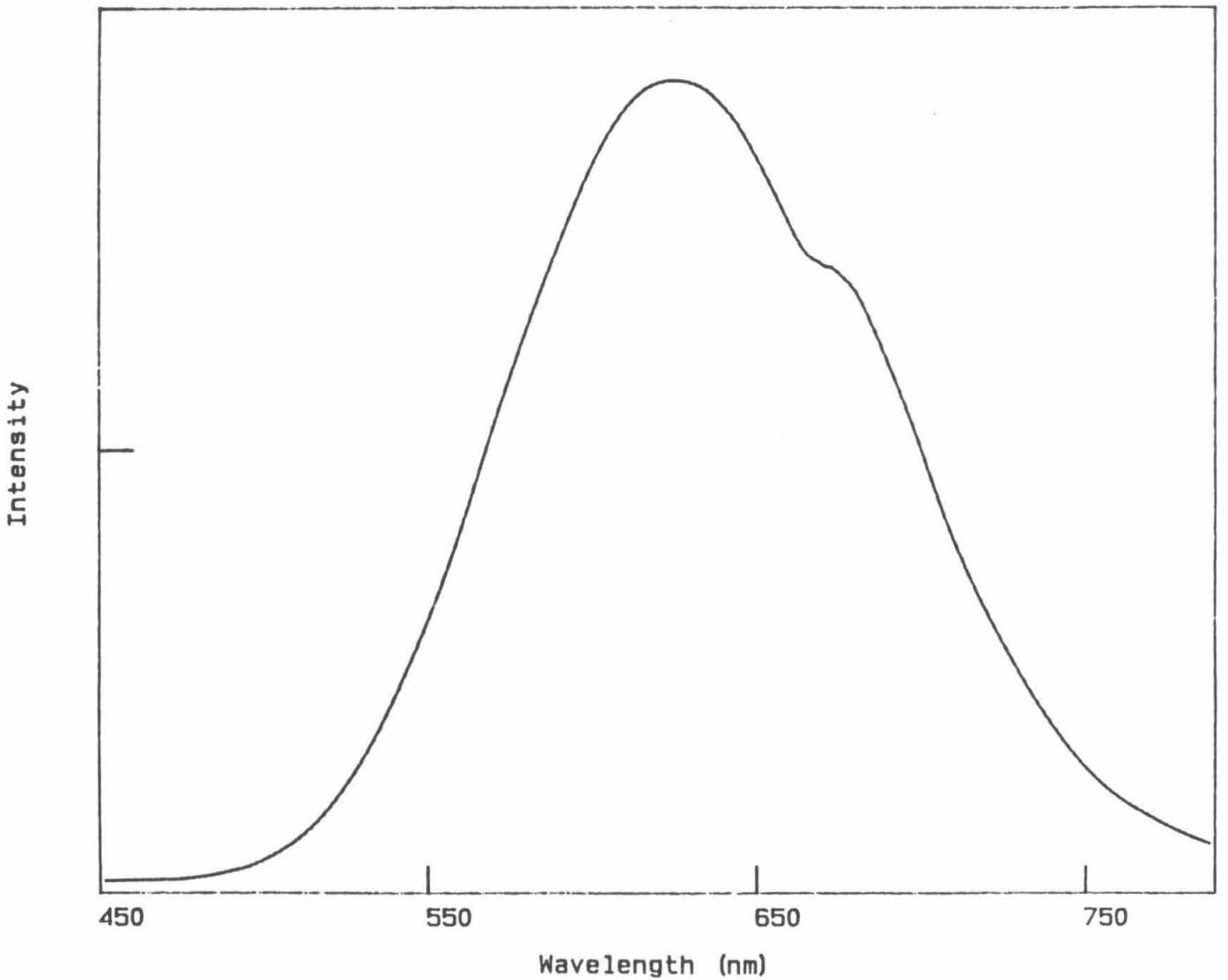
Intensity
450
550
650
750
Wavelength (nm)

Figure 5.12 (a) Electronic absorption spectrum of $[Pt_2(\mu\text{-dppm})_2(PPhMe_2)_2](PF_6)_2$ in acetonitrile (300 K). Absorption maxima at 404 and 330 nm.

(b) Uncorrected emission spectrum of $[Pt_2(\mu\text{-dppm})_2(PPhMe_2)_2](PF_6)_2$, powder sample, 300 K. Emission maximum at ~675 nm. (A grating anomaly occurs at ~667 nm.)

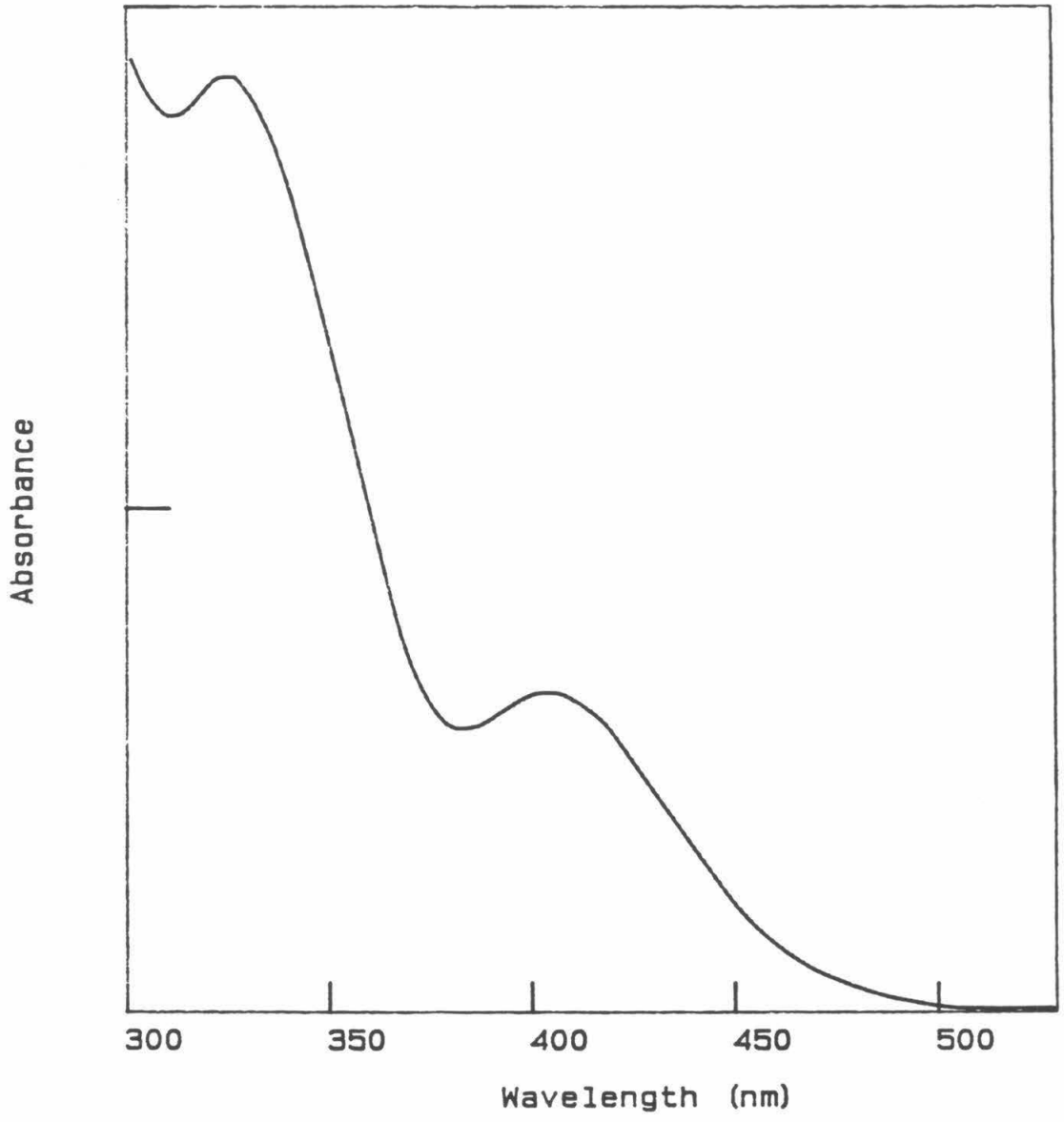
Absorbance
300
350
400
450
500
Wavelength (nm)

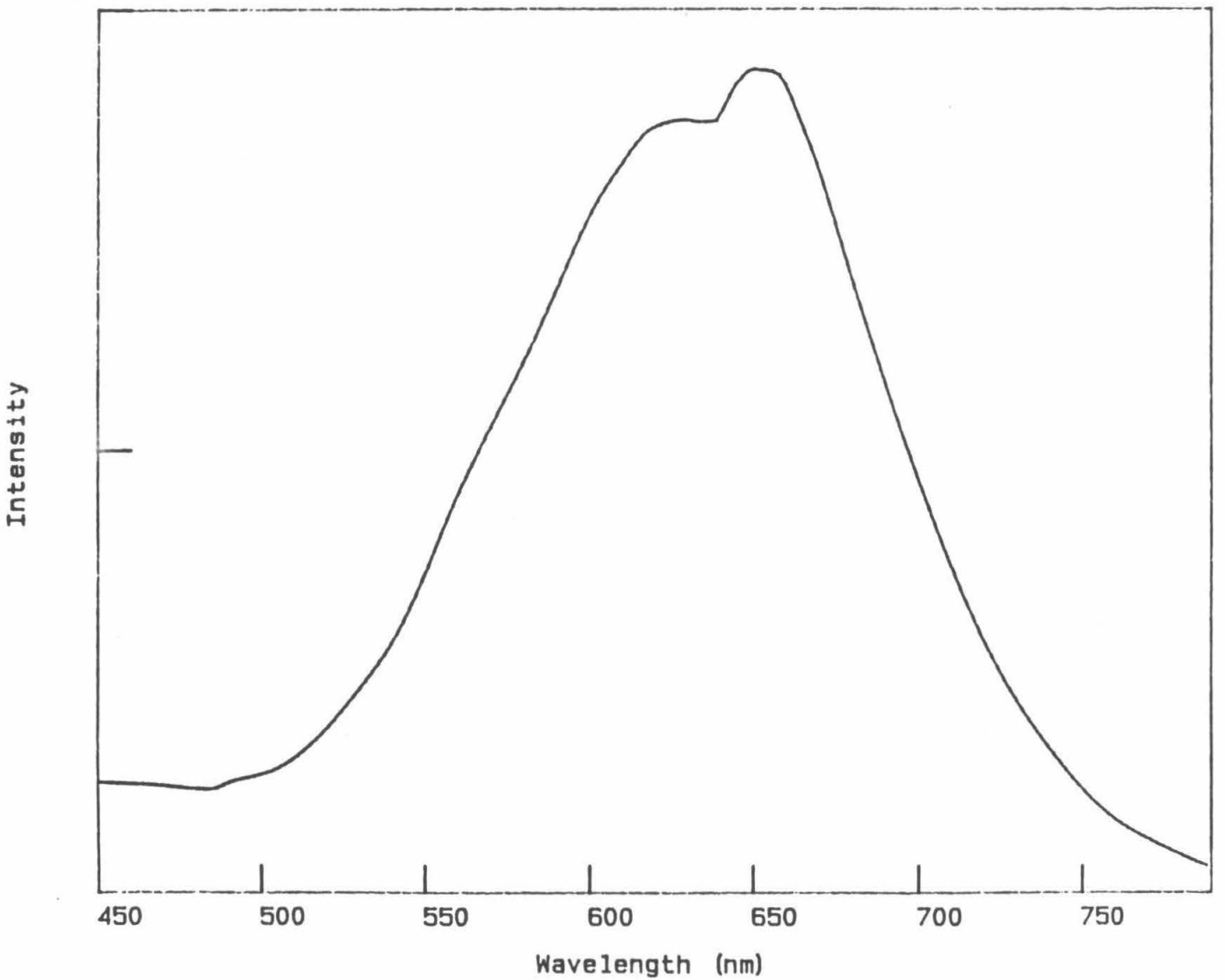
Intensity
450
500
550
600
650
700
750
Wavelength (nm)

weakest with its emission maximum at 675 nm at 300 K. Similar emission profiles were obtained for glass samples, run at 77 K, where the phosphine complex was dissolved in a 5:2 ethanol/methanol (v/v) mixed solvent system.

Attempts to measure the luminescent lifetime of the phosphine complexes were unsuccessful at both 300 and 77 K in the solid state. On the other hand, glass samples (5:2 ethanol:methanol) of the phosphine complexes gave luminescent lifetimes at 77 K on the order of 20 μs. The luminescent lifetimes measured for the three complexes were within experimental error, suggesting that they were the same or similar molecular species. Although these results are rather confusing, in light of the phosphine solubilizing ability of ethanol, the possibility exist that all the complexes were $Pt_2(\mu\text{-dppm})_2(CH_3CH_2OH)_2^{2+}$ or $Pt_2(\mu\text{-dppm})_2(CH_3OH)_2^{2+}$. These results indicate that axial ligand dissociation may be a facile deactivation pathway of the $Pt_2(\mu\text{-dppm})_2Cl_2$ excited state in solution.

A list of electronic absorption data of several platinum(I) and palladium(I) complexes is presented in Table 5.4.[8,20,24,25] Several similarities between the electronic absorption spectra of Pt(I) and Pd(I) dimers can be seen immediately. Both systems exhibit a multitude of electronic transitions, none of which is distinct or well resolved from the other. The extinction coefficients for the high energy transitions are quite large, characteristic of spin and orbitally allowed transitions. Difficulties arise when trying to compare the low energy electronic transitions of the Pt halide(X) molecule with those of either the Pt phosphine(L) or Pd halide(X) complexes. From comparison

Table 5.4

Absorption Band Maxima of Some Pt(I) and Pd(I) Dimers†

Platinum(I) Dimers	
$Pt_2(\mu\text{-dppm})_2Cl_2$	465 (<100), 427 (200), 380 (~2000), 360 (2600), 323(7800)
$Pt_2(\mu\text{-dppm})_2Br_2$	478, 441, 390, 360, 323
$[Pt_2(\mu\text{-dppm})_2(PPh_3)_2](PF_6)_2$	404 (15500), 350 (23000)
$[Pt_2(\mu\text{-dppm})_2(PPh_2Me)_2](PF_6)_2$	400 (7480), 335 (13400)
$[Pt_2(\mu\text{-dppm})_2(PPhMe_2)_2](PF_6)_2$	404 (5260), 330 (14000)
$[Pt_2(\mu\text{-dppm})_2(SnCl_3)_2$	450sh(15700), 438(16800), 360(24600), 303 (26700), 276sh (30800)
Palladium(I) Dimers	
$Pd_2(\mu\text{-dppm})_2Cl_2$	416 (7550), 347 (16800), 293 (25900)
$Pd_2(\mu\text{-dppm})_2Br_2$	428 (10600), 364 (17500), 301(23100), 285sh (21300), 258sh (29400)
$Pd_2(\mu\text{-dppm})_2I_2$	488 (13000), 439 (11900), 394(11900), 313 (20000), 280sh (23900), 262sh(28500)
$Pd_2(\mu\text{-dppm})_2(SCN)_2$	426 (14600), 303(21200), 259sh(30400)
$Pd_2(\mu\text{-dppm})_2(NCO)_2$	394(7390), 326sh(13500), 290sh(36300)
$Pd_2(\mu\text{-dppm})_2(N_3)_2$	428 (19900), 305sh (19700), 287sh(25000), 265sh (28100)
$Pd_2(\mu\text{-dppm})_2(NO_2)_2$	434 (11500), 362 (9300), 316sh (13800), 294sh (22000)
$Pd_2(\mu\text{-dppm})_2(SnCl_3)Cl$	495(14200), 422 (8640), 340 (18200), 294sh (18100), 260sh (31,700)
$Pd_2(\mu\text{-dppm})_2(SnCl_3)_2$	536 (21200), 500sh (17900), 417sh(6120), 353(19000), 261sh(35000)

†Some of the data taken from references 8, 20, 24, and 25.

of the molar extinction coefficients, the lowest energy electronic absorption bands observed for $Pt_2(\mu\text{-dppm})_2X_2$ are attributable to transitions different from those observed in the analogous $Pd_2(\mu\text{-dppm})_2X_2$ and $Pt_2(\mu\text{-dppm})_2L_2^{2+}$ complexes. Also, the temperature dependence of the emissive excited state lifetime of $Pt_2(\mu\text{-dppm})_2X_2$ is significantly different from that of $Pt_2(\mu\text{-dppm})_2L_2^{2+}$.

Finally, for $Pt_2(\mu\text{-dppm})_2Cl_2$, no intensity overlap between the lowest energy absorption band and the emission band is observed. This large "window" may be attributed to a significant Stokes shift, or it may be indicative of the presence of a very weak absorption band which is, as of yet, unobserved. The emission spectra of the $Pt_2(\mu\text{-dppm})_2Cl_2$ molecule show significant environment dependence, whereas, the corresponding excitation spectra are all identical to one another, showing no environment dependence. This apparent contradiction may be best explained by the presence of a lower energy absorption, too weak to be observed, which is directly related to the observed emission and is environment sensitive. Thus, the higher energy absorption bands observed in the excitation spectra, which are not environment sensitive, are not directly related to the emission band; instead, they merely communicate by various deactivation pathways with the lower energy state responsible for the observed luminescence.

REFERENCES

1. Brown, M. P.; Puddephatt, R. J.; Rashidi, M.; Manojlović-Muir, Lj.; Muir, K. W.; Solomun, T.; Seddon, K. R. *Inorg. Chim. Acta*, **1977**, *23*, L33.
2. Manojlović-Muir, Lj.; Muir, K. W.; Solomun, T. *Acta Cryst.* **1979**, *B35*, 1237.
3. Goldberg, S. Z.; Eisenberg, R. *Inorg. Chem.* **1976**, *15*, 535.
4. Brown, M. P.; Puddephatt, R. J.; Rashidi, M.; Seddon, K. R. *J. Chem. Soc. Dalton Trans.* **1978**, 516.
5. Brown, M. P.; Puddephatt, R. J. Rashidi, M.; Seddon, K. R. *J. Chem. Soc. Dalton Trans.* **1978**, 1540.
6. Brown, M. P.; Fisher, J. R.; Puddephatt, R. J.; Seddon, K. R.; *Inorg. Chem.* **1979**, *18*, 2808.
7. Cameron, T. S.; Gardner, P. A.; Grundy, K. R. *J. Organomet. Chem.* **1981**, *212*, 135.
8. Benner, L. S.; Balch, A. L. *J. Am. Chem. Soc.* **1978**, *100*, 6099.
9. Olmstead, M. M.; Hope, H.; Benner, L. S.; Balch, A. L. *J. Am. Chem. Soc.* **1977**, *99*, 5502.
10. Balch, A. L.; Benner, L. S.; Olmstead, M. M. *Inorg. Chem.*, **1979**, *18*, 2996.
11. Westland, A. D. *J. Chem. Soc.* **1965**, 3060.
12. Brown, M. P.; Puddephatt, R. J.; Rashidi, M.; Seddon, K. R.; *J. Chem. Soc. Dalton Trans.* **1977**, 951.
13. Brown, M. P.; Franklin, S. J.; Puddephatt, R. J.; Thomson, M. A.; Seddon, K. R. *J. Organomet. Chem.* **1979**, *178*, 281.
14. Nocera, D. G.; Winkler, J. R.; Yocom, K. M.; Bordignon, E.; Gray, H. B. *J. Am. Chem. Soc.*, **1984**, *106*, 5145.

15. Parker, C. A.; Rees, W. T. *Analyst* **1960**, *85*, 587.

16. Savas, M. M.; Mason, W. R. *Inorg. Chem.* **1987**, *26*, 301.

17. Boehm, J. R.; Doonan, D. J.; Balch, A. L. *J. Am. Chem. Soc.* **1976**, *98*, 4845.

18. Miller, T. D.; St. Clair, M. A.; Reinking, M. K.; Kubiak, C. P. *Organometallics* **1983**, *2*, 767.

19. Reinking, M. K.; Kullberg, M. L.; Cutler, A. R.; Kubiak, C. P. *J. Am. Chem. Soc.* **1985**, *107*, 3517.

20. Alves, O. L.; Vitorage, M.-C.; Sourisseau, C. *Nouv. J. Chim.* **1983**, *7*, 231.

21. Englman, R.; Jortner, J. *Molecular Physics* **1970**, *18*, 145.

22. Caspar, J. V.; Kober, E. M.; Sullivan, B. P.; Meyer, T. J. *J. Am. Chem. Soc.* **1982**, *104*, 630.

23. As the temperature was lowered from 300 to 77 K all of the $Pt_2(\mu\text{-dppm})_2Cl_2 \cdot$solvate lifetimes increased. In a few cases biphasic decays were observed. This biphasic decay may be due to the presence of $Pt_2(\mu\text{-dppm})_2Cl_2$ in different solvate environments. If, for example, one environment allows for greater solvent interaction with the $Pt_2(\mu\text{-dppm})_2Cl_2$ excited state than another environment, a superposition of these different luminescent lifetimes may be observed, resulting in a net multiphasic decay. As for $Pt_2(\mu\text{-dppm})_2Cl_2 \cdot C_6H_6$, this complex exhibited a monophasic decay throughout the entire temperature range studied.

24. Muralidharan, S.; Espenson, J. H. *J. Am. Chem. Soc.* **1984**, *106*, 8104.

25. Olmstead, M. M.; Benner, L. S.; Hope, H.; Balch, A. L. *Inorg. Chim. Acta* **1979**, *32*, 193.

CHAPTER 6

Energy Transfer Studies of $Pt_2(\mu\text{-dppm})_2Cl_2$

INTRODUCTION

An understanding of the nature of the excited state is necessary in order to intelligently discuss the observed excited state reaction chemistry. Traditional techniques used to elucidate excited state information are not ameniable to this $Pt_2(\mu\text{-dppm})_2Cl_2$ system since (*i*) these complexes do not luminesce in fluid solution at room temperature and (*ii*) absorption and/or emission band fine structure are not observed at low temperature. Instead, indirect methods for gaining the required information must be sought.

From data presented in Chapter 5, it is believed that the absorption band corresponding to the observed emission is not observed in solution electronic absorption or solid state excitation spectra. Both excitation spectra of the benzene and dichloromethane solvates of $Pt_2(\mu\text{-dppm})_2Cl_2$ show an ~3000 cm^{-1} window where no other transitions between the lowest absorption band and the emission band are observed (see Figures 5.4ab and 5.7ab). (A Stokes shift of this type or magnitude makes little physical sense; therefore, these high energy absorptions have been ruled out as being directly related to the emissive excited state.) The absorption band corresponding to the emissive excited state is assumed to have an extremely small molar extinction coefficient and is, logically, attributed to a singlet-triplet transition. Besides this argument, there is no other experimental evidence supporting the spin assignment of the emissive excited state. In energy transfer experiments, the conservation of spin is quite important. Investigating the energy transfer rates between $Pt_2(\mu\text{-dppm})_2Cl_2$ and other known triplet excited states may provide direct evidence for the triplet spin assignment of the emissive excited state.

From emission and lifetime studies of the solvate effect on powder $Pt_2(\mu\text{-dppm})_2Cl_2$ samples, it has been determined that the excited state is environment sensitive. Exactly what the excited state energy of the complex is in solution is unclear since direct measurement is impossible; however, indirect determination of its approximate energy is possible by conducting energy transfer experiments aimed at determining the energy at which the rate of transfer from donor to acceptor begins to drop off. Since $Pt_2(\mu\text{-dppm})_2Cl_2$ does not luminesce in fluid solution its role must be that of acceptor. A series of molecules which do luminesce in fluid solution and have excited state lifetimes greater than several hundred nanoseconds are employed as donors; in this experiment $W_6X_8Y_6^{2-}$ (X,Y = Cl, Br, I), $ReO_2L_4^+$ (L = pyridine and its derivatives), and $Ru(bpy)_3^{2+}$ (bpy = 2,2'-bipyridine) were used.

EXPERIMENTAL

Materials

All solvents, unless otherwise noted, were reagent grade and used as received without further purification. Dichloromethane (Burdick and Jackson, UV grade), used in the energy transfer quenching experiments, was dried and stored in glass solvent pots as described in the experimental section of Chapter 5.

Donors. Hexanuclear clusters, $(TBA)_2[W_6I_{14}]$, $(TBA)_2[W_6I_8Cl_6]$, $(TBA)_2[W_6Br_8I_6]$, $(TBA)_2[W_6Cl_8I_6]$, $(TBA)_2[W_6Cl_8Br_6]$, $(TBA)_2[W_6Cl_{14}]$ were prepared by Dr. Thomas Zietlow and used as received.[1] $(TBA)_2[W_6I_8Cl_6]$ required recrystallization from dichloromethane and petroleum ether prior to use. Rhenium dioxo complexes, $[ReO_2(4\text{-picoline})_4]BPh_4$, $[ReO_2(pyridine)_4]BPh_4$, and $[ReO_2(d_5\text{-pyridine})_4]BPh_4$ were prepared by Dr. Jay Winkler and used as received.[2] $[ReO_2(isoquinoline)_4]PF_6$ was prepared by Mr. John Brewer and used as received.[3] $[Ru(2,2'\text{-bipyridine})_3](PF_6)_2$ was prepared by Dr. Michael Hopkins and used as received.[4]

Acceptors. $Pt_2(\mu\text{-dppm})_2Cl_2 \cdot 0.5CH_2Cl_2$ was prepared as described in the experimental section of Chapter 5 and recrystallized from dichloromethane and iso-octane. Anthracene (Aldrich, 98%) was recrystallized from a hot 2:1:1 (v/v/v) acetone:ethanol:water mixture.

Physical Measurements

Stern-Volmer Quenching Procedures. A Nd:YAG pulsed laser system, previously described,[5] was used to measure the luminescent lifetimes as a function of quencher concentration. Energy transfer rate constants were calculated using Stern-Volmer analysis as described in the results

and discussion section of Chapter 2. Samples for all energy transfer experiments were prepared by placing the donor (~1 mg) into a quenching cell and evacuating it on a high vacuum line (limiting pressure < 10^{-3} Torr). (The quenching cell is described in the experimental section of Chapter 2.) Four to six mL of dichloromethane was distilled from the storage flask into the quenching cell under vacuum; the exact volume of dichloromethane used was recorded. Acceptor solutions were added following the same procedures for quencher addition outlined in the experimental section of Chapter 2. Figure 6.1 illustrates the energy transfer quenching of $(TBA)_2[W_6Br_8I_6]$ with $Pt_2(\mu\text{-dppm})_2Cl_2$.

In the ideal energy transfer experiment only the donor molecule should absorb the laser excitation; the acceptor should be unaffected by the laser excitation and remain in its ground state. The majority of the reported energy transfer experiments, however, were carried out using the laser's second harmonic, 355 nm, as the excitation wavelength, a wavelength at which the acceptor, $Pt_2(\mu\text{-dppm})_2Cl_2$, has an appreciable absorption. Therefore, to insure that the acceptor's excited state was not involved in initiating the energy transfer process, several measurements were made using the laser's first harmonic, 532 nm, as the excitation wavelength; ($Pt_2(\mu\text{-dppm})_2Cl_2$ has no absorption at this wavelength). Donors, $Ru(bpy)_3^{2+}$ and $ReO_2(py)_4^+$ which do have appreciable absorption at 532 nm were used in this control experiment. Nearly identical energy transfer rate constants were calculated for the data collected using 532 nm (no $Pt_2(\mu\text{-dppm})_2Cl_2$ absorption) and 355 nm (significant $Pt_2(\mu\text{-dppm})_2Cl_2$ absorption) excitation wavelengths. Thus, any excited state $Pt_2(\mu\text{-dppm})_2Cl_2^*$ molecules generated using 355 nm excitation appear to be

Figure 6.1 Stern-Volmer plot of the energy transfer quenching of $(TBA)_2[W_6Br_8I_6]$ with $Pt_2(\mu\text{-dppm})_2Cl_2$ in dichloromethane.

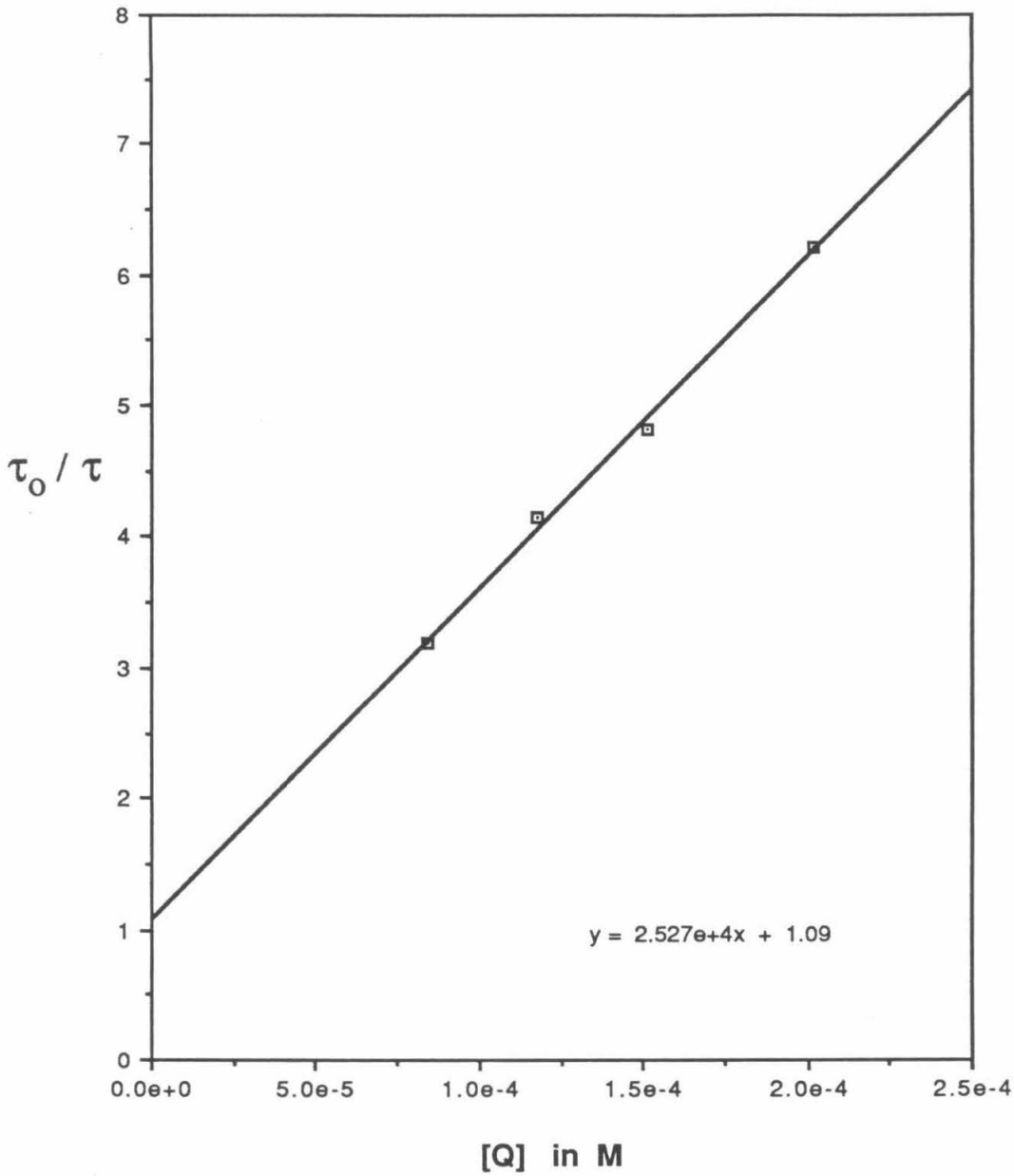
8
7
6
5
4
3
2
1
0
τ_o / τ
y = 2.527e+4x + 1.09
0.0e+0
5.0e-5
1.0e-4
1.5e-4
2.0e-4
2.5e-4
[Q] in M

uninvolved in the energy transfer process.

Emission Spectroscopy. Attempts to observe the luminescence from excited $Pt_2(\mu\text{-dppm})_2Cl_2$ were conducted on the emission instrument built at Caltech and described previously.[6] An excitation wavelength, 547 nm, was chosen in order to excite only the donor, $ReO_2(d_5\text{-py})_4^+$. Emission spectra were recorded between 585 and 825 nm. Samples were placed in NMR tubes equipped with 14/20 ground glass joints and capped with a septum. First, emission spectra of frozen dichloromethane solutions containing only $ReO_2(d_5\text{-py})_4^+$ (1×10^{-3} M) were measured. Next, emission spectra of frozen dichloromethane solutions containg 2×10^{-3} M $ReO_2(d_5\text{-py})_4^+$ and 1×10^{-2} M $Pt_2(\mu\text{-dppm})_2Cl_2$ were measured. Comparison between these emission spectra revealed subtle changes in the emission band profile of the $ReO_2L_4^+$ chromophore (not attributable to concentration changes).

RESULTS and DISCUSSION

There are several mechanisms (other than the intrinsic radiative and non-radiative processes) by which an excited state molecule, D*, can decay to its ground state, D: (1) energy transfer, (2) electron transfer, (3) a chemical reaction (other than electron transfer), (4) spin-catalyzed deactivation, (5) external heavy-atom effect, and (6) complex (excimer and exciplex) formation.[7]

Energy transfer is by far the most common deactivation pathway. Its basic requirement is that the acceptor molecule, A, possess an excited state, A*, in which the energy required for the $A \rightarrow A^*$ transition is approximately equal to or less than the $D^* \rightarrow D$ transition energy.[7-9]

The second prevalent deactivation pathway is electron transfer between the excited state donor and a ground state acceptor, such that either (*i*) $D^* + A \rightarrow D^+ + A^-$ or (*ii*) $D^* + A \rightarrow D^- + A^+$ is a favorable reaction.[7,10,11] In the first case (*i*), the donor must have an accessible oxidized state and D* must be of high enough energy such that it is energetically favorable to give up an electron from its excited state and reduce the acceptor. Similarly, the same type of requirements exist for the second case (*ii*), in which the donor must have an accessible reduced state and D* must be of high enough energy to oxidize the acceptor.

Chemical reactions between coordination complexes which do not involve electron transfer but rather some type of ligand loss or substitution are rare, since they are second order reactions which are usually unable to compete on the timescale of the donor's excited state lifetime.[7] If, however, such reactions were occurring, they would be

readily detected by changes in the electronic absorption spectrum which are not attributable to the donor or acceptor species.

The latter three processes are very rare, with very little, if any, evidence in support of them occurring between inorganic donors and acceptors.[7] Therefore, it is supposed that these processes are far too inefficient to compete with the more facile energy and electron transfer deactivation pathways.

Since no changes in the electronic absorption spectrum (aside from changes in acceptor concentration) were noted during the course of the quenching experiment, excited state deactivation by a chemical process (pathway 3) was ruled out. Although the acceptor and all donor molecules exhibit some type of oxidation wave more positive than -1 V *vs.* SCE, neither acceptor nor donor molecules (other than $Ru(bpy)_3^{2+}$) have a reduction potential less than +1.5 V *vs.* SCE. Therefore, deactivation by way of an electron transfer mechanism is not favorable.

The best way to prove energy transfer as being the operative deactivation pathway is to observe the luminescence from the excited acceptor molecule. Since $Pt_2(\mu\text{-dppm})_2Cl_2$, the acceptor, does not luminesce in fluid solution at room temperature, it is difficult to prove that energy transfer is the deactivation pathway. However, energy transfer mechanisms have been shown to occur even in frozen solutions according to the Perrin formula.[8] Excitation at 547 nm of a frozen dichloromethane solution containing $ReO_2(d_5\text{-py})_4^+$ and $Pt_2(\mu\text{-dppm})_2Cl_2$ did show subtle changes in the emission band profile of the $ReO_2L_4^+$ chromophore which may be due to emission from excited $Pt_2(\mu\text{-dppm})_2Cl_2$. This information alone is not definite proof of the energy transfer mechanism; however, combined with the unlikelihood that an

electron transfer or chemical reaction is occurring, electronic energy transfer from the donor to $Pt_2(\mu\text{-dppm})_2Cl_2$ is the most logical deactivation pathway available.

In fluid solution, there are two electronic mechanisms by which electronic energy transfer may occur: coulombic interaction (dipole-dipole mechanism) and exchange interaction (collisional mechanism). Detailed theoretical analysis of these mechanisms is available elsewhere.[12,13] However, the main difference between the two is that energy transfer by the coulombic interaction depends upon the oscillator strength of the $D^* \rightarrow D$ and, more importantly, $A \rightarrow A^*$ (A = acceptor, D = donor) transitions, whereas, the energy transfer by the exchange interaction is independent of these terms.[8] Thus, singlet-singlet transitions $[D(S_1) + A(S_0) \rightarrow D(S_0) + A(S_1)]$ are spin allowed by both coulombic and exchange interactions; triplet-triplet transitions $[D(T_1) + A(S_0) \rightarrow D(S_0) + A(T_1)]$ are spin forbidden by the coulombic interaction and spin allowed the exchange interaction; and both triplet-singlet $[D(T_1) + A(S_0) \rightarrow D(S_0) + A(S_1)]$ and singlet-triplet $[D(S_1) + A(S_0) \rightarrow D(S_0) + A(S_1)]$ are spin forbidden by both interactions (and rarely observed).

The majority of donors in this study are either tungsten hexanuclear dianionic clusters or rhenium dioxo monocationic monomers. Although the hexanuclear clusters are significantly larger in size than the rhenium monomers, they are both octahedral-like complexes. Also, although the hexanuclear clusters are tungsten(II) d^4 and the monomers are rhenium(V) d^2 molecules, the lowest energy absorption and emission in both systems arises from $d \rightarrow d$ transitions.[1,2] It has been experi-

mentally observed in organic systems that triplet-triplet energy transfer rates are not very sensitive to the type of orbitals involved.[8] Therefore, the difference in donor type, W *vs.* Re, is presumed to be of little consequence in this study.

The electronic energy transfer data between the various donors ($W_6X_8Y_6^{2-}$, $ReO_2L_4^+$, and $Ru(bpy)_3^{2+}$) and the acceptor ($Pt_2(\mu\text{-dppm})_2Cl_2$) are presented in Table 6.1 and plotted in Figure 6.2.[14] Since electronic energy transfer is observed from donor molecules, known to have triplet emissive excited states, to the acceptor, further evidence supporting the triplet spin label of the $Pt_2(\mu\text{-dppm})_2Cl_2$ excited state is gained.

The highest energy transfer rate of 2.1×10^9 M^{-1} sec^{-1} is observed with $(TBA)_2[W_6Br_8I_6]$ (λ_{max} = 752 nm). It is at this approximate energy that facile energy transfer between the donor and acceptor is believed to be occuring. Using the equation, k_{dif} (M^{-1} sec^{-1}) = $(2 \times 10^5)\cdot T/\eta$ where T = 300 K (temperature) and η = 0.004 P (viscosity), the diffusion controlled rate constant (k_{dif}) in dichloromethane is calculated to be ~1.5×10^{10} M^{-1} sec^{-1}. In triplet-triplet energy transfer experiments, exothermic energy transfer is not expected to occur with energy transfer rate constants, k_{et}, greater than k_{dif}. In fact, in many cases, upper limits for energy transfer quenching rate constants have been observed to be several orders of magnitude lower then the k_{dif} when one or both donor/acceptor molecules is a transition metal complex.[7] Activation barriers to energy transfer (similar to those observed in bimolecular photochemical reactions), although not required from a theoretical standpoint, may exist which keep the rate constants

Table 6.1

Energy Transfer Data Using $Pt_2(\mu\text{-dppm})_2Cl_2$ as the Acceptor

Donor	Emission Maximum nm	Emission Maximum cm^{-1}	k_q	$RT\ln k_q$
$Ru(bpy)_3^{2+}$	610	16393	$< 1 \times 10^6$	< 2880
$ReO_2(py)_4^+$	650	15385	8.1×10^7	3796.6
$ReO_2(py\text{-}d_5)_4^+$	650	15385	1.6×10^7	3458.4
$ReO_2(4\text{-pic})_4^+$	670	14925	2.9×10^6	3102.3
$ReO_2(isoquin)_4^+$	670	14925	3.6×10^7	3627.5
$W_6I_{14}^{2-}$	698	14327	1.8×10^8	3963.0
$W_6I_8Cl_6^{2-}$	701	14265	8.5×10^8	4286.8
$W_6Br_8I_6^{2-}$	752	13298	2.1×10^9	4475.2
$W_6Cl_8I_6^{2-}$	802	12469	2.6×10^8	4039.7
$W_6Cl_8Br_6^{2-}$	814	12285	3.1×10^7	3596.2
$W_6Cl_{14}^{2-}$	833	12005	$< 1 \times 10^6$	< 2880

Figure 6.2 Plot of the energy transfer data between donors ($W_6X_8Y_6^{2-}$, $ReO_2L_4^+$, $Ru(bpy)_3^{2+}$) and the acceptor, $Pt_2(\mu\text{-dppm})_2Cl_2$. (For an explanation of x axis error bars, please see reference 14.)

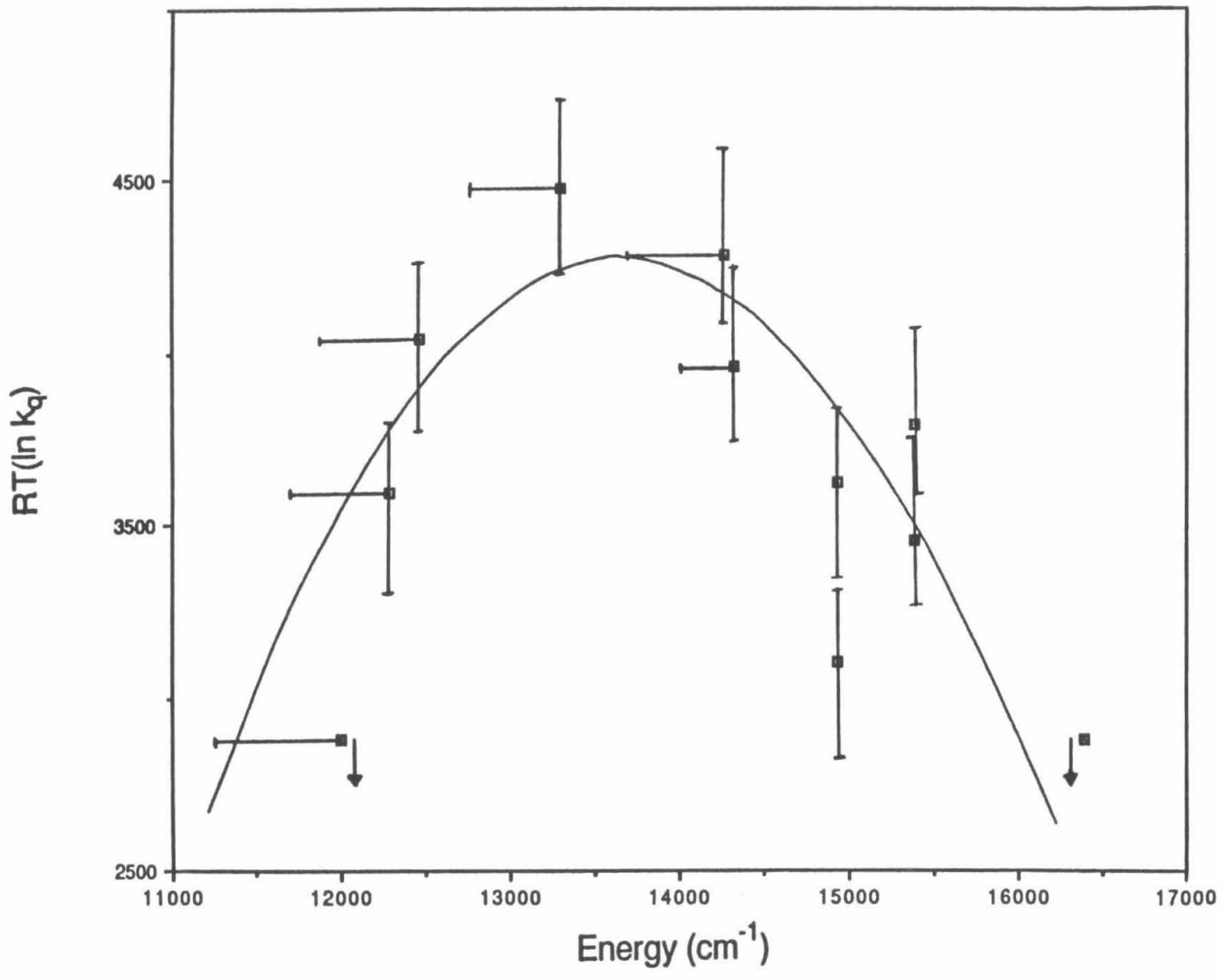
4500
3500
2500
RT(ln k_q)
11000
12000
13000
14000
15000
16000
17000
Energy (cm^{-1})

of the most facile energy transfer reactions below k_{dif}.[8]

When the acceptor's excited state energy level surpasses the donor's energy level, and the energy transfer becomes endothermic by several kilocalories per mole, energy transfer quenching is essentially shut down (see Figure 6.3a). This expected drop off in energy transfer rate constants is clearly observed in Figure 6.2. An estimate of the acceptor's excited state energy is obtained from the point at which the quenching rate begins to drop off as the energy transfer reaction becomes endothermic. Thus, the estimated energy of the $Pt_2(\mu\text{-dppm})_2Cl_2$ excited state in dichloromethane at room temperature is ~13000 cm^{-1}.

A similar drop off in transfer rates is observed for reactions in which the donor's excited state energy level is significantly greater than the acceptor's energy level (exothermic energy transfer reaction). Energy transfer theory,[9] which closely parallels Marcus theory for electron transfer, predicts a drop off of energy transfer rate constants in this the "inverted region".[10,11,17,18] In most cases, this theoretically predicted decrease in energy transfer rates is not observed; instead as the energy level difference between the donor and the acceptor becomes more exothermic, the energy transfer rate constants tend to saturate at some value, usually near k_{dif}.[8]

The most straightforward explanation for the saturation of the energy transfer rate constants as the system becomes more exothermic is depicted in Figure 6.3b. Typically, the acceptor molecule has several other higher lying electronic excited states. As the energy transfer reaction becomes more exothermic the donor's triplet level may overlap with these higher lying acceptor states; thus, the donor's energy may be transferred into these states and cascade down through established

Figure 6.3 (a) Donor and acceptor energy level schematic for endothermic energy transfer.

(b) Donor and acceptor energy level schematic for exothermic energy transfer. (Inverted region is not observed.)

(c) Donor and acceptor energy level schematic for exothermic energy transfer. (Inverted region is observed.)

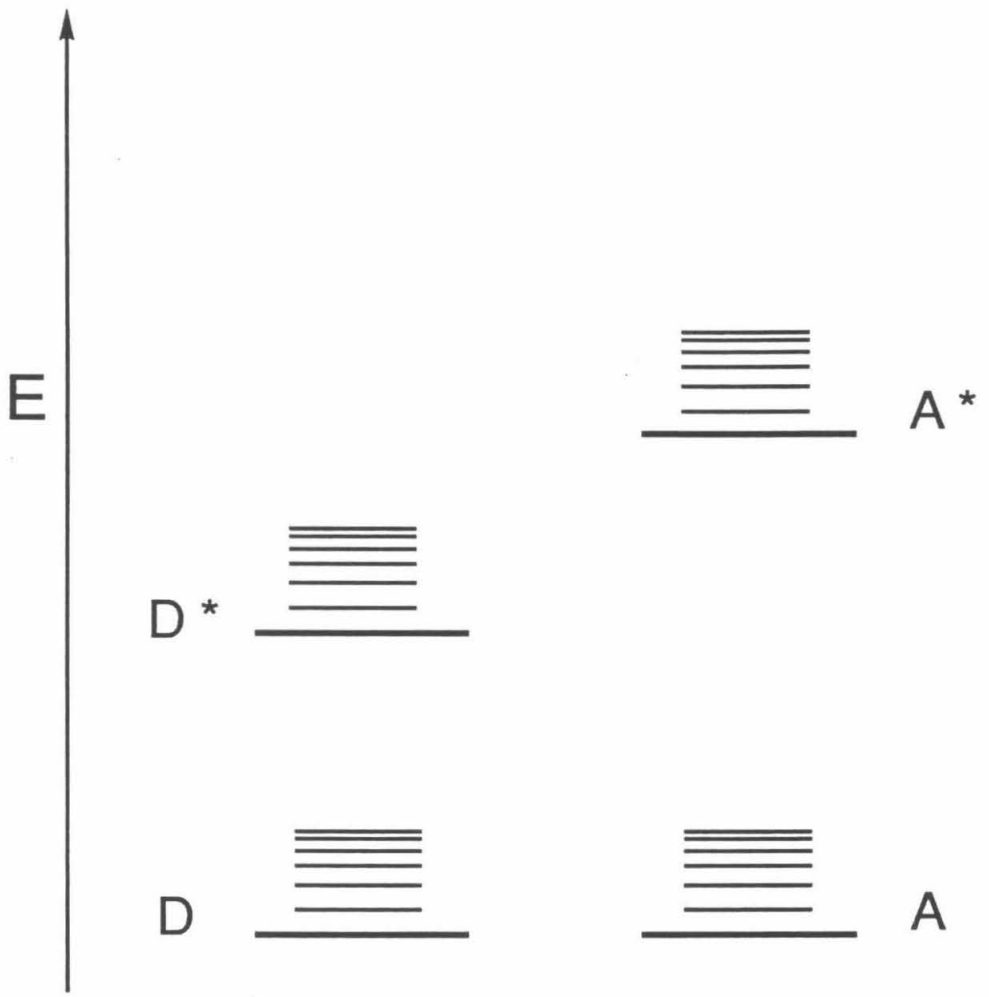
E
A *
D *
D
A

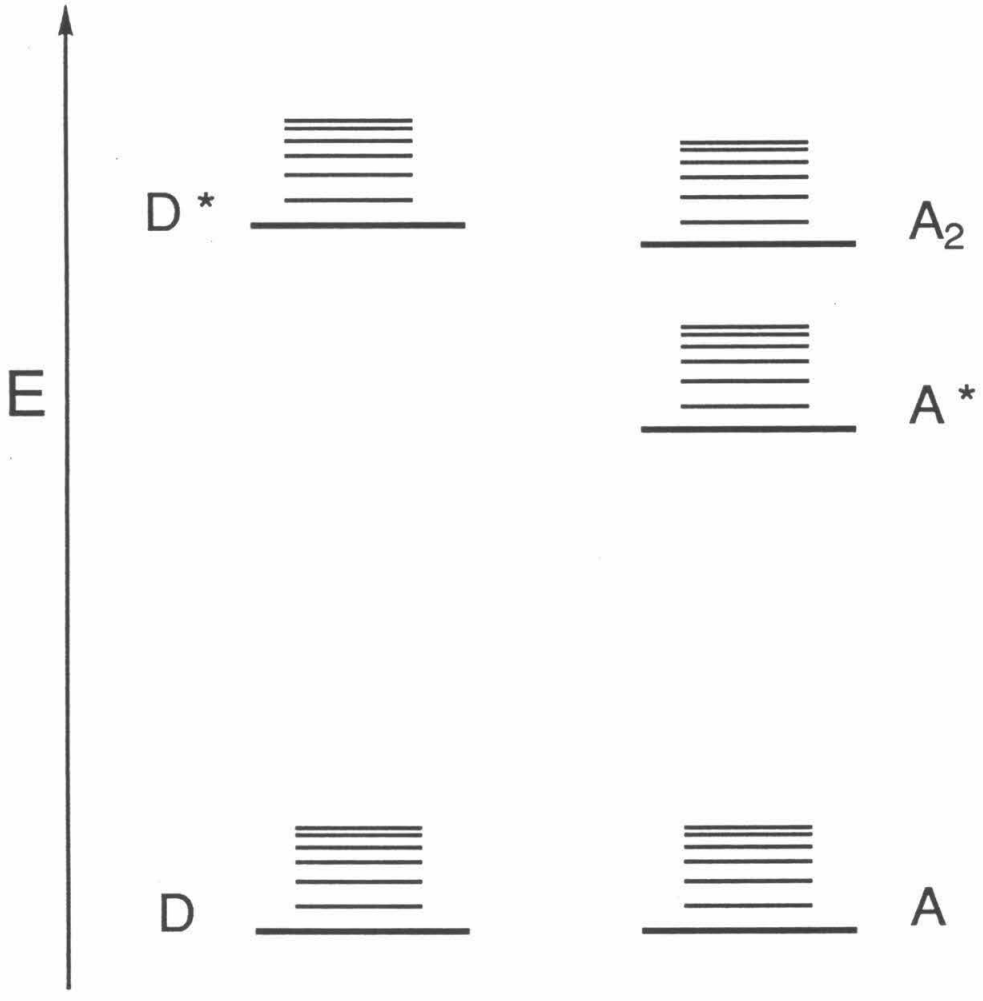
E
D *
D
A2
A *
A

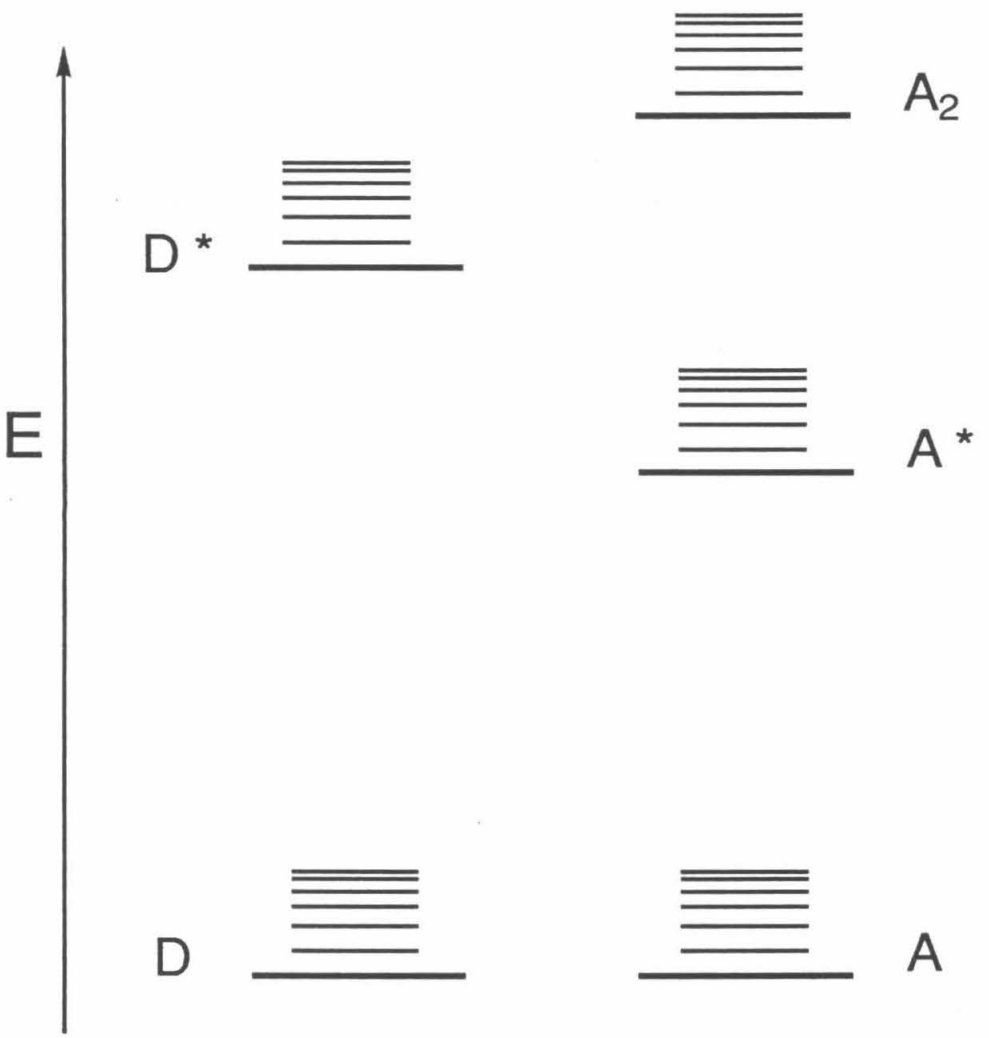
E
D
D *
A
A *
A2

deactivation pathways to the lowest triplet excited state of the acceptor. When this occurs, the anticipated inverted region is not observed. If, however, the situation arises in which the acceptor's additional electronic levels lie much higher in energy and are unable to accept the donor's excited state energy (see figure 6.3c), then the energy transfer rate constants should follow theory and the predicted decrease should be observed. It is this latter scenario which is proposed to be operative in the $Pt_2(\mu\text{-dppm})_2Cl_2$ system.

The energy transfer inverted region has been observed by a few researches in fluid solution, most notably by Engel and coworkers.[19,20] Their studies involved singlet-singlet energy transfer from various organic donors to azoalkane acceptors. In these systems, the exchange interaction was found to be the dominant energy transfer mechanism, and, a similar "window" or energy gap between the lowest electronic level and the next higher lying level was observed for the azoalkane acceptors.

In order to assert that the observed drop off in energy transfer rate is due to inherent properties of the acceptor molecule, $Pt_2(\mu\text{-dppm})_2Cl_2$, and not the nature of the donor molecules, information about energy transfer experiments of the donors with anthracene as the acceptor[21,22] was gathered and is presented in Table 6.2 and Figure 6.4. Clearly these data show the usual saturation of rates as the energy transfer reaction becomes more exothermic. Therefore, the marked decrease in energy transfer rate constants in the inverted region is attributable to the inherent characteristic of the $Pt_2(\mu\text{-dppm})_2Cl_2$ molecule.

Table 6.2

Energy Transfer Data Using Anthracene as the Acceptor†

Donor	Emission Maximum		k_q	$RT\ln k_q$
	nm	cm^{-1}		
$Ru(bpy)_3^{2+}$	610	16393	2.2×10^9	4485.0
$W_6I_{14}^{2-}$	698	14327	1.9×10^9	4454.4
$W_6Br_{14}^{2-}$	752	13298	1.1×10^8	3860.4
$W_6Cl_{14}^{2-}$	833	12005	1.0×10^7	3360.5

†Data taken from references 21 and 22.

Figure 6.4 Plot of the energy transfer data between donors ($W_6X_8Y_6^{2-}$, $Ru(bpy)_3^{2+}$) and the acceptor, anthracene. (Data taken from refences 21 and 22.)

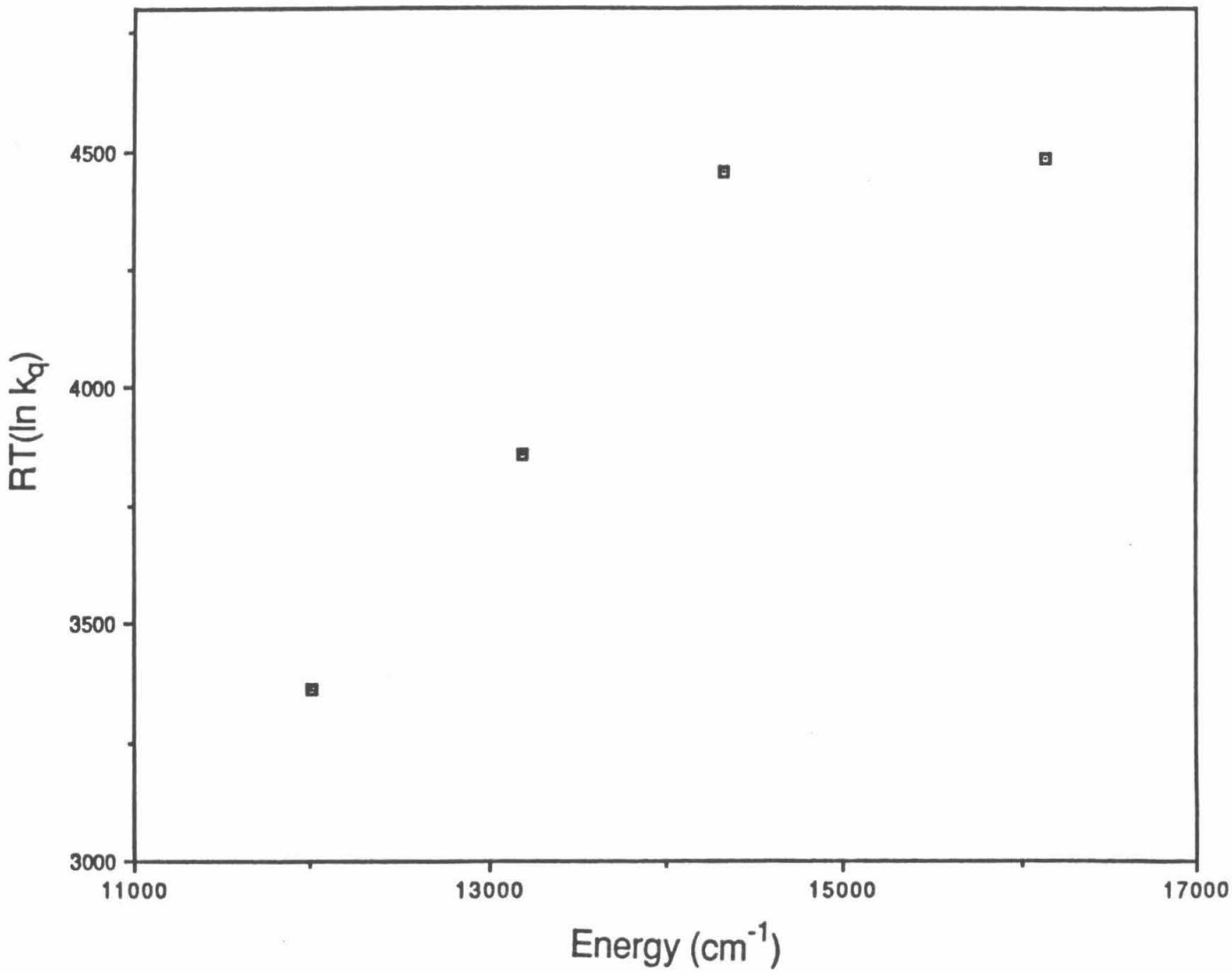
4500
4000
3500
3000
RT(ln k_q)
11000
13000
15000
17000
Energy (cm^{-1})

REFERENCES

1. Zietlow, T. C.; Nocera, D. G.; Gray, H. B. *Inorg. Chem.* **1986**, *25*, 1351.
2. Winkler, J. R.; Gray, H. B. *Inorg. Chem.* **1985**, *24*, 346.
3. Brewer, J. C.; Gray, H. B., unplublished results.
4. Broomhead, J. A.; Young, C. G. *Inorg. Synth.* **1982**, *21*, 127.
5. Parker, C. A.; Rees, W. T. *Analyst* **1960**, *85*, 587.
6. Nocera, D. G.; Winkler, J. R.; Yocom, K. M.; Bordignon, E.; Gray, H. B. *J. Am. Chem. Soc.* **1984**, *106*, 5145.
7. Balzani, V.; Moggi, L.; Manfrin, M. F.; Bolletta, F.; Laurence, G. S. *Coord. Chem. Rev.* **1975**, *15*, 321.
8. Turro, N. J. "Modern Molecular Photochemistry"; Benjamin/ Cummings: Menlo Park, CA, 1978, Ch. 9.
9. Scandola, F.; Balzani, V. *J. Chem. Ed.* **1983**, *60*, 814.
10. Kavarnos, G. J.; Turro, N. J. *Chem. Rev.* **1986**, *86*, 401.
11. Meyer, T. J. *Prog. in Inorg. Chem.* **1984**, *30*, 389.
12. Förster, T. *Disc. Faraday Soc.* **1959**, *27*, 7.
13. Dexter, D. L. *J. Chem. Phys.* **1953**, *21*, 836.
14. The error bars shown along the x axis for the $W_6X_8Y_6^{2-}$ complexes are derived from λ_{max} values reported by Zietlow *et al.*[1], Maverick *et al.*[15], and the Ph.D. thesis of Daniel G. Nocera;[16] x axis error bars for the $ReO_2L_4^+$ complexes are estimated.
15. Maverick, A. W.; Najdzionek, J. S.; Mackenzie, D.; Nocera, D. G.; Gray, H. B. *J. Am. Chem. Soc.* **1983**, *105*, 1878.
16. Nocera, D. G. "Spectroscopy, Electrochemistry, and Photochemistry of Polynuclear Metal-Metal Bonded Complexes", Ph.D. Thesis, Calif. Inst. of Tech.: California, 1984, pp 152-155.

17. Marcus, R. A. *J. Chem. Phys.* **1965**, *43*, 679.

18. Marcus, R. A. *J. Chem. Phys.* **1956**, *24*, 966.

19. Engel, P. S.; Steel, C. *Acc. Chem. Res.* **1973**, *6*, 275.

20. Engel, P. S.; Fogel, L. D.; Steel, C. *J. Am. Chem. Soc.* **1974**, *96*, 327.

21. Zietlow, T. C.; Hopkins, M. D.; Gray, H. B. *J. Solid State Chem.* **1985**, *57*, 112.

22. Wrighton, M.; Markham, J. *J. Phys. Chem.* **1973**, *77*, 3042.

CHAPTER 7

Electron Transfer Studies of $Pt_2(\mu\text{-dppm})_2Cl_2$ and Its Analogs

INTRODUCTION

Oxidation and reduction reactions are common in inorganic chemistry; thousands of examples are known. All redox reactions occur by either an inner-sphere (the complexes share one ligand in their coordination environment) or an outer-sphere (the complexes have separated coordination environments) electron transfer mechanism.[1] The electron transfer mechanism is also one of the more common excited state deactivation processes observed in inorganic photochemistry.[2-4] Rates of inner-sphere electron transfer are frequently limited by the rate of ligand substitution and are unlikely to be competitive with excited state decay rates.[2] Therefore, most of the excited state redox reactions occur by the outer-sphere electron transfer mechanism. Two examples of this type of reactivity are shown below:[5,6]

$$Ir_2(pz)_2(COD)_2 + MV^{2+} \underset{k_{q'}}{\overset{k_q}{\rightleftharpoons}} Ir_2(pz)_2(COD)_2^{+\bullet} + MV^{+\bullet}$$

$$\lambda_{em} = 684 \text{ nm}; \ \tau = 250 \text{ ns}$$

$$k_q = 8.7 \times 10^9 \text{ M}^{-1} \text{ sec}^{-1}; \ k_{q'} = 1.4 \times 10^9 \text{ M}^{-1} \text{ sec}^{-1}$$

and

$$Ru(bpy)_3^{2+} + TMPD \underset{k_{q'}}{\overset{k_q}{\rightleftharpoons}} Ru(bpy)_3^{+\bullet} + TMPD^{+\bullet}$$

$$\lambda em = 610 \text{ nm}; \ \tau = 600 \text{ ns}$$

$$k_q = 1.2 \times 10^{10} \text{ M}^{-1} \text{ sec}^{-1}; \ k_{q'} = 2.8 \times 10^{10} \text{ M}^{-1} \text{ sec}^{-1}$$

(where pz = pyrazine, COD = cyclooctadiene, MV^{2+} = methylviologen, bpy = 2,2'-bipyridine, and TMPD = N,N,N',N'-tetramethyl-1,4-phenylene-diamine). These transition metal complexes luminesce in room temperature, fluid solution and have excited state lifetimes on the order of 10^{-7} sec.

A few examples of transition metal complexes which do not luminesce

in fluid solution, but which have long-lived excited states (in fluid solution) are known. Keep in mind, that the lack of fluid solution luminescence does not rule out the possibility of excited state electron transfer reactivity. But rather, since luminescence is used as a tool for monitoring excited state electron transfer reactions, complexes which do not luminesce rarely have their excited state electron transfer reactivity investigated.

This chapter describes experiments designed to investigate the potential thermal and photochemical electron transfer reactivity of $Pt_2(\mu\text{-dppm})_2Cl_2$, which does not luminesce in fluid solution, and its analogs.

EXPERIMENTAL

Materials

All solvents, unless otherwise noted, were reagent grade and used without further purification. The dichloromethane (Baker) used in the electrochemical experiments was dried over calcium hydride and freshly distilled prior to use. The dichloromethane (Burdick and Jackson, UV grade) used in the electronic absorption and flash photolysis studies was also dried over calcium hydride and stored over Linde 3A molecular seives in a storage flask as described in the experimental section of Chapter 2. The acetonitrile (Burdick and Jackson, UV grade) used in the flash photolysis studies was dried over calcium hydride and stored over alumina in a storage flask as outlined in the experimental section of Chapter 2.

The platinum complexes, $Pt_2(\mu\text{-dppm})_2Cl_2 \cdot 0.5CH_2Cl_2$ and $[Pt_2(\mu\text{-dppm})_2(PPh_2Me)_2{}^{2+}](PF_6)_2$, were prepared as described in the experimental section of Chapter 5.

Tetracyanoethylene, TCNE, (Aldrich, 98%) was recrystallized twice from chlorobenzene and sublimated under vacuum. White crystalline chunks were obtained.

Tetracyanoquinodimethane, TCNQ, (Aldrich, 98%) was recrystallized twice from chlorobenzene and dried *in vacuo*. This complex darkens after several weeks in air; therefore, recrystallization and drying was carried out immediately prior to the EPR experiments.

Methylviologen hexafluorophosphate, MV^{2+}, and tetrabutylammonium hexafluorophosphate, $TBAPF_6$, were prepared and purified as outlined in the experimental section of Chapter 2.

Physical Measurements

Electrochemical Measurements. All cyclic voltammograms were measured in dichloromethane using the same equipment and operating procedures as detailed in the experimental section of Chapter 2. Several sets of electrochemical experiments were done. First, cyclic voltammograms were measured of $Pt_2(\mu\text{-dppm})_2Cl_2$ and $[Pt_2(\mu\text{-dppm})_2(L)_2(PF_6)_2$ where L = PPh_3, PPh_2Me, and $PPhMe_2$. Next, bulk electrolysis of a dichloromethane solution of 1×10^{-3} M TCNE and 0.1 M $TBAPF_6$ was performed. And, finally, cyclic voltammograms monitoring the progress of the $Pt_2(\mu\text{-dppm})_2Cl_2$ + TCNE thermal reaction were measured in conjunction with EPR experiments. These samples consisted of an N_2 purged dichloromethane solution of 1×10^{-3} M $Pt_2(\mu\text{-dppm})_2Cl_2$, 1×10^{-3} M TCNE, and 0.1 M $TBAPF_6$.

Electronic Absorption Spectroscopy. Spectra were recorded using the Shimatzu UV-260 spectrophotometer. The $Pt_2(\mu\text{-dppm})_2Cl_2$ + TCNE dark reaction was run in a special photometric cell which consisted of a central square precision quartz cuvette (1 cm pathlength), flanked on either side by a pyrex round bulb (2 in total), which were separated from the cuvette by teflon vacuum valves. A third teflon vacuum valve atop the photometric cell was used to keep the entire vessel under vacuum. The platinum complex and TCNE were placed in separate bulbs and the entire cell was evacuated on a high vacuum line (limiting pressure $<10^{-3}$ Torr). Under vacuum, ~4 mL of dichloromethane was distilled from the solvent pot into the bulb containing the platinum complex. This solution was transfered to the cuvette and an absorption spectrum was measured. Subsequently, some TCNE from the second bulb was added to the platinum solution in the cuvette and the progress of the ensuing

dark reaction was monitored by successive absorption scans.

Electron Paramagnetic Resonance Spectroscopy. All EPR spectra were measured on a Varian E-line Century Series spectrometer at 5 mW power. EPR spectra run in conjunction with electrochemical measurements were prepared under N_2 by syringing 0.5 mL of the electrochemical solution (described under the electrochemical measurements) into a N_2 purged EPR tube capped with a septum. All other EPR samples were prepared by mixing 1:1 dichloromethane solutions of 1×10^{-3} M or 5×10^{-4} M $Pt_2(\mu\text{-dppm})_2Cl_2$ with 1×10^{-3} M or 5×10^{-4} M TCNE (v/v) together in a graduated cylinder and syringing 0.5 mL into a quartz EPR tube. Most of these samples were prepared in air; however, several $Pt_2(\mu\text{-dppm})_2Cl_2$ + TCNE samples were prepared under N_2 or degassed completely. No significant differences between the EPR spectra of samples prepared in air, under nitrogen, or in degassed solutions were observed. Similar procedures were used for preparing $Pt_2(\mu\text{-dppm})_2(PPh_2Me)_2^{2+}$ + TCNE and $Pt_2(\mu\text{-dppm})_2Cl_2$ + TCNQ samples.

Microsecond Flash Photolysis Experiments. Flash photolysis studies were conducted on an apparatus constructed at Caltech and described elsewhere.[7,8] Flash lamp excitation wavelengths greater than 350 nm were used. Absorption changes were monitored at 360 and 605 nm. A 1:1 CH_2Cl_2:CH_3CN (v/v) mixed solvent containing ~1×10^{-4} M $Pt_2(\mu\text{-dppm})_2Cl_2$ and 5×10^{-3} M MV^{2+} was prepared in a flash photolysis cell consisting of a cylindrical pyrex compartment (15 cm pathlength), a 50 mL pyrex bulb, and a square cuvette (1 cm pathlength), each oriented 90° from one another. A set of control experiments to check for MV^{2+} and solvent contamination were done. The transient absorption at 605 nm of a CH_3CN solution of 5×10^{-3} M MV^{2+} and a 1:1 CH_2Cl_2:CH_3CN (v/v) mixed

solvent of 5×10^{-3} M MV^{2+} were measured; however, in both cases no $MV^{+\bullet}$ was detected.

Steady State Photolysis Procedures. A 1000 W high pressure Hg/Xe arc lamp equipped with Corning cutoff filters ($\lambda > 350$ nm) was used for the irradiations. Samples were prepared by placing $Pt_2(\mu\text{-dppm})_2Cl_2$ (~1 mg) in a two compartment spectrophotometric cell equipped with a teflon vacuum valve and evacuating on a high pressure vacuum line (limiting pressure $< 10^{-3}$ Torr). Dichloromethane was distilled from the storage flask into the spectrophotometric cell under vacuum. The dichloromethane solutions of $Pt_2(\mu\text{-dppm})_2Cl_2$ (various concentrations) were photolyzed over a period of 3 days. No electronic absorption spectral changes were observed over the course of the photolysis; hence, $Pt_2(\mu\text{-dppm})_2Cl_2$ is considered to be photo-stable in dichloromethane.

RESULTS and DISCUSSION

The redox properties of $Pt_2(\mu\text{-dppm})_2Cl_2$ and $Pt_2(\mu\text{-dppm})_2L_2$ have been investigated and the results are presented in Table 7.1. The $Pt_2(\mu\text{-dppm})_2Cl_2$ complex exhibits an irreversible oxidation +0.85 V *vs.* SCE. Similar studies performed by Nemra *et al.*[9] on $Pd_2(\mu\text{-dppm})_2Cl_2$ and $PtPd(\mu\text{-dppm})_2Cl_2$ in 1,2-dichloroethane show irreversible oxidations at +0.98 V and +0.96 V *vs.* SCE, respectively. In the Pd(I) and mixed Pd(I)Pt(I) dimers, the oxidation occurs by way of a one electron process; this same process is believed to occur in the platinum system. No return peak on the reverse is observed in the cyclic voltammogram at scans rates up to 500 mV/sec; therefore, the Pt(I,II) species produced must be fairly unstable, possibly reacting with the solvent.

No reduction wave was observed as far out as -1.5 V *vs.* SCE for the platinum(I) dimer. Irreversible two electron reductions were observed for $Pd_2(\mu\text{-dppm})_2Cl_2$ and $PtPd(\mu\text{-dppm})_2Cl_2$ at -1.26 V and -1.70 V *vs.* SCE, respectively.[9] From these results, a similar two electron irreversible reduction of $Pt_2(\mu\text{-dppm})_2Cl_2$ is expected to occur at a potential more negative than -1.70 V *vs.* SCE. Thus, for the most part, any electron transfer chemistry observed with the platinum(I) dimers will most likely involve a one electron oxidation of the complex.

Thermal and photochemical reactions designed to probe the electron transfer reactivity of these platinum complexes with various organic acceptors were undertaken. Tetracyanoethylene, TCNE, is very easily reduced, with a one electron reduction potential of +0.15 V *vs.* SCE.[10] Owing to the pronounced energy difference between neutral TCNE and $TCNE^{2-}$, the $TCNE^{-\bullet}$ has a high solution stability, making it an ex-

Table 7.1

Oxidation Potentials of $[Pt_2(\mu\text{-dppm})_2Y_2]^{n+}$

Complex	$\sim E_{1/2}$ *vs.* SCE
$Pt_2(\mu\text{-dppm})_2Cl_2$	+0.85 V
$[Pt_2(\mu\text{-dppm})_2(PPh_3)_2](PF_6)_2$	+1.3 V
$[Pt_2(\mu\text{-dppm})_2(PPh_2Me)_2(PF_6)_2$	+1.3 V
$[Pt_2(\mu\text{-dppm})2(PPhMe_2)_2(PF_6)_2$	+1.35 V

cellent one electron acceptor.[11] Upon mixing $Pt_2(\mu\text{-dppm})_2Cl$ with TCNE in deaerated dichloromethane, $TCNE^{-\bullet}$ was immediately produced, even in reactions where room light was rigorously excluded. Successive scans of the electronic absorption spectrum of the reaction mixture (Figure 7.1) clearly show an absorption band with the vibrational fine structure characteristic of the $TCNE^{-\bullet}$ growing in at ~440 nm.

Although ground state electron transfer from the platinum complex to TCNE should not occur based on ground state redox potentials, some type of adduct formation may occur which facilitates the electron transfer. Considering that several examples of small molecules adding thermally across the metal-metal bond of $Pt_2(\mu\text{-dppm})_2Cl_2$ are known to occur, the prospect for a $Pt_2(\mu\text{-dppm})_2Cl_2$-TCNE adduct forming prior to the electron transfer step is quite reasonable. Further oxidation of the platinum complex to produce a stable d^8-d^8 platinum dimer containing a tetracyanoethane bridge does not seem to occur due to the high stability of the $TCNE^{-\bullet}$.

Evidence for the proposed $Pt_2(\mu\text{-dppm})_2Cl_2^{+\bullet}$ / $TCNE^{-\bullet}$ adduct is obtained from EPR spectra. The EPR spectrum of the electrochemically generated $TCNE^{-\bullet}$ in dichloromethane (tetrabutylammonium hexafluorophosphate, $TBAPF_6$, present as electrolyte) and spectrum of the $TCNE^{-\bullet}$ generated by reduction with $Pt_2(\mu\text{-dppm})_2Cl_2$ in dichloromethane (no $TBAPF_6$ present) have several similarities, but, the overall shapes of the spectra are different.

The EPR spectrum of the electrochemically generated $TCNE^{-\bullet}$ is shown in Figure 7.2a. The EPR lines are significantly broadened from spectra previously reported for the $TCNE^{-\bullet}$.[12] This broadening is due to self-exchange between neutral TCNE and the radical facilitated by the

Figure 7.1 Electronic absorption spectrum of the thermal electron transfer reaction between $Pt_2(\mu\text{-dppm})_2Cl_2$ and TCNE in dichloromethane (room light excluded).

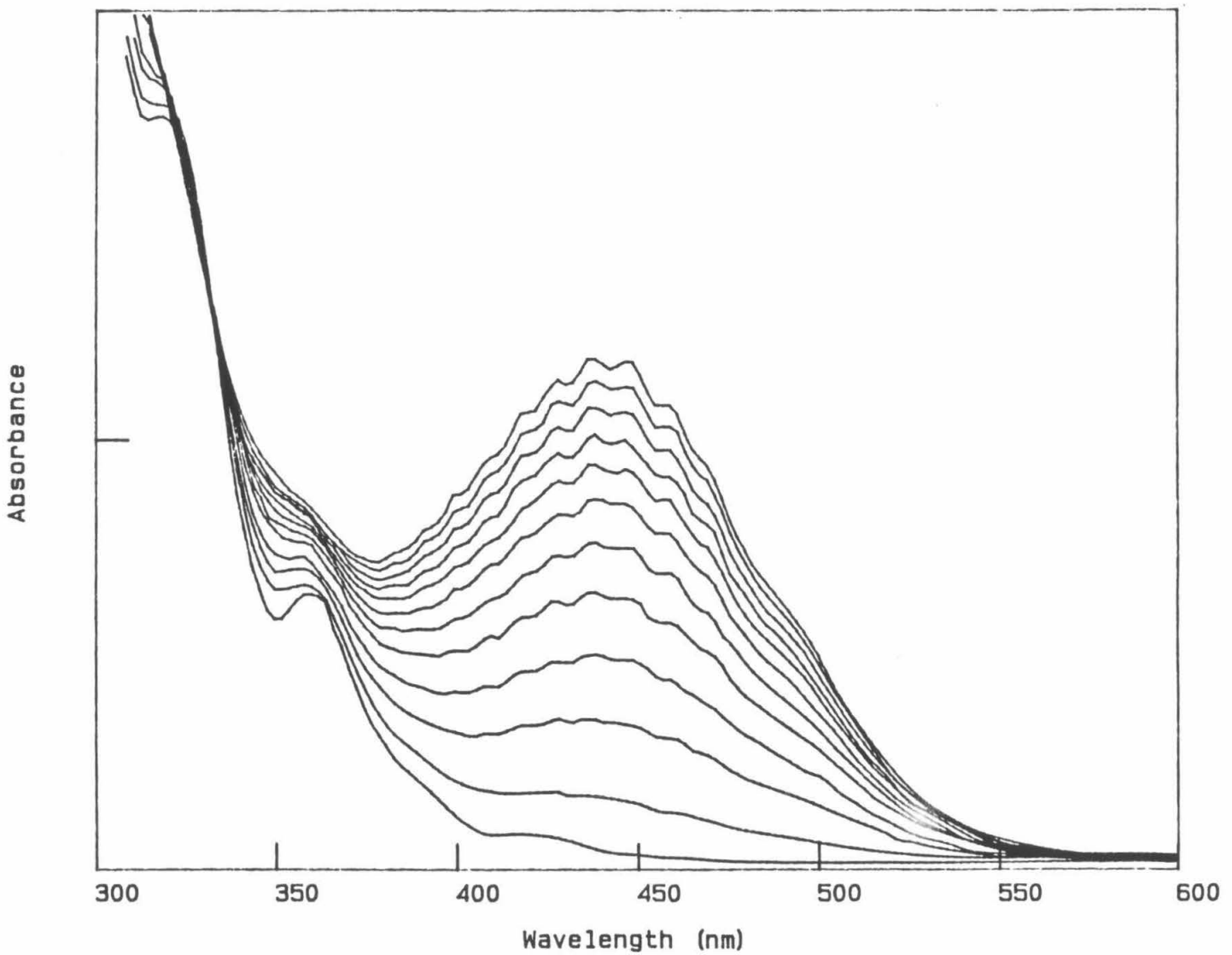
Absorbance
300
350
400
450
500
550
600
Wavelength (nm)

presence of the supporting electrolyte, $TBAPF_6$ (required for bulk electrolysis).[13] The uncoordinated $TCNE^{-\bullet}$ spectrum exhibits a total of 13 lines. The nine predominant lines (center of the spectrum) are expected for the four equivalent ^{14}N (I=1) nuclei; whereas, the smaller lines found at the beginning and end of the spectrum are best attributed to ^{13}C nuclei.[12] The spectrum has a g value of 2.001 and the spacing is 1.56 Hz; both results are in excellent agreement with previously reported results for $TCNE^{-\bullet}$.[12]

As for the EPR spectrum obtained when TCNE is reduced with $Pt_2(\mu\text{-dppm})_2Cl_2$, a similar g value of 2.000 and a range of line spacings 1.52 to 1.56 Hz is observed, see Figure 7.2b. From these results it is evident that the radical generated from this reaction does indeed resemble that of $TCNE^{-\bullet}$. However, in this spectrum, ~27 lines are observable. Since the total number of lines observed far exceeds that expected for uncoordinated $TCNE^-$ radical, it is presumed that the electron primarily localized on the TCNE also feels the presence of other nuclei in the vicinity such as ^{31}P (I = 1/2) and ^{195}Pt (I = 1/2). It is the observation of all these additional EPR lines which supports the supposition that some type of $Pt_2(\mu\text{-dppm})_2Cl_2$-TCNE adduct formation occurs to facilitate the electron transfer.

An EPR signal attributable to the oxidized platinum species was not observed. Since it is not uncommon for transition metal complexes to have spin lattice relaxation times which are too short to allow for signal detection at room temperature,[14] the absence of the oxidized platinum complex's signal is not unusual.

The overall shape of the EPR spectrum obtaining from the $Pt_2(\mu\text{-dppm})_2Cl_2$ + TCNE reaction differs from reaction mixture to reaction

Figure 7.2 (a) EPR spectrum of electrochemically generated $TCNE^{-\bullet}$ in dichloromethane (0.1 M $TBAPF_6$, 300 K).

(b) EPR spectrum of the thermal electron transfer reaction between $Pt_2(\mu\text{-dppm})_2Cl_2$ and TCNE in dichloromethane (300 K).

(c) A second EPR spectrum of the thermal electron transfer reaction between $Pt_2(\mu\text{-dppm})2Cl_2$ and TCNE in dichloromethane (300 K).

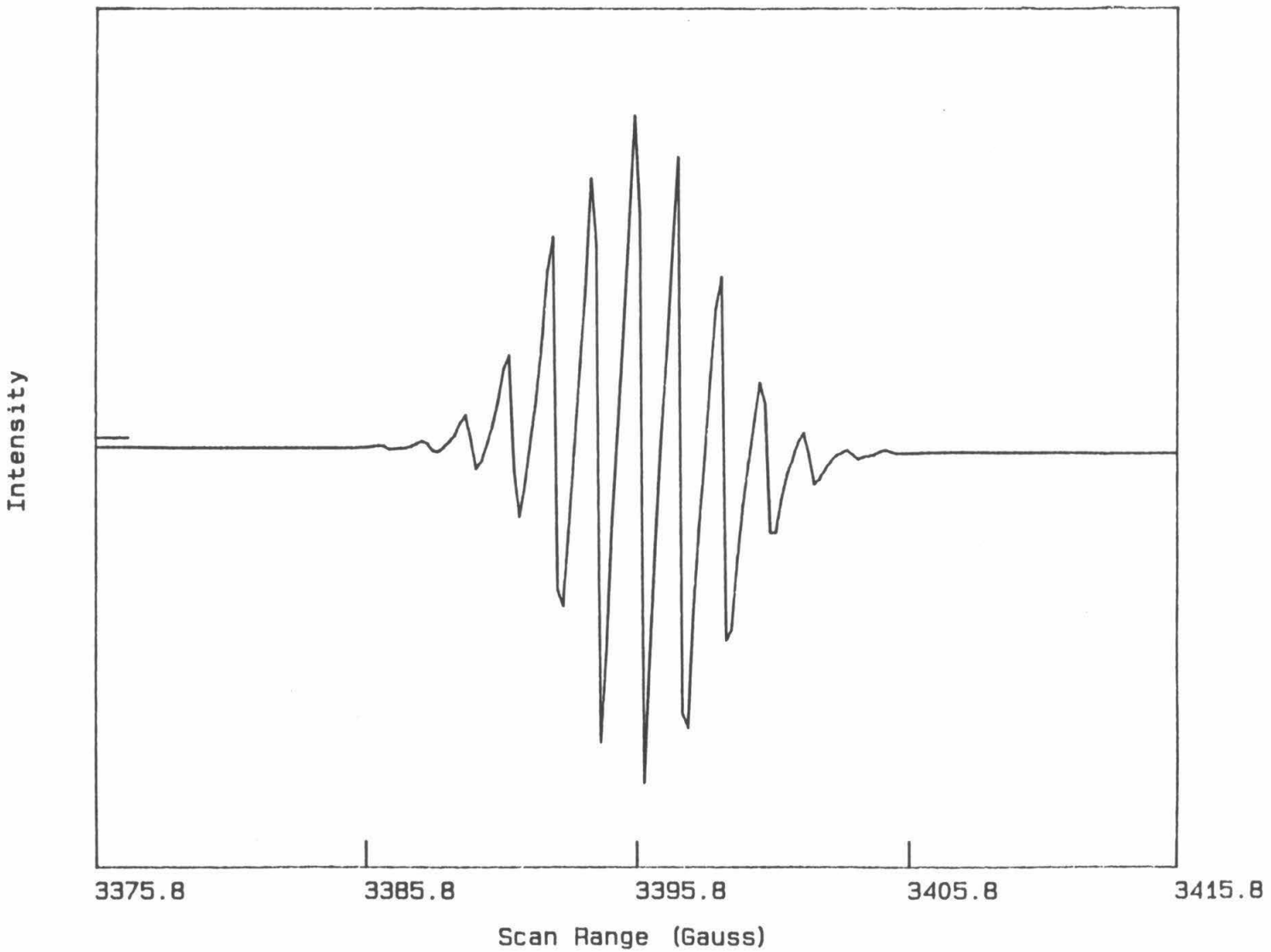
Intensity
3375.8
3385.8
3395.8
3405.8
3415.8
Scan Range (Gauss)

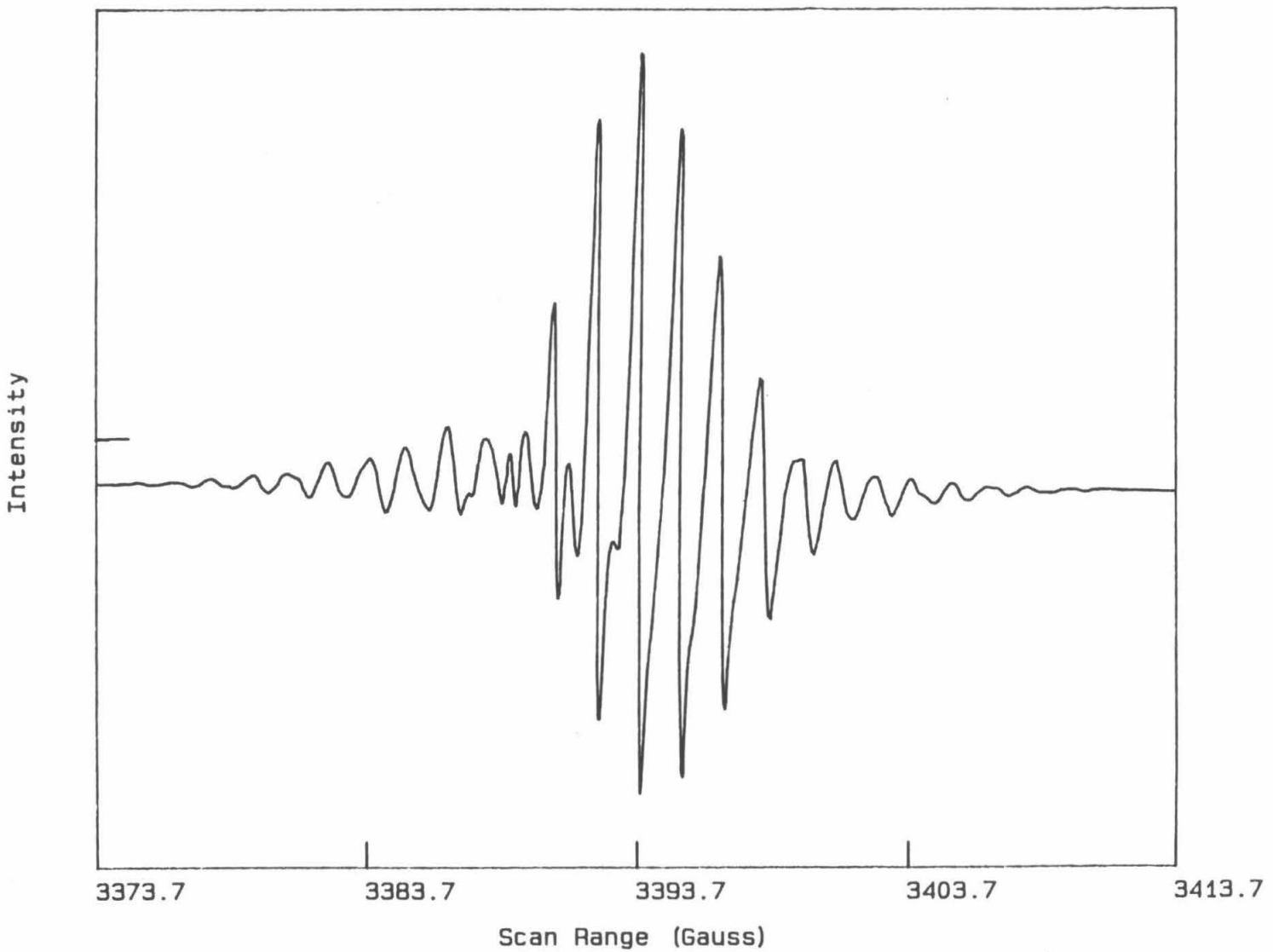
Intensity
3373.7
3383.7
3393.7
3403.7
3413.7
Scan Range (Gauss)

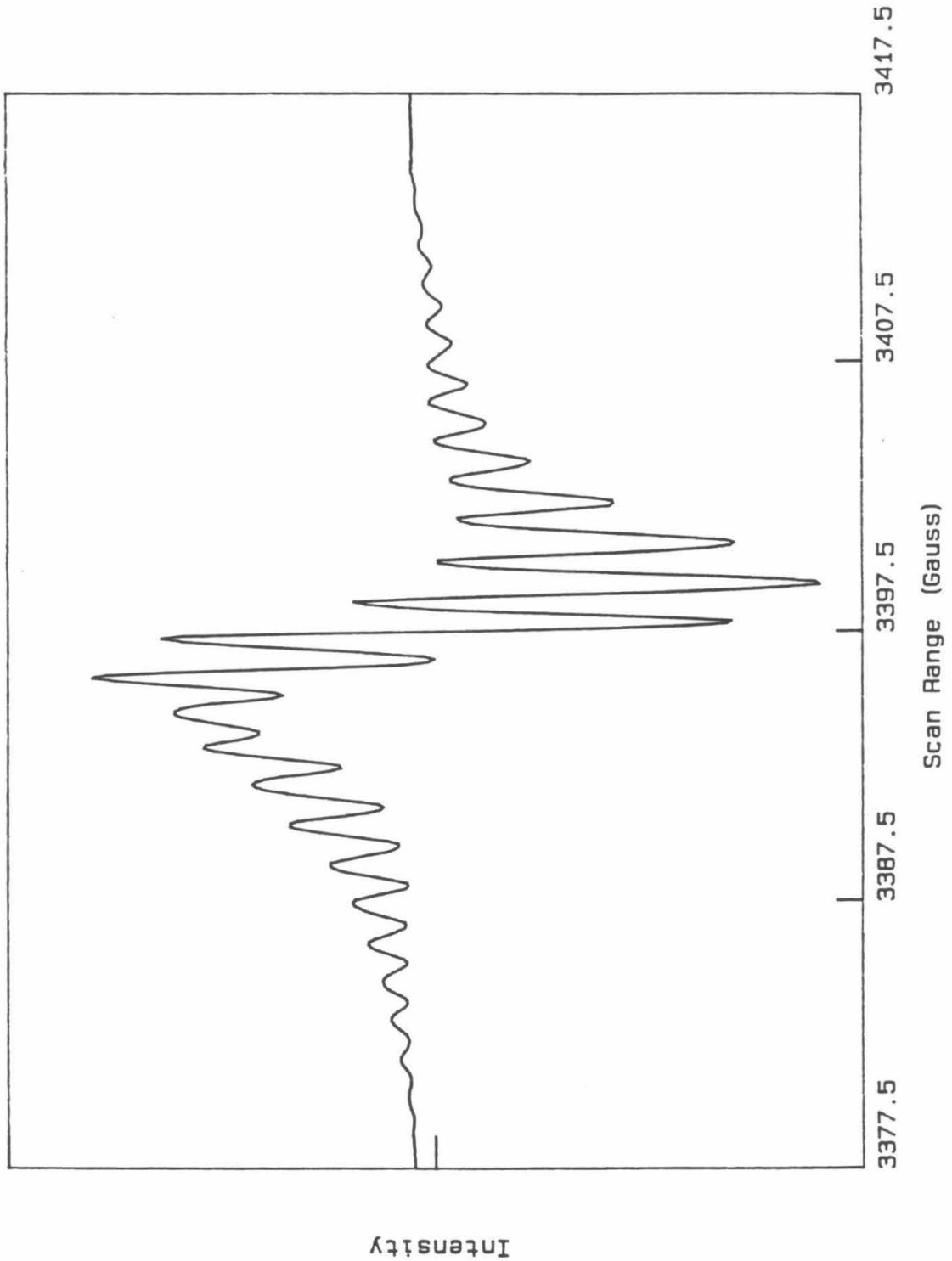
3377.5
3387.5
3397.5
3407.5
3417.5
Scan Range (Gauss)
Intensity

mixture, although about the same number of EPR lines are observed and the g value and range of line spacings are identical in all cases. (Examples of these differences may seen by comparing Figures 7.2b and 7.2c.) The difference in shape, along with the general complexity of the EPR spectrum itself, seems to indicate that the reaction mixture may contain several structural isomers of the $Pt_2(\mu\text{-dppm})_2Cl_2$-TCNE adduct.

Similar thermal electron transfer experiments between $Pt_2(\mu\text{-dppm})_2Cl_2$ and 7,7,8,8-tetracyanoquinodimethane, TCNQ were also conducted. TCNQ, like TCNE, is easy to reduce, $E_{1/2}$ = +0.127 V *vs.* SCE;[15] but unlike TCNE, TCNQ is a much bulkier electron acceptor and may not allow similar adduct formation to occur. Upon mixing the platinum complex with TCNQ a very complicated radical signal was observed. However, since the EPR spectrum of uncoordinated $TCNQ^{-\bullet}$ is reported to contain 43 lines, information regarding $Pt_2(\mu\text{-dppm})_2Cl_2$-TCNQ adduct formation was not forthcoming.

Surprisingly, reaction of $Pt_2(\mu\text{-dppm})_2(PPh_2Me)_2^{2+}$ with TCNE did not result in the formation of any radical species. There are two explanations for this lack of reactivity: (*i*) the phosphine groups in the axial positions of $Pt_2(\mu\text{-dppm})_2(PPh_2Me)_2^{2+}$ constricts access to the metal-metal bond, thus making adduct formation much more difficult than in the halide analog, and (*ii*) $Pt_2(\mu\text{-dppm})_2(PPh_2Me)_2^{2+}$ is ~45 mV more difficult to oxidize than $Pt_2(\mu\text{-dppm})_2Cl_2$.

In order to obtain additional information about the $Pt_2(\mu\text{-dppm})_2Cl_2$ + TCNE thermal reaction, its progress was simultaneously monitored by cyclic voltammetry and EPR over a 14 hour period. An N_2 purged

dichloromethane solution of 1×10^{-3} M $Pt_2(\mu\text{-dppm})_2Cl_2$, 1×10^{-3} M TCNE, and 0.1 M $TBAPF_6$ was prepared; 11 mL of the solutions was placed in the electrochemical cell and 0.5 mL was placed in a septum-sealed quartz EPR tube.

At first only the TCNE reduction and $Pt_2(\mu\text{-dppm})_2Cl_2$ oxidation waves were observed in the cyclic voltammogram, but, within a few minutes a new quasi-reversible wave at ~+0.3 V *vs.* SCE and an irreversible oxidation wave at ~+1.2 V *vs.* SCE appeared. After about 2 and a half hours the quasi-reversible wave at ~+0.3 V *vs.* SCE disappeared. And after 14 hours, the reduction wave of TCNE was substantially diminished (only 10% of the original signal remained) and only the irreversible oxidation wave at +1.2 V *vs.* SCE was observed.

The initial EPR spectrum obtained resembled the EPR spectra previously obtained for the thermal $Pt_2(\mu\text{-dppm})_2Cl_2$ + TCNE reaction (without electrolyte). However, as the reaction progressed, some of the EPR lines began to disappear and all the remaining lines began to sharpen. By the end of the experiment (14 hours later), the EPR spectrum consisted of 13 rather sharp lines, remarkably resembling uncoordinated $TCNE^{-\bullet}$. The results of these experiments are puzzling, especially in light of the fact that the EPR spectra of dichloromethane solutions of $Pt_2(\mu\text{-dppm})_2Cl_2$ + TCNE without electrolyte present do not show this unusual behavior with time. Naturally, these results raise questions about the role of the $TBAPF_6$ in this reaction.

One possiblity is that the electrolyte facilitates the further oxidation of the $Pt_2(\mu\text{-dppm})_2Cl_2^{+\bullet}$ / $TCNE^{-\bullet}$ adduct to produce a d^8-d^8 platinum dimer containing a tetracyanoethane bridge. Since the reaction was run at a 1:1 stoichiometry and only ~90 % of the TCNE was

consumed during the course of the reaction, possible platinum dimer decomposition may have occurred resulting in uncoordinated TCNE existing in its radical state. With this in mind, the transient quasi-reversible wave at ~+0.3 V *vs.* SCE may be attributable to the $Pt_2(\mu\text{-dppm})_2Cl_2^{+\bullet}$ / $TCNE^{-\bullet}$ adduct, the irreversible oxidation at ~1.2 V *vs.* SCE may be attributable to the d^8-d^8 platinum dimer (which is EPR silent), and the residual $TCNE^{-\bullet}$ (whose oxidation wave is observed in the final cyclic voltammogram) remains as the only species observed in the final EPR spectrum.

Further electron transfer experiments between $Pt_2(\mu\text{-dppm})_2Cl_2$ and methylviologen hexafluorophosphate, MV^{2+}, were investigated; the reduction potential of MV^{2+} is -0.45 V *vs.* SCE.[6] Unlike in the TCNE experiments, no ground state electron transfer between the platinum complex and MV^{2+} was observed. Flash photolysis of MV^{2+} in the presence of $Pt_2(\mu\text{-dppm})_2Cl_2$, however, resulted in the production of $MV^{+\bullet}$. Although a complete transient absorption spectrum of the $MV^{+\bullet}$ was not collected, an increase of the absorptions at 605 and 360 nm were observed and the characteristic blue color of the $MV^{+\bullet}$ radical was detected after several repetitive flashes.

Since a mixed solvent system, 1:1 (v/v) CH_2Cl_2:CH_3CN was used, several control experiments were done to rule out the possibility of MV^{2+} or solvent contamination; see insert in Figure 7.3a. Monitoring at 605 nm, the transient decay signal shown in Figure 7.3a was obtained. These data were evaluated according to the bimolecular rate equation:

$$1/\Delta C = 1/C_t - 1/C_o = kt$$

(where C_t is the concentration of the absorbing species at some time t, and C_0 is the inital concentration). Since the flash photolysis data obtained are in absorption units and $A = \varepsilon bC$, the bimolecular rate expression used to calculate the rate constant for back electron transfer, k_b, is modified as:

$$b\Delta\varepsilon/\Delta A = b\varepsilon_t/A_t - b\varepsilon_o/A_o = k_b t$$

or

$$1/\Delta A = (k_b/b\Delta\varepsilon)t.$$

The plot of $1/\Delta A$ *vs.* t is shown in Figure 7.3b. Since most of the absorption at 605 nm is due to the $MV^{+\bullet}$, $\Delta\varepsilon$ is approximated as $\Delta\varepsilon_{MV^{+\bullet}}$, whose value has been experimentally determined by Kosower *et al.*[16] as 13,000 $M^{-1}\,cm^{-1}$. The cell pathlength, b, is 15 cm and the slope of the $1/\Delta A$ *vs.* t plot is 0.07 sec^{-1}. Therefore, the back electron transfer rate constant is calculated to be 1.5 (±0.5) × 10^4 $M^{-1}\,sec^{-1}$. For stability, the oxidized platinum dimer may coordinate solvent, namely CH_3CN, which could account for the surprisingly slow back electron transfer rate. There is, however, no direct evidence for this proposed solvent coordination.

In conclusion, these experiments have shown that both ground state and excited state electron transfer from $Pt_2(\mu\text{-dppm})_2Cl_2$ are possible even though the platinum complex does not luminesce in fluid solution.

Figure 7.3 (a) Flash photolysis trace of the back electron transfer from $MV^{+\bullet}$ to the oxidized $Pt_2(\mu\text{-dppm})_2Cl_2$ in 1:1 dichloromethane:acetonitrile (v/v). [Insert: Flash photolysis trace of MV^{2+} in 1:1 dichloromethane :acetonitrile (v/v).] Absorption monitored at 605 nm.

(b) Plot of $1/\Delta A$ *vs.* t (sec) for the back electron transfer from $MV^{+\bullet}$ to the oxidized $Pt_2(\mu\text{-dppm})_2Cl_2$.

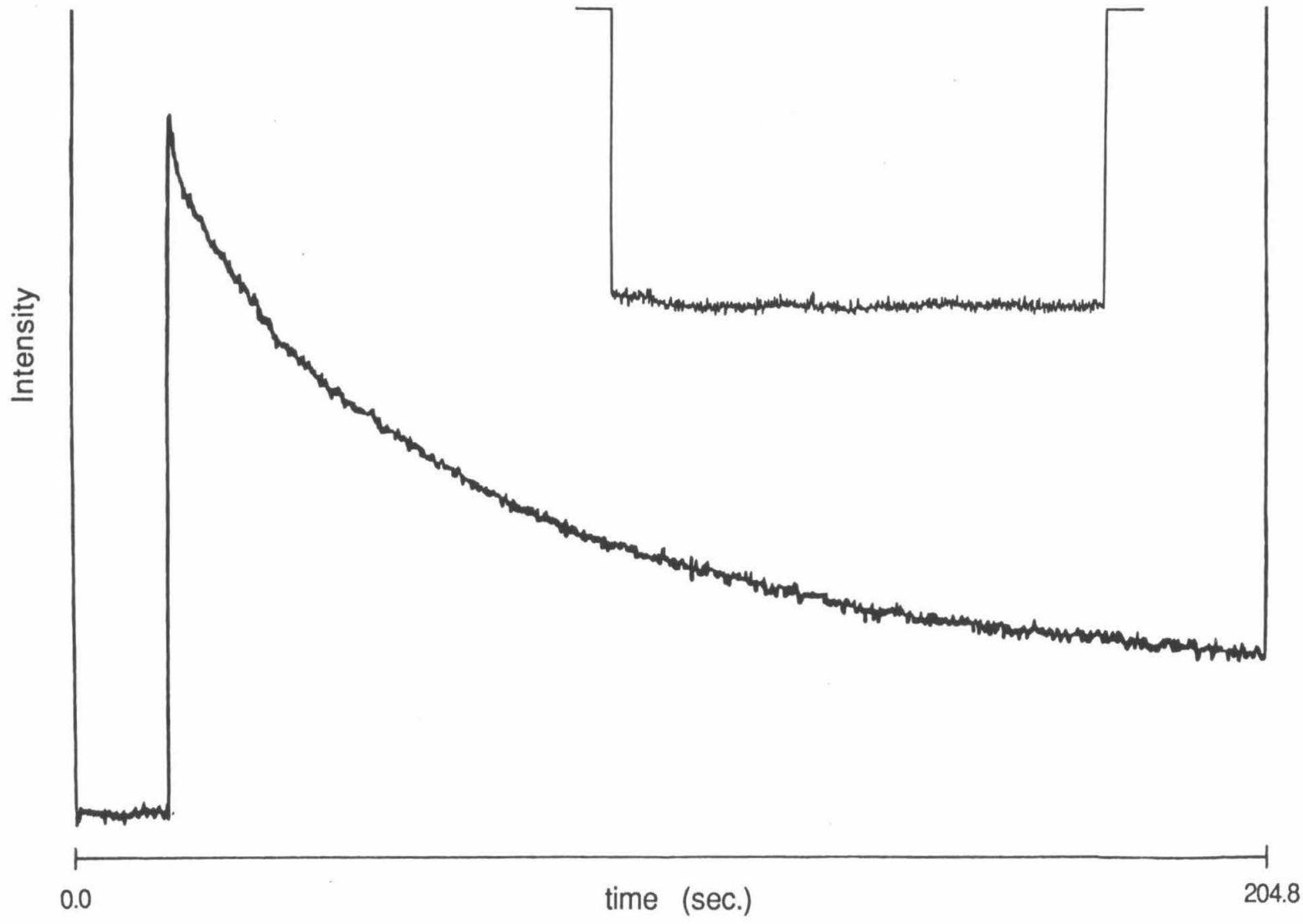
Intensity
0.0
time (sec.)
204.8

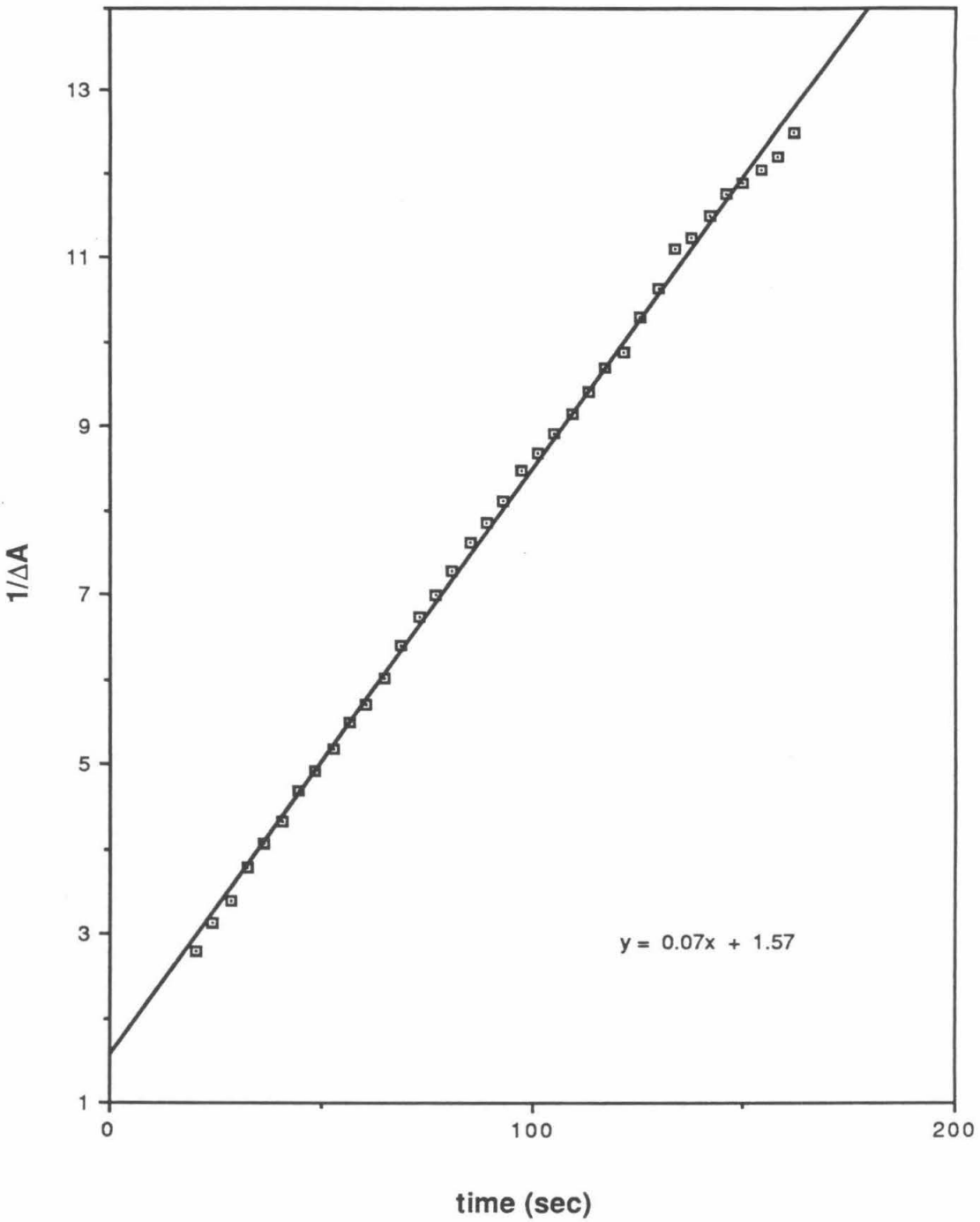
13
11
9
7
5
3
1
1/ΔA
0
100
200
time (sec)
y = 0.07x + 1.57

REFERENCES

1. Cotton, F. A.; Wilkinson, G. "Advanced Inorganic Chemistry, Fifth Ed."; Wiley: New York, 1988, pp 1306-1318.
2. Balzani, V.; Moggi, L.; Manfrin, M. F.; Bolletta, F.; Laurence, G. S. *Coord. Chem. Rev.* **1975**, *15*, 321.
3. Kavarnos, G. J.; Turro, N. J. *Chem. Rev.* **1986**, *86*, 401.
4. Meyer, T. J. *Prog. Inorg. Chem.* **1984**, *30*, 389.
5. Marshall, J. L.; Stobart, S. R.; Gray, H. B. *J. Am. Chem. Soc.* **1984**, *106*, 3027.
6. Bock, C. R.; Connor, J. A.; Gutierrez, A. R.; Meyer, T. J.; Whitten, D. G.; Sullivan, B. P.; Nagle, J. K. *J. Am. Chem. Soc.* **1979**, *101*, 4815.
7. Nocera, D. G.; Winkler, J. R.; Yocom, K. M.; Bordignon, E.; Gray, H. B. *J. Am. Chem. Soc.* **1984**, *106*, 5145.
8. Milder, S. J.; Goldbeck, R. A.; Kliger, D. S.; Gray, H. B. *J. Am. Chem. Soc.* **1980**, *102*, 6761.
9. Nemra, G.; Lemoine, P.; Braunstein, P.; de Meric de Bellefon, C.; Ries, M. *J. Organomet. Chem.* **1986**, 245.
10. Meites, L.; Zuman, P. "CRC Handbook Series in Organic Chemistry" 1976, Vol 1.
11. Webster, O. W.; Mahler, W.; Benson, R. E. *J. Am. Chem. Soc.* **1962**, *84*, 3678.
12. Phillips, W. D.; Rowell, J. C.; Weissman, S. I. *J. Chem. Phys.* **1960**, *33*, 626.
13. Weissman, S. I. *J. Am. Chem. Soc.* **1957**, *79*, 2086.
14. Drago, R. S. "Physical Methods in Chemistry"; Saunders: Philadelphia, 1977; Ch. 9.

15. Bard, A. J.; Faulkner, L. R. "Electrochemical Methods, Fundamentals and Applications"; Wiley: New York, 1980.

16. Hermolin, J.; Levin, M.; Ikegami Y.; Sawayanagi, M.; Kosower, E. M. *J. Am. Chem. Soc.* **1981**, *103*, 4795.

CHAPTER 8

Preliminary Investigations of $[Pt_2(CNCH_3)_6](BF_4)_2$

INTRODUCTION

Another class of d^9-d^9 platinum and palladium dimers exist which are unbridged, being supported only by a single metal-metal bond. These complexes, unlike the dppm bridged molecules, have a staggered geometry (see Figure 8.1).[1]

The thermal and photochemistry of these unbridged complexes are dominated by homolytic metal-metal bond cleavage reactions producing $15e^-$ radical species which rapidly react with an available substrate or the solvent to form d^8 monomeric complexes. For example:

$$[Pt_2(CNCH_3)_6]^{2+} + X_2 \xrightarrow{h\nu} 2\,[Pt(CNCH_3)_3X]^+$$

and

$$[Pt_2(CNCH_3)_6]^{2+} + X_2 \xrightarrow{\Delta} 2\,[Pt(CNCH_3)_3X]^+$$

(Such reactions have been investigated by several authors, most notably Balch *et al.*[2] and Kubiak and coworkers.[3,4])

Similar single metal-metal bond cleavage reactions are observed with $Mn_2(CO)_{10}$, which, upon photo-excitation, undergoes homolysis to produce $17e^-$ radical species.[5,6] Also, reactions of this type are seen with the dppm bridged palladium(I) and platinum(I) dimers which oxidatively add small molecules resulting in net metal-metal bond cleavage;[7-13] however, these complexes do not dissociate into monomers due to the presence of the dppm bridges which maintain the dimeric framework.

The $Pt_2(CNCH_3)_6^{2+}$ molecule shows great potential as a precursor for synthesizing new d^9-d^9 and d^8-d^8 A-frame dimers. Direct substitution of four $CNCH_3$ groups with two bridging ligands would afford new d^9-d^9

dimers; whereas, substitution of three $CNCH_3$ groups by two bridging ligands would produce d^8-d^8 A-frame complexes containing a bridging $CNCH_3$ group. Preliminary experiments along these lines are described in this chapter.

Figure 8.1 Structure of $[Pt_2(CNCH_3)_6](BF_4)_2$ and ORTEP of $[Pd_2(CNCH_3)_6](BF_4)_2$. (ORTEP taken from reference 1.)

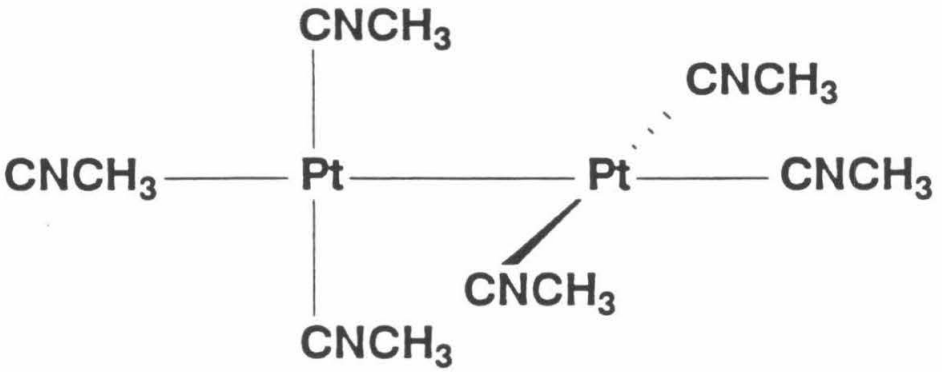
CNCH3
CNCH3
CNCH3
Pt
Pt
CNCH3
CNCH3
CNCH3

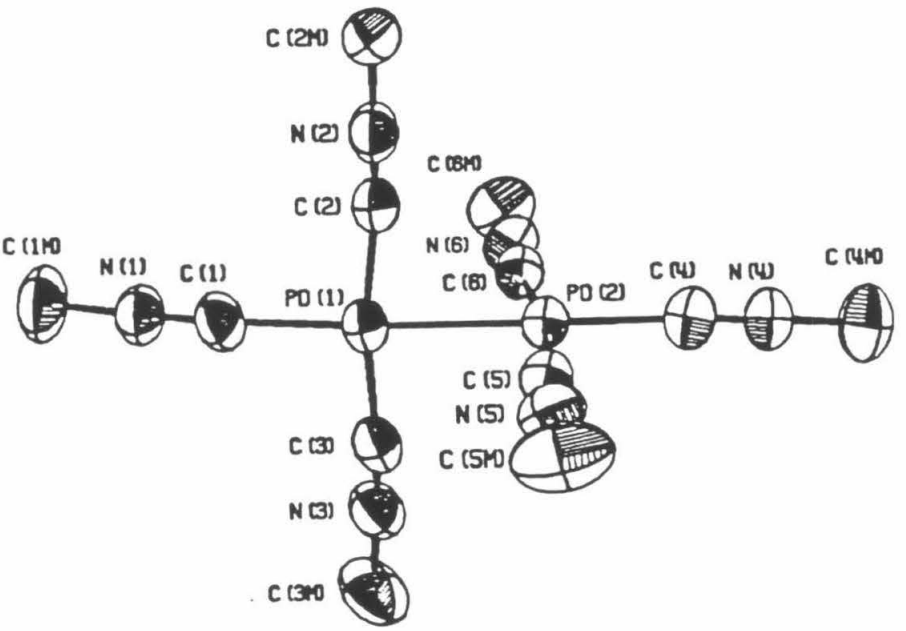
C (2M)
N (2)
C (2)
C (1M)
N (1)
C (1)
PD (1)
C (6M)
N (6)
C (6)
PD (2)
C (4)
N (4)
C (4M)
C (5)
N (5)
C (5M)
C (3)
N (3)
C (3M)

EXPERIMENTAL

Materials

All solvents, unless otherwise noted, were reagent grade and used without further purification.

$[Pt_2(CNCH_3)_6](BF_4)_2$ was prepared by published procedures.[2] To obtain the best results, it is important that the water solution containing K_2PtCl_4 and $NaBF_4$ be stirred for 30-45 minutes to attain the maximum $NaBF_4$ saturation.

Bis(diphenylphosphino)methane, dppm, (Aldrich, 98%) and bis(dimethylphosphino)methane, dmpm, (Aldrich, 98 %) were used as received. 1,3-Diisocyanopropane, $CN(CH_2)_3NC$, was prepared following published procedures,[14] was purified by column chromotography (Alumina, Woelm, Grade A), and gave a clean NMR spectrum.

Physical Measurements

Nuclear Magnetic Resonance. ^1H NMR spectra were recorded at 400 MHz on a JEOL GX-400 spectrometer, at 90 MHz on a Jeol FX90-Q spectrometer, and at 90 MHz on a Varian EM-390 spectrometer. ^1H chemical shifts are reported in ppm (δ) *vs.* CD_3CN (δ 1.98), $CDCl_3$ (δ 7.24), CD_2Cl_2 (δ 5.32), and $(CD_3)_2CO$ (δ 2.04). ^{31}P NMR spectra were recorded at 36.28 MHz on a JEOL FX90-Q spectrometer. The ^{31}P chemical shifts are reported in ppm (δ) *vs.* H_3PO_4 external standard. All NMR spectra were run at ambient temperature.

Electronic Absorption Spectroscopy. Absorption spectra were recorded on a Shimatzu 260-UV spectrophotometer.

Emission Spectroscopy and Lifetime Measurements. Emission spectra were measured using an emission instrument constructed at Caltech and

described previously.[15] Emission lifetimes were measured using a Nd:YAG laser system described elsewhere.[16] Low temperature, 77 K, spectra were collected using a liquid-nitogen-filled quartz finger dewar. Solid samples were placed in an NMR tube and sealed with a septum and parafilm. Acetonitrile solutions of $[Pt_2(\mu\text{-}CN(CH_2)_3NC)_2(\mu\text{-}CNCH_3)(CNCH_3)_2](BF_4)_2$ were placed in a two-compartment photometric cell equipped with a teflon vacuum valve and degassed (a minimum of 6 freeze/pump/thaw cycles) on a high vacuum lime (limiting pressure $< 10^{-3}$ Torr).

RESULTS and DISCUSSION

The electronic absorption spectrum of $[Pt_2(CNCH_3)_6](BF_4)_2$ reveals a shoulder at 296 nm and a larger broad absorption band maximizing at 272 nm (Figure 8.2a). Reinking *et al.*[4] report the molar extinction of the 296 nm absorption as 4350 cm^{-1} M^{-1} in acetonitrile. This complex does not luminesce in fluid solution or the solid state at room temperature; however, upon cooling the sample (powder) down to 77 K, yellow emission is observed (λ_{max} = 542 nm); see Figure 8.2b. This result implies that some facile deactivation pathway exist at room temperature. Since these complexes are known to readily undergo thermal and photochemical homolytic bond cleavage, the rupture of the metal-metal bond may be one of the temperature dependent deactivation pathways.

In order to synthesize another class of bridged d^9-d^9 dimers, a colorless acetontrile solution of $Pt_2(CNCH_3)_6^{2+}$ was added to a colorless acetonitrile solution of dppm (1:2 stoichiometry). The reaction was immediate as evidenced by the resulting bright orange solution. The absorption spectrum of this solution shows a new absorption at 452 nm; the absorption spectrum is presented in Figure 8.3a. The solvent was evaporated and an orange solid was obtained. Free $CNCH_3$ was detected. NMR analysis of the isolated complex clearly revealed the presence of the dppm ligand bridging two platinum centers δ = 5.57 ppm; see Figure 8.4. Bands attributable to methylisocyanide were located at δ = 2.83 and 2.50 ppm. Several smaller peaks, unassignable to the starting material or the proposed $Pt_2(\mu\text{-dppm})_2(CNCH_3)_n^{2+}$ complex were observed. These peaks are presumed to be decomposition products and d^8 monomeric $Pt(dppm)(CNCH_3)_2^{2+}$,[17] from comparison with NMR data of sim-

Figure 8.2 (a) Electronic absorption spectrum of $[Pt_2(CNCH_3)_6](BF_4)_2$ in acetonitrile (300 K). Absorption maxima at 296 (shoulder) and 272 nm.

(b) Uncorrected emission spectrum of $[Pt_2(CNCH_3)_6](BF_4)_2$, powder sample, 77 K. Emission maximum at 542 nm.

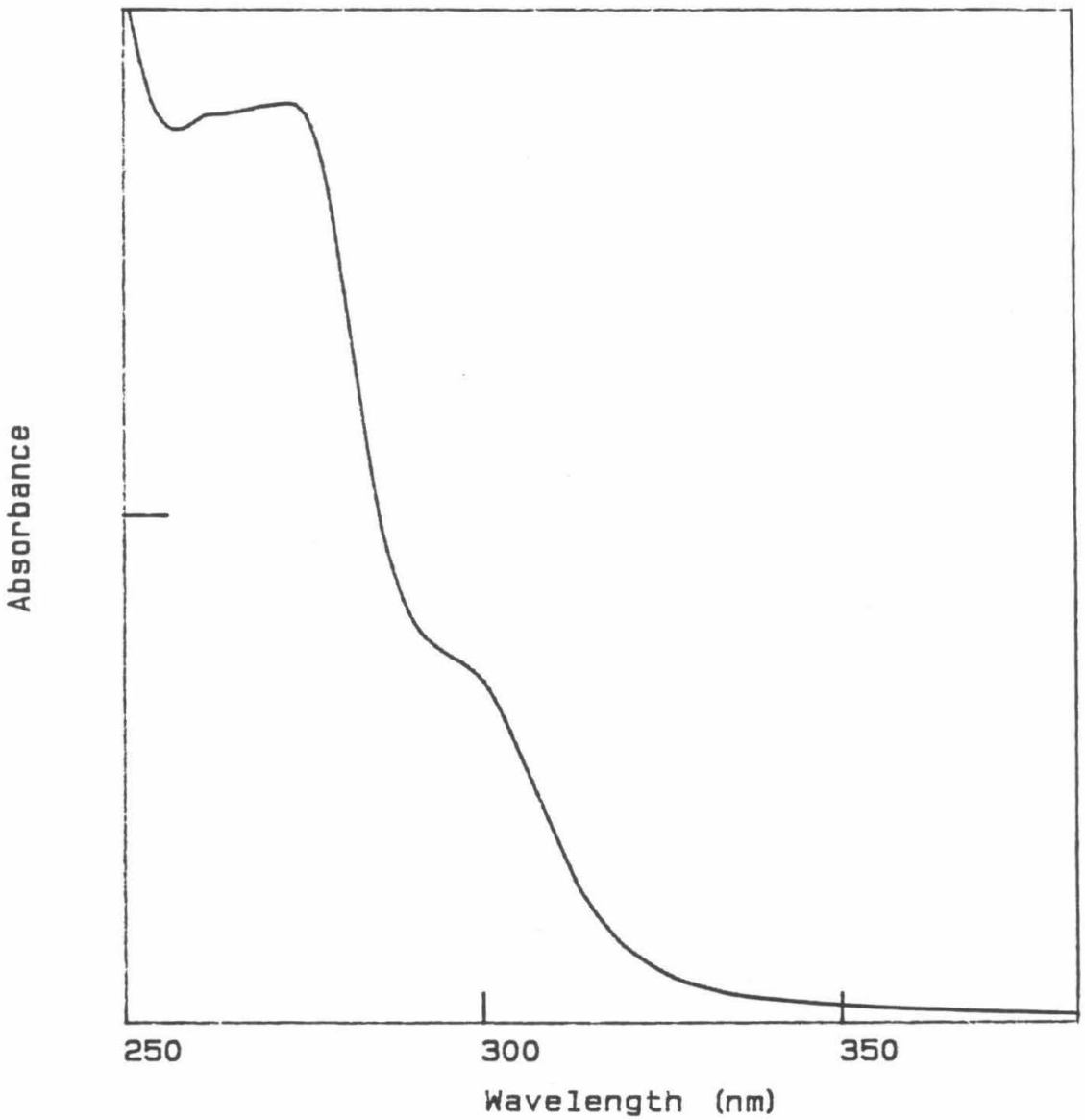
Absorbance
250
300
350
Wavelength (nm)

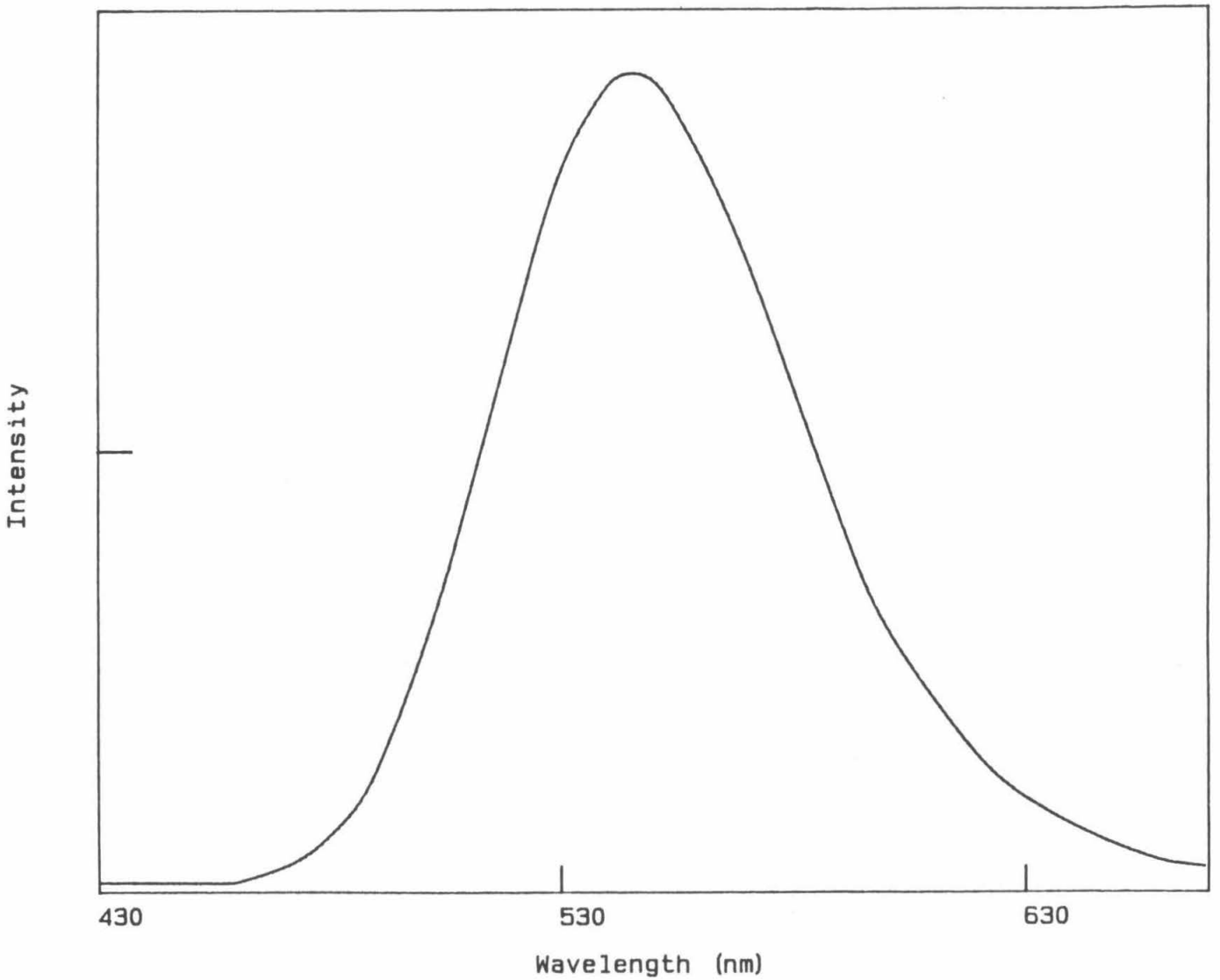
Intensity
430
530
630
Wavelength (nm)

Figure 8.3 (a) Electronic absorption spectrum of $[Pt_2(\mu\text{-dppm})_2(\mu\text{-}CNCH_3)(CNCH_3)_2](BF_4)_2$ in acetonitrile (300 K). Absorption maximum at 452 nm.

(b) Uncorrected emission spectrum of $[Pt_2(\mu\text{-dppm})_2(\mu\text{-}CNCH_3)(CNCH_3)_2](BF_4)_2$, powder sample, 77 K. Emission maximum at 604 nm. (A grating anomaly occurs at ~667 nm.)

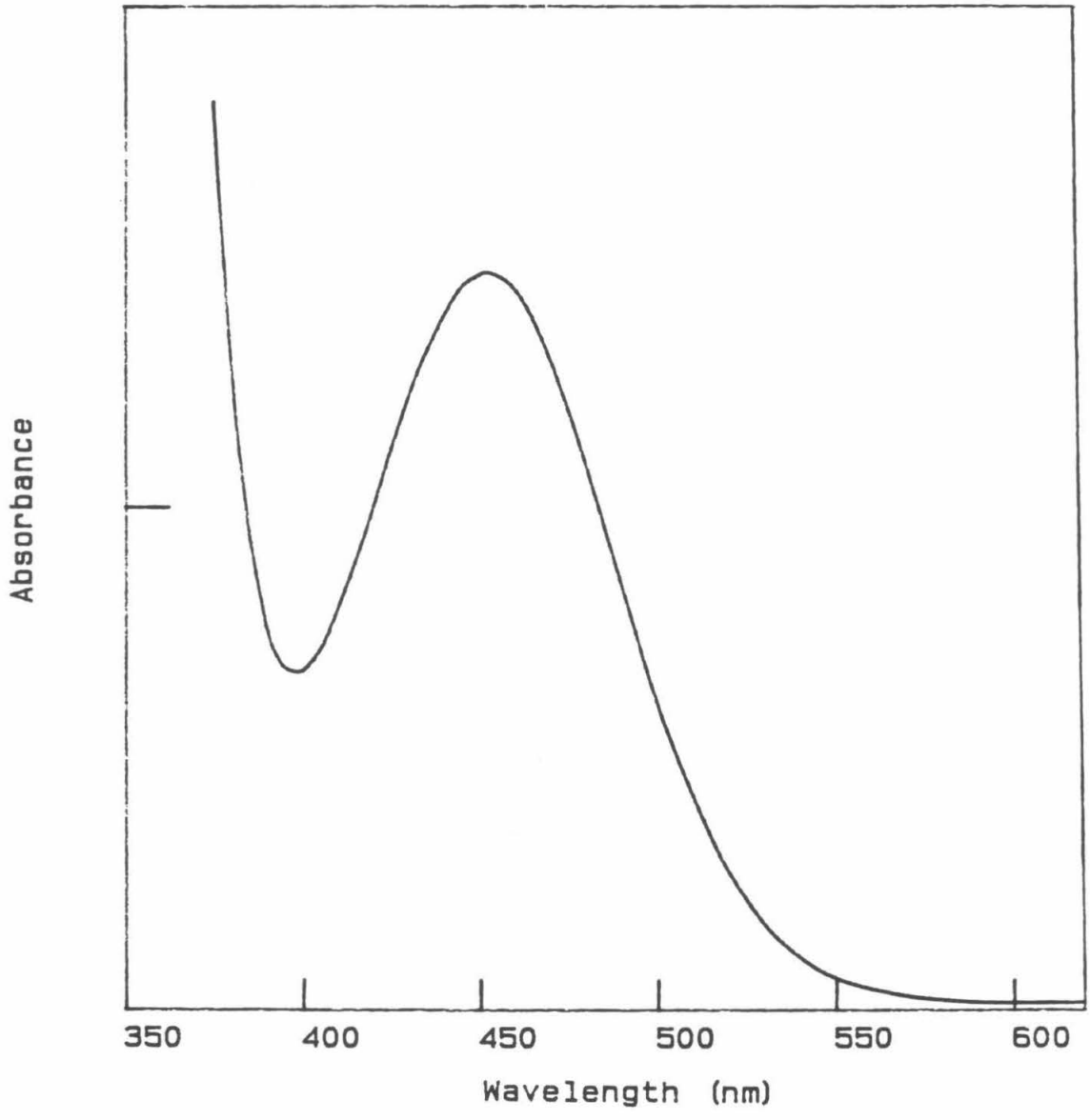
Absorbance
350
400
450
500
550
600
Wavelength (nm)

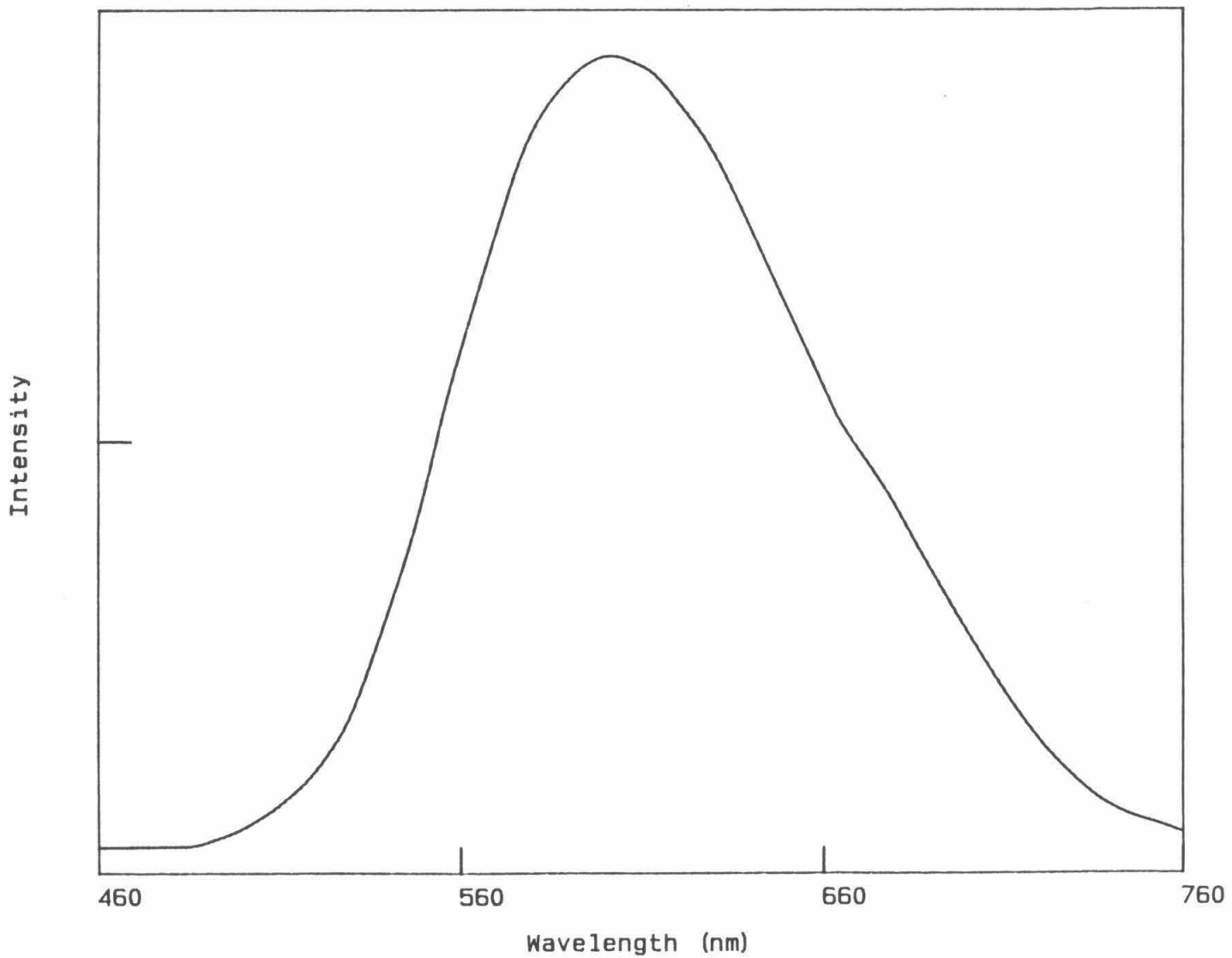
Intensity
460
560
660
760
Wavelength (nm)

Figure 8.4 ^{1}H NMR spectrum of the methylene protons in the bridging dppm ligand of $[Pt_2(\mu\text{-dppm})_2(\mu\text{-}CNCH_3)(CNCH_3)_2](BF_4)_2$ in d_6-acetone. $^{3}J(PtH)$ coupling 58.4 Hz; $^{2}J(PH)$ coupling 9.3 Hz.

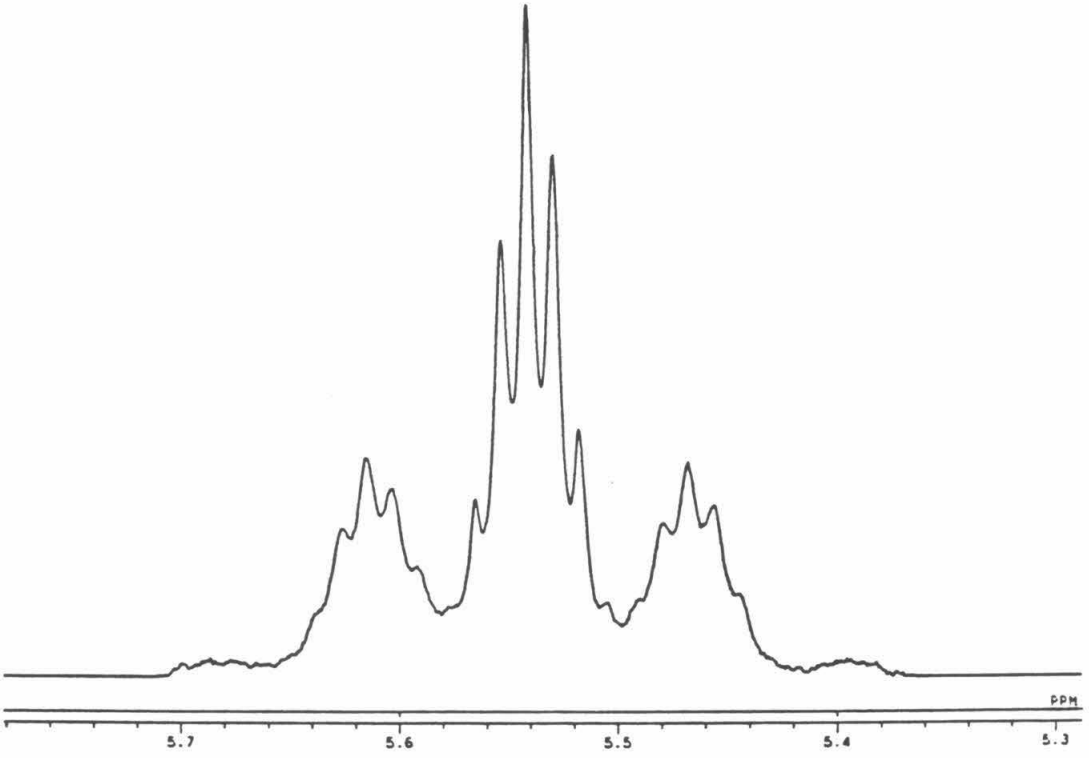
PPM
5.7
5.6
5.5
5.4
5.3

ilar platinum(II) monomers. The ^{31}P NMR revealed only one phosphorus signal at δ = 4.41 ppm.

Similar reaction between $Pd_2(CNCH_3)_6^{2+}$ and dppm afforded $Pd_2(\mu\text{-dppm})_2(\mu\text{-CNCH}_3)(CNCH_3)_2^{2+}$ which has been crystallographically characterized.[8] Based on the palladium reaction, the platinum complex obtained is presumed to be $Pt_2(\mu\text{-dppm})_2(\mu\text{-CNCH}_3)(CNCH_3)_2^{2+}$. Of course, additional characterization and possible structural evaluation is necessary to confirm this structural assignment. Attempts to grow crystals have been hampered by the slow decomposition of the complex when in solution. (Futher loss of $CNCH_3$ is detected when the sample remains in solution for prolonged periods of time.)

For this new dppm A-frame d^8-d^8 complex, as for the studied d^9-d^9 starting materials, no fluid solution or solid state luminesence at room temperature was observed. However at low temperature in the solid state, orange emission was detected (λ_{max} = 604 nm); see Figure 8.3b. Reaction of $Pt_2(CNCH_3)_6^{2+}$ with bis(dimethylphosphino)methane, dmpm, afforded a complex similar in absorption and emission properties as the complex formed from the $Pt_2(CNCH_3)_6^{2+}$ + dppm reaction.

Additional reactions between $Pt_2(CNCH_3)_6^{2+}$ and other bridging ligands were investigated in hopes of unearthing a dimeric complex which did show fluid solution emission at ambient temperature. Reaction of $Pt_2(CNCH_3)_6^{2+}$ with 1,3-diisocyanopropane, $CN(CH_2)_3NC$, resulted in the expected orange solution (λ_{max} = 443 nm, see Figure 8.5a) and also produced a species which luminesced in fluid solution at room temperature (emission spectra are shown in Figure 8.5b-d). These complexes appear to be air and possibly even moisture sensitive. Eventual decomposition of the product is observed. The emission lifetime of

Figure 8.5 (a) Electronic absorption spectrum of $[Pt_2(\mu\text{-}CN(CH_2)_3NC)_2(\mu\text{-}CNCH_3)(CNCH_3)_2](BF_4)_2$ in acetonitrile (300 K). Absorption maximum at 443 nm.

(b) Uncorrected emission spectrum of $[Pt_2(\mu\text{-}CN(CH_2)_3NC)_2(\mu\text{-}CNCH_3)(CNCH_3)_2](BF_4)_2$ in acetonitrile, 300 K. Emission maximum at 529 nm. (A grating anomaly occurs at ~667 nm.)

(c) Uncorrected emission spectrum of $[Pt_2(\mu\text{-}CN(CH_2)_3NC)_2(\mu\text{-}CNCH_3)(CNCH_3)_2](BF_4)_2$ in dichloromethane, 77 K. Emission maximum at 613 nm. (A grating anomaly occurs at ~667 nm.)

(d) Uncorrected emission spectrum of $[Pt_2(\mu\text{-}CN(CH_2)_3NC)(\mu\text{-}CNCH_3)(CNCH_3)_2](BF_4)_2$, powder sample, 77 K. Emission maximum at 626 nm. (A grating anomaly occurs at ~667 nm.)

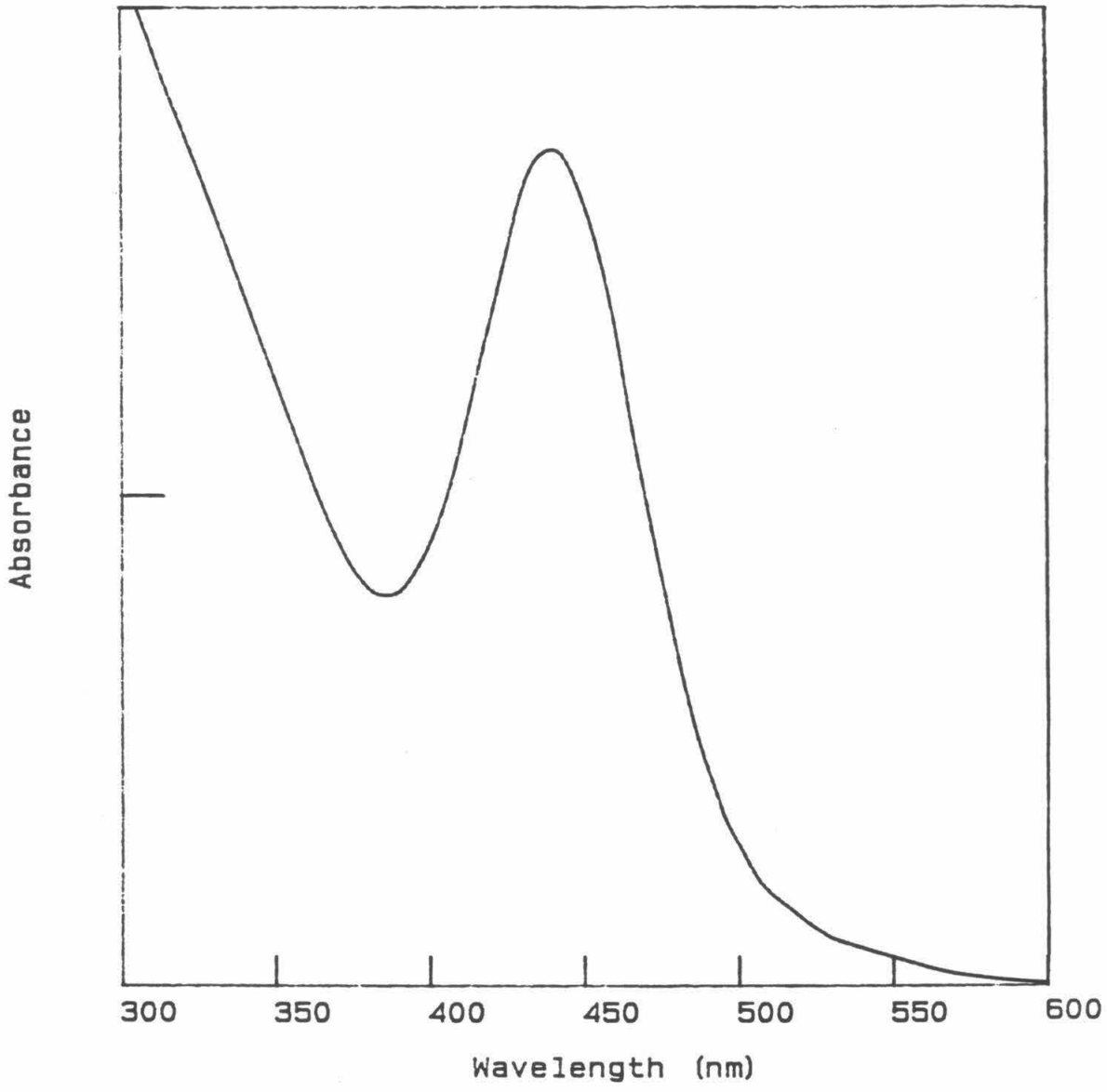
Absorbance
300
350
400
450
500
550
600
Wavelength (nm)

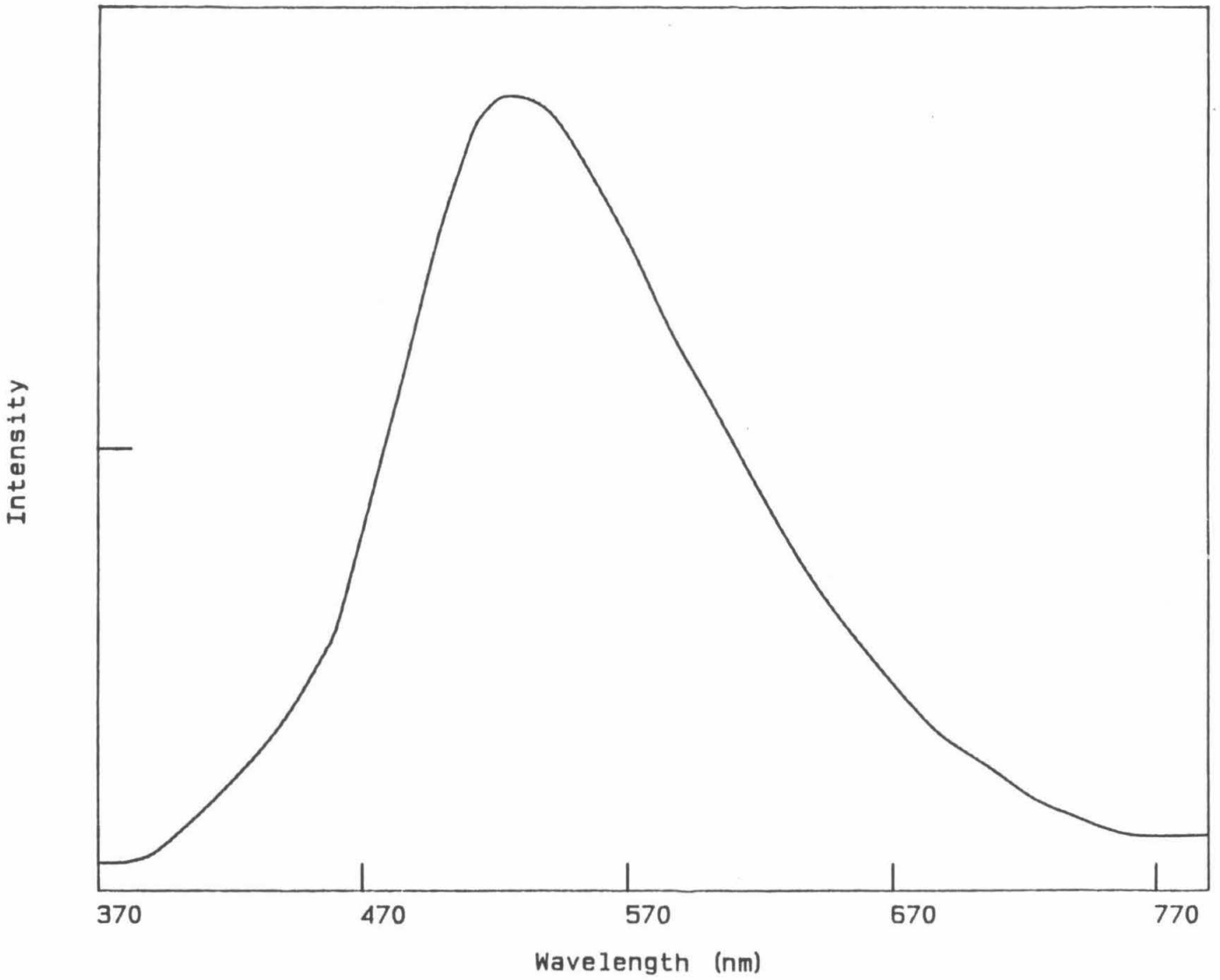
Intensity
370
470
570
670
770
Wavelength (nm)

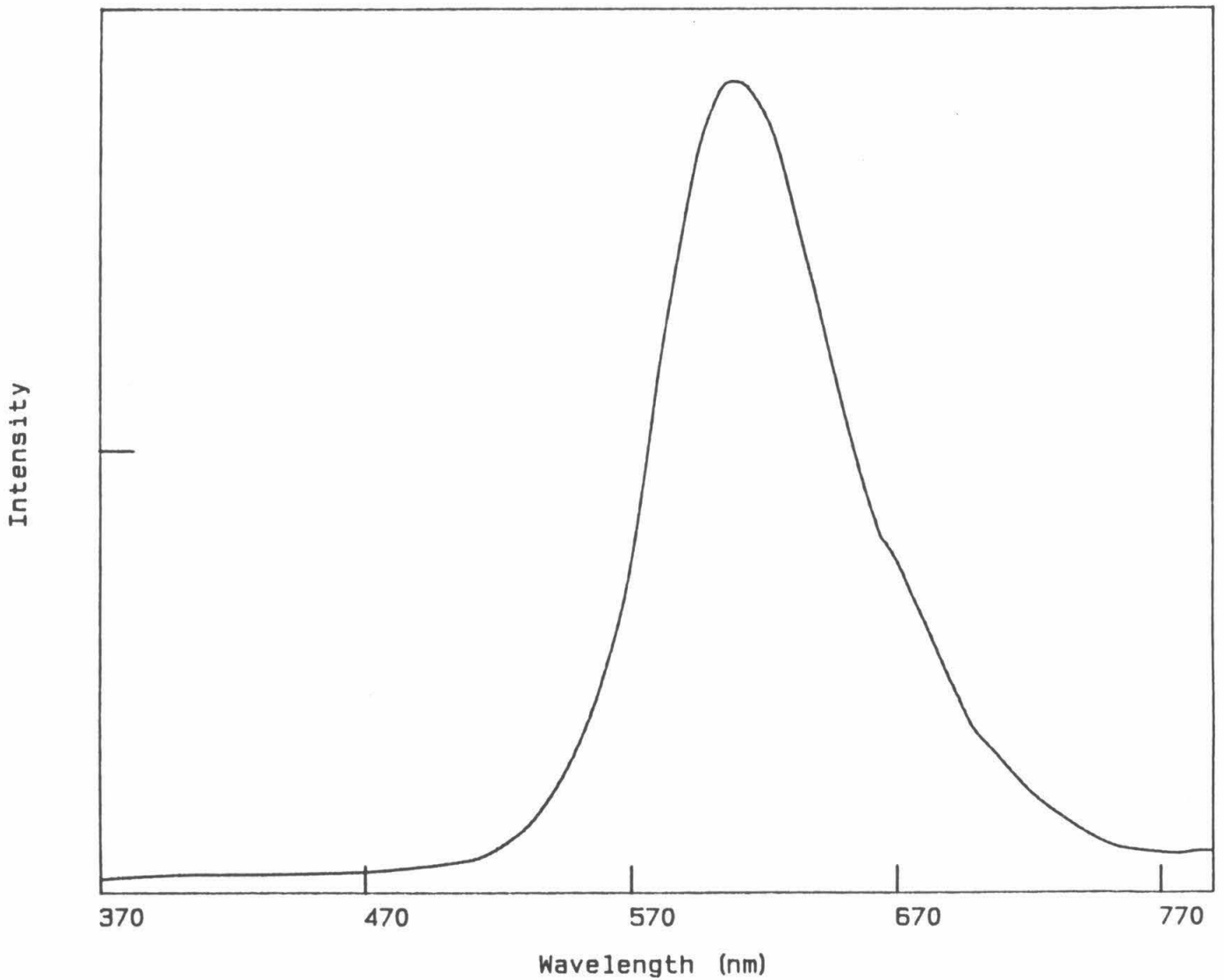
Intensity
370
470
570
670
770
Wavelength (nm)

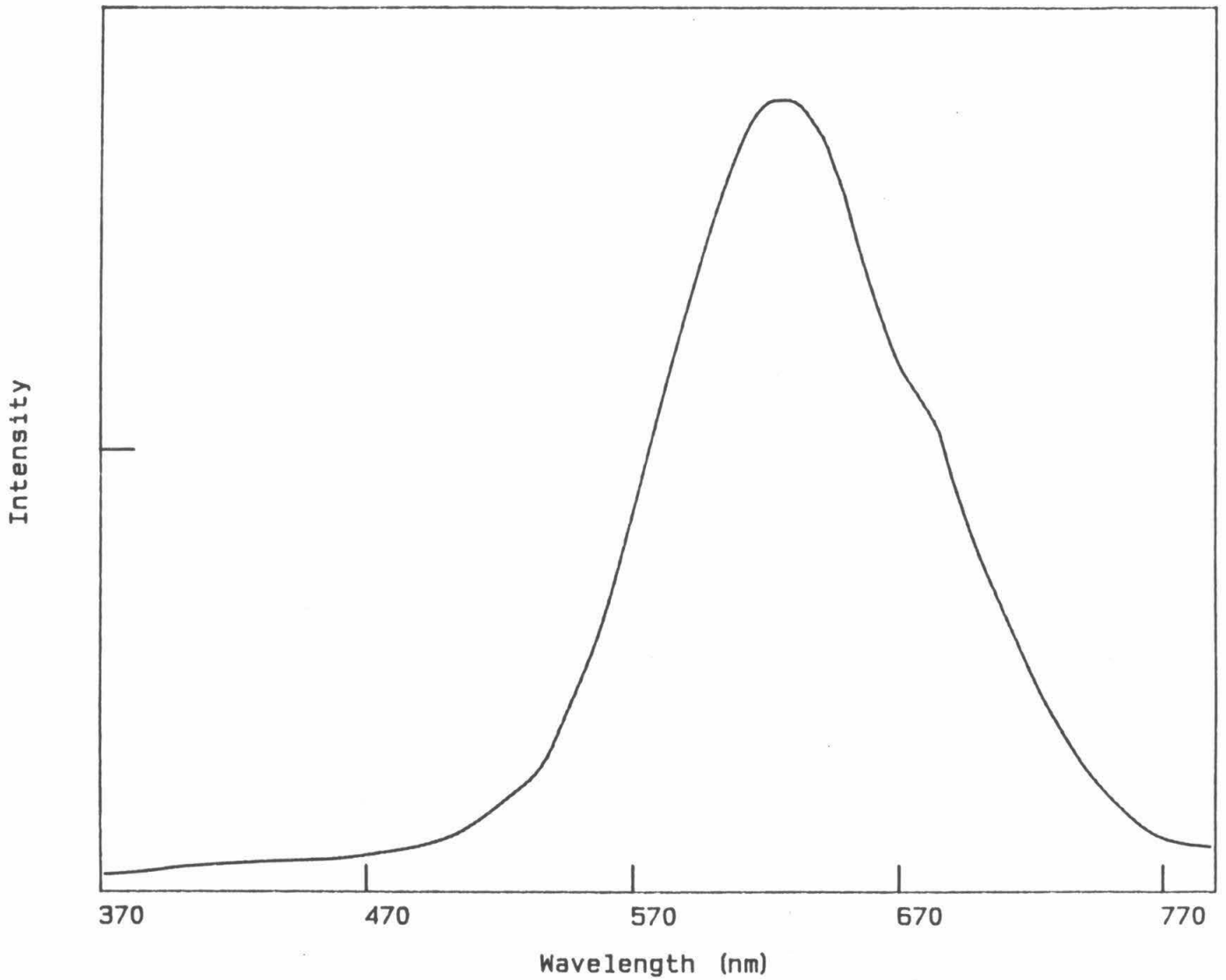
Intensity
370
470
570
670
770
Wavelength (nm)

this complex in room temperature fluid solution is 220 ns, and increases to 7.4 μs at 77 K in frozen solution. As in the dppm case, this complex is presumed to be $[Pt_2(\mu\text{-}CN(CH_2)_3NC)_2(\mu\text{-}CNCH_3)(CNCH_3)](BF_4)_2$.

Why is fluid solution emission observed with the bridging isocyanide ligand and not the phosphine bridging ligand? Apparently, the bridging isocyanide ligand is decreasing the platinum dimer's non-radiative rate constant. One possible non-radiative deactivation pathway in the dppm complex is rapid cleavage and reassembly of the Pt-P(dppm) bond.[18] Replacement of the neutral dppm bridging ligand with the bridging 1,3-diisocyanopropane ligand may hinder this deactivation pathway by inducing an electrostatic interaction between the Pt(+1) center and the formal negative charge on the carbon atom in the isocyanide ligand.

Obviously, further work in the areas of product characterization and photophysical analysis is required, and merited, on these reactions.

REFERENCES

1. Goldberg, S. Z.; Eisenberg, R. *Inorg. Chem.* **1976**, *15*, 535.
2. Boehm, J. R.; Doonan, D. J.; Balch, A. L. *J. Am. Chem. Soc.* **1976**, *98*, 4845.
3. Miller, T. D.; St. Clair, M. A.; Reinking, M. K.; Kubiak, C. P. *Organometallics* **1983**, *2*, 767.
4. Reinking, M. K.; Kullberg, M. L.; Cutler, A. R.; Kubiak, C. P. *J. Am. Chem. Soc.* **1985**, *107*, 3517.
5. Wrighton, M.; Bredesen, D. *J. Organomet. Chem.* **1973**, *50*, C35.
6. Wrighton, M. S.; Ginley, D. S. *J. Am. Chem. Soc.* **1975**, *97*, 2065.
7. Benner, L. S.; Balch, A. L. *J. Am. Chem. Soc.* **1978**, *100*, 6099.
8. Olmstead, M. M.; Hope, H.; Benner, L. S.; Balch, A. L. *J. Am. Chem. Soc.* **1977**, *99*, 5502.
9. Balch, A. L.; Benner, L. S.; Olmstead, M. M. *Inorg. Chem.*, **1979**, *18*, 2996.
10. Brown, M. P.; Puddephatt, R. J.; Rashidi, M.; Seddon, K. R. *J. Chem. Soc. Dalton Trans.* **1978**, 516.
11. Brown, M. P.; Puddephatt, R. J. Rashidi, M.; Seddon, K. R. *J. Chem. Soc. Dalton Trans.* **1978**, 1540.
12. Brown, M. P.; Fisher, J. R.; Puddephatt, R. J.; Seddon, K. R.; *Inorg. Chem.* **1979**, *18*, 2808.
13. Cameron, T. S.; Gardner, P. A.; Grundy, K. R. *J. Organomet. Chem.* **1981**, *212*, 135.
14. Weber, W. P.; Bokel, G. W.; Ugi, I. K. *Agnew. Chem. Int. Ed. Engl.* **1972**, *11*, 530.
15. Nocera, D. G.; Winkler, J. R.; Yocom, K. M.; Bordignon, E.; Gray, H. B. *J. Am. Chem. Soc.* **1984**, *106*, 5145.

16. Parker, C. A.; Rees, W. T. *Analyst* **1960**, *85*, 587.

17. Treichel, P. M.; Knebel, W. J.; Hess, R. W. *J. Am. Chem. Soc.* **1971**, *93*, 5424.

18. Muralidharan, S.; Espenson, J. H. *J. Am. Chem. Soc.* **1984**, *106*, 8104.

APPENDIX

Anisotropic Thermal Parameters and Listings of Observed and Calculated Structure Factors for $K_4[Pt_2(P_2O_5H_2)_4Cl]$ at 22 and 300 K

Table A.1

Anisotropic Parameters Pt_2Cl at 22 K.

$U \times 10^4$

Atom	U_{11}	U_{22}	U_{33}	U_{12}	U_{13}	U_{23}
Cl	241(11)	241(11)	378(64)	0	0	0
K1	172(5)	172(5)	107(9)	61(7)	0	0
K2	103(5)	103(5)	197(10)	15(6)	0	0
P	86(4)	82(4)	103(4)	-18(4)	13(4)	0(4)
O1	82(13)	137(14)	148(16)	-19(11)	26(12)	7(13)
O2	152(14)	68(13)	166(17)	-25(11)	27(14)	10(13)
O3	204(24)	174(24)	90(19)	-90(18)	0	0

Table A.2

Anisotropic Parameters Pt_2Cl at 300 K.

$U \times 10^4$

Atom	U_{11}	U_{22}	U_{33}	U_{12}	U_{13}	U_{23}
Cl	835(31)	835(31)	334(42)	0	0	0
K1	478(10)	478(10)	250(11)	202(12)	0	0
K2	338(8)	338(8)	490(18)	36(10)	0	0
P	202(5)	194(5)	241(5)	-29(4)	32(5)	8(5)
O1	284(18)	317(18)	418(23)	-48(15)	117(18)	2(19)
O2	352(20)	192(16)	544(28)	-52(14)	52(21)	82(19)
O3	491(37)	584(42)	235(22)	-335(30)	0	0

Table A3 (for deposit).

Structure Factors for Pt2Cl at 22 K.

The columns contain, in order,
l, 10Fo, 10Fc and 10[(Fo**2 - Fc**2)/sigma(Fo**2)].
A minus sign preceeding 10Fo indicates that Fo**2 is negative.

0 0 1

1	2150	2285	-62
2	2554	2606	-19
3	2953	3131	-58
4	1823	1866	-32
5	2241	2441	-78
6	2872	3131	-82
7	449	511	-26
8	1145	1190	-19
9	1603	1665	-22
10	726	783	-20
11	1577	1621	-14
12	1213	1284	-21
13	315	327	-2

1 1 1

0	3369	3229	40
1	1299	1118	121
2	2512	2426	32
3	3260	3379	-36
4	790	862	-56
5	1553	1638	-44
6	1910	2058	-65
7	49	96	-5
8	1620	1763	-62
9	1438	1532	-39
10	85	40	2
11	1172	1209	-13
12	726	757	-10

2 0 1

0	2069	1928	75
1	1550	1556	-4
2	1445	1446	0
3	2317	2310	3
4	1269	1287	-14
5	1790	1868	-45
6	1517	1576	-37
7	373	402	-20
8	1409	1493	-50
9	892	927	-22
10	235	206	10
11	1073	1092	-9
12	550	595	-19

2 1 1

0	480	563	-162
1	159	191	-63
2	343	342	1
3	229	219	13
4	411	415	-4
5	291	279	10
6	154	154	0
7	90	134	-13
8	267	270	-1
9	-58	99	-11
10	68	46	1
11	130	37	10
12	181	192	-1

2 2 1

0	2950	2894	18
1	555	508	52
2	217	45	116
3	2893	2896	-1
4	506	486	17
5	1128	1124	2
6	2223	2303	-32
7	110	9	10
8	1001	1042	-21
9	1259	1349	-41
10	232	256	-4
11	776	816	-15
12	827	862	-12

3 1 1

0	1484	1574	-68
1	776	649	143
2	373	295	106
3	1965	1951	8
4	684	644	41
5	921	937	-14
6	1423	1463	-26
7	233	233	0
8	732	759	-20
9	845	888	-29
10	148	164	-4
11	587	649	-35
12	619	681	-33

3 2 1

0	34	51	-10
1	317	372	-100
2	309	322	-20
3	988	991	-3
4	112	58	30
5	101	78	12
6	201	168	23
7	546	550	-2
8	-41	7	-2
9	132	84	13
10	157	164	-2
11	226	195	7
12	63	98	-3

3 3 1

0	3717	3724	-1
1	1750	1667	43
2	1829	1796	16
3	2612	2611	0
4	485	488	-2
5	1916	1901	6
6	2160	2189	-11
7	418	402	9
8	1558	1570	-5
9	1252	1293	-20
10	164	157	1
11	1299	1325	-10

4 0 1

0	793	767	29
1	1196	1209	-15
2	1048	876	146
3	2258	2306	-23
4	636	643	-7
5	468	425	39
6	586	549	31
7	191	250	-31
8	414	442	-19
9	1084	1125	-26
10	466	445	12
11	154	35	17

4 1 1

0	95	48	37
1	592	614	-31
2	516	547	-42
3	111	94	12
4	106	118	-8
5	651	639	11
6	184	224	-24
7	67	9	7
8	44	90	-9
9	217	223	-2
10	134	208	-23
11	64	124	-10

4 2 1

0	3273	3222	17
1	1281	1236	36
2	2442	2350	41
3	1898	1902	-1
4	394	409	-17
5	1422	1416	4
6	1246	1267	-15
7	538	562	-21
8	1235	1274	-25
9	1005	1057	-35
10	227	176	19
11	1075	1076	0

4 3 1

0	29	82	-32
1	138	118	22
2	530	498	40
3	383	376	9
4	67	12	14
5	54	11	8
6	397	400	-2
7	97	138	-18
8	18	3	0
9	143	147	-1
10	175	170	1
11	-95	10	-8

4 4 1

0	4155	4111	10
1	2032	1947	38
2	601	528	61
3	3325	3302	6
4	406	369	29
5	2573	2576	-1
6	3105	3146	-12
7	123	108	4
8	1573	1558	6
9	1369	1396	-12
10	623	564	28
11	1465	1462	1

5 1 1

0	2766	2736	12
1	1267	1221	36
2	611	566	52
3	1175	1168	6
4	113	55	28
5	1117	1120	-2
6	1502	1490	7
7	577	627	-41
8	610	581	21
9	741	744	-2
10	-39	30	-2
11	826	825	0

5 2 1

0	348	353	-6
1	291	300	-12
2	86	68	11
3	143	123	16
4	64	24	11
5	229	195	27
6	276	258	12
7	186	197	-7
8	197	200	-1
9	-104	48	-17
10	107	150	-10
11	243	210	11

5 3 1

0	3232	3223	3
1	684	661	27
2	1999	1955	24
3	3324	3286	13
4	638	644	-6
5	1345	1364	-13
6	1992	1975	8
7	178	116	30
8	1557	1569	-6
9	1524	1540	-8
10	125	86	10
11	1022	1029	-3

5 4 1

0	106	85	15
1	140	150	-9
2	320	349	-37
3	305	323	-20
4	99	74	12
5	83	46	12
6	394	383	9
7	57	110	-17
8	67	112	-13
9	172	169	1
10	235	200	15
11	36	20	1

5 5 1

0	1326	1416	-57
1	1002	978	17
2	1561	1536	13
3	3147	3114	14
4	1605	1573	16
5	1742	1727	6
6	1751	1697	24
7	212	167	18
8	1793	1817	-10
9	1205	1216	-5
10	231	200	9
11	1083	1037	20

6 0 1

0	1168	1269	-88
1	1194	1163	24
2	521	514	8
3	2059	2112	-27
4	1369	1384	-10
5	1461	1488	-17
6	1816	1816	0
7	341	350	-5
8	1404	1452	-29
9	1015	1027	-7
10	-66	40	-5
11	1037	1030	3

6 1 1

0	681	672	10
1	645	660	-16
2	53	83	-15
3	141	130	8
4	362	373	-11
5	686	672	12
6	138	107	12
7	107	65	12
8	-55	97	-16
9	364	355	5
10	120	185	-18
11	142	118	5

6 2 1

0	2849	2945	-38
1	510	435	86

Structure Factors for Pt2Cl at 22 K. Page 2

2	1567	1490	49
3	2497	2506	-4
4	348	317	30
5	982	937	36
6	1598	1591	3
7	124	88	13
8	1088	1080	5
9	1307	1325	-11
10	-142	20	-22
11	840	807	18

6 3 1

0	619	653	-39
1	97	103	-4
2	481	498	-20
3	32	37	-1
4	611	613	-2
5	77	65	4
6	222	194	17
7	67	102	-11
8	480	447	24
9	64	36	4
10	122	138	-5
11	113	126	-3

6 4 1

0	2132	2154	-11
1	1136	1099	30
2	1050	1035	13
3	1942	1927	7
4	729	717	11
5	1428	1417	7
6	1608	1608	0
7	379	378	0
8	1210	1214	-2
9	981	987	-4
10	153	23	26
11	1008	992	9

6 5 1

0	369	417	-60
1	84	84	0
2	173	148	20
3	285	265	19
4	165	153	8
5	68	20	8
6	351	316	27
7	122	76	15
8	-107	4	-21
9	142	173	-12
10	182	169	5
11	-79	31	-8

6 6 1

0	3254	3208	13
1	1044	993	33
2	1059	1076	-11
3	1763	1731	15
4	351	294	36
5	1280	1256	13
6	1499	1496	1
7	321	330	-4
8	650	612	20
9	960	920	19
10	102	47	6
11	846	847	0

7 1 1

0	2704	2775	-29
1	1216	1199	12
2	995	1010	-13
3	2871	2847	9
4	729	697	29
5	1753	1766	-7
6	2238	2216	10
7	119	2[illegible]	23
8	1464	1443	11
9	1241	1245	-2
10	226	172	18
11	1140	1108	17

7 2 1

0	425	455	-38
1	172	195	-23
2	304	329	-28
3	602	586	16
4	558	550	7
5	-65	2	-11
6	-63	11	-8
7	257	229	18
8	451	424	19
9	282	230	27
10	127	71	12
11	44	32	0

7 3 1

0	1606	1619	-8
1	621	594	29
2	1282	1264	14
3	1595	1570	15
4	638	608	28
5	797	775	18
6	1034	990	33
7	327	328	0
8	943	942	0
9	889	883	4
10	258	253	2
11	720	696	14

7 4 1

0	202	192	9
1	263	258	5
2	171	177	-4
3	191	181	8
4	-23	63	-12
5	384	383	0
6	-51	18	-6
7	95	86	2
8	-36	10	-2
9	163	124	14
10	107	73	7
11	-76	43	-8

7 5 1

0	2202	2227	-12
1	418	372	49
2	613	564	48
3	1491	1472	11
4	9[illegible]	1	23
5	495	463	27
6	1402	1365	23
7	301	298	1
8	532	533	0
9	1029	1010	12
10	149	53	21
11	617	597	12

7 6 1

0	313	293	19
1	329	345	-17
2	533	543	-11
3	461	449	11
4	112	81	11
5	262	264	-1
6	16	12	0
7	172	146	12
8	289	277	6
9	373	355	10
10	-115	47	-19

7 7 1

0	2457	2481	-8
1	1346	1328	9
2	1710	1674	17
3	1984	1961	10
4	565	547	11
5	1694	1690	2
6	1483	1458	11
7	420	375	23
8	1346	1314	14
9	952	947	2
10	191	123	15

8 0 1

0	3897	3935	-11
1	1568	1529	25
2	1677	1634	25
3	2761	2766	-1
4	283	245	31
5	2088	2072	7
6	2430	2437	-2
7	294	301	-5
8	1556	1558	-1
9	1416	1413	1
10	383	369	6
11	1450	1419	15

8 1 1

0	912	935	-21
1	57	85	-12
2	147	168	-16
3	538	541	-2
4	451	447	3
5	100	93	2
6	473	471	1
7	229	232	-2
8	113	124	-3
9	159	200	-17
10	274	255	9
11	84	1	6

8 2 1

0	2331	2376	-21
1	1003	992	9
2	1228	1224	2
3	2030	2009	11
4	404	407	-2
5	1414	1392	14
6	1426	1391	22
7	232	217	9
8	976	984	-5
9	918	937	-12
10	146	130	4
11	919	879	23

8 3 1

0	139	152	-10
1	423	444	-24
2	397	386	12
3	346	361	-14
4	269	278	-8
5	271	254	11
6	193	207	-9
7	488	472	12
8	472	475	-2
9	78	60	3
10	57	150	-23
11	448	401	25

8 4 1

0	866	861	4
1	132	36	43
2	513	444	66
3	1220	1200	14
4	627	616	9
5	211	43	67
6	843	817	20
7	240	261	-13
8	602	611	-7
9	904	907	-1
10	254	205	20

8 5 1

0	204	223	-17
1	372	354	17
2	345	381	-38
3	63	76	-4
4	143	135	4
5	326	313	10
6	95	90	1
7	186	226	-24
8	331	302	18
9	134	18	21
10	75	35	5

8 6 1

0	1876	1861	8
1	642	629	13
2	1172	1147	19
3	2016	1986	15
4	687	670	14
5	1043	1020	17
6	1370	1342	17
7	160	153	3
8	1151	1146	3
9	1105	1068	23
10	150	80	17

8 7 1

0	681	728	-46
1	84	70	5
2	203	193	7
3	143	135	3
4	308	293	11
5	120	81	14
6	272	254	11
7	57	52	1
8	105	27	13
9	129	145	-5
10	182	182	0

8 8 1

0	2812	2837	-8
1	1194	1180	7
2	1169	1163	3
3	2489	2473	5
4	508	514	-3
5	1769	1761	3
6	2188	2159	11
7	219	154	21
8	1483	1468	6
9	1246	1247	0
10	367	311	19

9 1 1

0	2622	2619	1
1	584	581	2
2	2241	2210	14
3	2703	2682	8
4	667	680	-11
5	1138	1123	10

6	1455	1411	26
7	70	1	8
8	1573	1563	5
9	1428	1408	11
10	202	77	34

9 2 1

0	708	728	-19
1	242	237	4
2	371	362	9
3	215	210	3
4	216	221	-2
5	339	308	24
6	148	166	-9
7	23	1	0
8	24	98	-13
9	-61	53	-8
10	-36	87	-10

9 3 1

0	1876	1877	0
1	859	822	33
2	198	34	78
3	1393	1400	-4
4	143	74	25
5	995	1006	-8
6	1541	1523	10
7	256	243	7
8	420	403	11
9	699	687	7
10	-32	31	-2

9 4 1

0	220	238	-16
1	51	21	6
2	215	243	-25
3	159	153	3
4	21	37	-1
5	-34	23	-3
6	-33	16	-2
7	-81	41	-15
8	78	85	-1
9	-41	77	-10
10	26	15	0

9 5 1

0	1584	1531	32
1	1180	1161	13
2	463	440	22
3	968	954	10
4	471	463	6
5	1206	1209	-2
6	1348	1334	8
7	607	624	-12
8	803	793	6
9	609	591	11
10	112	59	10

9 6 1

0	311	287	21
1	98	115	-8
2	123	138	-7
3	182	175	4
4	34	67	-6
5	164	146	9
6	276	259	10
7	-80	39	-13
8	190	240	-25
9	129	135	-1
10	229	142	30

9 7 1

0	2155	2193	-18
1	605	582	20
2	927	906	16
3	2641	2640	0
4	593	602	-8
5	1159	1175	-10
6	1925	1890	17
7	288	210	41
8	1267	1244	13
9	1353	1320	18
10	201	149	17

9 8 1

0	452	414	32
1	73	67	1
2	341	367	-22
3	258	255	2
4	117	118	0
5	157	166	-4
6	66	0	7
7	34	89	-10
8	81	62	3
9	120	56	12

9 9 1

0	1804	1840	-16
1	750	763	-8
2	1713	1737	-11
3	1703	1722	-8
4	750	746	2
5	1011	1024	-7
6	1151	1128	11
7	344	363	-8
8	1469	1446	9
9	1112	1109	1

10 0 1

0	2523	2532	-4
1	837	814	19
2	1000	998	1
3	1599	1561	22
4	178	198	-12
5	1015	999	11
6	1587	1588	0
7	457	467	-7
8	1001	986	9
9	1097	1084	7
10	164	169	-1

10 1 1

0	99	149	-30
1	228	247	-16
2	595	579	14
3	184	206	-13
4	110	114	-1
5	237	228	6
6	446	447	0
7	109	113	-1
8	98	88	2
9	205	201	1
10	278	272	3

10 2 1

0	1787	1814	-15
1	955	915	32
2	632	606	24
3	1695	1699	-2
4	597	571	21
5	1251	1233	12
6	1573	1554	11
7	319	293	16
8	996	982	9
9	923	901	13

10	19	15	0

10 3 1

0	59	63	-1
1	318	300	16
2	268	259	7
3	567	557	8
4	-23	46	-5
5	94	103	-3
6	182	186	-2
7	409	390	13
8	-64	38	-8
9	171	155	5
10	42	46	0

10 4 1

0	1937	1962	-13
1	510	505	5
2	1265	1267	-1
3	2039	2016	11
4	513	509	3
5	930	908	16
6	1248	1209	24
7	36	72	-5
8	1014	1032	-11
9	1098	1092	4
10	186	114	21

10 5 1

0	253	256	-2
1	252	248	3
2	558	551	6
3	135	75	23
4	63	38	5
5	267	242	16
6	228	206	12
7	91	134	-14
8	83	101	-4
9	86	60	4
10	92	138	-11

10 6 1

0	1769	1768	0
1	511	496	12
2	1292	1282	7
3	2202	2184	8
4	669	672	-2
5	1025	1004	14
6	1271	1226	28
7	135	69	18
8	1169	1168	0
9	1117	1104	7

10 7 1

0	84	33	12
1	-65	30	-11
2	459	445	11
3	346	358	-10
4	178	179	0
5	197	204	-4
6	166	176	-4
7	209	201	4
8	247	179	29
9	35	1	1

10 8 1

0	2144	2154	-4
1	881	881	0
2	842	850	-6
3	1448	1434	8
4	122	130	-3
5	1162	1169	-4
6	1367	1351	10
7	351	322	17
8	784	783	0
9	822	807	9

10 9 1

0	208	221	-9
1	55	58	0
2	192	178	8
3	237	230	4
4	-61	23	-7
5	104	133	-10
6	-10	112	-19
7	115	56	13
8	135	134	0
9	71	91	-3

10 10 1

0	1851	1842	3
1	714	725	-6
2	483	494	-6
3	1052	1066	-7
4	144	99	11
5	874	853	11
6	1368	1321	20
7	473	449	11
8	607	633	-12

11 1 1

0	1222	1217	3
1	442	435	6
2	517	479	31
3	1547	1535	7
4	569	569	0
5	703	678	19
6	1220	1197	15
7	130	119	3
8	761	783	-15
9	848	852	-2
10	120	86	6

11 2 1

0	164	183	-10
1	94	72	6
2	631	628	2
3	447	476	-25
4	247	218	18
5	-90	56	-22
6	-116	29	-26
7	141	145	-1
8	406	367	23
9	265	231	15
10	114	50	10

11 3 1

0	2171	2195	-11
1	1063	1060	2
2	1247	1230	11
3	1958	1947	5
4	567	582	-13
5	1441	1434	4
6	1635	1602	18
7	326	281	26
8	1300	1280	12
9	1041	1026	9
10	99	31	9

11 4 1

0	143	127	7
1	230	219	7
2	240	211	18
3	129	66	22

4	182	150	16
5	294	298	-3
6	208	185	11
7	40	11	2
8	58	85	-5
9	126	95	7
11 5 1			
0	2869	2883	-5
1	781	751	24
2	1308	1313	-3
3	2166	2159	3
4	113	43	19
5	1155	1149	3
6	1716	1687	15
7	166	109	20
8	1059	1030	18
9	1275	1236	22
11 6 1			
0	453	450	2
1	226	228	-1
2	582	590	-7
3	472	450	17
4	-66	6	-8
5	159	168	-4
6	-63	39	-8
7	121	124	-1
8	315	284	16
9	383	352	17
11 7 1			
0	1243	1255	-8
1	784	794	-8
2	844	856	-9
3	1186	1184	1
4	515	530	-12
5	999	1006	-4
6	951	942	6
7	342	326	9
8	857	846	7
9	658	640	11
11 8 1			
0	439	438	0
1	107	120	-5
2	62	27	5
3	95	88	2
4	169	185	-8
5	123	137	-4
6	229	255	-14
7	-40	45	-5
8	46	9	2
11 9 1			
0	1353	1385	-21
1	240	222	11
2	418	442	-18
3	1403	1395	4
4	145	166	-9
5	437	439	-1
6	1050	1036	9
7	43	8	2
8	441	462	-13
11 10 1			
0	109	138	-12
1	47	10	3
2	208	207	0
3	369	343	18
4	375	342	22
5	52	104	-11
6	104	85	4
7	132	125	2
8	400	346	28
11 11 1			
0	1191	1210	-10
1	757	783	-14
2	908	903	3
3	1501	1512	-5
4	824	807	8
5	1067	1096	-14
6	1186	1210	-11
7	241	222	6
12 0 1			
0	957	962	-3
1	511	481	25
2	575	595	-16
3	1040	1018	15
4	349	366	-12
5	704	673	23
6	582	576	4
7	227	205	10
8	442	419	14
9	482	498	-9
12 1 1			
0	179	184	-3
1	578	605	-23
2	166	148	9
3	74	98	-7
4	113	141	-12
5	766	758	6
6	213	197	8
7	-81	75	-17
8	203	223	-9
9	235	213	9
12 2 1			
0	1826	1813	7
1	535	513	19
2	773	763	8
3	1824	1818	2
4	460	461	0
5	850	855	-3
6	1436	1432	2
7	90	115	-6
8	994	957	23
9	1098	1074	13
12 3 1			
0	957	984	-21
1	85	108	-8
2	81	103	-7
3	361	369	-6
4	459	468	-7
5	257	231	15
6	424	380	29
7	-73	107	-23
8	109	92	4
9	149	134	4
12 4 1			
0	2724	2758	-13
1	1092	1090	1
2	1613	1612	1
3	2205	2172	15
4	400	401	0
5	1600	1581	10
6	1736	1683	27
7	235	240	-2
8	1386	1392	-3
9	1162	1169	-4
12 5 1			
0	578	575	2
1	125	106	7
2	-60	46	-12
3	272	268	3
4	161	164	-1
5	188	163	12
6	431	432	0
7	-82	9	-9
8	78	73	0
9	173	175	0
12 6 1			
0	1791	1809	-9
1	730	710	15
2	619	608	9
3	1422	1428	-3
4	342	365	-17
5	947	946	0
6	1511	1485	14
7	366	335	18
8	910	914	-2
9	949	937	6
12 7 1			
0	306	289	12
1	339	361	-17
2	73	91	-5
3	71	121	-16
4	-63	22	-7
5	474	467	5
6	202	229	-13
7	76	40	5
8	176	151	8
12 8 1			
0	924	907	12
1	306	285	14
2	476	471	3
3	1032	1038	-4
4	371	369	1
5	437	452	-10
6	713	711	1
7	155	151	1
8	481	488	-4
12 9 1			
0	165	174	-4
1	94	124	-11
2	-40	101	-20
3	148	152	-2
4	103	125	-7
5	88	153	-21
6	233	246	-6
7	132	53	16
8	270	259	5
12 10 1			
0	1215	1201	9
1	494	507	-9
2	799	810	-8
3	1564	1561	1
4	619	639	-14
5	867	852	10
6	1048	1055	-4
7	-30	56	-5
12 11 1			
0	108	134	-9
1	284	284	0
2	125	102	7
3	137	103	11
4	-59	58	-10
5	409	377	19
6	299	259	20
7	65	13	4
12 12 1			
0	2203	2189	5
1	774	772	0
2	1045	1032	6
3	1706	1719	-5
4	165	182	-4
5	1153	1168	-6
6	1431	1428	1
13 1 1			
0	1779	1766	6
1	815	822	-5
2	569	571	-1
3	1057	1036	14
4	61	53	1
5	963	955	5
6	1136	1132	2
7	410	408	1
8	510	504	3
9	641	633	4
13 2 1			
0	197	199	-1
1	166	149	8
2	-85	6	-14
3	448	462	-11
4	49	114	-17
5	311	344	-22
6	313	321	-4
7	227	181	19
8	155	182	-9
9	128	80	10
13 3 1			
0	1973	1981	-4
1	525	514	8
2	1284	1267	11
3	2210	2201	4
4	551	581	-23
5	959	958	0
6	1473	1452	12
7	106	47	11
8	1266	1260	3
9	1262	1235	15
13 4 1			
0	151	160	-4
1	-102	71	-32
2	125	133	-3
3	-48	14	-4
4	191	219	-15
5	-10	71	-7
6	104	20	13
7	55	53	0
8	183	193	-3
13 5 1			
0	1407	1408	0
1	695	700	-3
2	1141	1147	-3
3	1963	1942	10
4	852	844	5
5	1144	1155	-7
6	1293	1248	26

Structure Factors for Pt2Cl at 22 K. Page 5

7	120	12	17
8	1322	1276	25

13 6 1

0	134	162	-13
1	229	222	4
2	318	324	-4
3	230	233	-1
4	176	172	1
5	366	333	20
6	101	101	0
7	84	5	8
8	306	296	4

13 7 1

0	1326	1334	-5
1	360	373	-10
2	272	229	26
3	1113	1118	-3
4	224	234	-5
5	469	472	-2
6	1255	1244	6
7	256	255	0
8	571	575	-2

13 8 1

0	50	33	2
1	-17	90	-14
2	100	80	5
3	406	412	-4
4	80	61	3
5	26	65	-5
6	109	156	-15
7	309	269	20

13 9 1

0	1340	1353	-7
1	809	824	-11
2	665	671	-4
3	1017	1013	2
4	332	317	9
5	1025	1018	4
6	958	988	-19
7	374	339	18

13 10 1

0	295	283	7
1	15	19	0
2	104	89	4
3	425	443	-12
4	-68	38	-8
5	112	153	-13
6	184	171	4

13 11 1

0	2019	2007	5
1	598	619	-15
2	793	840	-33
3	1676	1668	4
4	196	183	5
5	908	949	-27
6	1480	1442	20

13 12 1

0	112	3	16
1	143	88	16
2	195	196	0
3	198	194	1
4	141	163	-7
5	214	176	15

13 13 1

0	1227	1281	-25
1	575	565	4
2	1066	1077	-5
3	1354	1366	-5
4	438	437	0

14 0 1

0	1638	1663	-14
1	219	212	3
2	973	988	-10
3	1967	1915	24
4	429	425	2
5	576	585	-6
6	1160	1142	10
7	88	81	1
8	914	895	11

14 1 1

0	104	119	-5
1	187	202	-8
2	-92	59	-21
3	159	173	-6
4	44	123	-19
5	116	170	-20
6	-68	42	-8
7	89	147	-16
8	122	91	7

14 2 1

0	1561	1573	-6
1	658	677	-15
2	1100	1107	-5
3	1440	1424	9
4	576	592	-11
5	905	918	-8
6	1138	1141	-1
7	333	339	-3
8	1185	1132	30

14 3 1

0	330	317	9
1	-28	64	-8
2	57	50	1
3	-41	25	-3
4	333	337	-2
5	-78	51	-12
6	99	25	11
7	-99	85	-21
8	231	279	-22

14 4 1

0	1897	1876	10
1	786	798	-9
2	400	396	3
3	1509	1493	9
4	-42	103	-18
5	1172	1181	-5
6	1456	1426	16
7	126	105	5
8	565	582	-10

14 5 1

0	240	225	9
1	44	40	0
2	55	53	0
3	217	175	20
4	77	102	-6
5	27	7	0
6	171	156	5
7	53	90	-6
8	103	23	10

14 6 1

0	1421	1435	-8
1	778	767	8
2	510	528	-13
3	1129	1118	6
4	343	335	5
5	955	988	-22
6	1152	1161	-5
7	334	335	0

14 7 1

0	154	135	8
1	76	87	-2
2	67	117	-14
3	264	235	15
4	-98	0	-14
5	-4	29	-1
6	-72	56	-10
7	108	106	0

14 8 1

0	1448	1455	-4
1	341	354	-9
2	1076	1096	-13
3	1524	1515	5
4	420	438	-12
5	612	621	-6
6	911	904	4
7	-65	97	-15

14 9 1

0	-99	26	-17
1	-53	58	-9
2	94	0	12
3	144	92	15
4	177	168	3
5	72	70	0
6	195	164	11

14 10 1

0	1454	1479	-14
1	416	423	-4
2	942	980	-26
3	1653	1643	5
4	497	504	-4
5	776	762	9
6	1108	1124	-9

14 11 1

0	159	130	10
1	-91	17	-12
2	220	205	6
3	201	203	0
4	-52	39	-5
5	-78	33	-8

14 12 1

0	1415	1424	-5
1	655	679	-16
2	672	705	-22
3	1037	1025	7
4	228	256	-13

14 13 1

0	112	84	6
1	110	68	9
2	156	165	-3
3	150	128	6

14 14 1

0	1016	1018	-1
1	464	479	-6

15 1 1

0	1825	1825	0
1	804	822	-12
2	754	765	-8
3	1662	1651	6
4	423	457	-23
5	1147	1149	-1
6	1547	1550	-1
7	177	209	-12
8	1064	1054	5

15 2 1

0	-69	83	-19
1	49	17	3
2	86	137	-16
3	595	590	3
4	232	221	5
5	181	199	-7
6	239	222	7
7	280	276	1

15 3 1

0	1264	1259	3
1	512	520	-6
2	700	718	-13
3	1156	1172	-10
4	357	388	-19
5	691	701	-6
6	980	967	7
7	226	237	-4

15 4 1

0	247	242	2
1	-89	17	-13
2	166	168	0
3	5	65	-6
4	109	151	-14
5	-106	31	-16
6	202	211	-3
7	-113	15	-16

15 5 1

0	1134	1125	5
1	263	274	-6
2	654	663	-6
3	1363	1358	3
4	307	329	-13
5	511	532	-13
6	867	810	35
7	84	19	7

15 6 1

0	39	63	-3
1	24	121	-21
2	536	501	24
3	359	310	28
4	255	247	3
5	242	245	-1
6	-54	54	-7
7	46	63	-2

15 7 1

0	1632	1673	-22
1	659	663	-2
2	1108	1125	-11

3	1447	1446	0
4	375	364	6
5	913	932	-12
6	1035	1048	-8

15 8 1

0	352	334	11
1	307	286	12
2	295	278	9
3	229	218	5
4	81	123	-10
5	196	219	-10
6	-115	13	-16

15 9 1

0	1928	1903	12
1	755	761	-4
2	633	666	-23
3	1575	1561	7
4	159	177	-6
5	1115	1125	-6

15 10 1

0	95	95	0
1	141	125	5
2	107	29	13
3	503	486	10
4	132	122	2
5	70	23	4

15 11 1

0	1133	1159	-16
1	619	624	-3
2	573	601	-19
3	948	963	-9
4	391	367	13

15 12 1

0	358	335	13
1	135	72	15
2	208	137	25
3	135	57	16

15 13 1

0	745	765	-13
1	199	195	1

16 0 1

0	1679	1696	-9
1	897	926	-20
2	1195	1188	4
3	1855	1845	4
4	670	695	-17
5	1460	1421	20
6	1354	1320	18
7	-113	96	-24

16 1 1

0	309	320	-6
1	248	262	-7
2	254	253	0
3	302	279	12
4	-102	16	-14
5	398	394	2
6	556	532	14
7	-37	37	-2

16 2 1

0	1700	1717	-8
1	427	452	-17
2	601	626	-18
3	1520	1518	1
4	95	171	-24
5	732	768	-24
6	1253	1240	7
7	96	46	7

16 3 1

0	498	467	21
1	374	355	11
2	76	140	-18
3	56	61	0
4	-63	60	-9
5	418	394	14
6	315	292	11
7	152	155	0

16 4 1

0	919	941	-15
1	464	477	-8
2	541	577	-25
3	714	716	-1
4	367	353	8
5	518	536	-11
6	675	698	-14

16 5 1

0	564	561	2
1	296	298	-1
2	352	329	13
3	112	125	-3
4	133	164	-10
5	410	374	20
6	159	125	9

16 6 1

0	1515	1502	7
1	409	417	-5
2	751	781	-21
3	1398	1372	15
4	277	304	-14
5	614	651	-24
6	1072	1062	6

16 7 1

0	322	331	-5
1	208	218	-4
2	94	122	-7
3	218	179	16
4	-107	19	-15
5	307	291	7

16 8 1

0	1664	1692	-14
1	751	770	-12
2	870	880	-6
3	1603	1605	0
4	462	450	7
5	1161	1159	0

16 9 1

0	393	375	10
1	62	93	-6
2	167	182	-5
3	186	220	-14
4	-56	67	-9

16 10 1

0	1225	1209	9
1	530	597	-46
2	571	595	-15
3	1214	1177	21

16 11 1

0	369	347	11
1	253	244	4
2	81	66	2

17 1 1

0	1551	1542	5
1	514	550	-23
2	1038	1049	-7
3	1647	1644	1
4	402	430	-17
5	897	910	-7
6	1062	1060	1

17 2 1

0	245	250	-2
1	-114	95	-30
2	411	405	3
3	279	297	-9
4	-80	129	-28
5	186	184	0
6	136	98	8

17 3 1

0	1245	1242	1
1	508	540	-21
2	441	466	-15
3	985	986	0
4	185	215	-12
5	693	694	0
6	992	975	10

17 4 1

0	181	220	-17
1	104	136	-9
2	-120	92	-31
3	89	115	-6
4	-30	113	-15
5	75	154	-19

17 5 1

0	1281	1260	12
1	560	581	-13
2	458	475	-10
3	956	960	-1
4	257	303	-23
5	691	693	-1

17 6 1

0	529	515	8
1	-21	112	-16
2	264	299	-18
3	404	380	13
4	91	120	-6
5	38	57	-1

17 7 1

0	1495	1490	2
1	579	601	-14
2	747	776	-19
3	1572	1548	12
4	386	430	-26

17 8 1

0	88	157	-20
1	-32	96	-12
2	195	212	-7
3	65	26	4
4	215	228	-5

17 9 1

0	1142	1149	-4
1	493	479	8
2	764	783	-12
3	1322	1326	-2

17 10 1

0	81	10	7
1	168	155	4

18 0 1

0	1801	1822	-10
1	533	571	-24
2	369	423	-32
3	1093	1081	6
4	40	40	0
5	703	720	-10

18 1 1

0	125	11	17
1	-138	31	-26
2	76	79	0
3	-149	25	-28
4	-102	7	-12
5	-41	18	-2

18 2 1

0	1199	1230	-18
1	695	686	6
2	770	800	-19
3	1083	1086	-1
4	358	381	-12
5	938	942	-2

18 3 1

0	258	260	-1
1	-137	35	-26
2	200	226	-11
3	49	28	1
4	159	162	0

18 4 1

0	1130	1123	4
1	150	208	-22
2	669	691	-14
3	1534	1514	10
4	479	504	-14

18 5 1

0	126	72	11
1	-74	78	-14
2	-83	20	-8
3	-36	30	-2
4	-91	23	-9

18 6 1

0	1244	1245	0
1	520	566	-30
2	889	890	0
3	1374	1357	9

18 7 1

0	118	119	0

Structure Factors for Pt2Cl at 22 K. Page 7

1	-103	49	-16	1	289	322	-16								19	5	1		
2	159	123	10	2	554	620	-42	0	1380	1357	12								
3	115	4	13	3	1056	1049	3	1	578	605	-16	0	1655	1605	24				
								2	602	637	-21	1	795	769	15				
	18	8	1		19	2	1	3	1329	1325	2	2	671	694	-14				
0	1357	1372	-8	0	188	230	-17		19	4	1				19	6	1		
1	585	607	-13	1	-88	85	-17												
				2	346	324	10	0	115	24	13	0	351	341	5				
	19	1	1	3	296	271	10	1	132	171	-12								
								2	-109	4	-13								
0	926	940	-8		19	3	1												

Table A4 (for deposit).

Structure Factors for Pt2Cl at 300 K.

The columns contain, in order,
k, 10Fo, 10Fc and 10|(Fo**2 - Fc**2)/sigma(Fo**2)|.
A minus sign preceeding 10Fo indicates that Fo**2 is negative.

Structure Factors for Pt2Cl at 300 K. Page 1

1 k 0

1	3172	3219	-14

2 k 0

0	2049	1945	57
1	461	548	-177
2	2842	2829	4

3 k 0

1	1440	1536	-78
2	-159	96	-123
3	3519	3592	-20

4 k 0

0	708	715	-9
1	-128	68	-84
2	3135	3100	12
3	-211	107	-142
4	3961	3963	0

5 k 0

1	2611	2602	4
2	244	295	-69
3	3129	3137	-3
4	-36	72	-24
5	1306	1383	-54

6 k 0

0	1063	1119	-57
1	479	489	-15
2	2756	2855	-41
3	517	513	5
4	1968	1948	11
5	341	360	-27
6	2854	2846	2

7 k 0

1	2439	2516	-36
2	415	405	15
3	1606	1594	8
4	185	142	42
5	2021	1990	16
6	174	199	-24
7	2279	2291	-5

8 k 0

0	3538	3649	-36
1	666	681	-19
2	2086	2092	-2
3	210	108	85
4	822	755	70
5	189	143	35
6	1601	1560	26
7	491	512	-25
8	2451	2432	7

9 k 0

1	2429	2460	-14
2	581	585	-4
3	1595	1575	13
4	189	190	-1
5	1349	1300	36
6	255	285	-35
7	1820	1814	3
8	341	334	7
9	1600	1639	-21

10 k 0

0	2235	2234	0
1	134	104	23
2	1610	1583	17
3	132	28	45
4	1617	1589	18
5	198	192	5
6	1503	1473	21
7	142	34	46
8	1658	1661	-1
9	188	202	-11
10	1387	1407	-12

11 k 0

1	1081	1067	12
2	137	125	8
3	1839	1838	0
4	152	122	22
5	2356	2351	2
6	275	267	8
7	1098	1071	23
8	256	247	9
9	1077	1094	-14
10	150	43	44
11	859	873	-10

12 k 0

0	782	758	25
1	161	134	21
2	1405	1377	20
3	647	669	-24
4	2324	2325	0
5	403	405	-2
6	1402	1391	7
7	210	225	-13
8	701	694	7
9	160	122	22
10	863	853	9
11	137	125	6
12	1480	1482	0

13 k 0

1	1350	1350	0
2	228	212	14
3	1637	1621	10
4	146	39	46
5	1257	1243	10
6	177	172	3
7	925	926	0
8	74	34	9
9	912	926	-12
10	158	171	-8
11	1353	1352	0
12	147	42	36
13	948	961	-8

14 k 0

0	1209	1196	9
1	151	57	46
2	1294	1269	18
3	264	221	37
4	1355	1357	-1
5	187	123	39
6	1076	1070	4
7	78	77	0
8	961	966	-4
9	87	32	13
10	1051	1057	-5
11	94	52	11
12	971	967	3
13	117	83	12
14	601	613	-8

15 k 0

1	1354	1352	2
2	119	43	27
3	981	975	4
4	108	110	-1
5	859	836	21
6	79	66	4
7	1177	1191	-10
8	225	173	34
9	1229	1214	11
10	38	60	-4
11	765	780	-13
12	157	142	7
13	470	501	-29
14	68	82	-3
15	567	590	-15

16 k 0

0	1309	1294	11
1	231	196	26
2	1171	1169	1
3	265	235	24
4	622	612	9
5	308	298	8
6	1031	1021	7
7	205	203	1
8	1223	1209	10
9	245	242	1
10	807	798	7
11	171	154	9
12	484	496	-11
13	-81	78	-23
14	576	581	-4
15	186	144	20
16	822	798	14

17 k 0

1	1162	1144	14
2	183	195	-7
3	815	824	-7
4	129	102	11
5	783	753	26
6	273	286	-10
7	1033	1019	10
8	118	49	20
9	806	792	12
10	94	49	11
11	609	618	-8
12	124	114	3
13	570	585	-13
14	136	105	11
15	762	755	6

18 k 0

0	1133	1119	11
1	111	0	23
2	860	863	-3
3	183	159	13
4	716	702	13
5	119	2	23
6	816	810	5
7	110	52	16
8	833	830	2
9	164	113	22
10	678	693	-12
11	121	54	18
12	519	541	-20
13	92	61	7

19 k 0

1	628	632	-3
2	128	83	16
3	863	859	3
4	-17	19	-1
5	978	966	10
6	159	131	12
7	705	704	0
8	120	102	6
9	513	517	-3
10	128	45	23
11	567	569	-1
12	158	28	35

20 k 0

0	452	470	-16
1	181	201	-11
2	725	714	9
3	310	307	2
4	916	906	8
5	197	176	11
6	763	740	19
7	216	180	19
8	412	435	-19
9	144	50	27
10	537	546	-7

21 k 0

1	606	593	11
2	143	145	0
3	756	737	15
4	124	36	20
5	694	696	-1
6	174	128	19
7	428	439	-8
8	114	13	19

22 k 0

0	589	589	0
1	39	55	-2
2	589	594	-4
3	-31	7	-1
4	643	631	10
5	126	34	20
6	467	457	6

0 k 1

0	2297	2284	6

1 k 1

1	1359	1157	133

2 k 1

0	1516	1525	-6
1	150	193	-52
2	545	479	76

3 k 1

1	773	676	120
2	203	337	-207
3	1718	1611	85

4 k 1

0	1136	1184	-48
1	435	504	-124
2	1272	1267	4
3	-134	128	-92
4	1930	1850	38

5 k 1

1	1200	1155	39
2	231	297	-92
3	717	725	-10
4	124	111	11

Structure Factors for Pt2Cl at 300 K. Page 2

5	924	925	0

6 k 1

0	1088	1147	-59
1	550	564	-21
2	529	467	87
3	-121	56	-67
4	1121	1110	10
5	132	25	57
6	948	887	48

7 k 1

1	1164	1140	22
2	197	174	28
3	598	586	15
4	241	180	65
5	445	451	-8
6	296	266	33
7	1117	1122	-3

8 k 1

0	1484	1483	1
1	196	80	102
2	960	971	-11
3	360	322	47
4	154	3	66
5	289	273	15
6	699	679	22
7	103	46	24
8	999	1011	-9

9 k 1

1	637	625	14
2	248	222	29
3	748	729	20
4	68	11	14
5	970	971	-1
6	148	114	23
7	595	601	-6
8	121	63	27
9	660	694	-28

10 k 1

0	813	831	-20
1	193	162	30
2	793	794	0
3	278	249	30
4	548	567	-24
5	234	201	29
6	479	470	10
7	126	25	37
8	766	791	-26
9	-35	49	-9
10	524	552	-23

11 k 1

1	450	444	7
2	158	77	51
3	920	912	7
4	180	127	39
5	674	680	-6
6	162	132	20
7	649	656	-8
8	104	85	8
9	284	292	-7
10	127	18	35
11	566	577	-8

12 k 1

0	365	353	14
1	396	391	5
2	572	573	-1
3	159	65	50
4	900	922	-21
5	107	52	21
6	609	635	-29
7	243	243	0
8	268	240	25
9	163	108	30
10	432	441	-9
11	141	135	3
12	585	593	-6

13 k 1

1	637	638	-1
2	173	137	26
3	516	532	-19
4	110	42	24
5	595	608	-14
6	147	148	0
7	342	365	-24
8	41	5	3
9	557	553	3
10	83	37	12
11	444	476	-33
12	77	51	6
13	437	439	-1

14 k 1

0	325	319	6
1	150	118	20
2	526	540	-15
3	58	33	5
4	669	671	-2
5	116	29	27
6	558	568	-10
7	135	78	25
8	324	346	-21
9	108	67	14
10	377	365	10
11	71	9	10
12	461	477	-15
13	68	31	7
14	284	294	-5

15 k 1

1	620	638	-19
2	142	23	41
3	422	426	-4
4	43	5	4
5	308	310	-1
6	27	54	-4
7	504	494	10
8	135	122	6
9	493	512	-19
10	83	33	11
11	437	429	6
12	111	46	18
13	194	179	9
14	141	20	31
15	303	307	-1

16 k 1

0	700	709	-9
1	200	131	42
2	424	423	0
3	225	210	11
4	301	307	-6
5	189	177	7
6	361	370	-8
7	113	98	5
8	543	551	-8
9	77	41	8
10	403	428	-24
11	157	128	13
12	167	166	0
13	-58	45	-9
14	304	294	7
15	156	57	31
16	315	310	2

17 k 1

1	455	462	-7
2	123	90	13
3	360	380	-18
4	119	50	21
5	367	384	-14
6	-84	4	-14
7	417	427	-9
8	-35	44	-6
9	397	383	11
10	112	72	12
11	222	220	1
12	87	27	11
13	295	310	-11
14	68	10	7
15	276	297	-15

18 k 1

0	418	436	-16
1	54	10	5
2	413	435	-21
3	94	39	13
4	210	251	-28
5	61	48	2
6	379	385	-5
7	101	21	16
8	388	406	-15
9	67	1	7
10	259	282	-16
11	120	10	23
12	235	255	-13
13	-40	29	-4

19 k 1

1	260	262	-1
2	84	29	10
3	411	405	5
4	113	49	16
5	461	452	7
6	54	11	4
7	322	315	5
8	-51	16	-5
9	202	177	13
10	98	37	13
11	283	265	12
12	144	62	25

20 k 1

0	260	275	-10
1	104	107	0
2	261	299	-27
3	139	96	15
4	426	412	11
5	115	70	13
6	267	286	-12
7	71	95	-6
8	163	207	-23
9	106	59	12
10	252	254	-1

21 k 1

1	271	278	-5
2	-61	26	-7
3	313	325	-8
4	-44	2	-3
5	266	275	-5
6	-75	39	-11
7	215	228	-7
8	-47	21	-4

22 k 1

0	166	207	-20
1	75	9	8
2	270	283	-8
3	115	4	18
4	266	282	-10
5	-55	1	-4

0 k 2

0	2673	2556	42

1 k 2

1	2570	2404	62

2 k 2

0	1451	1457	-4
1	270	340	-114
2	104	76	11

3 k 2

1	351	318	48
2	205	296	-118
3	1807	1746	31

4 k 2

0	964	825	140
1	385	449	-103
2	2310	2253	28
3	334	373	-58
4	622	546	74

5 k 2

1	654	599	72
2	-68	18	-20
3	1945	1910	19
4	219	254	-44
5	1434	1437	-1

6 k 2

0	479	513	-55
1	-89	68	-52
2	1433	1396	28
3	414	429	-22
4	1113	1072	36
5	267	163	99
6	1017	999	14

7 k 2

1	964	974	-10
2	277	263	20
3	1221	1199	18
4	270	155	103
5	629	606	27
6	395	403	-10
7	1515	1536	-12

8 k 2

0	1497	1474	16
1	249	124	114
2	1197	1210	-10
3	307	309	-2
4	458	378	91
5	253	273	-22
6	1034	998	32
7	187	120	49

8	1046	1057	-8

9 k 2

1	2002	1999	1
2	248	247	0
3	220	112	89
4	159	153	4
5	395	377	22
6	139	112	17
7	861	872	-10
8	242	223	17
9	1427	1436	-5

10 k 2

0	1070	1078	-7
1	455	439	20
2	575	548	32
3	153	96	39
4	1096	1094	1
5	336	347	-12
6	990	978	10
7	337	329	9
8	810	806	4
9	135	84	26
10	441	463	-17

11 k 2

1	503	472	37
2	425	448	-28
3	1027	1038	-10
4	165	126	27
5	1223	1247	-18
6	410	381	31
7	677	697	-21
8	25	13	1
9	412	418	-6
10	160	116	24
11	641	642	0

12 k 2

0	488	484	4
1	165	146	15
2	670	663	8
3	115	93	12
4	1313	1314	0
5	133	13	38
6	641	651	-10
7	144	110	18
8	345	351	-6
9	-94	82	-39
10	604	613	-9
11	132	52	29
12	729	725	2

13 k 2

1	519	529	-12
2	73	25	12
3	1053	1052	0
4	141	83	28
5	930	937	-5
6	170	193	-16
7	256	232	20
8	90	35	15
9	491	506	-15
10	117	71	17
11	642	667	-25
12	154	64	35
13	736	727	5

14 k 2

0	785	772	13
1	85	44	13
2	846	841	4
3	107	64	17
4	478	467	11
5	154	70	37
6	425	432	-7
7	122	75	18
8	712	740	-27
9	105	3	21
10	642	666	-23
11	148	139	4
12	505	529	-23
13	135	57	25
14	198	199	0

15 k 2

1	648	651	-3
2	149	118	17
3	554	585	-33
4	132	61	27
5	471	483	-12
6	285	258	22
7	802	809	-7
8	151	132	10
9	512	533	-20
10	64	38	4
11	413	431	-16
12	65	32	5
13	276	257	13
14	168	119	22
15	390	418	-17

16 k 2

0	780	776	3
1	157	114	23
2	564	564	0
3	115	96	7
4	371	380	-8
5	179	204	-16
6	599	603	-3
7	122	54	21
8	632	642	-10
9	108	92	5
10	419	425	-5
11	73	60	3
12	287	283	2
13	127	79	15
14	391	384	5
15	132	51	22

17 k 2

1	754	764	-9
2	209	195	9
3	381	371	9
4	18	55	-5
5	340	324	13
6	164	176	-6
7	559	577	-17
8	78	67	2
9	539	518	18
10	155	118	16
11	336	348	-9
12	125	74	16
13	331	319	8
14	96	66	7

18 k 2

0	420	443	-22
1	118	69	16
2	540	531	8
3	160	137	11
4	425	441	-14
5	27	16	0
6	542	525	15
7	127	118	3
8	355	366	-9
9	110	29	18
10	359	358	1
11	92	20	13
12	390	365	19
13	118	59	16

19 k 2

1	413	398	12
2	182	136	22
3	460	450	7
4	65	16	6
5	485	494	-8
6	157	97	23
7	391	394	-2
8	103	30	15
9	332	360	-22
10	137	116	8
11	346	348	0
12	57	5	5

20 k 2

0	280	266	9
1	54	68	-2
2	350	346	3
3	100	143	-16
4	578	575	2
5	106	54	12
6	412	416	-3
7	118	87	9
8	247	262	-9
9	89	38	10
10	308	290	12

21 k 2

1	301	304	-2
2	126	134	-2
3	431	454	-18
4	105	74	8
5	401	413	-8
6	184	163	10
7	247	235	7
8	118	2	20

22 k 2

0	340	380	-30
1	-65	38	-8
2	357	374	-12
3	59	3	4
4	259	277	-11
5	70	50	2

0 k 3

0	3089	3087	0

1 k 3

1	3251	3320	-21

2 k 3

0	2199	2177	11
1	-129	158	-131
2	2792	2794	0

3 k 3

1	1895	1901	-3
2	789	811	-27
3	2499	2530	-12

4 k 3

0	2077	2155	-43
1	88	110	-17
2	1798	1806	-5
3	313	345	-45
4	3087	3099	-3

5 k 3

1	1116	1107	7
2	130	135	-4
3	3013	2984	11
4	258	200	66
5	2885	2863	10

6 k 3

0	1846	1905	-36
1	192	163	34
2	2273	2330	-28
3	181	17	93
4	1867	1831	21
5	200	198	2
6	1689	1644	23

7 k 3

1	2558	2544	6
2	493	491	3
3	1456	1416	28
4	184	136	36
5	1308	1285	18
6	355	333	24
7	1735	1700	17

8 k 3

0	2570	2637	-30
1	422	443	-28
2	1803	1801	1
3	276	262	16
4	1066	1062	3
5	124	37	33
6	1571	1546	16
7	138	116	14
8	2172	2132	16

9 k 3

1	2314	2323	-4
2	149	154	-4
3	1162	1153	7
4	148	83	39
5	866	827	38
6	127	95	17
7	2130	2139	-5
8	169	173	-3
9	1478	1503	-14

10 k 3

0	1417	1412	3
1	159	105	39
2	1502	1516	-10
3	407	404	3
4	1610	1586	15
5	143	57	41
6	1770	1752	11
7	271	244	24
8	1184	1187	-2
9	189	152	24
10	902	885	12

11 k 3

1	1221	1209	10
2	334	346	-14
3	1668	1638	18
4	131	60	33

Structure Factors for Pt2Cl at 300 K. Page 4

5	1778	1753	14
6	282	279	3
7	974	966	7
8	107	66	16
9	956	940	14
10	228	212	12
11	1110	1112	-1

12 k 3

0	857	846	10
1	138	91	27
2	1427	1414	8
3	270	242	26
4	1821	1796	14
5	209	207	1
6	1136	1135	1
7	121	67	22
8	729	742	-12
9	95	73	8
10	1053	1044	7
11	144	96	21
12	1253	1243	6

13 k 3

1	846	827	18
2	302	305	-3
3	1687	1676	6
4	119	11	32
5	1497	1481	10
6	181	150	19
7	816	805	10
8	248	214	26
9	713	713	0
10	245	222	17
11	1164	1165	0
12	166	106	28
13	873	880	-4

14 k 3

0	1306	1283	17
1	198	147	36
2	1126	1129	-2
3	131	6	36
4	1128	1129	0
5	118	98	8
6	909	914	-3
7	208	196	8
8	1019	1000	15
9	106	17	20
10	1061	1066	-3
11	145	116	13
12	684	701	-16
13	124	72	17
14	622	614	5

15 k 3

1	1236	1230	4
2	324	325	0
3	882	866	14
4	97	46	14
5	895	894	1
6	224	189	22
7	1007	1006	0
8	133	55	26
9	1072	1056	13
10	240	207	21
11	627	632	-4
12	95	23	14
13	608	607	1
14	132	92	14
15	594	613	-12

16 k 3

0	1348	1348	0
1	232	196	26
2	1039	1022	13
3	103	66	12
4	567	549	17
5	84	86	0
6	884	882	1
7	191	134	30
8	1091	1084	5
9	152	131	10
10	765	766	-1
11	91	76	4
12	505	529	-22
13	145	96	17
14	555	556	-1
15	82	30	9

17 k 3

1	1149	1136	9
2	226	199	17
3	660	647	11
4	-16	53	-5
5	624	625	-1
6	228	196	20
7	999	983	12
8	137	40	28
9	853	846	5
10	174	114	26
11	562	565	-2
12	-64	72	-16
13	465	474	-7
14	179	94	33

18 k 3

0	777	769	7
1	146	24	34
2	744	743	0
3	48	51	0
4	886	861	21
5	114	8	21
6	827	839	-10
7	-70	32	-10
8	668	671	-2
9	74	44	6
10	514	524	-8
11	123	71	16
12	565	556	7
13	57	4	5

19 k 3

1	618	633	-13
2	148	150	0
3	829	815	11
4	-44	28	-4
5	807	788	15
6	202	169	17
7	643	632	9
8	137	37	26
9	516	508	7
10	93	70	5
11	568	557	8

20 k 3

0	436	443	-6
1	102	90	3
2	738	703	29
3	74	90	-4
4	793	795	-1
5	90	103	-3
6	669	642	22
7	115	50	16
8	427	430	-2
9	65	61	0

21 k 3

1	537	534	2
2	146	172	-11
3	702	689	10
4	124	0	21
5	651	630	17
6	88	114	-7
7	422	435	-9

22 k 3

0	616	594	17
1	74	27	6
2	533	542	-7
3	32	19	0

0 k 4

0	1661	1568	76

1 k 4

1	773	760	12

2 k 4

0	1254	1257	-2
1	320	346	-39
2	514	483	32

3 k 4

1	644	638	7
2	89	111	-17
3	510	496	14

4 k 4

0	561	554	10
1	134	128	6
2	416	405	15
3	172	24	85
4	540	425	97

5 k 4

1	214	41	125
2	192	17	98
3	555	597	-57
4	75	27	13
5	1382	1379	2

6 k 4

0	1153	1215	-56
1	256	253	3
2	294	250	50
3	455	469	-17
4	726	722	4
5	135	133	1
6	200	127	39

7 k 4

1	735	732	3
2	395	415	-28
3	498	512	-17
4	113	29	31
5	122	44	35
6	150	63	43
7	449	442	5

8 k 4

0	283	248	39
1	324	294	36
2	444	459	-19
3	205	175	26
4	476	469	8
5	161	97	37
6	608	604	4
7	216	186	23
8	459	459	0

9 k 4

1	556	564	-10
2	180	144	28
3	233	185	41
4	86	20	19
5	404	414	-11
6	75	17	13
7	563	571	-8
8	74	84	-4
9	493	510	-13

10 k 4

0	230	235	-5
1	126	97	17
2	485	489	-4
3	140	11	47
4	431	453	-26
5	80	23	14
6	521	532	-11
7	169	140	18
8	236	234	1
9	106	24	23
10	169	143	11

11 k 4

1	455	472	-20
2	188	161	21
3	507	516	-10
4	145	105	21
5	187	141	31
6	114	22	27
7	377	389	-11
8	147	87	28
9	161	138	13
10	183	163	12
11	594	598	-2

12 k 4

0	306	305	1
1	128	106	12
2	433	449	-18
3	290	280	9
4	326	326	0
5	147	102	23
6	325	344	-18
7	29	17	1
8	243	246	-2
9	105	75	11
10	443	462	-18
11	99	12	18
12	213	219	-3

13 k 4

1	92	107	-7
2	88	45	13
3	451	467	-17
4	148	94	25
5	603	599	4
6	122	72	19
7	212	234	-17
8	61	33	5
9	252	255	-2
10	-29	3	-1
11	191	197	-3
12	106	54	14
13	300	264	18

Structure Factors for Pt2Cl at 300 K. Page 5

14 k 4

0	366	365	0
1	115	63	20
2	389	387	2
3	225	204	16
4	240	225	11
5	55	57	0
6	252	272	-16
7	100	6	18
8	332	347	-13
9	104	90	4
10	281	288	-5
11	66	37	5
12	195	177	10
13	94	16	14
14	178	191	-4

15 k 4

1	387	391	-4
2	156	131	13
3	258	263	-4
4	100	46	15
5	212	230	-12
6	71	112	-14
7	291	276	11
8	-33	51	-7
9	247	241	4
10	112	68	13
11	243	227	11
12	-30	34	-3
13	214	224	-6
14	84	13	11
15	239	237	0

16 k 4

0	470	486	-15
1	78	12	11
2	215	209	4
3	36	2	2
4	228	242	-10
5	99	53	12
6	207	219	-8
7	86	17	12
8	307	292	11
9	120	50	19
10	241	245	-2
11	35	23	1
12	199	175	12
13	112	24	19
14	256	214	25

17 k 4

1	297	291	5
2	119	48	20
3	179	177	1
4	-53	37	-7
5	216	252	-25
6	140	47	28
7	284	285	0
8	63	88	-6
9	306	296	7
10	71	76	-1
11	93	121	-9
12	106	35	15
13	197	164	16

18 k 4

0	146	88	22
1	-15	11	0
2	222	231	-5
3	84	79	1
4	335	330	4
5	51	9	4
6	293	288	3
7	103	17	16
8	156	159	-1
9	98	59	9
10	118	109	3
11	-45	2	-3
12	194	213	-10

19 k 4

1	243	244	0
2	69	68	0
3	237	241	-2
4	-55	4	-5
5	149	177	-13
6	68	8	7
7	157	145	5
8	120	56	17
9	157	180	-11
10	78	52	5

20 k 4

0	231	223	4
1	-86	15	-12
2	170	198	-14
3	119	91	8
4	205	219	-8
5	87	17	10
6	129	131	0
7	-49	18	-4
8	177	167	4

21 k 4

1	162	146	6
2	87	22	10
3	181	203	-11
4	-104	9	-16
5	220	182	18
6	-56	25	-4

0 k 5

0	2208	2196	5

1 k 5

1	1668	1633	19

2 k 5

0	1705	1676	17
1	298	243	68
2	1088	1042	34

3 k 5

1	879	905	-27
2	78	7	20
3	1771	1749	11

4 k 5

0	321	272	61
1	485	503	-23
2	1333	1349	-12
3	112	38	27
4	2165	2171	-2

5 k 5

1	956	963	-6
2	178	154	21
3	1286	1300	-11
4	113	64	21
5	1571	1569	1

6 k 5

0	1307	1353	-37
1	476	478	-2
2	908	877	30
3	117	57	26
4	1288	1290	-1
5	120	26	33
6	1041	1036	3

7 k 5

1	1522	1528	-4
2	90	5	23
3	749	736	13
4	285	249	35
5	542	534	8
6	189	182	5
7	1306	1294	7

8 k 5

0	1787	1812	-15
1	174	77	59
2	1188	1201	-10
3	170	182	-10
4	222	120	73
5	238	226	10
6	901	888	12
7	153	68	38
8	1357	1366	-5

9 k 5

1	1070	1073	-1
2	258	238	19
3	799	791	8
4	81	20	15
5	909	899	9
6	112	112	0
7	1008	999	7
8	104	114	-4
9	910	925	-10

10 k 5

0	897	909	-12
1	197	161	29
2	964	973	-8
3	143	80	31
4	815	822	-7
5	185	180	5
6	836	817	17
7	128	139	-6
8	940	947	-6
9	111	92	7
10	555	588	-25

11 k 5

1	642	614	29
2	98	27	21
3	1123	1126	-2
4	203	157	31
5	916	914	0
6	156	81	35
7	770	774	-3
8	107	95	4
9	396	405	-8
10	47	50	0
11	737	738	0

12 k 5

0	467	460	8
1	428	450	-24
2	762	777	-15
3	126	127	0
4	1210	1192	13
5	114	94	8
6	757	766	-8
7	277	284	-5
8	322	325	-2
9	100	109	-3
10	581	594	-13
11	193	178	9
12	785	804	-12

13 k 5

1	669	668	1
2	252	245	6
3	834	823	10
4	118	38	25
5	877	889	-10
6	175	187	-7
7	430	427	3
8	108	72	11
9	594	603	-8
10	124	121	1
11	647	660	-11
12	151	80	26
13	594	595	-1

14 k 5

0	508	515	-7
1	122	58	23
2	679	680	0
3	61	36	5
4	864	856	7
5	113	11	23
6	675	678	-2
7	77	8	10
8	470	477	-6
9	121	60	19
10	543	543	0
11	83	51	7
12	559	566	-6
13	89	49	9
14	399	374	13

15 k 5

1	789	793	-3
2	85	83	0
3	538	540	-1
4	84	15	12
5	456	463	-7
6	124	122	0
7	617	619	-2
8	115	92	7
9	673	675	-1
10	-59	32	-8
11	483	507	-21
12	-26	33	-3
13	228	259	-20
14	-58	51	-9
15	361	391	-16

16 k 5

0	995	967	23
1	197	193	2
2	584	583	0
3	201	223	-14
4	349	334	12
5	205	202	1
6	434	464	-27
7	133	131	0
8	744	725	16
9	127	71	17
10	564	568	-3
11	178	162	8
12	214	229	-9

Structure Factors for Pt2Cl at 300 K. Page 6

13	115	83	9
14	371	359	9

17 k 5

1	670	668	2
2	156	150	3
3	443	433	8
4	135	52	24
5	398	418	-17
6	35	34	0
7	590	590	0
8	97	59	9
9	556	538	16
10	156	116	16
11	296	296	0
12	95	22	13

18 k 5

0	506	517	-10
1	64	36	4
2	532	536	-3
3	-89	25	-14
4	361	379	-14
5	111	48	15
6	522	535	-10
7	-56	39	-7
8	508	503	4
9	100	13	15
10	312	324	-9
11	140	11	28

19 k 5

1	321	336	-11
2	94	67	6
3	523	526	-2
4	101	40	12
5	563	570	-5
6	55	33	2
7	431	427	3
8	67	29	5
9	229	229	0

20 k 5

0	289	311	-16
1	142	129	5
2	409	408	1
3	110	116	-2
4	566	533	26
5	139	94	14
6	381	386	-3
7	151	99	17

21 k 5

1	337	355	-12
2	47	84	-6
3	426	432	-4

0 k 6

0	2775	2752	8

1 k 6

1	1896	1906	-5

2 k 6

0	1428	1423	3
1	179	172	6
2	1990	2015	-11

3 k 6

1	1287	1279	5
2	158	109	34
3	1885	1909	-12

4 k 6

0	666	629	41
1	146	128	13
2	1184	1169	13
3	258	267	-10
4	2656	2678	-8

5 k 6

1	1206	1210	-3
2	191	165	22
3	1763	1731	19
4	241	240	1
5	1507	1560	-30

6 k 6

0	1554	1565	-7
1	158	58	50
2	1397	1426	-21
3	177	151	20
4	1321	1317	3
5	216	218	-1
6	1264	1261	1

7 k 6

1	1803	1840	-22
2	135	34	41
3	900	870	27
4	26	16	1
5	1102	1085	13
6	44	3	4
7	1213	1199	8

8 k 6

0	1990	2034	-24
1	299	326	-31
2	1199	1183	12
3	148	113	21
4	753	714	38
5	53	40	3
6	1100	1096	3
7	168	182	-9
8	1665	1638	13

9 k 6

1	1249	1236	10
2	141	141	0
3	1161	1154	5
4	91	34	16
5	1014	1006	6
6	198	170	19
7	1441	1424	11
8	80	37	10
9	908	926	-12

10 k 6

0	1189	1186	2
1	281	252	26
2	1273	1260	9
3	139	118	10
4	972	968	3
5	155	106	25
6	1047	1049	-1
7	136	79	23
8	991	981	8
9	85	88	0
10	889	919	-20

11 k 6

1	968	955	12
2	125	5	34
3	1244	1231	9
4	91	90	0
5	1186	1186	0
6	92	29	15
7	764	749	13
8	89	112	-8
9	758	746	10
10	102	68	10
11	859	852	4

12 k 6

0	521	518	2
1	130	121	4
2	1057	1059	-1
3	256	241	11
4	1320	1318	0
5	234	243	-7
6	1013	1009	3
7	135	134	0
8	532	544	-11
9	121	119	0
10	711	710	0
11	143	146	-1
12	933	953	-12

13 k 6

1	789	772	16
2	196	189	4
3	1089	1091	-1
4	106	9	21
5	985	994	-7
6	156	91	27
7	789	805	-14
8	95	73	6
9	633	616	15
10	94	101	-2
11	882	869	10
12	-5	41	-3
13	587	589	0

14 k 6

0	833	821	10
1	90	38	13
2	850	841	7
3	75	1	10
4	985	971	11
5	149	92	23
6	789	810	-19
7	76	42	6
8	638	638	0
9	93	64	7
10	725	735	-9
11	96	2	14
12	638	626	10
13	146	53	27
14	543	536	4

15 k 6

1	1047	1028	15
2	110	105	1
3	678	669	7
4	99	86	4
5	601	591	9
6	-37	6	-2
7	705	698	5
8	82	3	11
9	872	871	0
10	130	106	8
11	587	580	6
12	152	109	16
13	450	463	-11
14	-60	10	-5

16 k 6

0	1026	1010	13
1	259	255	3
2	793	786	6
3	141	133	3
4	449	463	-12
5	87	61	6
6	629	640	-9
7	156	190	-17
8	862	861	0
9	146	98	17
10	622	627	-4
11	130	58	20
12	386	393	-6

17 k 6

1	729	731	-1
2	118	92	9
3	580	589	-8
4	43	16	2
5	661	632	24
6	102	94	2
7	746	746	0
8	-34	3	-1
9	607	611	-3
10	-88	43	-15
11	363	392	-23

18 k 6

0	723	708	12
1	59	22	4
2	556	570	-11
3	79	13	9
4	597	613	-13
5	76	5	8
6	615	612	2
7	100	2	15
8	610	601	7
9	140	19	27
10	411	432	-12

19 k 6

1	509	513	-3
2	94	62	7
3	642	633	6
4	97	3	13
5	624	633	-7
6	114	65	12
7	472	468	3

20 k 6

0	436	421	11
1	93	110	-5
2	545	552	-5
3	90	75	3
4	582	591	-7

0 k 7

0	375	394	-18

1 k 7

1	214	162	33

2 k 7

0	374	379	-5
1	118	77	24
2	119	30	27

Structure Factors for Pt2Cl at 300 K. Page 7

3 k 7

1	193	193	0
2	363	368	-6
3	345	360	-12

4 k 7

0	139	104	21
1	88	5	20
2	482	495	-15
3	177	108	43
4	124	97	10

5 k 7

1	465	475	-11
2	144	138	4
3	131	28	38
4	123	48	29
5	85	30	10

6 k 7

0	342	356	-15
1	103	78	11
2	137	101	19
3	120	40	28
4	273	252	18
5	55	57	0
6	227	214	6

7 k 7

1	129	97	17
2	143	167	-17
3	273	267	5
4	85	41	12
5	244	245	0
6	69	89	-6
7	292	320	-17

8 k 7

0	206	163	32
1	198	159	28
2	226	200	20
3	282	290	-8
4	190	192	-1
5	142	125	9
6	261	235	19
7	85	22	13
8	108	94	3

9 k 7

1	113	94	8
2	73	11	11
3	212	224	-10
4	108	13	24
5	390	400	-10
6	-51	29	-7
7	133	77	21
8	92	58	9
9	184	210	-11

10 k 7

0	297	281	15
1	93	54	12
2	198	187	8
3	243	226	14
4	177	164	8
5	138	74	25
6	76	10	11
7	58	98	-11
8	199	200	0

11 k 7

1	108	138	-12
2	148	104	17
3	121	145	-10
4	84	13	11
5	107	64	11
6	38	29	1
7	123	152	-11
8	116	74	12
9	80	74	1
10	126	70	16
9	35	36	0
10	202	241	-19

12 k 7

1	151	148	1
2	138	91	21
3	186	207	-15
4	-50	7	-5
5	94	103	-3
6	96	49	12
7	192	201	-5
8	54	20	4
9	-65	106	-29
10	53	56	0
11	165	151	5

13 k 7

1	261	257	3
2	99	103	-1
3	-29	36	-4
4	118	20	23
5	105	75	9
6	-43	0	-3
7	191	166	13
8	145	117	11
9	224	204	11
10	108	91	5
11	110	60	13
12	32	21	0
13	112	94	4

14 k 7

0	112	99	5
1	119	93	10
2	177	194	-10
3	-77	45	-15
4	123	81	14
5	81	45	8
6	153	151	0
7	109	79	9
8	89	115	-8
9	85	40	8
10	-53	66	-12
11	60	22	5
12	174	158	7
13	44	1	3

15 k 7

11	187	144	19
12	81	26	8

16 k 7

0	103	79	7
1	35	35	0
2	77	82	-1
3	-4	58	-5
4	161	181	-10
5	85	29	10
6	103	123	-7
7	60	10	5
8	138	97	14
9	-10	22	0
10	77	79	0
11	-61	7	-6

17 k 7

1	-94	40	-18
2	81	30	8
3	145	155	-4
4	48	14	3
5	215	178	18
6	-128	32	-29
7	-33	69	-9
8	85	4	10
9	17	61	-5
10	83	17	6

18 k 7

0	148	139	3
1	95	19	13
2	100	128	-9
3	58	13	4
4	73	55	3
5	44	11	2
6	35	60	-3
7	71	1	7
8	125	99	8

19 k 7

1	136	113	7
2	-97	4	-14
3	87	78	1
4	-21	24	-1
5	133	89	13

0 k 8

0	1161	1143	12

1 k 8

1	1417	1411	3

2 k 8

0	1302	1296	4
1	206	155	41
2	896	895	1

3 k 8

1	706	722	-17
2	112	63	21
3	1279	1251	17

4 k 8

0	420	392	29
1	86	93	-2
2	1043	1046	-3
3	86	24	16
4	1311	1330	-11

5 k 8

1	590	577	13
2	128	100	13
3	1230	1235	-3
4	76	50	7
5	1361	1373	-7

6 k 8

0	1037	1082	-39
1	50	71	-6
2	845	865	-18
3	262	272	-8
4	1021	1035	-12
5	-69	12	-10
6	591	590	0

7 k 8

1	1110	1146	-29
2	256	236	17
3	748	752	-4
4	-73	23	-13
5	449	459	-9
6	153	145	4
7	985	956	17

8 k 8

0	1186	1212	-20
1	104	54	16
2	836	870	-32
3	273	236	29
4	438	423	14
5	182	163	11
6	825	830	-4
7	79	20	10
8	1039	1036	1

9 k 8

1	1120	1121	0
2	124	97	11
3	420	425	-5
4	80	66	4
5	599	601	-2
6	134	137	-1
7	924	924	0
8	90	52	9
9	900	906	-4

10 k 8

0	814	826	-10
1	67	76	-2
2	734	744	-9
3	90	5	15
4	697	713	-15
5	-80	60	-20
6	759	786	-24
7	106	125	-7
8	644	647	-2
9	46	49	0
10	461	473	-8

11 k 8

1	583	584	-1
2	187	204	-11
3	882	883	0
4	42	44	0
5	777	773	3
6	141	137	1
7	575	591	-14
8	-30	2	-1
9	350	346	2

Structure Factors for Pt2Cl at 300 K. Page 8

10	130	138	-3
11	715	695	12

12 k 8

0	356	350	5
1	173	152	11
2	656	686	-27
3	103	18	18
4	951	945	4
5	24	43	-2
6	645	651	-5
7	143	105	14
8	330	315	10
9	72	130	-18
10	564	569	-3
11	106	47	13
12	599	601	-1

13 k 8

1	408	392	14
2	96	110	-4
3	840	836	3
4	110	79	9
5	837	830	5
6	163	150	5
7	383	384	0
8	-44	27	-4
9	393	427	-28
10	86	58	6
11	526	541	-13
12	-25	67	-7
13	523	499	14

14 k 8

0	575	561	12
1	53	43	1
2	665	662	2
3	157	125	13
4	528	542	-12
5	-56	18	-5
6	480	478	1
7	-41	31	-4
8	526	526	0
9	-37	70	-9
10	528	527	0
11	25	53	-3
12	442	431	8

15 k 8

1	688	687	1
2	121	116	1
3	457	469	-10
4	-3	5	0
5	333	360	-21
6	123	126	0
7	549	545	3
8	-84	32	-13
9	536	533	2
10	-63	78	-15
11	429	416	9

16 k 8

0	753	756	-2
1	65	67	0
2	454	477	-19
3	80	93	-3
4	332	329	2
5	30	68	-5
6	446	448	-1
7	106	52	12
8	609	583	21
9	-66	47	-10

17 k 8

1	574	559	12
2	87	139	-17
3	335	340	-3
4	62	13	5
5	383	391	-6
6	82	81	0
7	533	522	8

18 k 8

0	387	390	-2
1	45	24	2
2	424	414	7
3	-85	5	-11
4	424	432	-6
5	-33	1	-1

0 k 9

0	1444	1392	29

1 k 9

1	1186	1151	22

2 k 9

0	803	784	18
1	100	57	16
2	1094	1047	31

3 k 9

1	762	744	17
2	151	77	36
3	1024	1005	12

4 k 9

0	801	808	-6
1	144	127	10
2	804	805	0
3	139	80	26
4	1156	1147	6

5 k 9

1	674	672	1
2	35	27	1
3	1146	1135	8
4	139	99	17
5	874	901	-18

6 k 9

0	746	724	20
1	229	194	24
2	961	981	-17
3	43	13	3
4	786	772	13
5	39	91	-13
6	764	760	2

7 k 9

1	945	958	-10
2	80	132	-21
3	669	689	-18
4	-42	58	-10
5	692	711	-17
6	164	183	-10
7	755	758	-1

8 k 9

0	1066	1065	0
1	136	112	10
2	729	726	3
3	-39	22	-4
4	589	613	-22
5	-39	12	-3
6	718	720	-1
7	82	72	2
8	908	911	-1

9 k 9

1	961	980	-16
2	-59	35	-9
3	562	572	-9
4	44	42	0
5	487	507	-18
6	18	68	-7
7	876	878	-1
8	49	34	2
9	703	706	-1

10 k 9

0	764	782	-17
1	98	104	-2
2	695	687	7
3	128	83	16
4	703	698	4
5	84	34	10
6	729	735	-5
7	109	6	19
8	565	571	-5
9	-32	42	-4
10	519	560	-26

11 k 9

1	573	586	-12
2	147	114	13
3	702	740	-34
4	44	30	1
5	860	853	6
6	153	151	1
7	441	472	-26
8	-76	35	-11
9	501	512	-9
10	51	54	0
11	525	532	-4

12 k 9

0	401	411	-9
1	132	84	16
2	676	667	8
3	129	79	16
4	787	822	-30
5	74	98	-6
6	589	603	-12
7	-113	35	-23
8	422	423	0
9	69	46	3
10	518	514	3
11	65	6	6
12	584	571	8

13 k 9

1	488	487	0
2	-53	43	-8
3	781	763	15
4	103	20	15
5	603	629	-22
6	-56	34	-6
7	498	489	7
8	48	28	2
9	410	414	-3
10	-55	26	-5
11	574	571	1

14 k 9

0	654	645	7
1	111	35	16
2	597	603	-5
3	-13	11	0
4	489	501	-10
5	-93	37	-16
6	465	464	0
7	86	60	5
8	553	529	18
9	-83	21	-11
10	528	529	0

15 k 9

1	634	615	16
2	103	72	7
3	449	463	-11
4	56	22	4
5	429	433	-3
6	-98	32	-16
7	529	531	-2
8	46	3	3

16 k 9

0	557	562	-4
1	115	41	16
2	501	509	-5
3	128	20	22
4	373	374	-1
5	84	10	10
6	507	503	3

17 k 9

1	519	514	3
2	57	58	0
3	405	388	12

0 k 10

0	445	394	37

1 k 10

1	133	41	24

2 k 10

0	192	176	11
1	123	60	24
2	129	104	8

3 k 10

1	160	137	13
2	74	62	3
3	109	61	11

4 k 10

0	268	227	31
1	90	80	3
2	173	138	19
3	88	93	-1
4	278	284	-3

5 k 10

1	53	99	-13
2	70	49	4
3	94	56	10
4	27	80	-10
5	128	50	16

6 k 10

0	74	56	4
1	71	84	-3
2	59	11	6
3	43	71	-5
4	-12	78	-11
5	70	84	-3
6	-48	9	-2

7 k 10

1	30	67	-6
2	56	53	0
3	177	147	15
4	-62	11	-7
5	-94	5	-15
6	-77	15	-10
7	-71	61	-10

8 k 10

0	133	164	-15
1	145	136	4
2	101	78	7
3	76	43	6
4	115	119	-1
5	-59	3	-6
6	41	64	-3
7	71	93	-5
8	80	113	-6

9 k 10

1	158	16	38
2	70	58	2
3	-12	18	0
4	41	18	2
5	117	87	9
6	28	67	-5
7	65	63	0
8	-70	11	-7
9	60	21	3

10 k 10

0	-82	17	-12
1	76	97	-6
2	44	1	3
3	18	51	-3
4	54	77	-5
5	-62	56	-11
6	-56	29	-6
7	-11	48	-3
8	-81	3	-9
9	-75	24	-9
10	-123	27	-17

11 k 10

1	-32	31	-3
2	-79	8	-10
3	72	14	8
4	-74	2	-9
5	38	37	0
6	-83	25	-12
7	130	71	16
8	55	37	2
9	-42	10	-2
10	-116	11	-21
11	126	49	12

12 k 10

0	164	154	4
1	-70	5	-7
2	73	12	7
3	53	108	-13
4	56	64	-1
5	-24	98	-15
6	21	33	0
7	-83	36	-12
8	77	80	0
9	21	39	-1
10	30	77	-7

13 k 10

1	-72	66	-15
2	-58	46	-8
3	-40	28	-3
4	-63	16	-6
5	-91	1	-13
6	23	21	0
7	-135	12	-28
8	-30	1	-1
9	71	87	-3

14 k 10

0	-66	38	-9
1	48	32	1
2	64	21	5
3	-52	6	-4
4	71	28	6
5	-23	30	-2
6	-82	18	-10
7	-110	22	-18

15 k 10

1	-45	28	-4
2	53	10	3
3	-91	25	-13
4	-115	40	-22
5	72	56	2

0 k 11

0	1098	1095	1

1 k 11

1	910	904	4

2 k 11

0	817	792	22
1	37	15	2
2	634	610	16

3 k 11

1	499	500	0
2	93	86	2
3	925	908	10

4 k 11

0	227	204	15
1	113	70	13
2	799	782	14
3	96	0	15
4	986	932	32

5 k 11

1	580	558	19
2	65	102	-10
3	749	762	-11
4	-76	12	-10
5	756	751	3

6 k 11

0	709	714	-4
1	54	59	0
2	587	595	-6
3	61	58	0
4	677	661	13
5	-113	10	-21
6	555	565	-5

7 k 11

1	749	744	4
2	-48	14	-4
3	500	507	-6
4	-108	28	-20
5	418	440	-18
6	-80	15	-10
7	714	704	5

8 k 11

0	879	870	7
1	61	2	6
2	618	612	4
3	181	182	0
4	262	302	-27
5	57	120	-16
6	558	554	3
7	-76	54	-12
8	712	693	10

9 k 11

1	695	691	3
2	-53	71	-12
3	428	427	0
4	-105	15	-18
5	487	488	-1
6	-79	69	-16
7	547	533	10
8	-82	18	-9
9	605	604	0

10 k 11

0	566	580	-12
1	61	39	3
2	536	533	2
3	70	63	1
4	519	515	2
5	-60	58	-10
6	488	475	10
7	-61	16	-5
8	496	506	-7
9	-92	27	-12

11 k 11

1	417	404	10
2	-53	35	-6
3	623	611	10
4	101	30	13
5	583	558	20
6	-83	37	-11
7	421	435	-10
8	70	47	3

12 k 11

0	298	292	4
1	-69	106	-24
2	465	463	1
3	55	46	1
4	682	651	24
5	-96	52	-17
6	497	487	7
7	64	72	-1

13 k 11

1	390	398	-5
2	-71	54	-11
3	495	502	-6
4	56	26	3
5	500	500	0

14 k 11

0	395	393	1

0 k 12

0	819	771	30

1 k 12

1	545	556	-7

2 k 12

0	411	408	2
1	37	66	-5
2	588	577	7

3 k 12

1	457	441	14
2	14	18	0
3	543	552	-6

4 k 12

0	412	410	1
1	21	5	0
2	423	436	-10
3	103	55	11
4	668	663	3

5 k 12

1	457	443	12
2	31	2	1
3	527	529	-1
4	-34	21	-2
5	469	455	7

6 k 12

0	444	454	-8
1	-41	20	-3
2	481	495	-11
3	-48	79	-13
4	387	396	-6
5	-122	40	-24
6	523	495	15

7 k 12

1	515	528	-10
2	-127	23	-25
3	334	349	-10
4	-92	18	-12
5	406	433	-20
6	-117	9	-19
7	410	432	-11

8 k 12

0	579	568	8
1	11	86	-10
2	416	428	-9
3	-70	49	-10
4	307	343	-24
5	-77	20	-8
6	412	391	14
7	-102	29	-15
8	466	469	-1

Structure Factors for Pt2Cl at 300 K. Page 10

9 k 12

1	404	425	-16
2	-90	17	-12
3	466	442	17
4	-44	8	-2
5	342	351	-6
6	-91	4	-11
7	433	439	-3

10 k 12

0	368	367	0
1	-71	39	-9
2	400	419	-13
3	-123	41	-25
4	399	407	-5
5	-65	14	-6

11 k 12

1	362	354	5
2	-37	15	-2
3	370	408	-27

0 k 13

0	238	213	10

1 k 13

1	-47	117	-18

2 k 13

0	62	1	6
1	-29	1	-1
2	68	105	-7

3 k 13

1	90	3	12
2	-119	41	-26
3	-130	66	-24

4 k 13

0	51	11	3
1	-103	31	-18
2	68	6	6
3	-61	42	-8
4	145	176	-9

5 k 13

1	76	32	6
2	-51	14	-4
3	-85	145	-41
4	-102	42	-17
5	-117	89	-21

6 k 13

0	-89	22	-11
1	-142	57	-3[illegible]
2	85	97	-2
3	-101	7	-14
4	-96	50	-16
5	-127	43	-24

7 k 13

1	-134	95	-37
2	-129	50	-26
3	37	10	1
4	-165	9	-38

8 k 13

0	61	160	-27
1	-94	59	-16
2	-157	34	-22